The University Of Sheffield.

Investigating the structure/function relationships of leaves in wheat and its wild relatives

Matthew James Wilson

A thesis submitted to the University of Sheffield
for the degree of Doctor of Philosophy

The University of Sheffield
Faculty of Science
Department of Animal and Plant Sciences

September 2019

Acknowledgements

I would first like to thank my supervisor, Andy Fleming, who has provided the guidance and support that I have required throughout my PhD project. I would also like to thank my second supervisor, Colin Osborne, for the kind donation of seed and for his advice and encouragement. Likewise, I have appreciated the support of my iCASE supervisor, Richard Summers, whose enthusiasm for a project fairly low down on the applied scale has been invigorating.

This project was funded by a BBSRC iCASE studentship and I am grateful to both the BBSRC and RAGT Seeds for this opportunity. I am particularly thankful for the supervision of Lucie Griffe and also to everyone else in Ickleton for making me feel so welcome during my placement.

Without the help of many colleagues and collaborators, this research would have been impossible. I would like to thank Marjorie Lundgren and Jess Dunn for discussions regarding gas exchange analysis and would also like to express my appreciation to Ian Smillie – sorry for bothering you on what seemed like a monthly basis! With regards to imaging, I would like to acknowledge Craig Sturrock and Marc Fradera-Soler for their help with the µCT and image analysis training. I am particularly grateful to Alice Baillie for many hours of help with sample preparation and problem solving whilst developing the confocal protocol, and to Ellie Healicon for LithoGraphX troubleshooting. Thanks also to Darren Robinson for microscopy assistance. I would also like to thank Jen Sloan, Marion Bauch, Gemma Newsome and Heather Walker for their technical support (and so much more) and also the rest of D59 for their friendship and assistance.

Finally, I am indebted to my friends (particularly the pub group, the football squad and Caterpillar Club), my family – especially my parents - and Debs for making life outside of academia such a fulfilling experience, for which I am truly grateful.

Collaborations and publications

Some of the data presented in this thesis contributed to a larger, collaborative project with the University of Nottingham, resulting in the following publication:

- Lundgren, M.R., Mathers, A., Baillie, A.L., Dunn, J., Wilson, M.J., Hunt, L., Pajor, R., Fradera-Soler, M., Rolfe, S., Osborne, C.P., Sturrock, C.J., Gray, J.E., Mooney, S.J, & Fleming A.J., 2019. Mesophyll porosity is modulated by the presence of functional stomata. *Nature Communications*, 10(1), 2825.

The g_{smax} data from Chapter 2 was used in this publication to support the wheat gas exchange data collected by Dr Marjorie Lundgren and stomatal density/size data collected by Alice Mitchell.

The X-ray µCT data in Chapter 3 combines data from lines collected by Dr Marjorie Lundgren and Dr Radek Pajor with those analysed by myself using the same protocol (Scans were completed by Marc Fradera-Soler and Dr Craig Sturrock at the Hounsfield Facility, University of Nottingham). 3D reconstructions of µCT stacks were made by Dr Andrew Mathers and Dr Craig Sturrock. This data was also included in the above publication.

This publication also made use of the confocal data showing stomatal/mesophyll airspace development from Chapter 3, which I collected myself. Initial 3D cell geometry data, which eventually formed part of Chapter 4, also contributed to the aforementioned publication.

Stomatal size/density data and gas exchange data for some of the hexaploid lines used in Chapter 2 was collected by the MBiolSci project student George Thompson.

Seeds used to grow plants in this study were provided by my second supervisor, Professor Colin Osborne (2n and 4n wild lines), or by my BBSRC iCASE partner, RAGT Seeds Ltd (all *T. aestivum* and *T. durum* cultivars). *TaEPF1-OE* seeds used in Chapter 3 were provided by Jess Dunn, Dr Lee Hunt and Professor Julie Gray (University of Sheffield).

Abstract

In order to carry out photosynthesis, plants rely upon the exchange of CO_2 and water vapour. This is limited by pores on the epidermis (stomata), the internal arrangement of cells within the leaf, and the intercellular airspace network between the cells, through which gas must pass to the chloroplasts. How these leaf structures are co-ordinated, and the extent to which they individually influence photosynthesis, is open to debate and is the subject of this thesis.

Using modern bread wheat (*Triticum aestivum*), a hexaploid plant derived from tetraploid and diploid relatives, as the experimental organism, I first show using gas exchange analysis that diploid lines have the highest stomatal conductance (g_s) and lowest intrinsic water use efficiency (iWUE), whereas hexaploid lines have the lowest g_s and highest iWUE. These differences are linked to changes in stomatal size and density driven by changes in cell size linked to ploidy.

When the relationship between wheat g_s and leaf airspace was investigated using X-ray micro-computed tomography, a positive correlation was found. Analysis of differentiation patterns in the epidermis and subtending mesophyll provided evidence supporting a mechanistic link between g_s and airspace, indicating that functional stomata are required for the formation of intercellular airspaces within the leaf.

Finally, I report on the development of a 3D imaging protocol using confocal microscopy to extract wheat mesophyll cell geometry. This allowed the elucidation of a link between mesophyll cell size/shape and gas exchange, leading to the hypothesis that the evolution of higher ploidy levels in wheat may have been linked to gas exchange.

The work reported here provides a new insight into the relationship of stomatal function and leaf differentiation, and supports the idea that leaf water use rather than CO_2 assimilation may have been a driver in the selection of one of our major food crops.

Table of contents

Acknowledgements i

Collaborations and publications iii

Abstract v

Table of contents vii

Table of figures xi

List of tables xiv

List of equations xiv

Chapter 1. General introduction 1

1.1. Wheat as a crop and its domestication 1

1.2. Leaf form is related to leaf function 4

1.2.1. The primary leaf function is to carry out photosynthesis 4

1.2.2. The role of stomata in controlling photosynthetic gas flux 6

1.2.3. Mesophyll limitations of photosynthesis 8

1.2.4. Measuring leaf gas exchange 10

1.3. Wheat leaf morphology and anatomy 11

1.4. Water use efficiency is an important breeding target 14

1.5. Aims and objectives 15

Chapter 2. Changes in ploidy level affect stomata and leaf gas exchange in the Triticeae 17

2.1. Introduction 17

2.1.1. Stomatal size and stomatal density are associated with ploidy level 17

2.1.2. Other leaf structural parameters are also affected by ploidy level 18

2.1.3. What effect does variation in stomatal size and density have upon leaf level gas exchange? 19

2.1.4. Aims 22

2.2. Methods 22

2.2.1. Plant material and growth conditions 22

2.2.3. Stomatal size 25

2.2.4. Anatomical g_{smax} ... 26
2.2.5. Epidermal cell size ... 26
2.2.6. Leaf sections ... 27
2.2.7. Gas exchange analysis – steady state measurements ... 28
2.2.8. Data analysis ... 29
2.3. Results ... 29
2.3.1. Ploidy level affects stomatal density ... 29
2.3.2. Increasing ploidy level results in an increase in stomatal size ... 30
2.3.3. There is significant variation within the Triticeae for anatomical g_{smax} ... 32
2.3.4. Epidermal cell size changes with ploidy level ... 34
2.3.5. There is variation in leaf size within the Triticeae ... 35
2.3.6. There is variation in leaf vascular patterning ... 38
2.3.7. There is no trend of ploidy level and leaf thickness ... 40
2.3.8. Gas exchange in leaves of different ploidy under ambient conditions ... 41
2.4. Discussion ... 45
2.4.1. The size and arrangement of stomata is influenced by ploidy level in wheat ... 45
2.4.2. There is variation in organ size within the Triticeae but the relationship to ploidy level is not strict ... 47
2.4.3. Leaf vascular patterning and thickness and ploidy level ... 48
2.4.4. The effect of ploidy-related structural changes on leaf gas exchange ... 50
2.5. Conclusion ... 53
Chapter 3. How ploidy affects the internal structure of wheat leaves and implications upon photosynthesis ... 55
3.1. Introduction ... 55
3.1.1. The relationship of ploidy level and internal leaf structure ... 55
3.1.2. X-ray microtomography as a novel method for investigating leaf internal structure ... 58
3.1.3. Using fitting software to extract more information from gas exchange data – estimating mesophyll conductance ... 61
3.1.4. Other leaf components – chlorophyll and protein content ... 63
3.1.5. Carbon isotope discrimination and water use efficiency ... 64
3.1.6. What comes first, the stomata or the airspace? A chicken and egg hypothesis ... 65
3.1.7. Aims ... 66
3.2. Methods ... 67
3.2.1. Plant material and growth conditions ... 67

3.2.2. Using X-ray μCT to observe leaf internal characteristics 67
3.2.3. Physiological responses to changing environmental conditions – light intensity and CO_2 69
3.2.4. Quantification of chlorophyll content 70
3.2.5. Total soluble protein quantification 71
3.2.6. Stable isotopes as an indicator of water use efficiency 71
3.2.8. Confocal analysis of the stomatal lineage 72
3.2.8. Data analysis 73
3.3. Results **74**
3.3.1. Mesophyll porosity is positively correlated with stomatal density 74
3.3.2. Photosynthetic responses to changing levels of irradiance do not change significantly with ploidy level 78
3.3.1. Plants of different ploidy levels vary in their response to changes in CO_2 concentration 79
3.3.2. There are no clear trends between ploidy level and mesophyll conductance 85
3.3.3. There is variation in chlorophyll and total soluble protein content in the Triticeae 87
3.3.4. There are no significant differences in $\Delta^{13}C$ with ploidy level 88
3.3.5. Sub-stomatal cavities and intercellular airspaces form after the stomata have gained full function 90
3.4. Discussion: **94**
3.4.1. The patterning of intercellular airspaces in wheat leaves is positively correlated with stomatal conductance. 96
3.4.2. A more in-depth analysis reveals variation in photosynthetic parameters in the Triticeae 98
3.4.3. There is no trend with ploidy level and mesophyll conductance in wheat 99
3.4.4. Chlorophyll and protein content 101
3.4.3. iWUE is correlated with $\Delta^{13}C$ values in the Triticeae 102
3.4.5. Sub-stomatal cavities and intercellular airspaces form after the stomata have gained function 103
3.5. Conclusion **104**

Chapter 4. 3D imaging at cellular resolution: size and shape changes of mesophyll cells throughout wheat evolution 105
4.1. Introduction **105**
4.1.1. Changes in ploidy level have previously been associated with changes in mesophyll cell size and shape 105

4.1.2. Using confocal laser scanning microscopy to generate 3D image stacks of plant tissues ... 109
4.1.3. Image processing using LithoGraphX ... 112
4.1.4. Aims ... 113
4.2. Methods ... **114**
4.2.1. Plant material and growth conditions ... 114
4.2.2. Sample collection, fixation and storage ... 114
4.2.3. Sample preparation for confocal microscopy ... 114
4.2.4. Imaging leaf sections using confocal microscopy: ... 116
4.2.5. Image processing and reconstruction/segmentation using LithoGraphX ... 117
4.2.6. Data analysis ... 118
4.3. Results ... **120**
4.3.1. Increases in ploidy level in wheat result in changes in mesophyll cell size and shape ... 120
4.3.2. Mesophyll cell geometry is correlated with mesophyll airspace levels and exposed mesophyll surface area ... 128
4.4. Discussion ... **135**
4.4.1. Mesophyll cell size and shape is influenced by ploidy level in *Triticum* species ... 135
4.4.2. Mesophyll cell geometry is correlated with leaf airspace and the amount of exposed mesophyll surface ... 136
4.4.3. Method development and future prospects of using a confocal microscopy approach to quantify mesophyll cell geometric parameters ... 138
4.5. Conclusion ... **144**

Chapter 5. General Discussion ... 145
5.1 Wheat leaf form is responsible for function ... **145**
5.2. Future research directions ... **150**

Bibliography ... 153

Appendices ... 177
Appendix 1. Significance tables for Chapter 2 ... **177**
Appendix 2. Significance tables for Chapter 3 ... **187**
Appendix 3. Significance tables for Chapter 4 ... **193**

Table of figures

Figure 1.1. The geographical origins of modern bread wheat. 2
Figure 1.2. The evolution of modern bread wheat 3
Figure 1.3. The photosynthetic gas diffusion pathway within the leaf 5
Figure 1.4. Stomatal development in grasses 7
Figure 1.5. IRGAs can be used to measure leaf gas exchange 10
Figure 1.6. The basic arrangement of wheat leaf internal anatomy in transverse section 13

Figure 2.1. Stomatal anatomical characteristics 27
Figure 2.2. Measurements of leaf thickness and interveinal distance 28
Figure 2.3. There is variation in stomatal density between 2n, 4n and 6n wheat lines 30
Figure 2.4. Differences is stomatal density and size with ploidy level 31
Figure 2.5. There is variation in stomatal size between 2n, 4n and 6n wheat lines 33
Figure 2.6. Variation in anatomical g_{smax} between 2n, 4n and 6n wheat lines .. 34
Figure 2.7. There is variation in epidermal cell size between 2n, 4n and 6n wheat lines 36
Figure 2.8. There is variation in leaf size between 2n, 4n and 6n wheat lines . 39
Figure 2.9. There is variation in leaf vasculature between 2n, 4n and 6n wheat lines 41
Figure 2.10. There is variation in leaf thickness between lines 42
Figure 2.11. There is variation in leaf level gas exchange between 2n, 4n and 6n wheats 44
Figure 2.12. There is variation in stomatal density between modern 6n cultivars 52

Figure 3.1. Principles of X-ray µCT 59
Figure 3.2. µCT reveals variation in leaf airspace between 2n, 4n and 6n genotypes 75
Figure 3.3. There is variation in mesophyll porosity between 2n, 4n and 6n wheat lines 76
Figure 3.4. There is a positive correlation between mesophyll porosity and stomatal conductance (g_s) in the Triticeae with varying ploidy level 77

Figure 3.5. Exposed mesophyll surface area does not vary significantly between 2n, 4n and 6n Triticum lines 78
Figure 3.6. CO_2 assimilation response to changing irradiance levels in 2n, 4n and 6n accessions of the Triticeae 80
Figure 3.7. A_{sat} and quantum yield values extracted from light response curves vary amongst the Triticeae 81
Figure 3.8. The response of CO_2 assimilation to shifts in C_i varies between 2n, 4n and 6n wheat lines 82
Figure 3.9. Variation in C_i and A_{max} values at high CO_2 concentrations between 2n, 4n and 6n members of the Triticeae 84
Figure 3.10. There is variation in photosynthetic biochemistry between 2n, 4n and 6n lines of the Triticeae 86
Figure 3.11. Variation in mesophyll conductance in wheat lines of different ploidy 87
Figure 3.12. There is variation in leaf chlorophyll and total soluble protein ... 89
Figure 3.13. Carbon isotope discrimination ($\Delta^{13}C$) values for a range of 2n, 4n and 6n wheat lines 90
Figure 3.14. There is a negative correlation between $\Delta^{13}C$ and iWUE for 2n, 4n and 6n members of the Triticeae 91
Figure 3.15. There are gradients in stomatal density and mesophyll porosity along mature wheat leaves 93
Figure 3.16. *TaEPF1-OE* plants have a lower stomatal density and mesophyll porosity than wild-type Fielder plants 93
Figure 3.17. Mesophyll airspace formation is linked to the presence of fully differentiated stomata 95

Figure 4.1. Confocal microscopy can be used to generate high-resolution images of the leaf mesophyll 110
Figure 4.2. LithoGraphX software allows for the reconstruction and segmentation of individual mesophyll cells 119
Figure 4.3. Manual mesh cleaning in LGX 120
Figure 4.4. Mesophyll cells appear smallest in diploid plants, intermediate in 4n lines and largest in hexaploid accessions 121
Figure 4.5. There is variation in mesophyll cell surface area between 2n, 4n and 6n lines 122
Figure 4.6. There is variation in mesophyll cell volume between 2n, 4n and 6n lines 123
Figure 4.7. Relationships between mesophyll cell surface area and volume . 125

Figure 4.8. There is no significant variation in the surface area to volume ratio of wheat mesophyll cells for wheat lines of ranging ploidy level (2n, 4n, 6n) 126
Figure 4.9. There is significant variation in the mesophyll cell lobe number of wheat genotypes of ranging ploidy level (2n, 4n, 6n) 126
Figure 4.10. Variation in mesophyll cell lobing.....127
Figure 4.11. Mesophyll cell lobe number is correlated with other mesophyll cell geometric parameters in wheat leaves of varying ploidy levels 129
Figure 4.12. Mesophyll cell size parameters are inversely correlated with mesophyll porosity (%airpace/volume) in 2n, 4n and 6n Triticum lines.....130
Figure 4.13. Mesophyll cell shape parameters are correlated with mesophyll porosity (%airspace/volume) in 2n, 4n and 6n wheat genotypes 132
Figure 4.14. Mesophyll cell size parameters are correlated with exposed mesophyll surface area (Smes) in 2n, 4n and 6n wheat genotypes.....133
Figure 4.15. Mesophyll cell shape parameters are correlated with Smes in 2n, 4n and 6n wheat genotypes 134

List of tables

Table 2.1. A list of the Triticeae genotypes used in this study 23
Table 2.2. The subset of 11 *Triticum* lines selected for further analysis..... 24

List of equations

Equation 2.1. Anatomical g_{smax} 26
Equation 3.1. Mesophyll porosity 68
Equation 3.2. Exposed mesophyll surface area (S_{mes}) 68

List of abbreviations

A: CO_2 assimilation

A_{max}**:** Photosynthetic capacity

A_{sat}**:** Light saturated CO_2 assimilation

C_i**:** Leaf internal CO_2 concentration

CLSM: Confocal laser scanning microscopy

Δ^{13}C: Carbon isotope discrimination

EPF: Epidermal Patterning Factor

g_m**:** Mesophyll conductance

GMC: Guard mother cell

g_s**:** Stomatal conductance

g_{smax}**:** Anatomical maximum stomatal conductance

IRGA: Infra-red gas analyser

ITK: Insight Segmentation and Registration Toolkit

iWUE: Intrinsic water use efficiency

***J*:** Electron transport rate

LGX: LithographX

µCT: micro computed tomography

NA: Numerical aperture

PI: Propidium iodide

PS-PI: Pseudo-schiff propidium iodide

RBR: Retinoblastoma-related protein

Rubisco: Ribulose 1,5-bisphosphate carboxylase/oxygenase

SA/V: Surface area to volume ratio

SAM: Shoot apical meristem

S.E.M: Standard error of the mean

S_c**:** Exposed chloroplast surface area

SMC: Subsidiary mother cell

S_{mes}**:** Exposed mesophyll surface area

v/v: Volume/ volume

V_{cmax}**:** Maximum carboxylation rate of Rubisco

w/ v: Weight/ volume

WUE: Water use efficiency

Φ: Apparent quantum yield of photosynthesis

Chapter 1. General introduction

1.1. Wheat as a crop and its domestication

Wheat (*Triticum aestivum*) is a monocot cereal crop from the grass (Poaceae) family, which provides around 20% of the global calorific and dietary protein intake (Reynolds *et al.*, 2012; Hawkesford *et al.*, 2013; Shiferaw *et al.*, 2013) and is the staple crop for 40% of the global population (Peng *et al.*, 2011). It is the most widely cultivated crop in the world with more than 220 million hectares grown worldwide yearly (Balfourier *et al.*, 2019), and can be grown in a vast range of environmental conditions (Shewry, 2009; Shiferaw *et al.*, 2013). In 2013, a total of 713 million tonnes of wheat were produced globally (Long *et al.*, 2015).

The origins of wheat can be traced back to the 'Fertile Crescent' region of the Near East (Abbo & Gopher, 2017) (Figure 1.1), which includes parts of Turkey, Syria, Iraq, Iran, Israel, Jordan and Lebanon, where it was domesticated from its wild ancestors around 8000-10,000 years ago at the dawn of modern agriculture (Marcussen *et al.*, 2014; El Baidouri *et al.*, 2017; Balfourier *et al.*, 2019). Both cultivated and wild species of the *Triticum* genus (of which *T. aestivum* is a member) have a chromosome number of n=7, and vary in ploidy level from diploid (2n), tetraploid (4n) and hexaploid (6n) (Berkman *et al.*, 2013). Like many other crop species, modern bread wheat is polyploid, specifically allohexaploid (AABBDD), in nature, and this is the result of two separate hybridisation events involving three different diploid species (Marcussen *et al.*, 2014; Vergauwen & De Smet, 2017; El Baidouri *et al.*, 2017; Ramírez-González *et al.*, 2018) (summarised in Figure 1.2).

The advent of new genetic resources has enabled greater clarification of the origins of wheat (El Baidouri *et al.*, 2017; Ramírez-González *et al.*, 2018), which has also been aided by archaeobotanical research (Abbo & Gopher, 2017). The initial polyploidisation event has been hypothesised to have been between the diploid species *T. urartu* (which provided the A genome) and an unknown relative of *Aegilops speltoides* (the source of the B genome) (Marcussen *et al.*, 2014; El Baidouri *et al.*, 2017). This resulted in the formation of tetraploid *Triticum turgidum* (AABB), from which the

domesticated species *T. durum* (durum wheat) and *T. dicoccon* (emmer wheat) have been derived (Avni *et al.*, 2017; Maccaferri *et al.*, 2019). This was then followed by a second hybridisation between tetraploid domesticated emmer and *A. tauschii* (the donator of the D genome) to form modern hexaploid bread wheat (AABBDD) (Marcussen *et al.*, 2014; El Baidouri *et al.*, 2017). The *Triticum* genus also contains many more species at each ploidy level, including the domesticated 2n species einkorn (*T. monococcum*) and domesticated 6n spelt (*T. spelta*). Around 95% of wheat currently cultivated worldwide is hexaploid bread wheat, and the majority of the remaining 5% is tetraploid durum wheat (Peng *et al.*, 2011). Einkorn, emmer and spelt, although less commonly grown, are still cultivated in small quantities (Shewry, 2009; Haas *et al.*, 2019).

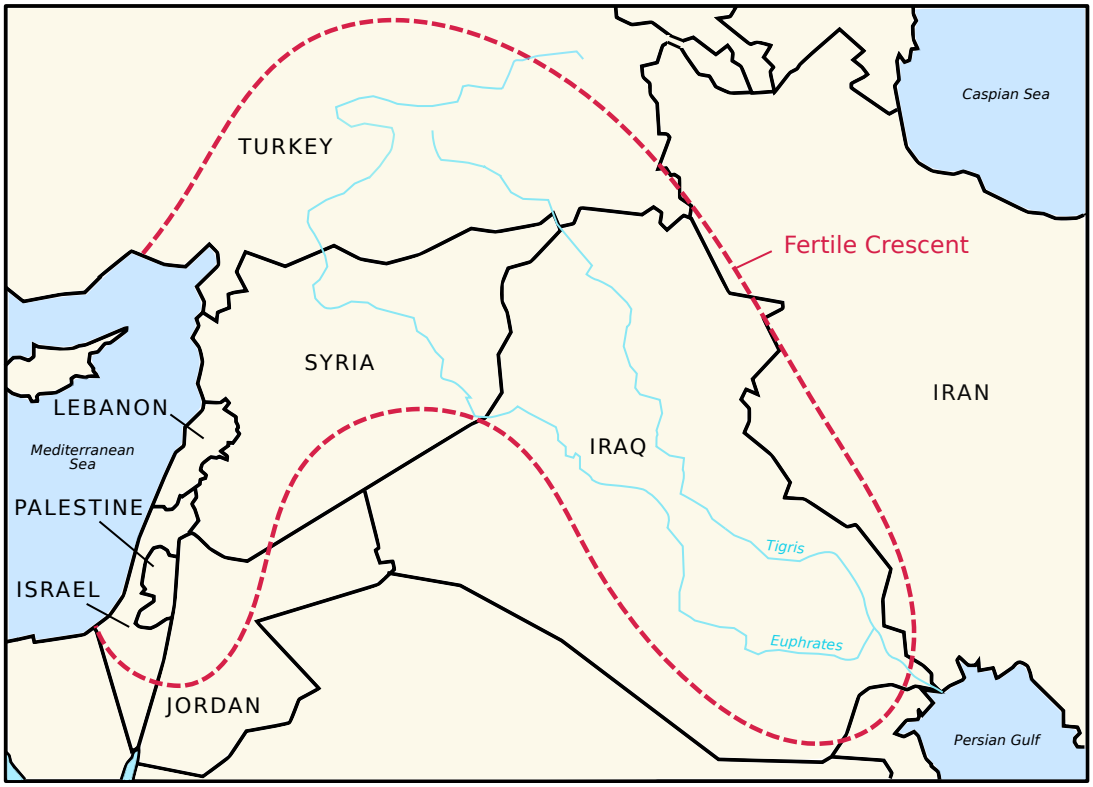

Figure 1.1. The geographical origins of modern bread wheat.
Modern hexaploid bread wheat (*T. aestivum*) was domesticated (around 8000–1000 years before present) from its wild ancestors in the Euphrates–Tigris basin in the Near East – a region named the Fertile Crescent (shown by the red dashed line).

The domestication of 6n wheat has been associated with the selection of desirable traits. Unlike its wild relatives, hexaploid wheat is indehiscent as it has a non-brittle rachis (thus lowering seed losses at harvesting) (Dubcovsky & Dvorak, 2007; Allaby *et al.*, 2017), and has free threshing, rather than hulled grain (Doebley *et al.*, 2006; Dubcovsky & Dvorak, 2007).

In addition to these genetic domestication syndrome traits, yield and its components have also been affected throughout the evolution of hexaploid wheat, with increased yield being suggested to be a major driver of selection (Peng *et al.*, 2011; Preece *et al.*, 2017).

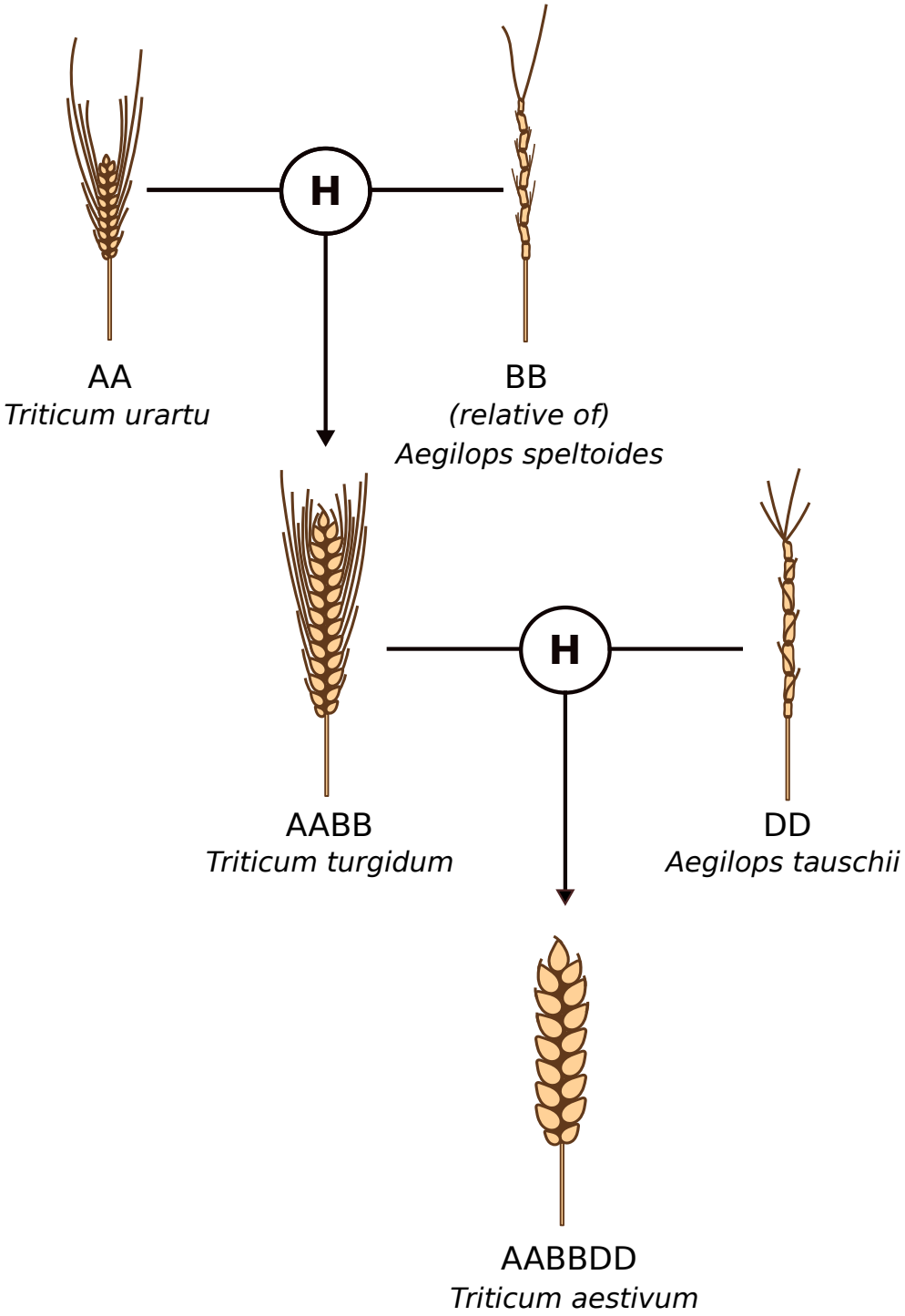

Figure 1.2. The evolution of modern bread wheat
Hexaploid wheat has evolved as the result of two separate hybridisation events. Hybridisation events resulting in allopolyploid formation are identified with an H. Hybridisation of the diploid species *T. urartu* (AA) with an unknown relative of *A. speltoides* (BB) generated a tetraploid species containing the A and B genomes: *T. turgidum*. A second hybridisation event between domesticated tetraploid wheat (AABB) and *A. tauschii* (DD) led to the formation of modern hexaploid wheat, *T. aestivum* (AABBDD).

Grain yield is a highly complex trait, being influenced by many parameters, one of which is grain size. This has been shown to increase with ploidy level in the Triticeae, and it is likely that this is one of the traits that led to the preferential selection of polyploid lines (Purugganan & Fuller, 2009; Gegas *et al.*, 2010; Preece *et al.*, 2015; Hughes *et al.*, 2019). It has been hypothesised that a variety of quantitative traits were also selected for, including plant height and spike characteristics (Peng *et al.*, 2011) in addition to growth rate, duration of the growth period and the increased allocation of biomass to reproductive tissue in comparison to vegetative tissue (Preece *et al.*, 2017). Another potential influence upon grain yield is variation in photosynthesis, which in theory is directly responsible for dry matter production when no other conditions are limiting (Parry *et al.*, 2010; Evans, 2013). Changes in specific environmental pressures - such as periods of drought (Balfourier *et al.*, 2019) - may also have had an impact upon the evolution of wheat, with lines conferring higher resilience against such events being either unconsciously or preferentially selected for (Milla *et al.*, 2015).

1.2. Leaf form is related to leaf function

1.2.1. The primary leaf function is to carry out photosynthesis

Photosynthesis is the biochemical process by which plants utilise intercepted solar radiation (in the visible spectrum, wavelengths of 400-700nm) to drive the oxidation of water (H_2O) and reduction of CO_2, eventually resulting in the release of oxygen and the production of simple carbon compounds used for growth (Zhu *et al.*, 2008; 2010). The photosynthetic process is carried out in organelles named chloroplasts, and has long been known to be separated into two distinct steps, the light-dependent and light-independent reactions (Raines, 2003; Allen & Martin, 2007). The products of the photophosphorylatory light-dependent reactions (ATP and NADPH) are in turn used to drive the carbon fixation reactions (Kirchhoff, 2013). These light-independent reactions act to synthesise sugars used for growth, which requires the action of ribulose 1,5-bisphosphate carboxylase/oxygenase (Rubisco) (Ducat & Silver, 2012).

Photosynthesis has not just biochemical components but also physical ones, as the diffusion of gas from the atmosphere to the site of carbon fixation in the chloroplasts is essential to this process, i.e., the biochemistry has a spatial structure at a distance from the CO_2 and light source (Flexas *et al.*, 2012). The primary role of leaves is as photosynthetic organs, and as such they have specific, highly specialised anatomies (Terashima *et al.*, 2011; Tomas *et al.*, 2013; Ren *et al.*, 2019). Firstly, the epidermis is dotted with microscopic pores named stomata, which act as the point of entry and exit for photosynthetic gas exchange (Lawson & Blatt, 2014; Endo & Torii, 2019). Beneath stomata lie sub-stomatal cavities (Hepworth *et al.*, 2018), and these are connected to a three-dimensional network of airspaces that intersperses the chlorenchyma tissue (Ishizaki, 2015). This provides a route through which gas can efficiently diffuse to and from the chloroplasts found around the perimeter of mesophyll cells. CO_2 must overcome several points of resistance along this route, including the leaf boundary layer and stomatal and mesophyll resistances that are determined by their anatomy (see Figure 1.3).

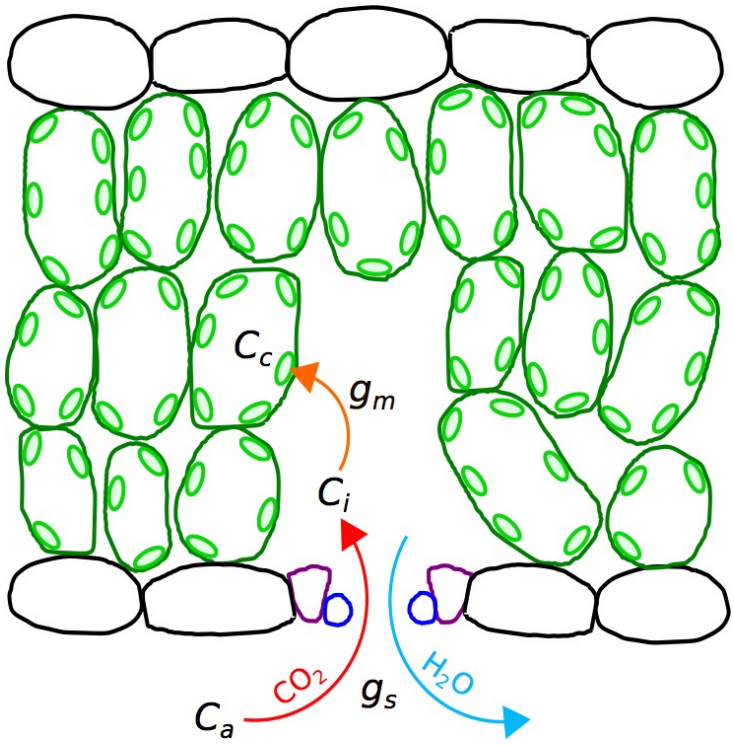

Figure 1.3. The photosynthetic gas diffusion pathway within the leaf
CO_2 enters leaves through stomata and diffuses through the mesophyll to the site of carboxylation at chloroplasts. C_a is the atmospheric CO_2 concentration; C_i is the leaf internal CO_2 concentration and C_c is the CO_2 concentration at the chloroplast. Water vapour also diffuses out of the leaf via this pathway in reverse. g_s is the rate of gas diffusion across the pore, or stomatal conductance, whilst g_m is the inverse of the resistance to gas diffusion across the mesophyll, mesophyll conductance.

1.2.2. The role of stomata in controlling photosynthetic gas flux

Stomata, as the interface between the leaf and the environment, are expected to have a major impact upon the rates of gas exchange and thus photosynthesis (Hepworth *et al.*, 2018). In grasses, such as *Triticum* species, each stoma is comprised of an aperture flanked by a pair of dumbbell shaped guard cells and subsidiary cells (Raissig *et al.*, 2016; Endo & Torii, 2019). This characteristic arrangement is thought to enable the rapid opening and closure of grass stomata in response to environmental stimuli (Franks & Farquhar, 2006; Lawson & Blatt, 2014).

Grass stomatal development follows specific, defined stages, and differs from the development of stomatal complexes in eudicots (summarised in Figure 1.4). Firstly, the epidermal cell files that have the capability to form stomata are determined (Raissig *et al.*, 2016), and this is followed by the asymmetric division of cells within this file to form guard mother cells (GMCs) alongside larger sister cells (Facette & Smith, 2012; Vatén & Bergmann, 2012; Raissig *et al.*, 2016; Hepworth *et al.*, 2018). Subsequently, a second asymmetric division occurs, this time in the epidermal cells that flank the newly differentiated GMCs, resulting in the formation of subsidiary mother cells (SMCs) (Serna, 2015; Endo & Torii, 2019). These cells then increase in size until each complex precursor consists of a pair of immature subsidiary cells flanking the mature GMC (Vatén & Bergmann, 2012; Hepworth *et al.*, 2018). The final division in the stomatal development pathway is symmetrical in nature and the GMC is split into two immature guard cells (Hepworth *et al.*, 2018; Endo & Torii, 2019). Following this, the guard cells elongate into their stereotypical dumbbell shape (Liu *et al.*, 2009) and eventually separate to form a central stomatal aperture or pore (Hepworth *et al.*, 2018) – see Figure 1.4. These patterns of division are highly regular and ensure that neighbouring stomatal complexes are separated by at least one epidermal cell (Bergmann & Sack, 2007; Pillitteri & Torii, 2012). The frequency of stomata is established during leaf development, and is influenced by many environmental factors including light, humidity and CO_2 concentration (Bergmann & Sack, 2007).

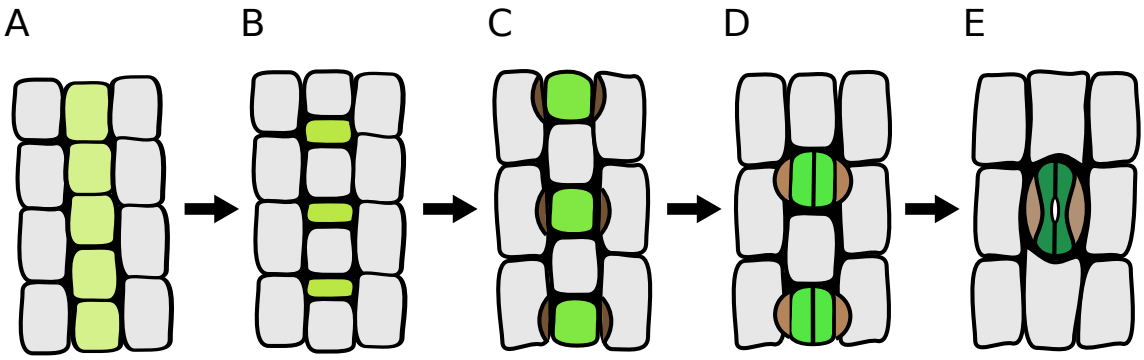

Figure 1.4. Stomatal development in grasses
A) Stomatal files are determined (stomatal file shown in green). **B)** Cells undergo an asymmetrical division, forming guard mother cells (GMCs – highlighted in green). **C)** A subsequent asymmetrical division in cells flanking GMCs (green cells) produces subsidiary mother cells (SMCs – indicated by brown cells). **D)** A symmetrical division results in the formation of two guard cells (green). **E)** Guard cells elongate and separate to form a pore. Mature grass stomata are stereotypically dumbbell shaped (in green) and flanked by a pair of subsidiary cells (shown in brown).

As stomatal behaviour is responsible for the control of not only CO_2 uptake but also the loss of water vapour through transpiration (Farquhar & Sharkey, 1982; Miner *et al.*, 2017), stomatal conductance - or g_s - (the rate of gas diffusion across the pore, see Figure 1.3) is indicative of the rate of photosynthesis and also of crop water use (Vialet-Chabrand *et al.*, 2017; Lawson & Vialet-Chabrand, 2019). Stomatal density, size, distribution and pore area are responsible for determining resistance to gas diffusion and therefore g_s (Dow *et al.*, 2014; Vialet-Chabrand *et al.*, 2017; Faralli *et al.*, 2019a). Whilst a high g_s is linked with higher rates of CO_2 assimilation (A), it is also associated with an increase in the loss of water vapour. As such there is a delicate balance between CO_2 uptake and water losses in order that an appropriate leaf water status is maintained (Matthews *et al.*, 2017). Stomatal conductance, therefore, has a direct impact upon the water use efficiency (WUE), or the 'crop per drop' of plants. At a leaf level, the ratio between photosynthesis and water vapour loss through stomata (A/g_s) is defined as the intrinsic water use efficiency (iWUE) (Flexas *et al.*, 2016; Lawson & Vialet-Chabrand, 2019). Crops with a higher WUE require less water to produce the same yield, and are more resilient to drought conditions (Condon *et al.*, 2004; Faralli *et al.*, 2019a). When water is not limiting, it has been shown that there is a strong positive correlation between the rate of g_s and grain yield in wheat (Fischer *et al.*, 1998; Evans, 2013), however, it has also been observed that a reduced g_s in wheat has a positive impact upon iWUE (Dunn *et al.*, 2019).

1.2.3. Mesophyll limitations of photosynthesis.

In addition to stomatal limitations affecting the availability of CO_2 for carboxylation at chloroplasts, the diffusion of CO_2 inside the leaf is subject to several 'barriers' (Flexas *et al.*, 2012). Mesophyll conductance (g_m) - the inverse of the resistance to CO_2 diffusion through the leaf mesophyll (Flexas *et al.*, 2008)(see Figure 1.3) - has until fairly recently been comparatively under-investigated, despite the potentially large limitations it can have upon rates of photosynthesis (Griffiths & Helliker, 2013). Previous studies have shown that g_m is positively correlated with carbon assimilation in several species (Flexas *et al.*, 2008; Niinemets *et al.*, 2009), including hexaploid wheat (Jahan *et al.*, 2014; Barbour *et al.*, 2016). Mesophyll conductance has been observed to be positively correlated with g_s (Buckley & Warren, 2014; Tholen *et al.*, 2014) (although not in wheat (Jahan *et al.*, 2014; Barbour *et al.*, 2016)), and it has been established that both stomatal and mesophyll resistances may limit photosynthesis to a similar degree (Niinemets *et al.*, 2009; Terashima *et al.*, 2011). It has also been demonstrated that g_m can respond to environmental conditions in a plastic manner, for example to changes in CO_2 concentration, water availability and light intensity (Flexas *et al.*, 2008; Terashima *et al.*, 2011).

The arrangement of cells in the leaf mesophyll may also limit CO_2 supply to chloroplasts and, consequently, limit the rate of photosynthesis (Terashima *et al.*, 2011; Tholen *et al.*, 2012; Barbour *et al.*, 2016). Obstacles to diffusion include the intercellular airspace network, area and thickness of exposed cell walls, plasma membranes and the cytoplasm (Kaldenhoff, 2012). The gaseous phase of diffusion (through leaf airspaces) has been hypothesised to limit diffusion to a lower extent than the liquid phase (cellular components) (Evans *et al.*, 2009; Tomas *et al.*, 2013; Buckley, 2015), with the major influences on gas flux being the amount of surface area of mesophyll cells exposed to intercellular airspaces, S_{mes} (and subsequently the exposed chloroplast surface area, S_c) (Sage & Sage, 2009; Terashima *et al.*, 2011; Tholen *et al.*, 2012; Ren *et al.*, 2019). These anatomical characteristics of the mesophyll are also known to impact upon leaf water transport (Ren *et al.*, 2019). Nevertheless, g_m is not entirely determined by leaf structure, and is also influenced by the

action of aquaporins and carbonic anhydrases (Evans *et al.*, 2009; Buckley & Warren, 2014). Since it has obvious implications for the photosynthetic rate of plants, modifying g_m has been suggested as an alternative to altering g_s as a method for improving crop WUE (Flexas *et al.*, 2013; 2016; Flexas, 2016).

Despite their potential role in influencing gas diffusion for photosynthesis, the regulation of intercellular airspace formation in the leaf mesophyll is not well understood (Ishizaki, 2015). Since plant cell walls divide by establishing an internal cell wall, mother and daughter cells are adhered to one another, so intercellular airspaces must be formed post-cell division (Smith, 2001). Whilst airspaces can be formed by lysigeny (cell breakdown) or expansigeny (cell expansion), in many leaves it is thought that they are formed as the result of schizogeny – the partial separation of cells following the localised degradation of primary cell wall components by enzymes (Jeffree *et al.*, 1986; Jarvis *et al.*, 2003; Ishizaki, 2015). In order to ensure the correct localisation and size of airspaces are formed, the cell separation process is thought to be highly controlled and occurs at cell junctions (Knox, 1992; Ishizaki, 2015). In order to constrain separation, cell walls at the corners of airspaces are thought to be reinforced (Willats *et al.*, 2001; Jarvis *et al.*, 2003). In wheat, the cytoskeleton has also been hypothesised to play a key role in the formation of intercellular airspaces (Panteris & Galatis, 2005; Giannoutsou *et al.*, 2013). Localised rings of microtubules and resultant cellulose microfibril deposition act to define areas of restricted cell growth, whilst intervening regions are still able to expand. This has been suggested to be followed by the schizogenous formation of intercellular airspaces at the sites where cell expansion is constricted, implying that the mesophyll airspace network in wheat is formed via a combination of expansigeny and schizogeny (Panteris & Galatis, 2005; Giannoutsou *et al.*, 2013).

1.2.4. Measuring leaf gas exchange

The exchange of CO_2 and H_2O is required for photosynthetic function. These leaf gas exchange parameters can be quantified *in vivo* using an infra-red gas analysis system (IRGA) (Long & Bernacchi, 2003; Johnson & Murchie, 2011). In these systems, a leaf is clamped into an airtight cuvette sealed with foam gaskets without the need for it to be removed from the plant. Whilst not a direct measure of leaf gas exchange, comparison of CO_2 and water vapour concentrations (as determined by differences in absorbance in the infra-red) between a sample cell and an empty reference cell, alongside a measure of the flow rate of gas through the leaf chamber (Figure 1.5), allows for the calculation of the CO_2 assimilation rate (A – indicative of photosynthetic rate) per unit area of leaf (Busch, 2018). Further physiological parameters can also be obtained using these instruments including C_i (leaf internal CO_2 concentration) and g_s (derived from the transpiration rate) (Johnson & Murchie, 2011; Evans & Santiago, 2014; Busch, 2018), and relationships between CO_2 assimilation and the biochemical components of photosynthesis can be elucidated using the well-established model of photosynthesis created by Farqhuar, von Caemmerer and Berry (Farquhar *et al.*, 1980).

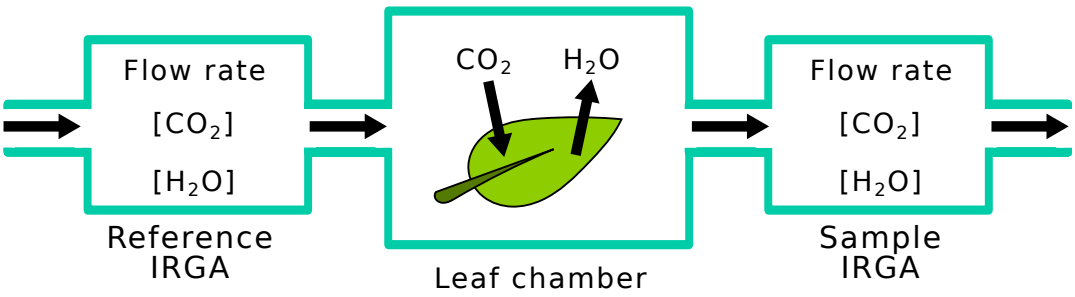

Figure 1.5. IRGAs can be used to measure leaf gas exchange
A simplified schematic of a typical open infra-red gas exchange analysis (IRGA) system. Comparisons of CO_2 and H_2O concentrations between reference and sample IRGAs, alongside a measure of flow rate across the chamber, allow for the estimation of leaf-level photosynthetic gas exchange parameters such as A and g_s.

One advantage of using these systems is that they allow users to exert high levels of environmental control and allow for the simple manipulation of parameters influencing leaf physiology and gas exchange, including: incident light (both light quality and intensity),

temperature, humidity and CO_2 concentration. In addition to providing real-time estimates of gas exchange under particular conditions, programmes such as light response and CO_2 response curves can be run, and these allow for the extraction of more in depth datasets and parameters, such as g_m (Bellasio *et al.*, 2015; Sharkey, 2016). Whilst IRGAs are an extremely practical tool for the measurement of CO_2 and water fluxes, calibration issues, gasket leaks and incorrect calculations of leaf area may limit data utility (Johnson & Murchie, 2011), so correct setup and appropriate protocols must be used. Gas exchange analysis has frequently been used to assess the physiological performance of wheat (Araus *et al.*, 1986; Yin *et al.*, 2009; Driever *et al.*, 2014; Dunn *et al.*, 2019). Although there is a large amount of variation depending on experimental conditions, the mean light-saturated A of modern hexaploid wheat lines grown in the field has been shown to range between 20 and 30 µmol m^{-2} s^{-1} under ambient carbon dioxide concentrations (Driever *et al.*, 2014) with g_s in the range of 0.30-0.45 mol m^{-2} s^{-1} in field-grown plants (Gaju *et al.*, 2016).

1.3. Wheat leaf morphology and anatomy

Despite being a major food crop, detailed analyses of wheat leaf structure are comparatively few in number (Dunstone & Evans, 1974; Parker & Ford, 1982; Jellings & Leech, 1984), and it appears that no new studies have investigated the physiological effects of changes in ploidy upon wheat leaf anatomy and morphology in depth since the early 1990s (Pyke *et al.*, 1990). Members of the Triticeae (across each of the ploidy levels) have a similar basic leaf structure (Parker & Ford, 1982). As with other grasses, leaves consist of a proximal sheath and a distal lamina (or leaf blade), and a membrane called the ligule connects these tissues (Kaplan, 2001; Sluis & Hake, 2015; Lewis & Hake, 2016). The lamina of the wheat leaf is flat, narrow, elongated and tapers to a point (Ocheltree *et al.*, 2012; Nelissen *et al.*, 2016). Grass leaf blades have a central midrib and lateral vasculature runs parallel to this (Kaplan, 1973; Sack & Scoffoni, 2013). Grass leaves develop in a basipetal manner, with older, more differentiated cells found towards the tip of the lamina (Lewis & Hake, 2016). Wheat leaves are amphistomatous (Rebetzke *et al.*, 2001), with both adaxial and abaxial surfaces punctuated by stomata, which are

restricted to distinct epidermal cell files within each leaf surface (Hepworth *et al.*, 2018).

Internal leaf anatomy also follows a similar basic arrangement in *Triticum* species across 2n, 4n and 6n ploidy levels (see Figure 1.6). Unlike the stereotypical differentiation of the chlorenchyma tissue into distinct palisade mesophyll and spongy mesophyll layers observed in eudicot leaves, in wheat and its wild relatives there is no clear distinction between these layers (Parker & Ford, 1982; Jellings & Leech, 1984). Mesophyll cells contain a large number of chloroplasts and are the location for the majority of leaf photosynthesis in C_3 plants. In wheat leaves, over 50% of the leaf is comprised of mesophyll cells (Jellings & Leech, 1984; Pyke *et al.*, 1990), and in hexaploid varieties, these have been shown via classical histology techniques to be stereotypically elongated and to have high levels of distinctive lobing (Parker & Ford, 1982; Jellings & Leech, 1984; Jung & Wernicke, 1990). This is hypothesised to increase the available surface area of mesophyll cells for gas exchange (Sage & Sage, 2009). This characteristic lobed appearance is thought to be determined by the action of cytoskeletal components, which manipulate the cell into this shape (Jung & Wernicke, 1990; Jung *et al.*, 1993; Panteris & Galatis, 2005; Giannoutsou *et al.*, 2013). In monocot plants, such as wheat, the mesophyll cells derive from the L2 layer of the shoot apical meristem (SAM). Cells within the SAM are pluripotent, allowing for the differentiation into lateral organs such as leaves (Fleming, 2006; Braybrook & Kuhlemeier, 2010; Byrne, 2012). In the grasses, shoot development occurs in distinct phytomers which consist of a leaf, an axillary meristem and an internode (Pautler *et al.*, 2013).

Despite having the same basic structure, previous comparisons of wheat species of differing levels of ploidy have shown differences in both the frequency of intercellular airspaces and also the area of exposed mesophyll, in addition to altered vascular patterning (Parker & Ford, 1982). It has been previously observed that 6n varieties have generally larger mesophyll cells with a greater number of lobes than their 4n and 2n counterparts (Jellings & Leech, 1984; Pyke *et al.*, 1990), and that mesophyll cell size was negatively related to CO_2 assimilation rates (Dunstone & Evans, 1974). 2n lines have been reported to have higher

photosynthetic rates and rates of stomatal conductance than tetraploid and hexaploid wheats (Austin *et al.*, 1982). When intercellular airspace was compared between ploidy levels, it was determined that diploid *T. urartu* had a higher level of leaf porosity than hexaploid *T. aestivum*. The authors hypothesised that the higher photosynthetic rates displayed by diploid plants may be associated with an increased observed amount of exposed mesophyll surface area (Austin *et al.*, 1982).

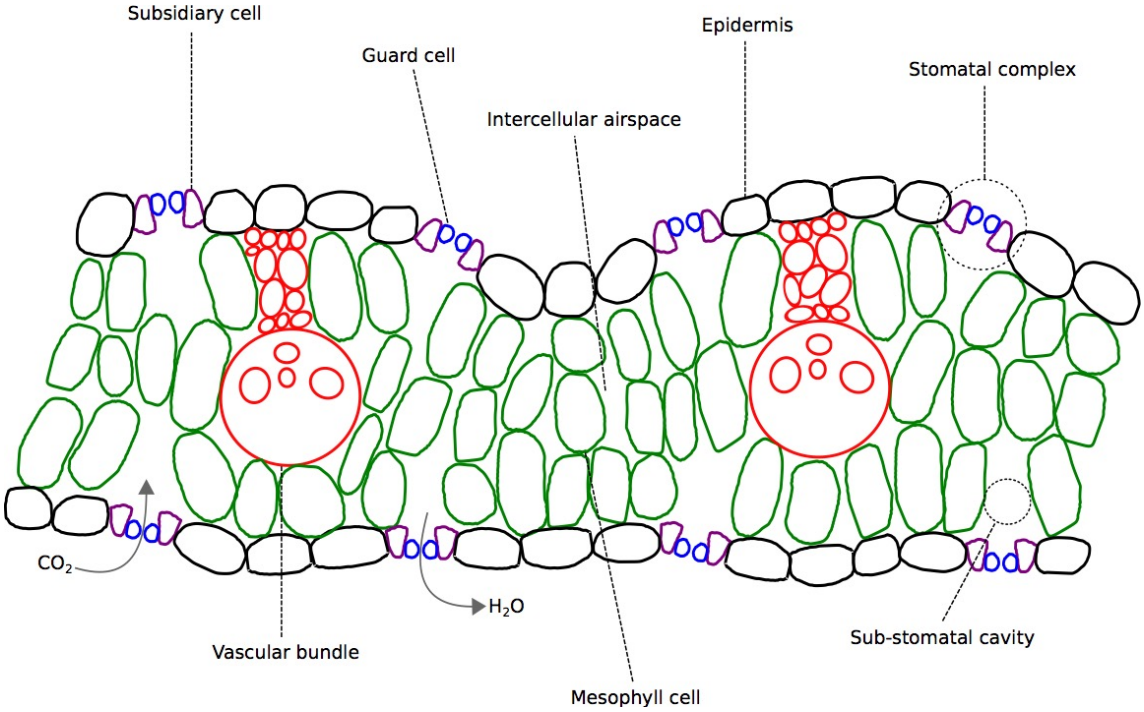

Figure 1.6. The basic arrangement of wheat leaf internal anatomy in transverse section
Unlike eudicots, there is no clear distinction of the mesophyll into palisade and spongy layers. Mesophyll cells (green) are interspersed by a network of intercellular airspaces and leaf vasculature (shown in red) runs parallel to the longitudinal axis. The epidermis (black) is regularly punctuated by stomatal complexes comprising of a pair of guard cells (blue) flanked by subsidiary cells (purple). These allow for the control of the diffusion of CO_2 into and water vapour out of the leaf.

It is therefore apparent that a greater understanding of the changes in wheat leaf structure associated with its evolution (and concurrent shifts in ploidy) and how this has impacted physiological function is required. Whilst ecophysiologists have often investigated these structure/function relationships (Tosens *et al.*, 2012), observations of how this may relate to leaf development are less common. Furthermore, our comprehension of how leaf structure influences photosynthetic function has previously been limited by an absence of accurate and efficient techniques for measuring the 3D structural parameters associated with mesophyll cells and their associated network of intercellular airspaces. Traditional 2D

histological methods have primarily been used to characterise wheat leaf structural components in the past (Parker & Ford, 1982; Jellings & Leech, 1984), but by their very nature, these techniques do not provide an accurate estimation of the complex 3D features of the internal leaf environment (Théroux-Rancourt *et al.*, 2017). Recent advances in 3D imaging have increased the feasibility of generating appropriate datasets, of which this project takes advantage. For example, the re-appropriation of X-ray micro-computed tomography (X-ray µCT) techniques enables the 3D quantification of leaf airspace (Pajor *et al.*, 2013; Mathers *et al.*, 2018), whilst improved protocols for imaging deep into thick plant tissues using confocal microscopy now allows for the quantification of mesophyll cell geometries in 3D. Previous work carried out by members of my lab has investigated how alterations in leaf internal anatomy affect photosynthetic gas flux (Lehmeier *et al.*, 2017), and also explored the relationships between stomatal function and mesophyll structure (Lundgren *et al.*, 2019).

1.4. Water use efficiency is an important breeding target

With climate change being predicted to influence water availability via increased frequency of droughts (Lobell *et al.*, 2011; Wheeler & Von Braun, 2013), and increasing global populations (estimated to reach between nine and ten billion by 2050) placing more pressure on reserves, it will be essential to improve crop drought tolerance. At the same time, the potentially conflicting aim of improving crop yield in order to meet increased future demand (with demand for cereals such as wheat potentially doubling) is also of great importance (Godfray *et al.*, 2010; Hawkesford *et al.*, 2013; Long *et al.*, 2015). Wheat yields have increased steadily since the Green Revolution of the 1960s, but yield increases are beginning to stagnate, and as such there is a growing need to identify methods by which wheat production can be maintained or increased (Ray *et al.*, 2012; 2013). As such, improved crop WUE has been suggested as one agronomic trait which may help to reduce yield losses resulting from drought events (Bertolino *et al.*, 2019; Leakey *et al.*, 2019). Further understanding of the relationship of wheat leaf structure to photosynthetic function and crop water-use is therefore of utmost importance to future wheat breeding programmes. One aspect that has

been under-explored is how the ploidy changes associated with the evolution of modern bread wheat from wild ancestors has impacted these aspects of leaf function. The research reported in this thesis addresses this fundamental problem in plant biology.

1.5. Aims and objectives

The overarching aim of this project was to increase our understanding of how leaf structure in wheat and its wild relatives influences photosynthetic function. The aims can be listed as follows:

1) To characterise the relationships between stomatal patterning, size and leaf gas exchange in a range of wild and domesticated wheat lines of varying ploidy levels.

2) Elucidate the relationships between mesophyll porosity and physiological function in the leaves of wheat and its wild relatives.

3) Explore the changes in cell size and shape that have occurred during the evolution of modern hexaploid bread wheat from tetraploid and diploid ancestors, and how this may influence leaf function.

To achieve these aims, the following objectives were pursued:

1) A screen of stomatal morphology, basic leaf structure and steady state measurements of leaf gas exchange parameters using an infra-red gas analysis (IRGA) system was conducted on a wide range of Triticeae varieties, including lines from 2n, 4n and 6n species.

2) An X-ray µCT technique was used to characterise differences in the amount of leaf airspace associated with the changes in ploidy level that have accompanied the evolution of modern bread wheat, and the effect of leaf structure upon physiological function was subject to further analysis.

3) A confocal microscopy technique for the 3D imaging of mesophyll cell geometry was developed. Using this, the changes in wheat mesophyll cell size and shape associated with changing ploidy levels during the evolution of modern wheat, and the impacts of this upon leaf function were investigated.

Chapter 2. Changes in ploidy level affect stomata and leaf gas exchange in the Triticeae

2.1. Introduction

Wheat leaf function requires the gaseous exchange of CO_2 from the atmosphere to the chloroplasts of mesophyll cells, where it is fixed into carbohydrate. In order to enable this flux of CO_2 entry and water vapour loss, the leaf surface is punctuated with pores named stomata, which are responsible for controlling the flow of carbon and water. Clearly the arrangement and anatomical characteristics of these pores can directly influence leaf gas exchange and physiology. The extent to which these parameters vary according to ploidy level in wheat, and the impact this has on photosynthetic gas exchange, in particular water use efficiency, is analysed in this chapter.

2.1.1. Stomatal size and stomatal density are associated with ploidy level

It has long been suggested that polyploidy in angiosperms results in an increased guard cell length/stomatal size in plants with a higher ploidy level (Sax & Sax, 1937, Masterson, 1994; Beaulieu *et al.*, 2008). This has been shown to be the case for many dicots, trees and shrubs (Beaulieu *et al.*, 2008), including crop species such as banana (Vandenhout *et al.*, 1995), coffee (Mishra, 1997) and cannabis (Parsons *et al.*, 2019). This phenomenon has also been shown in monocots (Beaulieu *et al.*, 2008), including *Aegilops* (Aryavand *et al.*, 2003) and barley (Borrino & Powell, 1988) and several studies have indicated that there are differences in stomatal density and stomatal size between ploidy levels in wheat species (Austin *et al.*, 1982; Wang & Clarke, 1993; Maosong *et al.*, 2008; Khazaei *et al.*, 2010).

Previous investigations have shown that there is a negative correlation between stomatal size and stomatal density, with smaller stomata generally present at a higher frequency per leaf area than larger stomata (Beaulieu *et al.*, 2008; Franks *et al.*, 2009). In the Triticeae, diploid species have been shown to have a higher stomatal density than tetraploid and

hexaploid lines (Austin *et al.*, 1982). The frequency of stomata was also shown to be increased in tetraploid genotypes in comparison to hexaploid cultivars (Austin *et al.*, 1982; Wang & Clarke, 1993; Khazaei *et al.*, 2010). These previous studies have also indicated that hexaploid wheat stomata are larger than their tetraploid and diploid counterparts, and that diploid guard cells are the shortest, with the stomata found on tetraploid plants having intermediate stomatal size (Wang & Clarke, 1993; Khazaei *et al.*, 2010).

2.1.2. Other leaf structural parameters are also affected by ploidy level

In addition to wheat, many other domesticated crop species - including cotton and potato - are polyploids (Meyer *et al.*, 2012; Renny-Byfield & Wendel, 2014; Salman-Minkov *et al.*, 2016), and it has been suggested that an increase in ploidy leads to increases in cell (Kondorosi *et al.*, 2000; Katagiri *et al.*, 2016) and organ size, including increased seed/grain size (Dubcovsky & Dvorak, 2007; Hughes *et al.*, 2019) and leaf size (Milla & Matesanz, 2017; Zhang *et al.*, 2019), and this has been observed previously in wheat (Dunstone & Evans, 1974). Final organ size is determined by cell size and number (Mizukami, 2001; Zhang *et al.*, 2019). However, evidence from Arabidopsis suggests that this relationship may not be as simple as theorised, and that increases in cell volume are not necessarily a direct response to genome duplication (Tsukaya, 2013).

With respect to wheat, it has previously been observed that diploid members of the Triticeae have narrower leaves than their tetraploid and hexaploid counterparts (Austin *et al.*, 1982). It has been suggested that this results in the genesis of alternative arrangements of leaf vasculature, such as differing vein densities and interveinal distance. Additionally, it would also be expected that the internal architecture of the leaf – the arrangement of mesophyll cells and intercellular airspaces – would also show the effects of ploidy (Austin *et al.*, 1982; Parker & Ford, 1982). This aspect of ploidy on organ structure, and how it may impact photosynthesis and water use, has been less well investigated and is the focus of work described later in this thesis (see Chapters 3 and 4).

2.1.3. What effect does variation in stomatal size and density have upon leaf level gas exchange?

As indicated above, stomata are the access point for leaf gas exchange and, when open, allow CO_2 into the leaf and the egress of water vapour. As such, stomatal density and stomatal size can have a significant impact on both water use and photosynthesis (Franks & Beerling, 2009; Dow *et al.*, 2014; Lawson & Blatt, 2014). A higher stomatal conductance positively impacts the rate of CO_2 assimilation, but does come with the trade-off of a reduction in the water use efficiency of the plant (Lawson & Blatt, 2014). When water is not limiting, g_s can display a strong positive correlation with grain yield, as has been observed in winter wheat (Fischer *et al.*, 1998; Evans, 2013).

With respect to wheat, Austin *et al.* (1982) reported that diploid species had a higher maximum photosynthetic rate than tetraploid and hexaploid wheats, in addition to also having a higher rate of stomatal conductance. This may be partly explained by the higher frequency of stomata found on diploid leaves. Conversely, the opposite pattern has also been noted in both well-watered and droughted lines, with g_s in hexaploid lines shown to be larger than in diploid plants, with tetraploid plants showing intermediate rates of stomatal conductance (Xiong *et al.*, 2006).

This relationship between stomatal density and conductance can be further investigated by the analysis of mutant plants with greater or fewer stomata than the wild type, generated by changing the expression of genes encoding regulators of stomatal formation. This allows the physiological responses to altered stomatal frequency to be investigated. For example, several studies have shown that over-expression of genes encoding *EPIDERMAL PATTERNING FACTOR1* (*EPF1*) and *EPF2* in Arabidopsis results in plants with a lower stomatal density and, consequently, reduced stomatal conductance (Doheny-Adams *et al.*, 2012; Franks *et al.*, 2015; Hepworth *et al.*, 2015). Similar phenotypes have been observed in crop plants such as barley (Hughes *et al.*, 2017) and rice (Caine *et al.*, 2019; Mohammed *et al.*, 2019). Recently, colleagues have manipulated *EPF* expression in wheat, again showing that overexpression of this peptide results in both reduced stomatal density and conductance relative to control non-transformed plants (Dunn *et al.*, 2019). Conversely,

manipulating an increase in the frequency of stomata via overexpression of *STOMAGEN/EPFL9* (a positive regulator of stomatal development) led to a corresponding increase in stomatal conductance under ambient CO_2 concentrations in Arabidopsis (Doheny-Adams *et al.*, 2012; Tanaka *et al.*, 2013).

In addition to stomatal density, stomatal size can also impact upon gas exchange. Larger stomata have a greater aperture area and respond at a slower rate than smaller stomata to triggers for opening/closing (Drake *et al.*, 2013; Lawson & Blatt, 2014). It is therefore apparent that density and size work in tandem to determine stomatal conductance. As a result, it is possible to estimate the potential maximum rate of g_s using these characteristics. This parameter is termed the anatomical g_{smax} (Dow *et al.*, 2014; McElwain *et al.*, 2015; de Boer *et al.*, 2016).

In addition to controlling CO_2 uptake, stomata are also responsible for balancing this against water loss and as such g_s is an important parameter determining crop water use. Improving the water use efficiency, or 'crop per drop', of a crop is of utmost importance and is thus a vital breeding target in the future (Bertolino *et al.*, 2019; Leakey *et al.*, 2019). For example, it has been shown that manipulation of stomatal density using the transgenic approaches described above has a direct impact on crop WUE (Hughes *et al.*, 2017; Caine *et al.*, 2019; Dunn *et al.*, 2019). Plants with a higher WUE require less water to produce similar yields, and are more drought tolerant than those with a lower WUE (Farquhar & Sharkey, 1982; Condon *et al.*, 2004; Lawson & Vialet-Chabrand, 2019).

Variation in stomatal conductance has been associated with variation in iWUE (A/g_s) of cultivars in soybean (Gilbert *et al.*, 2011) and investigated in rice cultivars (Hubbart *et al.*, 2007; Xiong *et al.*, 2016). With respect to wheat, it has previously been shown that domesticated lines display a relatively large amount variation in g_s (Rebetzke *et al.*, 2001; Condon *et al.*, 2007; Sadras *et al.*, 2012), although stomatal size and density was only measured in one of the studies (Sadras *et al.*, 2012). Stomatal conductance was shown to correlate with yield when measured for a range of wheat cultivars under well-watered field conditions (Fischer *et al.*, 1998), but anatomical parameters of stomata were not recorded in these lines.

Variation for other photosynthetic parameters, including CO_2 assimilation, has also been investigated in modern *T. aestivum* lines (Driever *et al.*, 2014; Gaju *et al.*, 2014), and the WUE of a range of wheat lines has also previously been investigated (Farquhar & Richards, 1984). Other studies have also explored variation in g_s and iWUE in a narrower range of wheat lines (Jahan *et al.*, 2014; Barbour *et al.*, 2016; Wang *et al.*, 2015; Ouyang *et al.*, 2017; Faralli *et al.*, 2019b).

In the first of these studies (Jahan *et al.*, 2014), the authors found variation in both g_s and water-use efficiency across nine genotypes. They suggested that increasing leaf age had a negative effect on g_s but did not investigate leaf structure. Barbour *et al.* (2016), found that there was a large amount of variation in g_s and iWUE within a mapping population of *T. aestivum* and their parent lines, but again did not carry out analyses of stomatal density or size to try to explain these differences. Wang *et al.*, 2015, focused more on the genetic basis of stomatal conductance and related photosynthetic traits, and also investigated the effect of drought stress, finding variation in g_s for 150 doubled haploid lines. Ouyang *et al.* (2017) primarily focused on rice but included two wheat lines in their study and found that these had different rates of stomatal conductance associated with changes in stomatal density. Faralli *et al.* (2019b) observed significant variation in stomatal density in a panel of eight varieties of hexaploid winter wheat, and also found that this was positively correlated with the speed of stomatal opening and had knock-on effects on iWUE.

As water becomes a scarcer resource in the 21st century, improving the WUE of crop plants, such as wheat, in order to maintain yields to meet future demand has been identified as a major agronomic aim (Bertolino *et al.*, 2019; Leakey *et al.*, 2019). As such, a better understanding of the mechanisms underpinning the impact of variation in leaf structure and stomata on gas exchange will be of great importance for future breeding programmes.

2.1.4. Aims

In this chapter I aim to determine whether the distribution and size of stomata vary with ploidy level for a wide range of accessions of the Triticeae. This analysis was extended to include a range of other leaf structural parameters, including epidermal cell size and leaf size, as well as other characteristics contributing to gross structure, such as the leaf vasculature. These data form the foundation for investigations (reported in subsequent chapters) into whether leaf structural variation in wheat linked to ploidy level influences leaf-level photosynthetic gas exchange.

2.2. Methods

2.2.1. Plant material and growth conditions

Seeds of 26 wild and domestic wheat lines (shown in Table 2.1) of various ploidy levels (diploid, tetraploid and hexaploid), were sown in module trays containing a mixture of 6:1 Levington M3 compost (ICL, Suffolk, UK): perlite (Sinclair Pro, Cheshire, UK) and placed into a controlled environment growth chamber (Conviron PGR15; Conviron, Winnipeg, MB, Canada) in the Sir David Read Controlled Environment Facility (University of Sheffield, Sheffield, UK). All *T. aestivum* and *T. durum* cultivars were provided by RAGT Seeds (Ickleton, Cambs, UK). All other lines were taken from the stocks of Prof. Colin Osborne (The University of Sheffield, Sheffield, UK). The environmental conditions in the chamber were as follows: air temperature = 21˚C:16˚C, 16h light = 400 µmol $m^{-2}s^{-1}$ at bench level (425 µmol $m^{-2}s^{-1}$ at the top of the canopy), 8h dark, 60% relative humidity. After initial screens of stomatal density, A and g_s, a smaller subset of 11 lines was selected for further analysis (Table 2.2).

After germination, seedlings were transplanted into 1 litre pots containing the same compost mixture. Five grams of Osmocote Exact 5-6 slow release fertiliser (ICL, Suffolk, UK) was added to each pot and mixed into the top layer of compost.

Table 2.1. A list of the Triticeae genotypes used in this study

Ploidy level	Species name	Domestication status	Cultivar /accession no.
2n	*Triticum baeoticum*	Wild	TRI 18344
2n	*Triticum baeoticum*	Wild	TRI 19028
2n	*Triticum urartu*	Wild	TRI 6735
2n	*Triticum urartu*	Wild	TRI 17128
2n	*Triticum monococcum*	Domesticated	TRI 28870
4n	*Triticum araraticum*	Wild	TRI 18513
4n	*Triticum araraticum*	Wild	TRI 16599
4n	*Triticum dicoccoides*	Wild	TRI 18505
4n	*Triticum dicoccoides*	Wild	TRI 18530
4n	*Triticum dicoccon*	Domesticated	TRI 16877
4n	*Triticum durum*	Domesticated	Anvergur
4n	*Triticum durum*	Domesticated	Aventadur
4n	*Triticum durum*	Domesticated	Surmesur
4n	*Triticum durum*	Domesticated	Voilur
6n	*Triticum aestivum*	Domesticated	Cashel
6n	*Triticum aestivum*	Domesticated	Conqueror
6n	*Triticum aestivum*	Domesticated	Conversion
6n	*Triticum aestivum*	Domesticated	Cougar
6n	*Triticum aestivum*	Domesticated	Crusoe
6n	*Triticum aestivum*	Domesticated	Gallant
6n	*Triticum aestivum*	Domesticated	Sacramento
6n	*Triticum aestivum*	Domesticated	Scout
6n	*Triticum aestivum*	Domesticated	Shamrock
6n	*Triticum aestivum*	Domesticated	Shango
6n	*Triticum aestivum*	Domesticated	Skyfall
6n	*Triticum aestivum*	Domesticated	Stigg

Table 2.2. The subset of 11 *Triticum* lines selected for further analysis

Ploidy level	Species name	Domestication status	Cultivar /accession no.
2n	*Triticum baeoticum*	Wild	TRI 18344
2n	*Triticum urartu*	Wild	TRI 6735
2n	*Triticum monococcum*	Domesticated	TRI 28870
4n	*Triticum araraticum*	Wild	TRI 18513
4n	*Triticum dicoccoides*	Wild	TRI 18505
4n	*Triticum dicoccon*	Domesticated	TRI 16877
4n	*Triticum durum*	Domesticated	Anvergur
4n	*Triticum durum*	Domesticated	Voilur
6n	*Triticum aestivum*	Domesticated	Cougar
6n	*Triticum aestivum*	Domesticated	Crusoe
6n	*Triticum aestivum*	Domesticated	Shango

2.2.2. Stomatal density measurements

Impressions of the leaf epidermis were taken in order to calculate the stomatal density (mm^{-2} of the leaf surface). Dental putty (Coltene Whaledent, Switzerland) was used to generate a negative impression of both the abaxial and adaxial leaf surfaces. The putty was mixed prior to application to the middle third of the lamina, where it was allowed to solidify before removal. This produces a permanent record of the leaf epidermis. From these negative casts, positive impressions of both the adaxial and abaxial epidermis were made via the application of two layers of clear nail varnish. Once these had dried, the nail varnish impressions were peeled off the putty and mounted onto slides under a coverslip.

Counts were carried out via light microscopy (Nikon Labophot; Nikon, Tokyo, Japan). Each stomatal complex within the field of view was counted and the density was scaled up to 1 mm^2. A total of five counts either side of a major vein were made for both epidermises and a mean density was calculated. The abaxial and adaxial values were summed to calculate the total average stomatal density. This was carried out on the fully developed fifth leaf on the main tiller for a total six plants per line.

2.2.3. Stomatal size

Sections of leaf material of around 1 cm^2 were excised from the plant and fixed immediately in 3:1 ethanol: acetic anhydride (v/v) – samples were then vacuum infiltrated for 1 hour before being stored for a minimum of four hours at 4˚C. Next, samples were washed first with a 50% ethanol solution followed by 70% ethanol. If samples were not to be imaged immediately, they were stored in this solution at 4˚C until necessary.

Once required, the sample was treated with chloroform for 10 minutes before undergoing progressive rehydration via stepwise changes in ethanol concentration (first 70%, second 50%) before a final wash in water. The leaf tissue was then submerged in bleach (0.2 M NaOH containing 1% sodium dodecyl sulphate (w/v)) for 15 minutes prior to another rinse with water. If samples were also to be imaged on the confocal, they were next treated with a starch digestion solution (PBS + 0.1% Tween-20 and 0.01% alpha-amylase (Sigma-Aldrich, UK) overnight at 37˚C to remove starch grains. For staining, samples were first treated in 1% (w/v) periodic acid (Sigma-Aldrich, UK) for 40 minutes before being stained with the fluorescent stain pseudo-schiff propidium iodide (0.1 M $Na_2S_20_5$, 0.15 N HCl, 0.01% (w/v) propidium iodide (Sigma-Aldrich, UK)) for a minimum of 4 hours. This coloured the stomata a magenta/pink colour that could still easily be observed on a light microscope. After staining, samples were cleared in a clearing solution made up of 200 g chloral hydrate (Sigma-Aldrich, UK), 20 ml glycerol and 30 ml water before being mounted directly onto microscope slides using a drop of mountant (3 g 20% (v/v) Arabic gum in 10 g chloral hydrate and 1 g glycerol) and covered with a coverslip. Coverslips were sealed using nail varnish.

A total of 10 pictures containing a minimum of three stomata were taken for both the abaxial and adaxial surfaces per leaf sample (Olympus BX51 with DP71 camera; Olympus, Tokyo, Japan). The guard cell length, stomatal complex width, complex area, pore width and pore area were all measured using FIJI (ImageJ) software (Schindelin *et al.*, 2015). Measurements are summarised in Figure 2.1. All samples were imaged within 48 hours of mounting to reduce the likelihood of desiccation, which could result in cell shrinkage, and thus, inaccurate collection of

data. This was repeated for six leaves per line. As with the stomatal density measurements, the fifth leaf on the main tiller was chosen for stomatal size measurements.

2.2.4. Anatomical g_{smax}

For each of the lines for which stomatal size characteristics (Table 2.2) were measured, the anatomical g_{smax} was also estimated using Equation 2.1, taken from Dow *et. al,* (2014; 2017):

Equation 2.1. Anatomical g_{smax}

$$\text{Anatomical } g_{smax} = d \,.\, D \,.\, a_{max} / (v \,.\, (l + (\pi/2) \,.\, \sqrt{(a_{max}/\pi)}))$$

In this equation, d is equivalent to the diffusivity of water in air at 22˚C (m^2s^{-1}), D is stomatal density (mm^{-2}) and a_{max} is mean maximum stomatal pore area (μm^2) – see Figure 2.1. v is the molar volume of air at 22˚C (m^3mol^{-3}), l is pore depth (µm), and π is a mathematical constant (approximated to 3.142). l is assumed to be equivalent to guard cell width at the middle of the stoma. Estimated values were generated for each surface of the leaf and summed to calculate the total anatomical g_{smax}. Values of stomatal density from individual leaves (measured as described in 2.2.2) were used in the equation, whilst mean values for each genotype were used for a_{max} and l.

2.2.5. Epidermal cell size

Alongside stomatal parameters, measurements of epidermal cell size (cell length, cell width and cell length x width) were also made on samples from which stomatal anatomical characteristics were recorded. Samples were again imaged using light microscopy. Epidermal cell length and width were both determined using ImageJ software. Multiplying these two values together gave an estimation of the epidermal cell area.

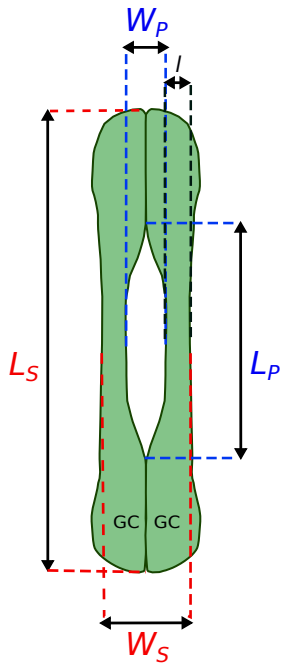

Figure 2.1. Stomatal anatomical characteristics
Ls and *Ws* are equivalent to the length and width of the complex respectively. Stomatal complex area was calculated using the equation: π.½*Ls* . ½*Ws*. Pore area (a_{max}) was measured using the equation: π. ½*Lp* . ½*Wp*, where *Lp* is the pore length and *Wp* the pore width. Guard cell width at the centre of the stoma, *l*, was recorded as a proxy for pore depth. a_{max} and pore depth values are required for the calculation of anatomical g_{smax}.

2.2.6. Leaf sections

In order to measure leaf thickness and vascular characteristics, thin hand sections of the widest part of the fully expanded leaf blade (leaf 5) were cut in the transverse plane - perpendicular to the vasculature - using a razor blade. Sections were then immediately mounted on slides in distilled water and imaged via light microscopy (Olympus BX51 with DP71 camera; Olympus, Tokyo, Japan). Leaf thickness was measured using ImageJ to quantify the distance between the abaxial and adaxial epidermis both at veins and between veins and a mean value was calculated (Figure 2.2). The number of veins per leaf width was also measured to provide an estimate of vein density. In order to measure leaf section width in transverse section, images were stitched together to form a composite of the entire leaf section using the Stitching plugin for ImageJ (Preibisch *et al.*, 2009). Mean interveinal distance was calculated by measuring between two veins (Figure 2.2). This was completed across the entire leaf width and then averaged.

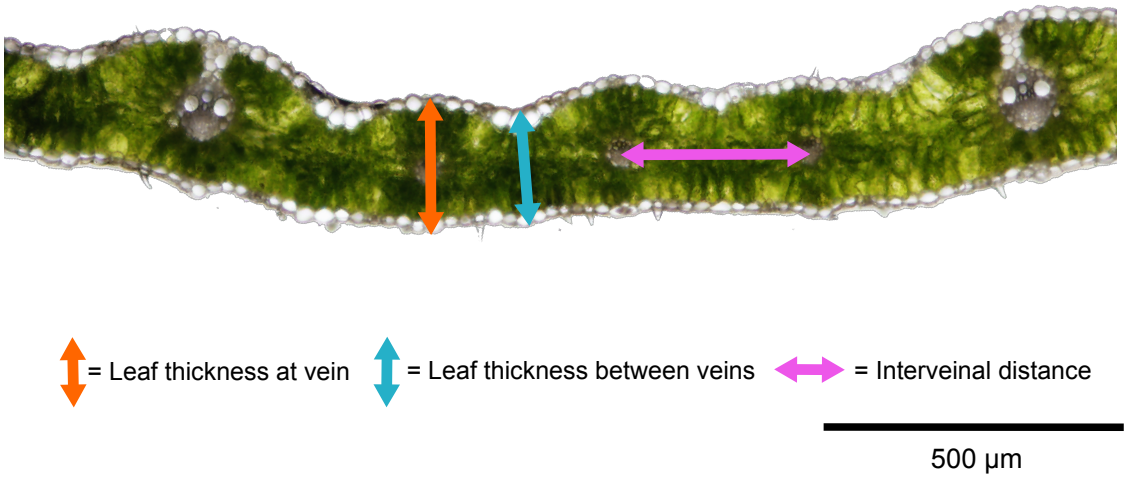

Figure 2.2. Measurements of leaf thickness and interveinal distance
Measurements were made on transverse sections cut by hand. Leaf thickness at and between veins was measured, and mean leaf thickness calculated from these values. Interveinal distance measurements were made between veins along the entire width of the leaf.

2.2.7. Gas exchange analysis – steady state measurements

Steady state IRGA measurements were carried out using a LI-COR 6800 (LI-6800) portable photosynthesis system (LI-COR Biosciences, Lincoln, NE, USA) with the Multiphase Flash Fluorometer (6800-01A) used as a light source. For these gas exchange experiments, the leaf cuvette conditions were set to mirror those of the growth chamber as closely as possible. As such, the temperature exchanger was set at 21˚C and chamber light intensity was set at 425 µmol $m^{-2}s^{-1}$ (90% red, 10% blue). Relative humidity was set at 60% and maintained using Drierite™ (Drierite, OH, USA) as a self-indicating desiccant and Stuttgarter masse (Pall, NY, USA) as a humidifying agent. The reference CO_2 concentration was set at 400 µmol mol^{-1}. 8 g CO_2 cartridges (LISS, Hungary) were used to supply this, and wet soda lime (LI-COR Biosciences, Lincoln, NE, USA) was used to scrub CO_2 as required. Chamber fan speed was set at 10,000 rpm and the flow rate was set at 300 µmol s^{-1}.

All gas exchange analysis measurements were again carried out on the middle third of the newly fully expanded fifth leaf on the main tiller of well-watered plants. This ensured that all plants were measured at the same developmental stage, despite differing rates of growth. The leaf blade was clamped into the IRGA chamber and allowed to acclimate to

chamber conditions for at least 20 minutes – until both A and g_s values were stable. Leaf width was measured, and the value inputted into the console for the calculation of the correct leaf area within the cuvette. Once stable, the AutoLog program was used to log data every 10 seconds for a period of 10 minutes. Prior to the running of each program the reference and sample IRGAs were matched. From datasets generated in this manner, mean A and g_s values over the 10-minute period were calculated. At least six plants per genotype (see Table 2.1) were analysed in this manner. In order to estimate instantaneous water use efficiency (iWUE), assimilation rates were divided by stomatal conductance (A/g_s).

2.2.8. Data analysis

Statistical analyses of the datasets were carried out using GraphPad Prism 8 (Graphpad Software Inc.). Datasets were assessed for normality and significant differences between lines were identified using one-way analysis of variance (ANOVA). When individual lines were compared with each other, significance was determined if P= <0.01. When grouped by ploidy level, significance was determined if P= <0.05. When detected, Tukey's HSD was used as a multiple comparisons test to determine significance in the differences in means between lines (to 99% or 95% confidence respectively). Comparisons between 4n wild and domesticated lines were carried out via the use of an unpaired, two-tailed t test (P= <0.05). All error bars on graphs indicate +/- one standard error of the mean (S.E.M.).

2.3. Results

2.3.1. Ploidy level affects stomatal density

In order to test the hypothesis that there is a link between ploidy level and stomatal frequency, I analysed a series of wheat lines (Table 2.1) with ploidy level varying from 2n to 4n and 6n. As shown in Figure 2.3, a general trend of decreasing stomatal density was observed as ploidy level increased. Statistical analysis (one-way ANOVA followed by a Tukey's multiple comparisons test) indicated that there was significant variation within species and ploidy level ($F_{(25,105)}$= 39.67, P= <0.0001). Details of the

multiple comparisons tests for this figure, and for all subsequent figures presenting data from the full range of accessions in this chapter, are available in Appendix 1. When lines were grouped into their respective ploidy levels (Figure 2.3B), it was found that ploidy has a significant effect upon stomatal density (ANOVA, $F_{(2,23)}$= 87.73, P= <0.0001) with 2n lines having the highest stomatal frequency (a mean of 111.8 stomata mm^{-2}), 4n plants an intermediate stomatal density (78.5 mm^{-2}), and the 6n varieties having the fewest stomata per area (69.7 mm^{-2}). Domesticated 4n lines had a lower number of stomata per area (75.4 mm^{-2}) than the wild members of the 4n ploidy level (82.2 mm^{-2}), but this was not found to differ significantly with domestication status (unpaired t test, $t_{(7)}$= 1.938, P= 0.0938). Example images summarising the observed differences in stomatal density with ploidy level are shown in Figure 2.4A-C.

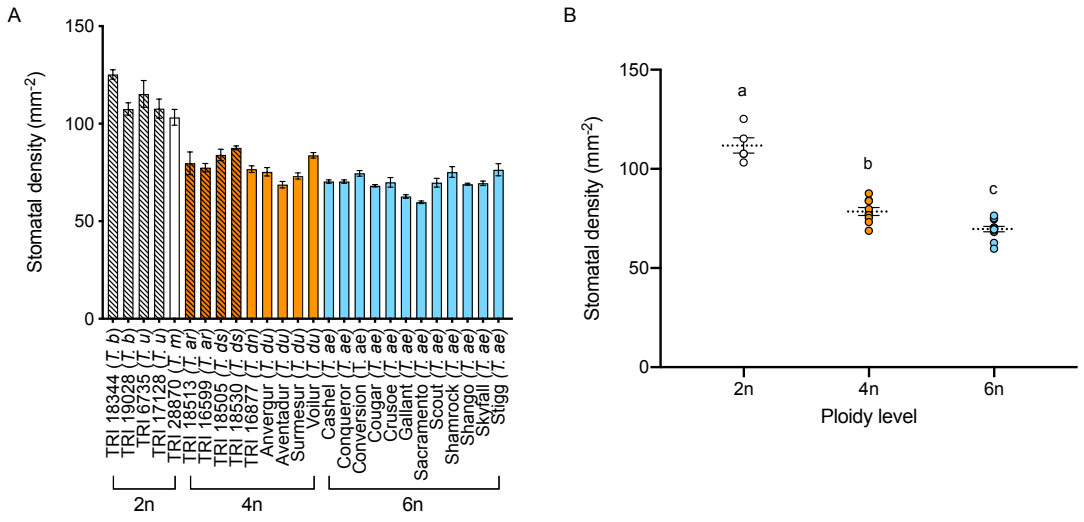

Figure 2.3. There is variation in stomatal density between 2n, 4n and 6n wheat lines
A) Mean stomatal density of a range of *Triticeae* accessions including 2n, 4n and 6n species (as indicated- see Table 2 for key to accession data). Solid bars indicate domesticated cultivars, hatched bars, non-cultivated. B) Mean stomatal density of 2n, 4n and 6n wheat lines, with data grouped from those shown in (A). Samples indicated with the same letter cannot be distinguished from each other (P=<0.05). (Tukey HSD post one-way ANOVA). Error bars = S.E.M. n = minimum of 5 per line.

2.3.2. Increasing ploidy level results in an increase in stomatal size

To investigate to what extent the observed shifts in stomatal density with ploidy level were linked to any change in stomatal size, I performed an analysis of various stomatal dimensions in accessions representing 2n, 4n and 6n wheat lines (highlighted in Table 2.2). These results, shown in Figure 2.5, revealed shifts in aspects of stomatal size linked to changes

in ploidy level. Example images summarising the differences in stomatal size between 2n, 4n and 6n accessions are shown in Figure 2.4D-F. Measurement of guard cell length suggested an increase with increasing ploidy level (Figure 2.5A) and statistical analysis indicated a significant variation with ploidy level (ANOVA, $F_{(10,109)}$= 76.01, P= <0.0001). When grouped by ploidy (Figure 2.5B), guard cell length was shown to differ significantly (ANOVA, $F_{(2,8)}$= 47.98, P= <0.0001) with 6n lines having the longest stomata on average (76.2 µm). The guard cells of 4n lines had an intermediate length (68.8 µm), whilst 2n lines had the shortest guard cells in comparison to the other ploidy levels (56.6 µm). Similarly to stomatal density, it was found that there was no significant effect of domestication status upon guard cell length within the 4n group. (unpaired *t* test, $t_{(3)}$= 0.5396, P= 0.6269). Wild lines had a mean guard cell length of 67.9 µm, whilst this was only slightly higher in cultivated 4n varieties (69.5 µm).

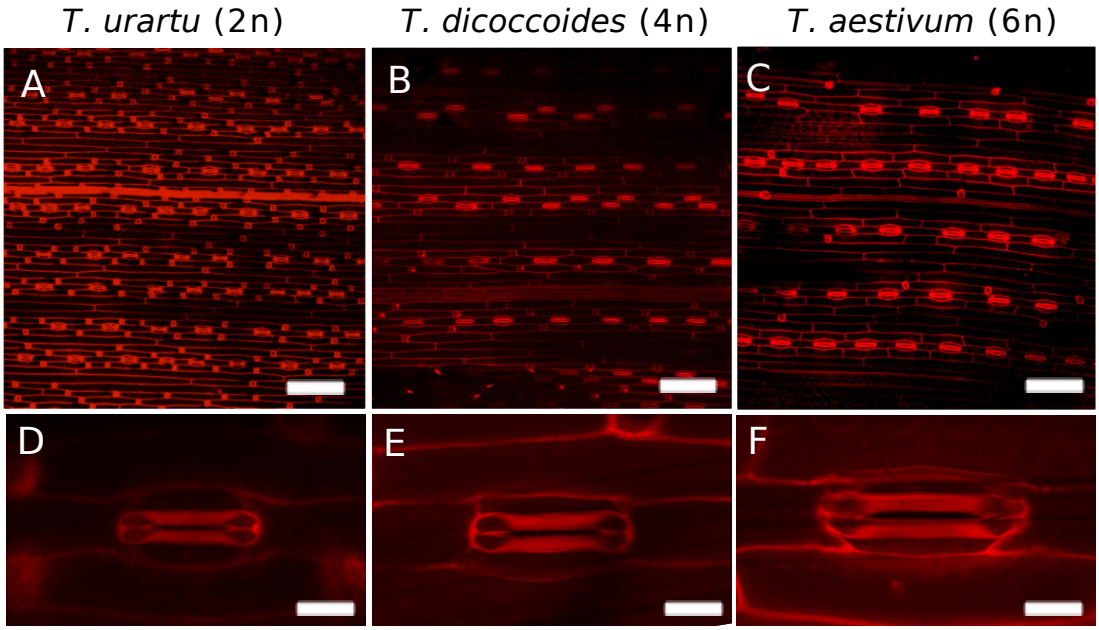

Figure 2.4. Differences is stomatal density and size with ploidy level
There is variation in stomatal density and size between 2n, 4n and 6n wheat lines. **A–C)** Confocal microscopy images of stomatal density of example 2n, 4n and 6n lines. **D–F)** Confocal microscopy images showing the difference in stomatal size between ploidy levels for example 2n, 4n and 6n lines. For (A–C) scale bars = 100 µm; for D–F = 20 µm.

The width of the stomatal complex followed a similar pattern to guard cell length, as shown in Figure 2.5C, with plants of higher ploidy level possessing wider stomatal complexes (ANOVA, $F_{(10,109)}$= 57.25, P= <0.0001). When grouped by ploidy (Figure 2.5D), stomatal width was found to be lowest in 2n genotypes (12.8 µm), middling in the 4n lines (15.3 µm) with

the widest stomata found in 6n cultivars (18.6 µm). These values were shown to be significantly different by one-way ANOVA followed by Tukey's HSD ($F_{(2,8)}$= 93.28, P= <0.0001). Width of stomata was also shown to not be significantly different in 4n wild (15.6 µm) and 4n domesticated (15.2 µm) accessions (unpaired t test, $t_{(3)}$= 0.6245, P= 0.5765).

Consequently (and unsurprisingly), it was also found that there was significant variation in stomatal complex area between genotypes, as shown in Figure 2.5E (ANOVA, $F_{(10,109)}$= 111.5, P= <0.0001). When lines were grouped into their corresponding ploidy level (Figure 2.5F), stomatal complex area was shown to be significantly higher (via one-way ANOVA - $F_{(2,8)}$= 190.3, P= <0.0001) in the 6n varieties (1113.7 µm^2) than the 4n (827.0 µm^2) lines, which were in turn themselves significantly larger than their 2n (569.5 µm^2) counterparts. Once again, domestication was not shown to have a significant effect upon stomatal complex area (unpaired t test, $t_{(3)}$= 0.06033, P= 0.9557), with this value being similar for wild (828.7 µm^2) and domesticated (825.8 µm^2) genotypes.

2.3.3. There is significant variation within the Triticeae for anatomical g_{smax}

Stomatal size and density parameters determine the theoretical anatomical maximum rate of stomatal conductance (g_{smax}). To investigate whether the variation in these parameters (described above) led to a similar variation in theoretical conductance, I analysed g_{smax} for representative 2n, 4n and 6n wheat lines (using Equation 2.1., p26). These data, shown in Figure 2.6A, showed that there was significant variation between lines (ANOVA, $F_{(10,49)}$= 6.854, P= <0.0001). When varieties were grouped together by ploidy level (Figure 2.6B), it found that there was a tendency for decreasing g_{smax} with higher ploidy, ($F_{(2,8)}$= 7.475, P= 0.0148), although it was not possible to distinguish differences between 2n (1.793 mol m^{-2} s^{-1}) and 4n (1.683 mol m^{-2} s^{-1}) groups, or the 4n and 6n (1.453 mol m^{-2} s^{-1}) groups at 95% confidence. However, 2n plants were found to have a significantly higher anatomical g_{smax} than those in the hexaploid group. When differences between wild (1.725 mol m^{-2} s^{-1}) and cultivated (1.656 mol m^{-2} s^{-1}) 4n lines were investigated, it was shown that these were not significantly different from one another (unpaired t test, $t_{(3)}$= 0.5909, P= 0.5962).

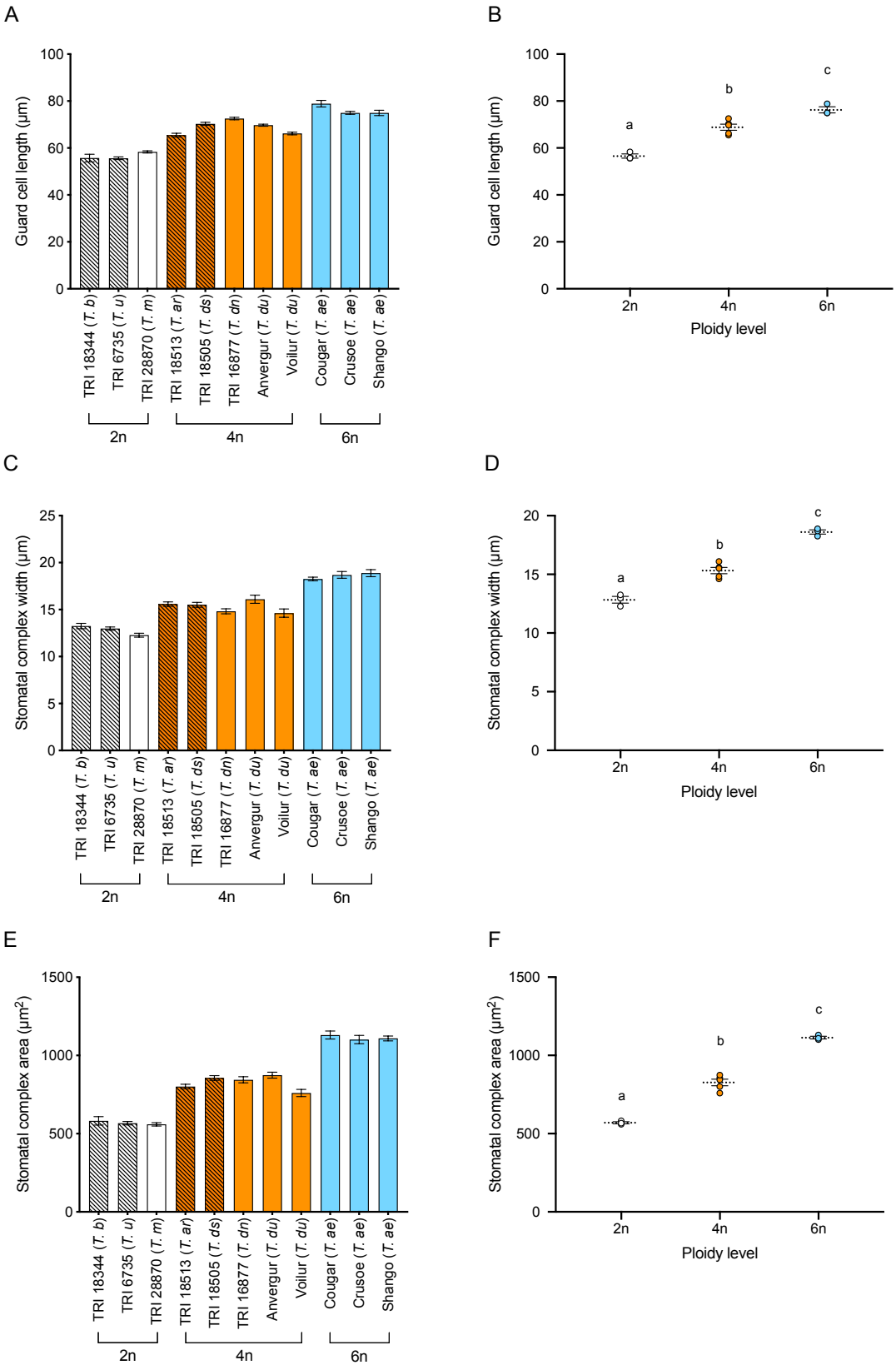

Figure 2.5. There is variation in stomatal size between 2n, 4n and 6n wheat lines
A) Mean guard cell length for lines across the three ploidy levels (2n, 4n, 6n) as indicated. See Table 2 for key to accession data. **B)** Mean guard cell length by ploidy level, data grouped from those shown in (A). **C)** Mean stomatal complex width for each of the lines shown in (A). **D)** Stomatal width grouped by ploidy, as in (B). **E)** Mean stomatal complex area for each of the lines shown in (A). **F)** Mean stomatal area grouped by ploidy level, as in (B). Samples indicated with the same letter cannot be distinguished from each other (P=<0.05). (Tukey HSD post one-way ANOVA). Error bars = S.E.M. n = min of 5 per line.

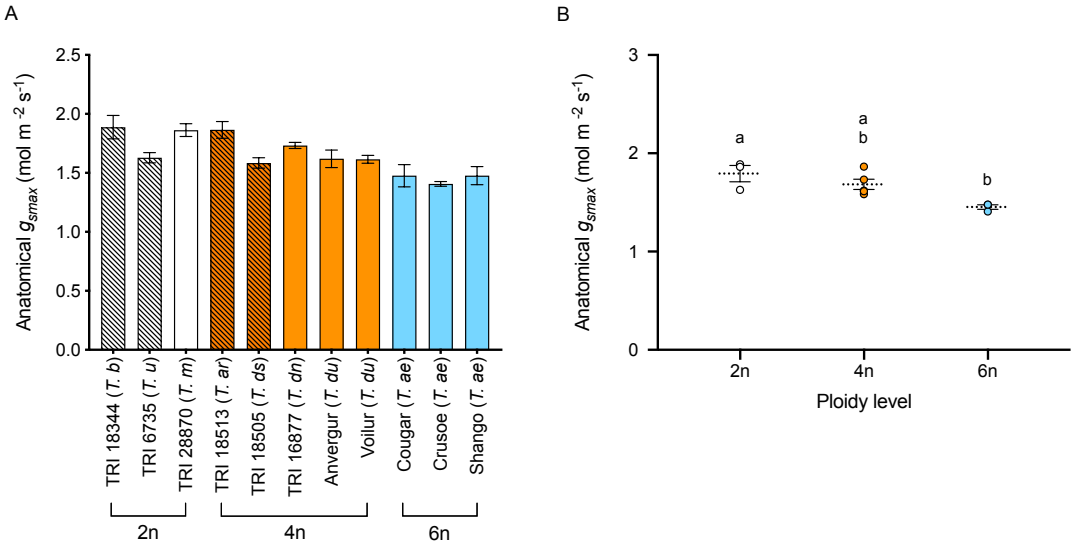

Figure 2.6. Variation in anatomical g_{smax} between 2n, 4n and 6n wheat lines
A) Mean anatomical g_{smax} across all of the genotypes of each ploidy level (2n, 4n, 6n) as indicated. See Table 2 for key to accession data. **B)** When grouped by ploidy level, data grouped from those shown in (A), there are no significant differences in anatomical g_{smax}. Samples indicated with the same letter cannot be distinguished from each other (P=<0.05). (Tukey HSD post one-way ANOVA). Error bars = S.E.M. n = min of 5 per line.

2.3.4. Epidermal cell size changes with ploidy level

Typical of grasses, wheat leaves are constructed from rows of cells along the longitudinal axis so that stomata form in files in which guard cells differentiate in a pattern alternating with epidermal cells that do not undergo stomatal differentiation. To investigate the extent to which the differences in stomatal size in wheat lines of different ploidy level reflected general shifts in epidermal cell size, I analysed epidermal cells in representative 2n, 4n and 6n wheat lines. The results, shown in Figure 2.7A,C,E; indicated that there was significant variation in epidermal cell length (ANOVA, $F_{(10,49)}$= 13.58, P= <0.0001), width (ANOVA, $F_{(10,49)}$= 6.854, P= <0.0001), and area (ANOVA, $F_{(10,49)}$= 23.13, P= <0.0001) amongst the lines. When grouped by ploidy level (Figure 2.7B,D,F), analysis revealed a significant increase in epidermal cell length, width and area as ploidy level increased. Thus, the 2n lines had significantly shorter (179.8 µm) epidermal cells than 4n lines (239.5 µm), which also were shown to be significantly shorter than the hexaploid varieties (270.0 µm) (ANOVA, $F_{(2,8)}$= 145.3, P=<0.0001). When 4n wild and domesticated grouped plants were compared, it was found that domestication did not have a significant effect upon epidermal cell length (unpaired t test, $t_{(3)}$= 0.8908, P= 0.4387). Epidermal cell width was shown to follow a similar trend, with

2n genotypes (23.4 µm) having narrower cells than 6n lines (34.5 µm), with 4n lines (30.3 µm) having intermediate epidermal cell width (ANOVA, $F_{(2,8)}$= 94.44, P=<0.0001). Domestication was not shown to have a significant effect upon epidermal cell width between the 4n wild and domesticated genotypes when grouped (unpaired t test, $t_{(3)}$= 0.1177, P= 0.9137). Consequently, epidermal cell area was found to be significantly higher (ANOVA, $F_{(2,8)}$= 176.0, P=<0.0001) in hexaploid plants (9321 µm^2) than tetraploids (7062 µm^2) and diploids (4207 µm^2). Statistical analysis of the wild and cultivated tetraploid groups showed no significant difference in epidermal cell area with domestication status (unpaired t test, $t_{(3)}$= 0.5958, P= 0.5933).

2.3.5. There is variation in leaf size within the Triticeae

Variation in leaf epidermal cell length and width in a grass leaf suggests that there may be variation in resultant leaf size or, alternatively, if leaf size remains unchanged, that there is an alteration in the number of cells from which a leaf is composed. To investigate these alternatives, I measured leaf size parameters in representative lines for 2n, 4n and 6n wheat lines. Measurements of leaf width (Figure 2.8A) showed that there was significant variation within the lines analysed for this parameter (one-way ANOVA; $F_{(10,59)}$= 62.28, P= <0.0001). The leaves of 2n plants were significantly narrower than those of the domesticated lines (both 4n and 6n). The domesticated tetraploid lines had significantly wider leaves than their wild relatives, and the durum wheat leaves were significantly wider than leaves of the hexaploid Cougar and Crusoe lines, but comparable in width to the hexaploid Shango line. When values were grouped for ploidy level and compared (Figure 2.8B), the mean leaf width was seen to be lower for diploid lines (6.5 mm) than tetraploid (9.4 mm) and hexaploid genotypes (9.7mm). These differences were not statistically significant at the 0.05 confidence limit (ANOVA, $F_{(2,8)}$= 4.145, P= 0.0582), but the relatively large variation observed in the tetraploid lines may have confounded this analysis.

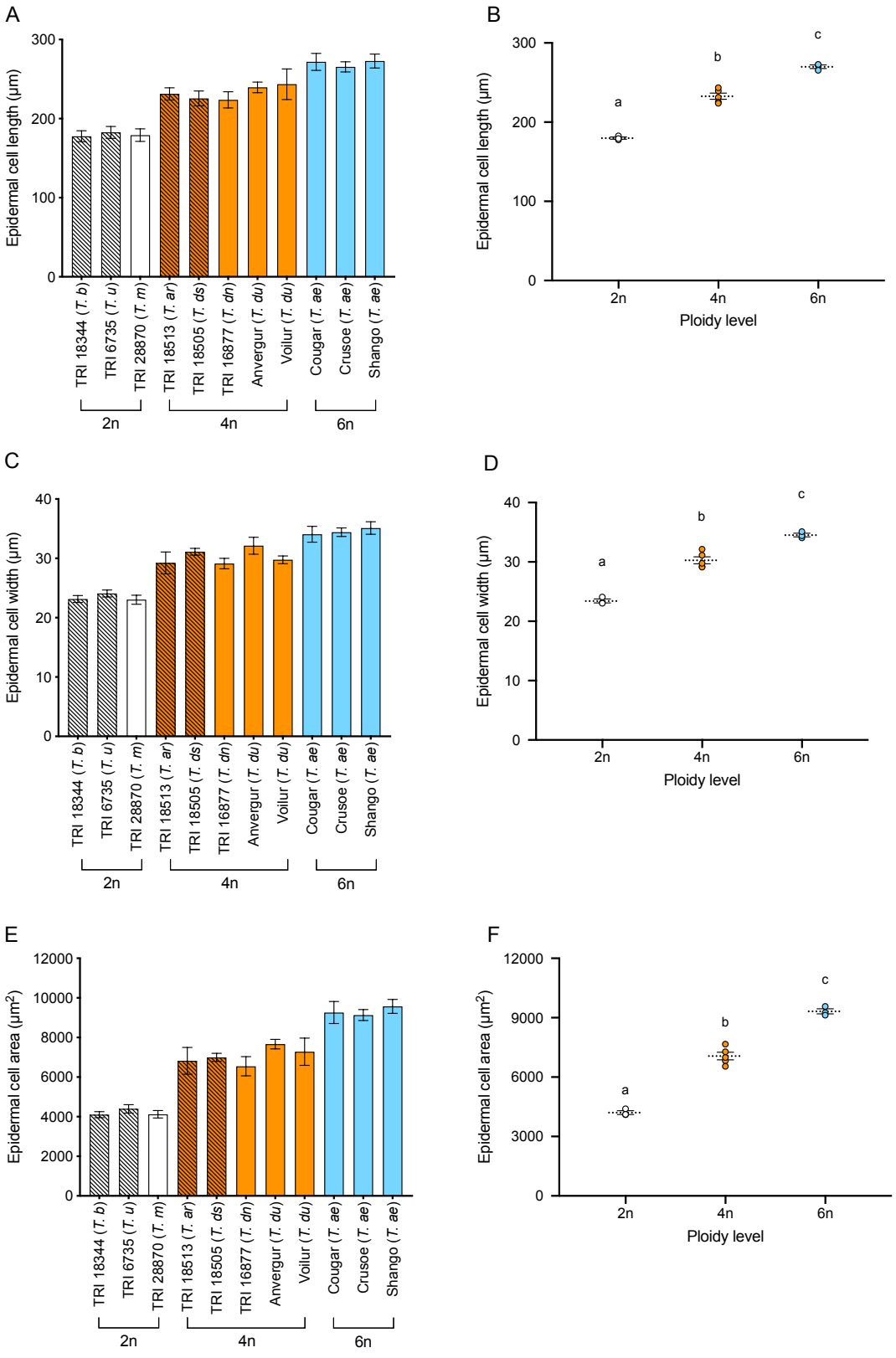

Figure 2.7. Variation in epidermal cell size between 2n, 4n and 6n wheat lines
A) Mean epidermal cell length for lines across the three ploidy levels (2n, 4n, 6n) as indicated. See Table 2 for key to accession data. **B)** Mean epidermal cell length by ploidy level, data grouped from those shown in (A). **C)** Mean epidermal cell width of each of the lines, as in (A). **D)** Mean epidermal cell width when lines grouped into ploidy levels, as in (B). **E)** Mean epidermal cell area of each variety, as in (A). **F)** Epidermal cell area grouped by ploidy, as in (B). Samples indicated with the same letter cannot be distinguished from each other (P=<0.05). (Tukey HSD post one-way ANOVA). Error bars = S.E.M. n = min of 5 per line.

If the tetraploid data were split into wild and domesticated lines, mean leaf width was shown to be narrower in the wild lines (7.3 mm) in comparison to the cultivated varieties *T. dicoccon* and *T. durum* (10.8 mm). This difference was shown to be significant via statistical analysis (unpaired *t* test, $t_{(3)}$= 6.573, *P*= 0.0072), suggesting a significant effect of domestication upon leaf width.

When leaf length measurements were analysed (Figure 2.8C), it was again found that that there was significant variation between genotypes (ANOVA, $F_{(10,59)}$= 19.19, *P*= <0.0001). Leaves of the wild 4n line TRI 18505 (*T. dicoccoides*) and the domesticated 4n TRI 16877 (*T. dicoccon*), were longer than those of 2n and the other tetraploid plants. Both of these lines were longer also than the hexaploid lines Cougar and Shango. TRI 18505 had significantly longer leaves than the domestic wheat line Crusoe, but TRI 16877 did not. Again, similarly to leaf width, when grouped into ploidy levels (Figure 2.8D), the 2n lines had the shortest mean leaf length (272.0 mm), whilst 4n and 6n plants had leaves of similar length (315.3 and 314.2 mm respectively). When analysed via one-way ANOVA, however, it was found that these differences in leaf length with ploidy level were not significant ($F_{(2,8)}$= 1.581, *P*= 0.2638). Unlike leaf width, leaf length was not found to be significantly impacted by domestication status for 4n lines (unpaired *t* test, $t_{(3)}$= 0.05994, *P*= 0.9560), with wild accessions having a mean leaf length of 313.5 mm compared to 316.6 mm in domesticated cultivars.

The combined changes in leaf width and length led to significant shifts in leaf area, as shown in Figure 2.8E,F. A one-way ANOVA followed by a post-hoc Tukey test revealed that 2n lines had a significantly smaller leaf area than the other lines ($F_{(10,59)}$= 45.26, *P*= <0.0001), as did the 4n wild species *T. araraticum* (Figure 2.7E). The 4n accession TRI 18515 (*T. diccocoides*) was not found to have significantly smaller leaves than several of the domesticated lines (Voilur, Cougar and Crusoe). Of the 4n domesticated lines, emmer wheat (TRI 16877), had the largest leaf area whilst area was lowest in the durum wheat variety Voilur. Of the *T. aestivum* lines, Cougar had the smallest mean leaf area, whilst it was greatest in plants of the cultivar Shango. When the grouped leaf area data for each ploidy level was investigated (Figure 2.8F), it was found that leaf

area differed significantly with ploidy level (ANOVA, $F_{(2,8)}$= 5.254, P= 0.0349). 2n lines had the smallest mean leaf area (1761.1 mm^2), whilst mean leaf area for 4n and 6n plants was similar (2959.6 and 3059.9 mm^2 respectively). Leaf area was shown to not be significantly different between 4n wild (2294 mm^2) and domesticated lines (3404 mm^2), despite significant differences in leaf width, although the P value was found to be close to the 95% limit (unpaired t test, $t_{(3)}$= 3.038, P= 0.0560).

2.3.6. There is variation in leaf vascular patterning

Variation in leaf size and constituent epidermal cell size raises the question of whether there is an alteration in the density and distribution of the vascular bundles, which service the cells within the leaf. In wheat leaves, vascular bundles are arranged in longitudinal arrays parallel with the cells files in which the stomata are distributed.

I therefore measured vascular density in representative lines for the 2n, 4n and 6n wheat lines. As shown in Figure 2.9, there is variation in leaf vasculature in the wheat lines analysed. Vein density per mm leaf width (Figure 2.9A) was shown to vary significantly between lines (ANOVA, $F_{(10,53)}$= 29.77, P= <0.0001). When grouped by ploidy level (Figure 2.9B) it was apparent that there was a higher number of veins per mm in the leaves of 2n plants compared to those of the 6n accessions (3.3 mm^{-1} compared to 2.4 mm^{-1}), which were not significantly different from the vein density in 4n lines (2.5 mm^{-1}) (ANOVA, $F_{(2,8)}$= 10.10, P= 0.0065). When the means of the 2n and 4n groups were compared, it was shown via a post-hoc Tukey test that these values were also significantly different from one another at the 95% confidence limit. The tetraploid group was split into wild and domesticated genotypes in order to assess the effect of domestication upon the frequency of veins (2.620 mm^{-1} for wild lines and 2.583 mm^{-1} in domesticated cultivars). It was found that domestication status did not have a significant effect upon the density of vascular bundles (unpaired t test, $t_{(3)}$= 0.1171, P= 0.9142), despite being previously shown to significantly impact leaf width.

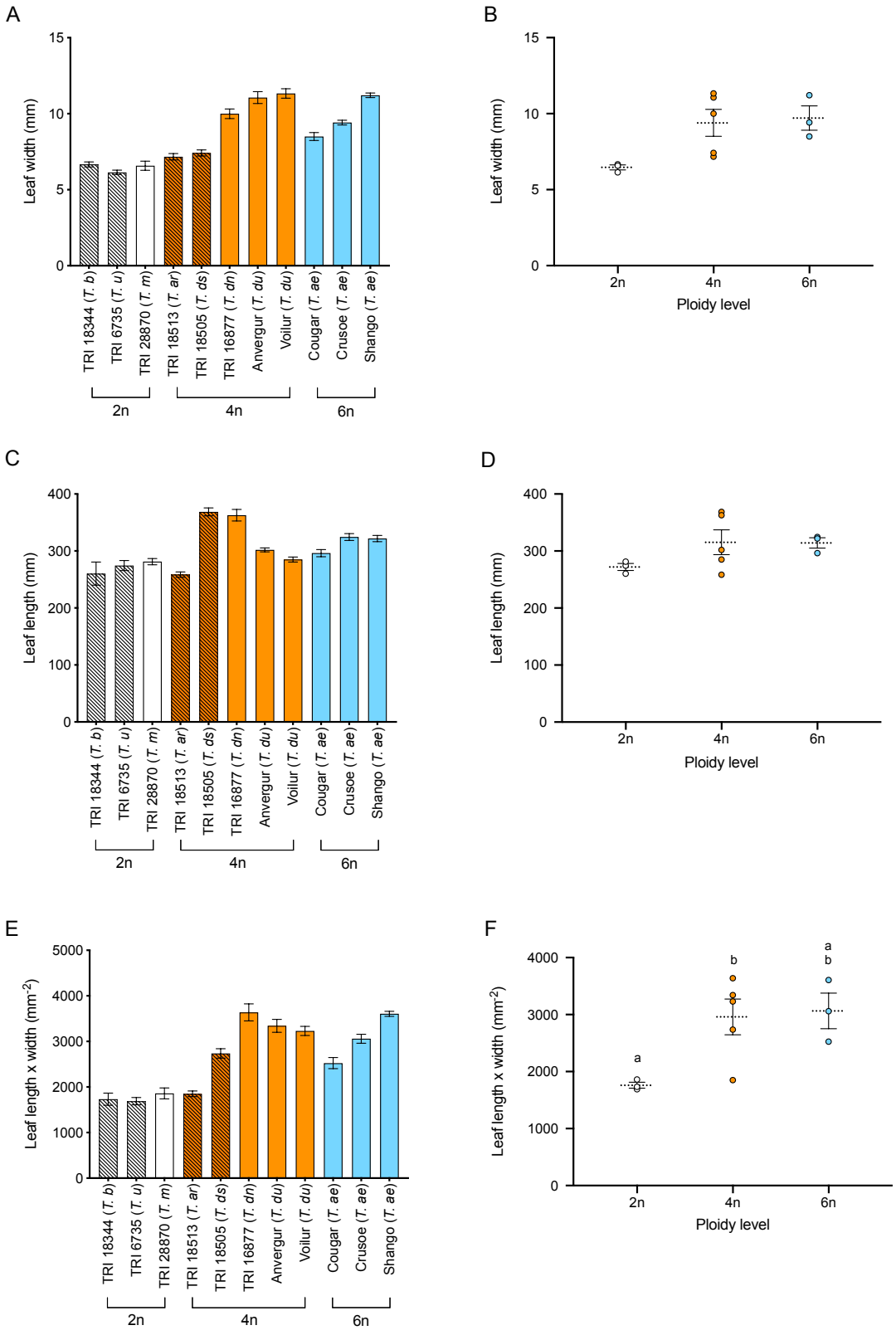

Figure 2.8. There is variation in leaf size between 2n, 4n and 6n wheat lines
A) Mean leaf width for lines across the three ploidy levels (2n, 4n, 6n) as indicated. See Table 2 for key to accession data. **B)** When grouped by ploidy level, there are significant differences in leaf width. **C)** Mean leaf length for each of the lines**. D)** Leaf length grouped by ploidy level. **E)** Mean leaf area (length x width) across all genotypes. **F)** Leaf area grouped into ploidy level. Letters indicate significant differences between means (P=<0.05), Tukey HSD post one-way ANOVA. Error bars are equivalent to +/- 1 S.E.M. n = minimum of 5 per line).

Similarly to vein density, the distance between vascular bundles was shown to vary significantly in the lines investigated (ANOVA, $F_{(10,53)}$= 40.69, P= <0.0001) (Figure 2.9C). When lines within each ploidy level were grouped (Figure 2.9D), it was shown that ploidy level had a significant impact upon interveinal distance (ANOVA, $F_{(2,8)}$= 11.35, P= 0.0046). Interveinal distance was significantly lower in the 2n lines compared to the hexaploid varieties. 4n genotypes (393.4 µm) were also observed to have a statistically significantly larger interveinal distance than their 2n counterparts (307.3 µm), but 4n and 6n leaves could not be distinguished with respect to interveinal distance. As with vein density, the mean distance between veins was also compared between the wild (*T. araraticum* and *T. dicoccoides*) and domesticated (*T. dicoccon* and T. *durum*) species under investigation. It was shown that there was no significant difference (unpaired *t* test, $t_{(3)}$= 0.5201, P= 0.6390) in interveinal distance between wild (379.7 µm) and domesticated groups (402.4 µm).

2.3.7. There is no trend of ploidy level and leaf thickness

As cell size, leaf size and vasculature were all shown to vary with ploidy, leaf thickness was the next structural parameter that was investigated, as this may be expected to respond to ploidy in a similar manner and may impact upon leaf-level gas exchange. Although analysis of leaf thickness revealed that there was significant variation between the lines (ANOVA, $F_{(10,115)}$= 45.26, P= <0.0001) and Tukey's HSD could be used to identify differences between means of individual lines (99% confidence) (Fig. 2.10A), there was no obvious trend in leaf thickness between plants of different ploidy level (Fig. 2.10B). Although tetraploid varieties were thickest and diploid lines the thinnest, there was no significant difference in mean leaf thickness between 2n (260.2 µm), 4n (285.6 µm) and 6n (275.9 µm) genotypes (ANOVA, $F_{(2,8)}$= 1.716, P= 0.2398). Domestication within the 4n ploidy level was shown to have no significant effect upon leaf thickness (unpaired *t* test, $t_{(3)}$= 3.007, P= 0.0574), despite wild accessions being thicker on average (302.9 µm) than their cultivated counterparts (274.0 µm).

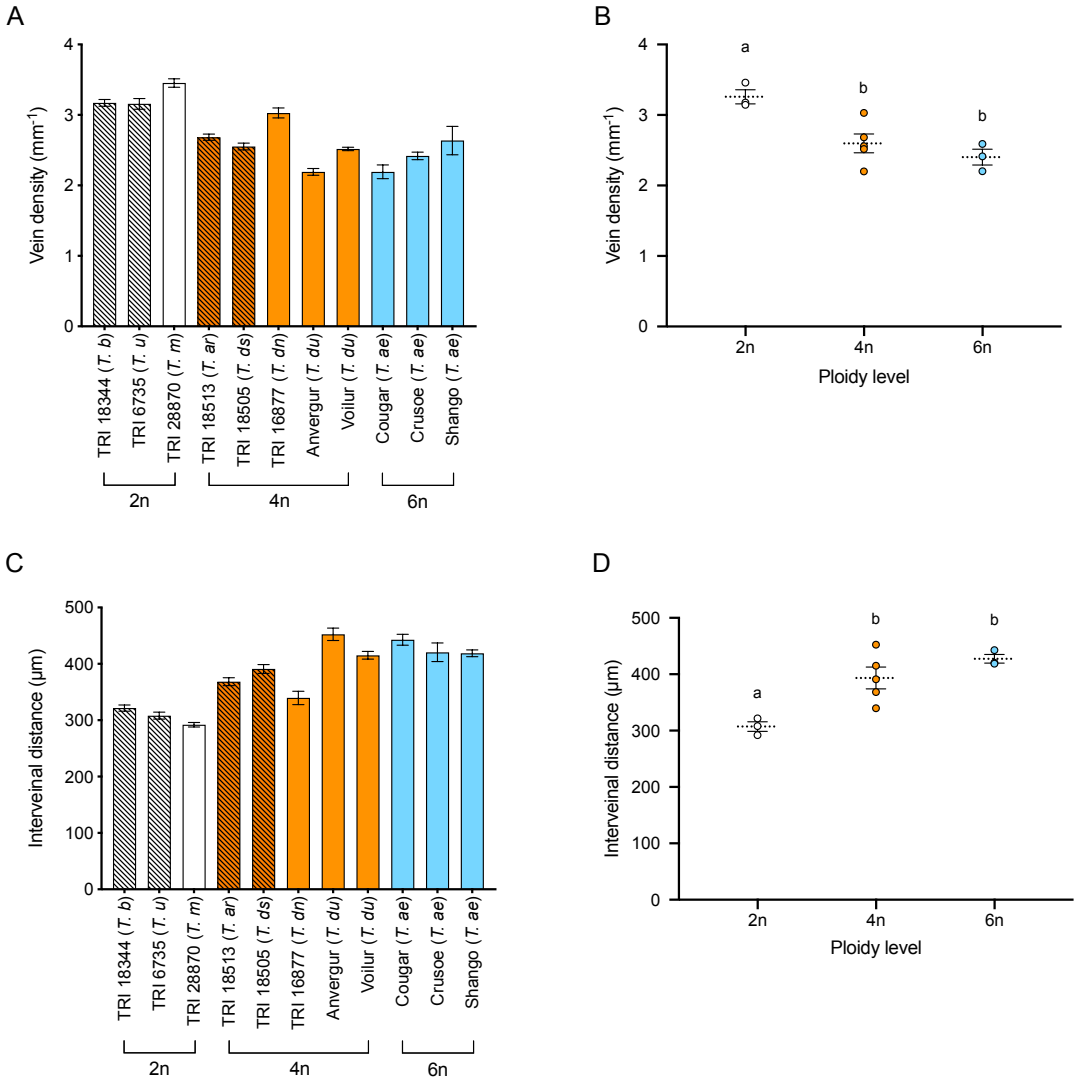

Figure 2.9. There is variation in leaf vasculature between 2n, 4n and 6n wheat lines
A) Vein density per mm leaf width for lines across the three ploidy levels (2n, 4n, 6n) as indicated. See Table 2 for key to accession data. **B)** Mean vein density by ploidy level, data grouped from those shown in (A) **C)** Mean interveinal distance for the lines shown in (A)**. D)** Interveinal distance by ploidy level, data grouped from those shown in (C) Samples indicated with the same letter cannot be distinguished from each other (P=<0.05), Tukey HSD post one-way ANOVA. Error bars = S.E.M. n = minimum of 5 per line).

2.3.8. Gas exchange in leaves of different ploidy under ambient conditions

To investigate whether the variation in leaf structural parameters described above was reflected in altered photosynthetic gas exchange, I performed a series of steady-state IRGA measurements on the same lines in which variation in stomatal density was investigated (Table 2.1). As shown in Figure 2.11A, there was significant variation in the CO_2 assimilation rate, *A*, within the members of the Triticeae investigated

(one-way ANOVA; $F_{(25,129)}$= 2.780, P= <0.0001), but with no obvious trend with ploidy level. Using a post-hoc Tukey's HSD test, it was established that the domesticated 2n and 4n lines (TRI 28870 and TRI 16877 respectively), had a lower photosynthetic rate than several of the other genotypes. When members of each ploidy level were grouped (Figure 2.11B), the mean assimilation values were as follows: 2n = 21.6 µmol m^{-1} s^{-1}, 4n = 21.2 µmol m^{-1} s^{-1}, 6n = 21.1 µmol m^{-1} s^{-1}. There was no significant difference in assimilation rate based on ploidy level (ANOVA, $F_{(2,23)}$= 0.1703, P= 0.8445). However, when the tetraploid group was further split into its constituent wild and domesticated units, it was shown that the cultivated varieties (*T. dicoccon* and the *T. durum* lines had significantly lower rates of CO_2 assimilation (20.53 µmol m^{-1} s^{-1}) than wild members of the same ploidy level (20.53 µmol m^{-1} s^{-1}) (unpaired t test, $t_{(7)}$= 3.124, P= 0.0167).

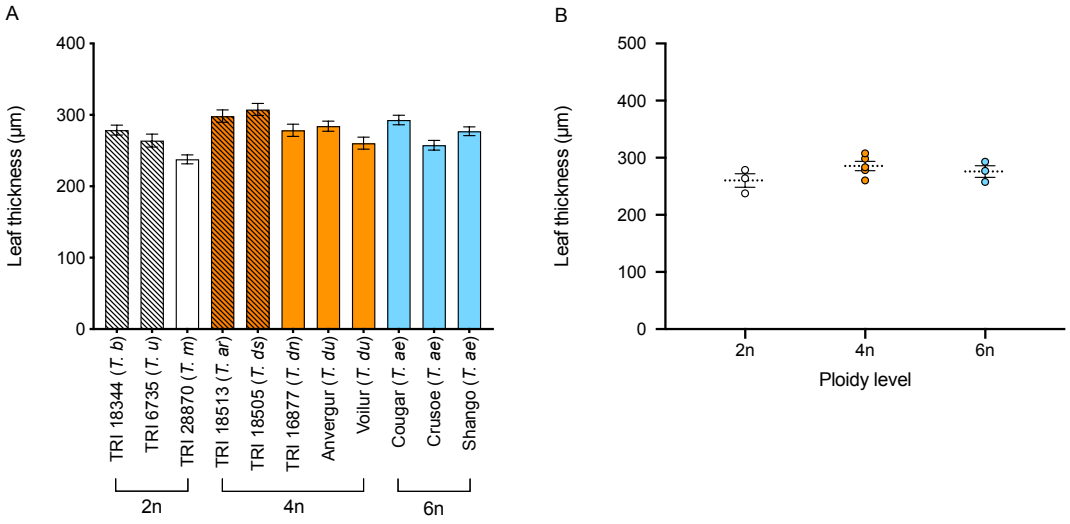

Figure 2.10. Variation in leaf thickness between 2n, 4n and 6n wheat lines
A) Leaf thickness for lines across the three ploidy levels (2n, 4n, 6n) as indicated. See Table 2 for key to accession data. **B)** Mean leaf thickness by ploidy level, data grouped from those shown in (A). Tukey HSD post one-way ANOVA. Error bars = S.E.M. n = minimum of 5 per line).

Under the same environmental conditions, it was found that there was significant variation in g_s between genotypes (one-way ANOVA; $F_{(25,129)}$= 8.130, P= <0.0001), as shown in Figure 2.11C, with an apparent trend of diploid plants having a higher stomatal conductance relative to other ploidy levels. Tetraploid lines showed a lot of variation in g_s, with domesticated 4n plants (*T. dicoccon* and *T. durum*) having relatively low g_s values (comparable to those shown by the hexaploid lines) while wild

4n lines generally had a higher stomatal conductance. When the mean rate of g_s was calculated for grouped ploidy data, the 2n lines had the highest stomatal conductance (0.61 mol m^{-2} s^{-1}), 6n varieties the lowest g_s values, with 4n lines showing an intermediate g_s level (0.53 and 0.43 mol m^{-2} s^{-1} respectively). This variation in g_s value was significant (ANOVA: $F_{(2,23)}$= 13.59, P= 0.0001). A post-hoc multiple comparisons test (Tukey's HSD) showed that g_s was not significantly different between the diploid and tetraploid plants but was significantly lower in the hexaploid cultivars than both 2n and 4n genotypes (Figure 2.11D). As with A, it was found that stomatal conductance was significantly higher (unpaired t test, $t_{(7)}$= 4.254, P= 0.0038) in wild 4n lines (0.61 mol m^{-2} s-1) than domesticated tetraploid lines (0.46 mol m^{-2} s^{-1}).

As a result of the variation in assimilation and stomatal conductance, significant differences in iWUE between were also be observed between the wheat lines (one-way ANOVA; $F_{(25,122)}$= 8.130, P= <0.0001). As shown in Figure 2.11E, although there is variation within ploidy levels, it appears that the varieties of *T. durum* (4n domesticated) and *T. aestivum* (6n) had a higher iWUE than the wild tetraploids and the diploid genotypes. This was explored using one-way ANOVA and post-hoc Tukey's HSD ($F_{(2,23)}$= 26.16, P= <0.0001). The mean iWUE value for the 2n lines (35.8 µmol mol^{-1}) was lower than that for 4n (41.7 µmol mol^{-1}), and this was found to be significant at the 95% confidence limit (Figure 2.11F). Furthermore, the mean iWUE across all the hexaploid cultivars was greater still at 50.5 µmol mol^{-1}, and this was found to be significantly higher than that of both the 2n and 4n lines. When the 4n ploidy level was separated via domestication status, it was shown that domestication had a significant effect upon iWUE (unpaired t test, $t_{(7)}$= 4.035, P= 0.005), with cultivated varieties having a higher iWUE (45.5 µmol mol^{-1}) than their wild relatives (36.9 µmol mol^{-1}).

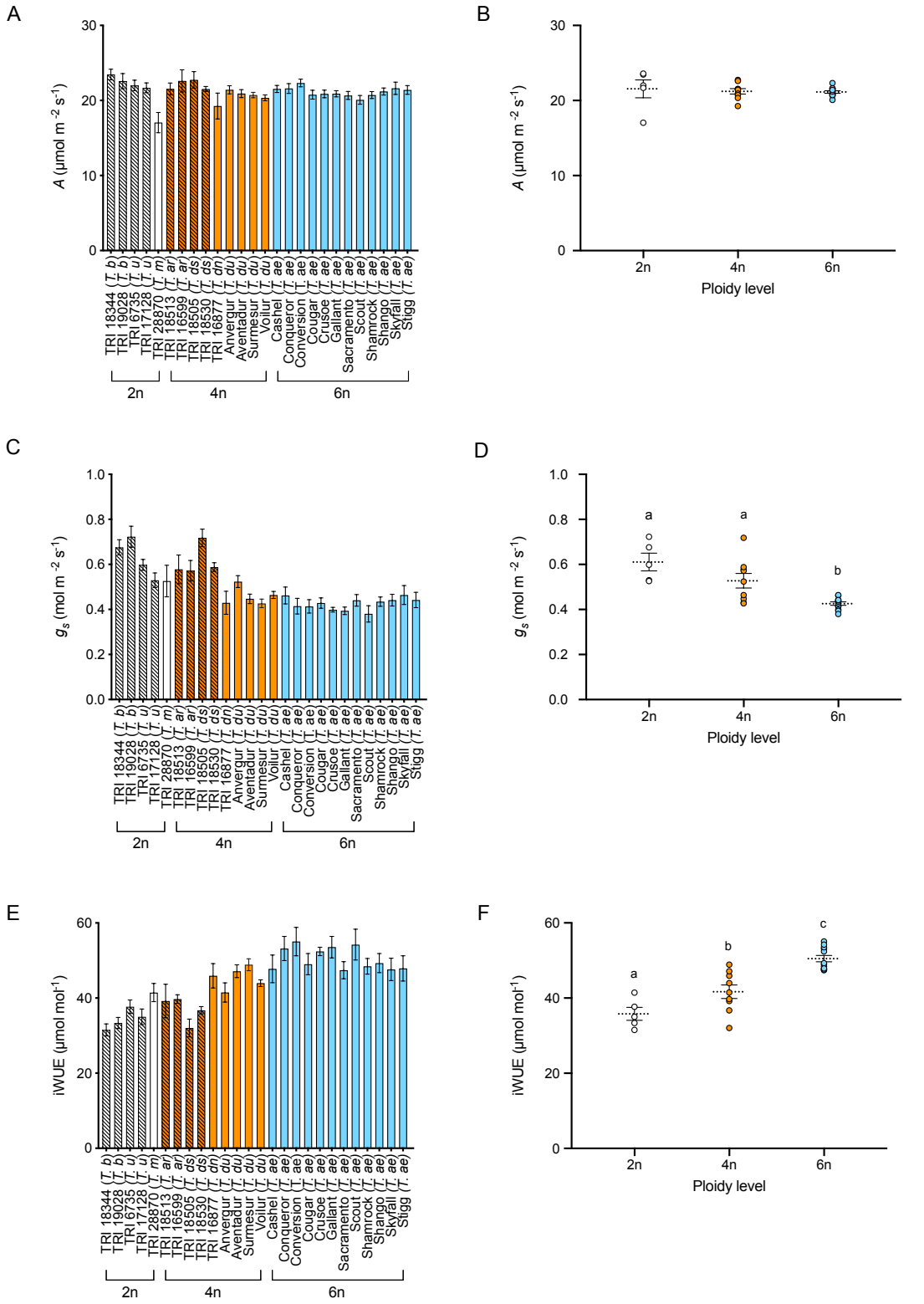

Figure 2.11. There is variation in leaf-level gas exchange between 2n, 4n and 6n wheats **A)** CO_2 assimilation for lines across the three ploidy levels (2n, 4n, 6n), as indicated. See Table 1 for key to accession data **B)** Mean assimilation rate by ploidy level, data grouped from those shown in (A). **C)** g_s for the wheat lines shown in (A). **D)** Mean g_s by ploidy level, data grouped from those shown in (C). **E)** iWUE for the wheat lines shown in (A). **F)** Mean iWUE by ploidy level, data grouped from those shown in (A) and (C). Samples indicated with the same letter cannot be distinguished from each other (P=<0.05). Tukey HSD post one-way ANOVA. Error bars = S.E.M. n = minimum of 5 per line.

2.4. Discussion

The relationships between ploidy level and stomatal anatomy and leaf structure and the effects that these have upon physiological function in the Triticeae have been investigated previously (Austin *et al.*, 1982). This chapter aimed to further explore these relationships and to elucidate the mechanisms resulting in these physiological differences shown by leaves of different ploidy level. Using a wide range of 2n, 4n and 6n genotypes, the hypothesis that stomatal density and size are affected by genome size - and that other leaf structural parameters were affected in a similar manner - was tested. Furthermore, the impact that these changes in leaf form have on leaf-level gas exchange, and the associated impacts this may have upon wheat water use efficiency, were investigated.

2.4.1. The size and arrangement of stomata is influenced by ploidy level in wheat

The negative correlation between polyploidy and stomatal density and size is a well-established phenomenon (Masterson, 1994; Beaulieu *et al.*, 2008). The data presented here confirms a previously observed pattern in the Triticeae, with 6n plants having significantly fewer stomata than 4n plants, which in turn have a significantly lower stomatal frequency than diploids (Austin *et al.*, 1982; Wang & Clarke, 1993; Maosong *et al.*, 2008; Khazaei *et al.*, 2009). A greater number of modern bread wheat (6n) varieties were used in our study, as was a wider range of tetraploid lines and species, providing a more global view of the phenomenon. From our data, it is apparent that there is significant variation within modern hexaploid wheat for stomatal density. Given the importance of stomata with respect to plant water use, this may prove useful for the breeding of drought tolerant crops.

Alongside this variation in the frequency of stomata, it was also observed that stomatal size was affected by ploidy level. The data showed that this is a result of not only changes in the length of the guard cells but also that the width of the stomatal complex increases with ploidy, thus increasing complex area. This increase in stomatal size results in a greater pore area (Franks & Beerling, 2009), and analysis of anatomical

g_{smax} suggests that the theoretical maximum rate of conductance allowed by stomatal anatomy is also significantly different between ploidy levels. Although pore size is reduced in lines of lower ploidy level, the increased stomatal density of these plants counteracts this. Smaller stomata have a smaller distance across which gas must diffuse as the depth of the pore is reduced (Franks & Beerling, 2009). The connection of operational stomatal conductance and anatomical g_{smax} reveals a link between leaf function and stomatal development and anatomy (Dow *et al.*, 2014).

My results showed that, in addition to this trend of increasing stomatal size with increasing ploidy level, epidermal cell size was also larger in 6n lines, intermediate in tetraploids and smallest in diploid plants. As cell size and ploidy have often been shown to have a close relationship (Kondorosi *et al.*, 2000), this is unsurprising. Our results indicate that all cell files in the leaf, both stomatal and epidermal, respond to increasing ploidy in a similar manner. Thus, the observed increase in stomatal size is not a specific outcome of increasing ploidy level, rather it is an unavoidable consequence of a general increase in cell size linked to increasing ploidy. As both stomata and epidermal size respond to increasing ploidy comparably, it is likely that stomatal index values would not significantly differ with ploidy, although this could be investigated further in future.

Previous studies on stomatal structure and ploidy level have generally focussed on flag leaves. Our results suggest that trend observed are also apparent in younger leaves, i.e., leaf 5. Use of younger leaves in this study allowed for a higher throughput of plants, with the use of smaller plants allowing for an efficient use of growth room space. In future it would be interesting to carry out similar experiments upon leaves of other developmental stages, including flag leaves, although this would probably require the use of field or glasshouse conditions which, of necessity, bring in an environmental component of variability, making data interpretation more difficult.

2.4.2. There is variation in organ size within the Triticeae but the relationship to ploidy level is not strict

As cell size and number are responsible for determining organ size, it would be expected that leaf size differences would follow the same trend observed in stomata and epidermal cells. In this investigation it was found that there was a trend for 2n wheat lines to have smaller leaf blades, being slightly narrower and shorter than those of 4n and 6n plants. In Austin *et al.*, 1982, flag leaf width and area were shown to be greatest in 6n, intermediate in 4n and lowest on 2n lines. However, whereas stomata and epidermal cell size appears to be related to ploidy level, we speculate that leaf size may be influenced more by domestication status, as the leaves of cultivated *T. dicoccon* (emmer wheat) and *T. durum* were shown to be wider than those of their wild relatives of the same ploidy level. This effect was not previously described in Milla & Matesanz (2017), although total area for light capture was stated to be higher in domesticated plants. As cell size and cell number are both equally responsible for determining final organ size (Mizukami, 2001; John *et al.*, 2013), I suggest that the larger leaves possessed by cultivated tetraploid varieties may be the result of an increased cell number in comparison to the wild members of this ploidy level, as also suggested by Dunstone & Evans (1974). It is possible that domesticated plants having larger leaves may have been a preferable trait for selection even prior to the advent of modern breeding techniques. Grain size is often suggested as an important trait associated with domestication and selection (Dubcovsky & Dvorak, 2007; Brown *et al.*, 2009), and is often paralleled by an increase in leaf size (Dunstone & Evans, 1974; Milla & Matesanz, 2017). As such, larger leaves may have potentially led to the preferential selection of these plants.

Additionally, it has previously been suggested that specific leaf area (SLA, leaf area per unit leaf dry mass) increases with domestication in durum wheat (Milla & Matesanz, 2017), and it may be of interest to examine changes in this parameter with ploidy in the future. A higher SLA has previously been suggested to provide growth advantages in grain crops as it is indicative of increased early vigour (Rebetzke *et al.*, 2004), although is also associated with a reduction in photosynthetic capacity per unit area (Richards, 2000).

2.4.3. Leaf vascular patterning and thickness and ploidy level

As leaf vasculature is arranged longitudinally along the leaf blade in wheat, it may be expected that changes in leaf size, especially width, would have an impact upon the arrangement of veins within the leaf structure. Similarly to Austin *et al.* (1982), vein density per mm leaf width was shown to be significantly higher in diploid species than hexaploid genotypes. Whilst shown to be intermediate to 2n and 6n plants, the vascular bundle density of tetraploids was not shown to be significantly different to hexaploid varieties. The interveinal distance was shown to follow the same pattern with increasing ploidy, i.e., 2n lines, with more veins per leaf width, had a smaller interveinal distance than found in tetraploid and hexaploid leaves, although this was only significant in 6n leaves. Tetraploid plants were intermediate, but interveinal distance was only significantly different from the 2n ploidy group. Other studies (Parker & Ford, 1982), have also noticed that veins of diploid species of the Triticeae were more closely spaced than those in hexaploids. It has been suggested that the more compact arrangement of vasculature in 2n leaves reduces the distance over which photosynthate and water must travel and is, thus, potentially partly responsible for the higher rates of photosynthesis shown by diploid lines (Austin *et al.*, 1982).

Venation is thought to have a major influence upon leaf hydraulics and thus stomatal function (Sack & Holbrook, 2006; Sack & Scoffoni, 2013). In future experiments, it may be useful to measure differences in vein size between ploidy levels, as the dimensions of these may shift with increasing genome size to a similar degree as guard and epidermal cells. It has previously been found in a range of dicot species that xylem conduit size scales independently of other cell types (John *et al.*, 2013). However, it has also been suggested that within the Proteaceae that changes in xylem size are positively correlated with the sizes of guard and epidermal cells and negatively correlated with both vascular and stomatal density (Brodribb *et al.*, 2013).

These coordinated changes in size and density of vascular systems and stomata are suggested to be essential to maintain effective function and it has suggested that the distance between veins and stomata may be a

limiting factor for gas exchange (Brodribb *et al.*, 2010; Rockwell & Holbrook, 2017). The decrease in stomatal density with increasing ploidy should in theory be paralleled by vein density decreases, in order to reduce excess water loss (Brodribb *et al.*, 2013). Similarly to the packing constraints that result in stomatal size/density trends, it has been hypothesised that increased vascular density requires an appropriate reduction in cell size (Feild & Brodribb, 2013). The diameter of vascular bundles has an impact upon hydraulic transport, with larger veins having greater hydraulic conductance (Sack & Scoffoni, 2013). Hydraulic conductance has previously been suggested be correlated with photosynthetic capacity (Brodribb *et al.*, 2007) and stomatal conductance (Sack & Holbrook, 2006). Thus, in future, it may also be of interest to measure this parameter in order to further understand the coordination of stomata and vasculature and the associated effects upon leaf gas exchange.

With respect to leaf thickness, it might be expected that cell size increases would result in an increase in this parameter (John *et al.*, 2013), but our results showed that there was no significant effect of ploidy level or domestication on leaf thickness. It has also previously been suggested that domestication does not have a significant effect upon leaf thickness in common bean (*Phaseolus vulgaris*) (Navea *et al.*, 2002). Previous work in the Triticeae has shown that there is variation in leaf thickness, but that this is not related to the ploidy level, with lines with the thickest and thinnest leaves shown both to be diploids (Parker & Ford, 1982). Our results suggested a trend for domesticated plants to be thinner within a ploidy level, but this difference in thickness was not found to be statistically significant. Thicker leaves have been associated with higher levels of photosynthesis (Oguchi *et al.*, 2005; Terashima *et al.*, 2011), but conversely may also increase the diffusion path length for both water and CO_2 (Brodribb *et al.*, 2010; Drake *et al.*, 2019). Leaf thickness is a fairly plastic parameter and is influenced by environmental conditions. As such, under different conditions, it may be that leaf thickness is significantly affected by changes in ploidy dependent on environment, and this may be of future research interest.

I suggest that this apparent maintenance of leaf thickness independent of thickness may be made possible via the adoption of differing packing strategies of mesophyll cells and/or the structure and arrangement of the mesophyll cells and adjacent intercellular airspaces. How the internal structure of the wheat leaf blade is affected by changes in ploidy is further investigated in Chapters 3 and 4.

2.4.4. The effect of ploidy-related structural changes on leaf gas exchange

My results show that under ambient growth conditions there is no significant difference in the rate of CO_2 assimilation dependent on ploidy level, despite significant variation amongst the lines under investigation. Previous experiments (Austin *et al.*, 1982) focussed on differences in maximum rates of photosynthesis as opposed to those under operating environmental conditions and found that maximum photosynthetic rates (A_{max}) were higher in diploids, middling in tetraploids and lowest in hexaploids. In that study, A_{max} was shown to positively correlate with several anatomical parameters, including vein density and stomatal density (Austin *et al.*, 1982). It has previously been noticed that there is much variation in photosynthetic capacity (A_{max}) between *T. aestivum* lines, and that high yields are not necessarily correlated with the highest rates of photosynthesis (Driever *et al.*, 2014; Gaju *et al.*, 2014). Responses of photosynthesis in lines of different ploidy to changing environmental conditions, such as and light intensity CO_2 concentration, will be investigated further in the next chapter.

Despite the lack of a relationship between photosynthetic rate and ploidy level, I found that there were differences in stomatal conductance with ploidy. The rate of stomatal conductance, g_s, was significantly lower in the hexaploid varieties than the 4n and 2n lines investigated. These results agree with those of Austin *et al.* (1982), but contrast with those presented by Xiong *et al.* (2006). It is likely that these differences in stomatal conductance are driven by the associated changes in stomatal density that occur with altered ploidy level. All of my experiments were carried out under favourable environmental conditions, and water was not limiting. It may be possible that under drought conditions hexaploid

lines maintain g_s for longer, thus presenting higher rates of conductance than their 4n and 2n relatives when water is limited. In wheat, it has been shown using transgenic approaches that reductions in stomatal density lead to reduced rates of stomatal conductance (Dunn *et al.*, 2019). My results show that the reduction in stomatal conductance found in the hexaploid cultivars resulted in these lines having an improved iWUE in comparison to diploid and tetraploid varieties, a phenotype also found in transgenic wheat having a lower g_s as a consequence of overexpressing EPF1, and thus a lower stomatal density (Dunn *et al.*, 2019). I suggest that during the domestication of wheat from its wild relatives there has been a stepwise selection for plants with a reduced frequency of stomata and an increased size of these pores, and that the resulting reductions in g_s and improvements in iWUE have at least partially underpinned this selection process.

Reduced g_s and a corresponding increase in iWUE is a potential trait that could be a target for modern cereal breeders. Improvements in iWUE would increase the resilience of wheat to future drought events, which are likely to increase in frequency with climate change. Furthermore, the moderate reductions in stomatal density, with resulting reductions in the rate of g_s shown in Dunn *et al.* (2015) were found to not have a negative influence on crop yield. As such, small reductions in stomatal density may result in improved water use efficiency at little to no cost in grain yield, although this must be investigated further. Although a transgenic approach might be the most effective means of achieving this, similar to previous authors, our results demonstrate that there is significant variation in stomatal density within modern bread wheat lines (Jahan *et al.*, 2014; Barbour *et al.*, 2016; Wang *et al.*, 2015). Indeed, in collaboration with a colleague (Jess Dunn) I have carried out a preliminary screen of an even wider panel of 6n wheat lines (32 cultivars including seven of the cultivars analysed in this study), grown in the field at RAGT Seeds (Ickleton, Cambs, UK – measurements taken on seedlings drilled in Autumn 2015) which shows that there is a large amount of variation in stomatal density in modern wheat cultivars (Figure 2.12). Although counting stomata is a useful screening method, it may be more appropriate in future to utilise a more high-throughput approach in a breeding context, for example using thermal imaging to observe

differences in stomatal conductance and WUE (Leinonen *et al.*, 2006; McAusland *et al.*, 2013).

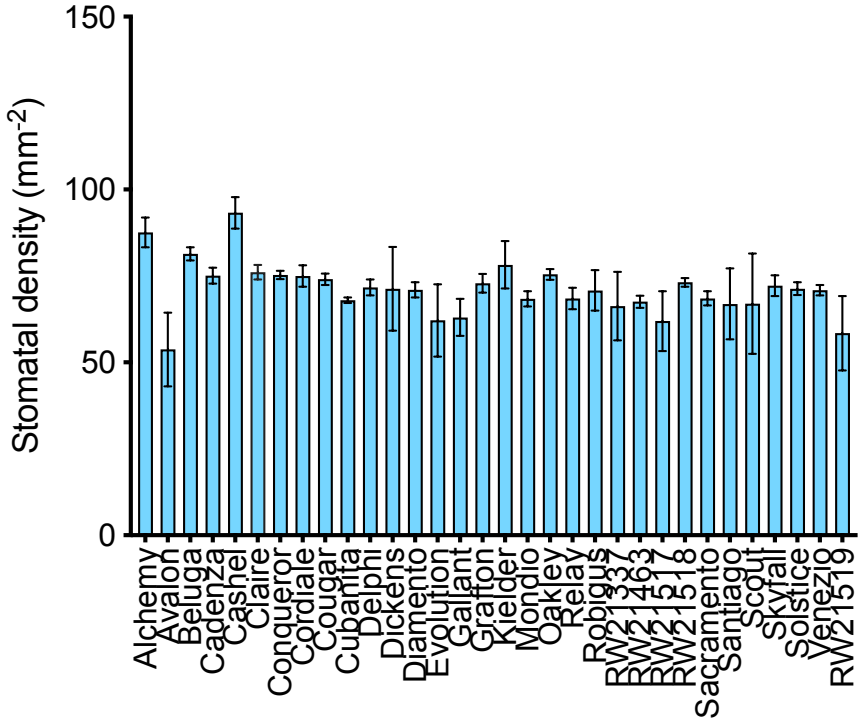

Figure 2.12. There is variation in stomatal density between modern 6n cultivars
A screen of stomatal density for 32 lines of hexaploid bread wheat grown in the field suggests that there is lots of variation within the 6n ploidy level, which could be used to improve drought tolerance.

Whilst under water-limited conditions a high g_s is detrimental, under a well-watered regime it has been shown that a high g_s confers a high grain yield in wheat (Fischer *et al.*, 1998). Additional benefits of a higher stomatal conductance include greater evaporative cooling potential (Dunn *et al.*, 2019). However, it is likely that the drought tolerance improvements associated with reduced g_s would outweigh these potential benefits.

It is also clear that there is potential to improve the water use efficiency of durum wheat, normally grown in Mediterranean regions more prone to drought events (Shewry, 2009). It is likely that there are other domesticated wheat lines that will show the reduced stomatal density phenotype, and in the future, a more focused screen of hexaploid varieties may be useful in determining which varieties may be useful for improving water use efficiency gains.

2.5. Conclusion

In this chapter I have shown that stomatal size and density vary with ploidy level in wheat. I also observed that other leaf structural aspects, such as epidermal cell size and leaf vasculature, change with ploidy level, but that leaf thickness is not affected. These changes in leaf form were shown to have an impact upon stomatal conductance without affecting CO_2 assimilation (under ambient conditions) and thus highlighted the potential for improvements in iWUE that may be unlocked in the future by selection of these traits. At a mechanistic level, the data in this chapter focussed on the leaf epidermis (stomata), but the internal structure of the leaf, notably the mesophyll, is also likely to influence leaf performance. The extent to which mesophyll structure in wheat varies with ploidy level is the focus of the next chapter.

Chapter 3. How ploidy affects the internal structure of wheat leaves and implications upon photosynthesis

3.1. Introduction

The internal structure of the leaf, and in particular leaf airspace, has been suggested to have a direct impact upon the rate of CO_2 diffusion to the site of carbon fixation in the chloroplasts of mesophyll cells (Terashima *et al.*, 2011; Ren *et al.*, 2019). This chapter makes novel use of a 3D imaging technique, X-ray microtomography (X-ray µCT), to characterise differences in leaf airspace and, by combining with gas exchange analysis, explores the relationship of leaf internal architecture to photosynthetic function. In particular, I examine changes in these relationships across the different ploidy levels exemplified by the wheat species introduced in the previous chapter, leading to inferences on how wheat leaf structure and function have evolved.

3.1.1. The relationship of ploidy level and internal leaf structure

As with the distinct patterns exhibited by external anatomical parameters, such as the stomata, it has been noticed in previous studies that leaf internal architecture differs with ploidy level, and that this has an impact on photosynthesis (Austin *et al.*, 1982; Parker & Ford, 1982). Consideration of this topic first requires an understanding of wheat leaf structure. The chlorenchyma of wheat leaves does not have the stereotypical differentiation of palisade and spongy mesophyll layers seen in many eudicot plants. Instead, leaves of each wheat ploidy level are built along a similar basic structure consisting of lobed mesophyll cells with no clear distinction of layers (Jellings & Leech, 1984; Jung & Wernicke, 1990). These lobed cells are punctuated by a fairly regular pattern of intercellular airspaces through which CO_2 and water vapour can diffuse throughout the leaf (Parker & Ford, 1982; Jellings & Leech, 1984). The arrangement and amount of airspace within the leaf would thus be expected to have an impact upon rates of photosynthesis, specifically mesophyll conductance (g_m). For example, an increased exposed surface area of the mesophyll tissue is hypothesised to enable

higher rates of exchange of CO_2 and water vapour between the stomata and the chloroplasts (Loreto *et al.*, 1992; Terashima *et al.*, 2011; von Caemmerer & Evans, 2015). The connectivity and patterning of airspaces within the leaf has also been suggested to play a vital role in ensuring effective gas exchange throughout the leaf volume (Long *et al.*, 1989). Mesophyll cell size and shape are also thought to impact photosynthesis (Ren *et al.*, 2019) and this topic is the focus of experiments described later in in Chapter 4.

Previous experiments investigating the impact of ploidy upon leaf gas exchange have typically prioritised effects upon stomatal conductance and differences in leaf biochemistry and physiology, as opposed to structural changes within the chlorenchyma tissue. One study (Parker & Ford, 1982), did estimate the percentage of air-filled space (analogous to mesophyll porosity, %age airspace per volume) within flag leaves of diploid (*T. urartu, T. monococcum*) and hexaploid wheats (*T. aestivum*). The authors showed that there was variation in this parameter, with leaves of the wild 2n species (*T. urartu*) containing a higher percentage of airspace than the other two varieties, with the lowest porosity observed for the domesticated einkorn (2n) line. However, a further study investigating the effect of ploidy upon leaf internal anatomy in the Triticeae found that the proportion of leaf airspace showed no specific trend with ploidy level (Jellings & Leech, 1984).

Associated with leaf airspace is the exposed surface area of the mesophyll (S_{mes}). It has been hypothesised that a greater S_{mes} has a positive effect upon gas exchange, as CO_2 and H_2O diffuse at different rates in the gas phase (apoplastically) than in the liquid phase through cells (symplastically) (Flexas *et al.*, 2012; Tholen *et al.*, 2014; Buckley, 2015). An increase in S_{mes} results in a greater available surface area for gaseous CO_2 diffusion, and thus a greater theoretical maximum flux of CO_2 to the chloroplasts (Terashima *et al.*, 2011). Parker and Ford (1982), showed that, in the *Triticum* genotypes under investigation, exposed surface area of the mesophyll responded in the same manner as mesophyll porosity, with diploid *T. monococcum* having the lowest S_{mes}, whilst it was highest in *T. urartu* (2n) and intermediate in the hexaploid cultivar. The authors suggest that the higher rates of photosynthesis shown in *T. urartu* were

potentially the result of a reduced resistance to the diffusion of CO_2 into the mesophyll cells associated with a greater S_{mes} (Parker & Ford, 1982).

The impact of ploidy level on mesophyll conductance in the Triticeae has not been investigated, however, several studies have shown that there is a large amount of genotypic variation in g_m between hexaploid wheat cultivars (Driever *et al.*, 2014; Jahan *et al.*, 2014; Barbour *et al.*, 2016; Olsovska *et al.*, 2016; Ouyang *et al.*, 2017). This large-scale screen of 64 *T. aestivum* genotypes carried out by Driever *et al.* (2014) found that not only was there variation in g_m, but that this correlated with photosynthetic capacity. It has also previously been shown that 11 Australian cultivars had significant variation in mesophyll conductance, and that whilst this showed a positive relationship with CO_2 assimilation (A), there was no significant relationship between g_m and leaf iWUE (Jahan *et al.*, 2014). Additionally, Barbour *et al.* (2015), found that mesophyll conductance varied three-fold within a mapping population of 150 lines of *T. aestivum*, and that it was correlated with light-saturated photosynthetic rate but not g_s. Mesophyll conductance in wheat has also been shown to be positively correlated with the assimilation rate of CO_2 in several other studies (von Caemmerer & Evans, 2015; Olsovska *et al.*, 2016). For example, Olsovska *et al.* (2016) also found that there was significant variation (again nearly three-fold) in g_m for four hexaploid wheat lines of varying geographical origins (both Europe and Mexico). Ouyang *et al.* (2017) also found variation in g_m for the two wheat lines investigated and suggested that the higher rates of mesophyll conductance shown by wheat over rice resulted from having a higher S_{mes} in the wheat lines than the rice cultivars used in the same study.

It has also been hypothesised that, in the short-term, mesophyll conductance can be influenced by changes in environmental conditions (Flexas *et al.*, 2008). Whilst CO_2 and light have been shown to have no effect upon rates of g_m (Tazoe *et al.*, 2009), mesophyll conductance in wheat has been shown to be impacted by temperature (von Caemmerer & Evans, 2015), leaf age (Loreto *et al.*, 1994) and season (Sun *et al.*, 2015). When four wheat lines were subjected to drought it was shown that g_m displayed a variable response to water stress (Olsovska *et al.*, 2016). Having high g_m, low g_s plants is potentially a desirable trait in future

breeding programmes, as it may enable improvements in WUE whilst maintaining yields and productivity (Barbour *et al.*, 2016).

3.1.2. X-ray microtomography as a novel method for investigating leaf internal structure

The concept of X-ray µCT relies upon the material or tissue being imaged having variation in density, similarly to the way in which 2D radiographs can be used to investigate bones in medicine. CT scanning builds upon this by recording a series of 2D images whilst rotating the sample relative to the X-ray source and the detector (Landis & Keane, 2010; Salvo *et al.*, 2010). When a sample is exposed to the X-ray beam, the density of the microstructure of the sample, along with atomic number and the X-ray strength, is responsible for determining the X-ray attenuation coefficient (Flannery *et al.*, 1987; Mathers *et al.*, 2018). If the beam is not absorbed or blocked, it will pass through the sample. X-rays that are transmitted through the sample are converted into visible light using a scintillator, which is then detected and used to create 2D projections (Landis & Keane, 2010; Salvo *et al.*, 2010). This series of 2D slices can then be reconstructed in order to render a 3D image consisting of voxels (3D/xyz pixels) representing the individual X-ray absorption of the sample at that point (Dhondt *et al.*, 2010; Landis & Keane, 2010). This process is summarised in Figure 3.1.

Originating as a non-destructive imaging technique for medical use and biomedical research (Ritman, 2011), X-ray µCT is now widely used in computer sciences, earth sciences, chemistry, palaeontology and materials science (Staedler *et al.*, 2013), however, it is only relatively recently that this imaging technique has been on plant tissues (Stuppy *et al.*, 2003; Dhondt *et al.*, 2010) and is comparatively underused to image plant structures (Staedler *et al.*, 2013). X-ray µCT analysis has been frequently used to non-invasively determine the structure of root systems (Flavel *et al.*, 2012; Mooney *et al.*, 2012; Tracy *et al.*, 2012) , and has also been used to investigate xylem embolism and anatomical characteristics of woody tissues in tree species (Steppe *et al.*, 2004; Mayo *et al.*, 2010; Choat *et al.*, 2016). Imaging of flowering structures, seeds and fruits in 3D is another novel use of this technique in plants (Stuppy *et al.*, 2003;

Dhondt *et al.*, 2010; Herremans *et al.*, 2015; Jhala & Thaker, 2015; Tracy *et al.*, 2017).

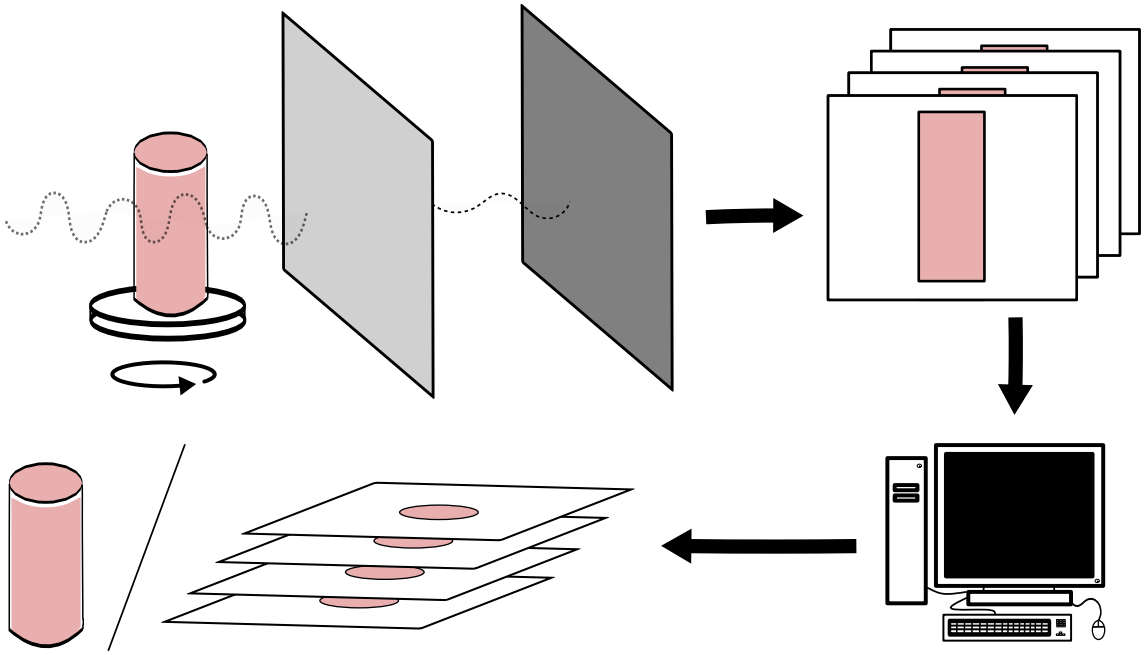

Figure 3.1. Principles of X-ray µCT
A sample is exposed to an X-ray beam – dense tissue blocks the X-ray, whilst it passes through less dense areas of a sample. The signal is picked up by a detector and used to create 2D projections. These slices are then reconstructed using computer software to create a 3D image of the sample.

The use of this technique to successfully observe leaf internal structure has previously been carried out on several eudicot plant species including: *Arabidopsis thaliana* (Pajor *et al.*, 2013; Dorca-Fornell *et al.*, 2013; Lehmeier *et al.*, 2017; Mathers *et al.*, 2018; Lundgren *et al.*, 2019), tomato and pea (Mathers *et al.*, 2018). Furthermore, this imaging method has been used to successfully derive internal structural parameters such as mesophyll porosity and the exposed mesophyll surface area for the monocot crop species barley, oats and rice (Mathers *et al.*, 2018). Additionally, µCT scanning has been successfully used on herbarium samples to investigate leaf venation (Schneider *et al.*, 2018).

In the case of leaves, the intercellular airspace network is low density in comparison to the higher density cellular material (Dhondt *et al.*, 2010; Pajor *et al.*, 2013; Mathers *et al.*, 2018). This difference in density within the leaf allows for quantitative leaf architectural parameters to be

inferred, as the beam passes through the leaf airspaces and is absorbed or reflected by the surrounding cells (Dhondt *et al.*, 2010; Pajor *et al.*, 2013; Mathers *et al.*, 2018). This technique allows for high levels of resolution (between 2.5 – 2.75 µm) and it is possible to image thick samples without the need for tissue fixation (Pajor *et al.*, 2013; Mathers *et al.*, 2018). This resolution is however limited by the size of the sample, and higher resolution images also require longer scanning and processing (Pajor *et al.*, 2013).

CT scanning has been successfully used to investigate the effect that manipulation of cell cycle gene expression has upon leaf internal architecture in Arabidopsis. This study showed that an increase in mesophyll porosity and a change in its distribution occurred when retinoblastoma-related protein (RBR) was suppressed, altering cell division patterns (Dorca-Fornell *et al.*, 2013). It was found that the increased mesophyll porosity associated with suppression of RBR resulted in plants with higher rates of stomatal conductance. Further investigations into the effects of the promotion or repression of cell proliferation in Arabidopsis showed using X-ray µCT that tissue porosity and the pattern of airspaces within leaves were altered compared to the wild type when the cell cycle genes were manipulated (Lehmeier *et al.*, 2017). Analysis of A_{sat} in these lines suggested that a reduction in mesophyll porosity resulted in an increase in photosynthetic capacity and g_m, but no significant differences in g_s.

In addition to this use of CT imaging to elucidate the relationships between leaf airspace parameters and photosynthetic performance in a model species, Mathers *et al.* (2018), used this technique to investigate mesophyll porosity and S_{mes} for a variety of dicot and monocot crop species, as well as comparing the accuracy of a 2D analysis of these parameters with that provided by the 3D analysis enabled by X-ray µCT. This showed that whilst it is possible to estimate porosity to a similar level of precision using 2D analysis, CT scans generally gave a significantly higher S_{mes} value. A similar result, showing the underestimation of mesophyll surface area (between 15-30% lower when uncorrected) using 2D methods was also shown in a wider range of species in a separate study (Théroux-Rancourt *et al.*, 2017).

Reconstructions captured using X-ray µCT were also recently used to examine the intercellular airspace parameters of 19 species from the Bromeliaceae, incorporating species utilising both C_3 and CAM photosynthesis pathways (Earles *et al.*, 2018).

3.1.3. Using fitting software to extract more information from gas exchange data – estimating mesophyll conductance

In addition to the steady state survey measurements carried out in Chapter 2, IRGA systems can also be used to extract more physiological data providing information regarding plant performance. For example, measuring photosynthetic rate responses to changing irradiance allows for the maximum rate of leaf photosynthesis under saturated light (A_{sat}) to be determined (along with other parameters such as the quantum yield of photosynthesis - Φ). Whilst steady state measurements can be carried out at saturating light to determine A_{sat}, more information is available if light response curves are carried out (Johnson & Murchie, 2011). CO_2 response curves (A/C_i curves) are another method frequently used to explore differences in photosynthetic performance. Investigating the response of A to C_i at a range of concentrations of CO_2 under saturating light conditions allows for the biochemical determinants of photosynthesis that are carried out in the mesophyll to be separated from boundary layer and stomatal effects (Long & Bernacchi, 2003).

The FvCB model (Farquhar *et al.*, 1980) is the most frequently used model to investigate how photosynthesis responds to environmental changes. This model assumes that the biochemical photosynthetic reactions are limited by one of three processes. Photosynthesis may be Rubisco-limited - usually when the CO_2 concentration is low (<20 Pa) - or limited by the regeneration of RuBP - normally at higher CO_2 concentrations above 30 Pa CO_2 (Sharkey *et al.*, 2007). When chloroplast reactions have a higher capacity than that of the leaf to use their products, primarily triose phosphate, then the leaf is triose phosphate use (TPU) limited. Under this condition A neither responds to increasing CO_2 concentrations, nor increasing O_2 concentration and as such this step often determines the maximum photosynthetic rate (A_{max}).

By assuming that A is equal to 100% of the lowest rate allowed by these limitations (also assuming that all parts of the leaf respond to environmental change in the same manner) it is possible to model CO_2 assimilation. A changes as predicted by the limiting state until one of the other processes becomes the limiting one (Sharkey *et al.*, 2007). Each limiting state results in a different response to CO_2, and therefore plotting A against CO_2 concentration and modelling responses allows for the biochemical parameters driving photosynthesis to be examined. The parameters that can be fitted include the V_{cmax}, or maximum Rubsico carboxylation rate; J – the electron transport rate, and g_m – mesophyll conductance. There are several freely available, peer-reviewed fitting tools available, each of which have their own advantages and disadvantages and each make their own assumptions (Sharkey *et al.*, 2007; Bellasio *et al.*, 2015).

Photosynthetic variation has previously been identified within *Triticum* species of varying ploidy levels. Several studies have observed that A_{max} - the photosynthetic capacity - is higher in diploid lines than in tetraploid and hexaploid genotypes (Austin *et al.*, 1982; Jellings & Leech, 1984; Warner & Edwards, 1993). It has also been found that there are significant differences in A_{max} within the hexaploid ploidy level. As previously mentioned, a screen of 64 hexaploid *T. aestivum* lines has indicated significant genotypic variation in photosynthetic capacity (Driever *et al.*, 2014). Variation in this parameter was also found when a panel of 15 genotypes, including modern, landrace and synthetic hexaploid lines was investigated (Gaju *et al.*, 2016) and a screen of a mapping population (150 lines) also showed significant variation in A_{max} (Jahan *et al.*, 2014; Barbour *et al.*, 2016). Photosynthesis under high light conditions has previously been shown to vary with ploidy level (Dunstone & Evans, 1974), and it has also been shown that tetraploid durum wheat has a higher A_{sat} than hexaploid *T. aestivum* (Biswas & Jiang, 2011). Additionally, there has also been shown to be genotypic variation in A_{sat} in a range of 13 Australian wheat varieties (Sadras *et al.*, 2012). Previous experiments have also identified variation in V_{cmax} and J amongst hexaploid wheat lines (Driever *et al.*, 2014; Carmo-Silva *et al.*, 2017). Although there are no published wide-scale studies comparing how these fitted parameters are affected by

ploidy level in the Triticeae, it has been noticed that both V_{cmax} and J are higher in 4n *T. durum* than 6n bread wheat (Biswas & Jiang, 2011).

Recently, a screen of Rubisco activity suggested that there was significant variation in carboxylation velocity (V_c) amongst 25 genotypes of the Triticeae, including 2n, 4n and 6n varieties (Prins, *et al.*, 2016). More historical studies have also investigated the carboxylation activity of Rubisco, and whilst one study has shown that there were no significant differences in carboxylase and oxygenase activity between *Triticum* species of different ploidy levels (Holbrook *et al.*, 1984), a further study found that Rubisco activity was higher on a leaf nitrogen basis in 6n *T. aestivum* than 2n *T. monococcum*, despite similar initial responses of A to increasing CO_2 concentrations on a leaf area basis (Evans & Seemann, 1984).

3.1.4. Other leaf components – chlorophyll and protein content

Other leaf components, such as chlorophyll content and Rubisco content, are also indicators of photosynthetic performance. As such it is important to investigate whether there are any differences in these parameters with changing ploidy level in the Triticeae. Levels of chlorophyll, as the major photosynthetic pigment, have been associated with rates of CO_2 assimilation (Buttery & Buzzell, 1977; Gaju *et al.*, 2014; Croft *et al.*, 2017) and are indicative of leaf nitrogen status (Cartelat *et al.*, 2005), as components of the photosynthetic machinery are responsible for a large proportion of leaf nitrogen (Evans, 1983; Evans, 1989). Whilst it has been suggested that diploid wheat leaves have a higher content of chlorophyll than hexaploid counterparts (Watanabe *et al.*, 1994), the converse to this has also been found (Kaminski *et al.*, 1990). Prior studies have shown that hexaploid wheat contains a large amount of genotypic variation for leaf chlorophyll content (Babar *et al.*, 2006; Gaju *et al.*, 2016; Hamblin *et al.*, 2014; Sid'ko *et al.*, 2017), as does 4n *T. dicoccoides* (Nevo *et al.*, 1991).

Rubisco content has previously been observed to increase in a stepwise manner with changes in ploidy on a per mesophyll cell basis, although these changes are less pronounced on a per leaf volume basis as a result

of concurrent changes in mesophyll cell number per volume (Dean & Leech, 1982a), and in some cases it was found that there was no significant difference in Rubisco content (on a per leaf nitrogen basis) (Evans & Seemann, 1984). Rubisco content has also been discovered to vary in hexaploid wheat and to be positively correlated with photosynthetic capacity (Driever *et al.*, 2014; Carmo-Silva *et al.*, 2017). Measuring total soluble protein is a useful proxy for the measurement of Rubisco as this enzyme is thought to comprise the majority of leaf protein (Driever *et al.*, 2014). Leaf total soluble protein has previously been shown to be positively correlated with Rubisco content in *T. aestivum* (Carmo-Silva *et al.*, 2017). Despite this apparent importance, Driever *et al.* (2014) suggested that in comparison to other previously mentioned traits, variation in Rubisco content is a minor contributor to the variation of leaf photosynthesis in hexaploid wheat.

3.1.5. Carbon isotope discrimination and water use efficiency

In addition to the iWUE values presented in the previous data chapter, it is possible to estimate the WUE of a plant via the use of carbon isotope analysis (Adams & Grierson, 2001; Seibt *et al.*, 2008; Cernusak *et al.*, 2013). This can be approximated via examination of the carbon isotope discrimination ($\Delta^{13}C$) of the leaf tissue. This method makes use of the discriminatory nature of Rubisco, which favourably carboxylases the ^{12}C isotope over heavier ^{13}C (Farquhar & Sharkey, 1982; Farquhar & Richards, 1984; Adams & Grierson, 2001). Plants with a lower internal CO_2 concentration have been shown to have a higher ratio of ^{13}C: ^{12}C, as discriminatory fixation is reduced. As g_s influences C_i, $\Delta^{13}C$ is therefore a useful proxy for estimating plant water loss, and reduced discrimination is indicative of higher WUE (Farquhar & Richards, 1984; Cernusak *et al.*, 2013). Many authors have discussed the relationship between carbon isotope discrimination and water use efficiency in crop species (Hubick & Farquhar, 1989; Rajabi *et al.*, 2008; Centritto *et al.*, 2009; Gilbert *et al.*, 2011; Adiredjo *et al.*, 2014).

In both hexaploid *T. aestivum* (Farquhar & Richards, 1984; Rebetzke *et al.*, 2002; Merah *et al.*, 2001) and tetraploid *T. durum* (Araus *et al.*, 1997; Rizza *et al.*, 2012), it has been found that there is a negative correlation

between leaf carbon isotope discrimination and water use efficiency, and $\Delta^{13}C$ has been negatively correlated with stomatal density in *T. durum* (Merah *et al.*, 2001). Differences in $\Delta^{13}C$ between ploidy levels in the Triticeae have also been explored previously (Khazaei *et al.*, 2009). The authors established that diploid wheat genotypes had a higher $\Delta^{13}C$ than tetraploid and hexaploid accessions, and that carbon isotope discrimination was negatively associated with water use efficiency across all species and genotypes, and positively correlated to stomatal density (Khazaei *et al.*, 2009). It may be expected that the differing stomatal characteristics and internal structures showcased by the Triticeae would result in differing $\Delta^{13}C$ values (Araus *et al.*, 1997; Cao *et al.*, 2012), which may or may not correlate with the iWUE values calculated in the previous chapter.

3.1.6. What comes first, the stomata or the airspace? A chicken and egg hypothesis

The link between stomata and the intercellular airspace network within the leaf is accepted as being fundamental to leaf form and function, however, the mechanism by which the differentiation of stomata and mesophyll airspace formation are linked to form a fully functioning network is unknown. When discussing this relationship between stomata and leaf airspace, an important question to ask is which develops first: do stomata develop above sub-stomatal cavities, or is the converse of this true? The development of stomata and establishment of leaf porosity have been shown to be linked (Kessler & Sinha, 2004; Bergmann, 2004), and it has been found that a lack of mesophyll airspace subtending the epidermis does not affect stomatal development (Sachs, 1979; Lightner *et al.*, 1994), suggesting that stomata form prior to the underlying airspaces found in the mesophyll layer. It has recently been hypothesised that initial mesophyll cell separation occurs sub-epidermally as part of the usual developmental lineage of the leaf blade, but that the final size and distribution of intercellular airspaces is controlled by the presence of mature stomata on the epidermis (Dow *et al.*, 2017). The authors of this study suggest that genes associated with stomatal development are involved in determining the density of the mesophyll and interlayer coordination in Arabidopsis, although the signals for this have not yet been identified (Dow *et al.*, 2017). If this is the case, it suggests that

stomatal density and mesophyll porosity are causally linked, and consequently that mesophyll porosity and leaf gas exchange are coordinated.

It has also previously been suggested that signalling between the mesophyll layer and guard cells is important for correct stomatal responses to environmental stimuli (Mott *et al.*, 2008; 2014), and stomatal patterning has also been theorised to be influenced by the internal anatomy of the leaf (Bergmann, 2004; Casson & Gray, 2008), with epidermal files in monocot plants - such as wheat - not containing stomata when positioned above vascular bundles (Bergmann, 2004; Martin & Glover, 2007).

One way in which this hypothesis can be tested is via the use of stomatal development mutants. *EPIDERMAL PATTERNING FACTOR* (*EPF)* overexpressors, which have a reduced stomatal density phenotype as they are negative regulators of stomatal development, are useful tools for investigating stomatal development and impacts upon leaf physiology and mesophyll development. For this reason, transgenic wheat lines (*TaEPF1-OE*) that have previously been generated by colleagues at the University of Sheffield (Dunn *et al.,* 2019) were chosen to investigate how a reduced stomatal phenotype may influence sub-epidermal development of the mesophyll tissue. Likewise, developmental gradients are easily observable in grass leaf blades, with younger tissue being found closer to the base of the leaf. This allows for investigation of the mesophyll layer at each point of the stomatal development pathway, which may help to further highlight links between stomatal maturation and airspace formation.

3.1.7. Aims

In this chapter, I aim to explore how ploidy level affects mesophyll airspace levels in a wide range of *Triticum* lines, in addition to carrying out investigations into the impact of ploidy upon physiological gas-exchange parameters including photosynthetic capacity and mesophyll conductance. Finally, a combination of a transgenic approach, alongside the use of leaf development gradients, was used to attempt to identify

any potential mechanistic link between stomatal function and intercellular airspace development.

3.2. Methods

3.2.1. Plant material and growth conditions

Unless noted, all plant material used in this chapter was grown as per section 2.2.1. A summary of the 2n, 4n and 6n wheat lines used is available in Table 2.2.

3.2.2. Using X-ray µCT to observe leaf internal characteristics

X-ray µCT scans were carried out at the Hounsfield Facility at the University of Nottingham by Radek Pajor, Marc Fradera-Soler and Craig Sturrock. Data analysis was performed by myself (with technical advice from Marc Fradera-Soler and Craig Sturrock). For the analysis, the middle third of the mature fifth leaf of wheat plants was analysed. A 5 mm diameter cork borer was used to remove a leaf disc from the leaf blade, avoiding the midrib. The leaf discs were placed into a tube between two polystyrene plugs at an angle of 45° in order to keep the sample static during the scanning process and thus maximise image quality. Each sample was imaged using a GE phoenix nanotom X-ray µCT scanner (GE Inspection Technologies, PE, USA). Scans were carried out using a spatial resolution of 2.75 µm, energy levels of 65 kV and 140 µA, whilst collecting 2400 projections with an exposure time of 750 ms. For the domesticated 2n (*T. monococcum*) and 4n lines (*T. dicoccon*, *T. durum*), the protocol was adapted slightly so that a 1-2 cm^2 strip of leaf was mounted and imaged as opposed to a leaf disc. In addition to having greater stability during the scan period, a reduced level of mechanical damage was inflicted to the leaf sample. This resulted in a larger volume of tissue from which porosity data could be extracted. Radiographs were assessed for movement or shrinkage, and this was corrected for if present. If samples shifted by more than three pixels in x or y, the stack was discarded. The 2D radiographs acquired were then reconstructed into 3D via the use of a filtered back-projection algorithm. A total of three scans per genotype were carried out.

Volumes were aligned using VGSTUDIO software (Volume Graphics GmbH, Germany) and 3D images were converted into stacks of tiff images. These stacks were then utilised to form a mask using Avizo software (Thermo Fisher Scientific, Massachusetts, USA), which acted to separate the sample from the background of the image (polystyrene) via a binarisation process. Separated stacks were then cropped to a region of interest, removing any areas around the edge of the sample, which may have been mechanically damaged during the excision process. If present, the major veins and/or the midrib was also avoided.

Using the IsoData function in ImageJ along with minimum algorithms ('Max Entropy" and 'Li' algorithms), aligned and cropped stacks were then thresholded to extract stacks of images showing only plant tissue and the previously created mask. Any variations in brightness due to filament decay were accounted for by switching the algorithms when required. Noise was considered to be equivalent for each sample. Image stacks were used as the input for the ImageJ Image Calculator, and stacks consisting exclusively of pore space were generated. The ImageJ Particle Analyser plugin (Sezgin & Sankar, 2004) was used to extract numerical structural information (total pore area/volume, total mask area/volume, perimeter area) of the intercellular airspace within the leaf, including mesophyll porosity (% airpace/volume) and exposed mesophyll surface area (S_{mes}). Mean porosity was calculated using Equation 3.1, whilst mesophyll surface area was calculated using Equation 3.2.

Equation 3.1. Mesophyll porosity

$$\text{Mesophyll porosity (\%)} = \frac{(\Sigma \text{ Total pore area})}{(\Sigma \text{ Total mask area})} \times 100$$

Equation 3.2. Exposed mesophyll surface area (S_{mes})

$$S_{mes} = \frac{((\Sigma \text{ Perimeter area}) \times \text{resolution})}{\text{Total mask volume}}$$

3.2.3. Physiological responses to changing environmental conditions – light intensity and CO_2

Light response curves and CO_2 response A/C_i curves were carried out on the subset of lines identified in the previous chapter (see Table 2.2) using a LI-COR LI-6800 under ambient O_2 concentrations. Conditions for the light response curves were as follows: flow rate: 400 µmol s^{-1}, relative humidity: 60%. Sample CO_2 was set at 400 µmol mol^{-1} and the mixing fan set at 60% (around 10000 rpm). The temperature exchanger was set to 21˚C. The width of the fully developed fifth leaf of each plant was recorded before the middle part of the leaf blade was clamped into the chamber with a light level set at 2000 µmol $m^{-2}s^{-1}$. The leaf width was used to calculate leaf area inside the chamber. The leaf was left to acclimate until A and g_s reached stable values. Once the leaf was at steady state, the response curve was logged using the following light intensity values: 2000, 1800, 1500, 1200, 1000, 800, 600, 500, 400, 300, 200, 150, 100, 50, 25, 0, 2000 (µmol $m^{-2}s^{-1}$; 90% red, 10% blue light). The minimum wait time at each light level before the value was logged was set as 180 s, with a maximum wait of 300 s. IRGAs were matched after each log event.

For the A/C_i curves, the values of relative humidity, temperature and fan speed were the same as for the light response curves. Light intensity was set at 2000 µmol $m^{-2}s^{-1}$. A/C_i curves were carried out in 2 stages: for the first half of the curve, the flow rate was set at 200 µmol s^{-1}. The leaf was clamped as before and left to acclimate with reference CO_2 set at 400 µmol mol^{-1}. Once photosynthesis and stomatal conductance were stable, this was dropped in a stepwise manner as follows: 400, 300, 200, 100, 75, 50, 25, 5 µmol mol^{-1} (the minimum wait before logging was set at 90 s, with a maximum of 120s) before being brought back up to ambient. At this stage, flow was increased to 400 µmol s^{-1} and once the plant had re-acclimated to ambient air conditions, the reference CO_2 concentration was increased stepwise to 1600 µmol mol^{-1} (400, 500, 600, 800, 1000, 1300, 1600 µmol mol^{-1}), with a maximum wait time of 300 s (minimum of 180 s). After each point was logged, IRGAs were matched. For both sets of response curves, a minimum of five biological replicates was used and the same part of the leaf was clamped as for the light curves.

The excel fitting tool presented by Sharkey (2016) – updated from Sharkey *et al.*, (2007) was selected for its ease of use and because it fitted values informing of V_{cmax}, J, and g_m. This tool was used to fit these parameters for each curve and mean values were calculated for each genotype with leaf temperature adjusted to 21˚C. The default Γ* (photorespiratory compensation point) values from tobacco were used as it was deemed comparable to that previously measured for wheat (Walker *et al.*, 2017). Light response curves were also fitted using this tool – as per Buckley & Diaz-Espejo (2015) - and values of A_{sat} and Φ were estimated.

3.2.4. Quantification of chlorophyll content

Using a 0.4cm diameter cork borer, four leaf discs were excised from the region of the leaf blade upon which gas exchange analysis had been carried out. These were then instantly flash frozen in liquid nitrogen before being stored at -80˚C. When required, one leaf disc was removed from storage and its weight was determined. 200 µl of ice-cold 80% acetone (v/v) was added to each leaf disc along with three ball bearings (3 mm) in a screw-top eppendorf tube.

Once in acetone, samples were kept on ice and in the dark to stop degradation. Leaf tissue was ground using a MP Bio FastPrep system (MP Biomedicals, China). Samples were ground three times at 9.5 m/s for 30 seconds, or until homogenised. Tubes were then placed onto an orbital shaker and incubated on ice for a period of 15 minutes. 1 ml ice-cold 80% acetone was next pipetted into fresh eppendorf tubes and 100 µl of sample was added to each corresponding tube of acetone, before being spun for 15 minutes in a pre-cooled centrifuge (4˚C, 3000 rpm).
The chlorophyll content of each extraction was recorded using a Shimadzu UV-2600 spectrophotometer (Shimadzu, Kyoto, Japan). 1 ml of the supernatant of each sample was pipetted into a cuvette, and absorbance was measured against a blank of 80% acetone at wavelengths of 645 nm, 663 nm and 710 nm. Total chlorophyll (a + b) content was calculated from absorbance readings using the equations presented by Porra *et al.* (1989). Chlorophyll content was then expressed on a per area basis.

3.2.5. Total soluble protein quantification

Leaf discs (0.4 cm diameter) were taken from the leaf and flash frozen in liquid nitrogen and stored at -80˚C. When required, the weight of an individual leaf disc was measured and placed into a screw-top eppendorf tube. 500 µl of extraction buffer (100 mM Tris HCl buffer, pH 8; 100 mM $MgCl_2$, 1 mM EDTA, 0.05% (v/v) Triton X, 10 mM dithiothreitol (DTT), 50 mM 2-mercaptoethanol and H_2O) was added and this was ground using a MP Bio FastPrep homogeniser (MP Biomedicals, China). After grinding, a further 500 µl of extraction buffer was added to the sample and this was vortexed. Samples were then centrifuged at 4˚C for five minutes at 13000 rpm before the supernatant was removed and respun for a further five minutes at 13000 rpm and 4˚C. At this stage, samples were either aliquoted and then frozen at -80˚C for later analysis, or immediately used for the Bradford assay to estimate total protein content.

Bradford reagent has differing absorbance at 595 nm with differing protein contents. Standard curves were generated using bovine serum albumin (BSA) as the standard on a Shimadzu UV-2600 spectrophotometer (Shimadzu, Kyoto, Japan) (range of standard concentration = 0-20 µg/ml). A cuvette consisting of 50 µl extraction buffer and 950 µl Bradford reagent (Sigma-Aldrich, UK) was used as a blank, whereas 50 µl sample and 950 µl Bradford reagent was used for sample cuvettes. Cuvettes were left at room temperature for 20 minutes to incubate. Absorbance was tested against the standard curve, and protein content in µg ml^{-1} was estimated. This was converted to µg mg^{-1} using the leaf disc weight recorded previously.

3.2.6. Stable isotopes as an indicator of water use efficiency

Three frozen leaf discs from the middle third of the leaf blade were placed into screw-cap tubes and dried in a freeze drier overnight. These samples were then homogenised using a FastPrep (MP Biomedicals, China). Around 1 mg of ground, dried sample was weighed out and sealed into a tin capsule in a 96-well plate before being placed into an isotope ratio mass spectrometer (IRMS, Sercon, UK) at the Sheffield Biomics Facility to determine the $\delta^{13}C$ (carbon isotope composition) of the leaf

material relative to the PeeDee belemnite carbonate standard (PDB). $\Delta^{13}C$ values were calculated using equation 3.3 (Cernusak *et al.*, 2013).

Equation 3.3. $\Delta^{13}C$

$$\Delta^{13}C = \frac{\delta^{13}C_{air} - \delta^{13}C_{plant}}{1 + \delta^{13}C_{plant}}$$

3.2.7. Using µCT to investigate leaf developmental gradients

Seeds of the transgenic wheat line *TaEPF2-OE* (Dunn *et al.*, 2019) and its corresponding wild type (Fielder) were sown and grown up to leaf 5 as described previously. In order to examine the stomatal density gradient of the leaf, dental putty impressions were taken in three areas: towards the tip of the leaf, in the middle of the leaf and at the base of the leaf lamina adjacent to the ligule. Nail varnish impressions were created, and stomatal density counts made from these as described in 2.2.2. Plants were then transferred to the Hounsfield Facility at the University of Nottingham to be imaged using an X-ray µCT scanner.

For this process, a section of leaf towards the tip was excised from the plant and from this, a 5 mm leaf disc was removed, avoiding the midrib. Sample preparation and scan settings were as described in 3.2.2. Once the scan was completed, a second leaf section was taken from the middle of the leaf blade and the process was repeated (using the same side of the midrib as the previous leaf disc). A third sample of the leaf was taken from an area at the base of the leaf close to the ligule. Scans were processed as previously described and mesophyll porosity was determined for each region of the leaf blade.

3.2.8. Confocal analysis of the stomatal lineage

Seeds of the transgenic wheat line *TaEPF2-OE* and its corresponding wild type (Fielder) were sown on wetted filter paper in petri dishes, which were sealed with micropore tape and left to germinate in a growth cabinet (Snijders Scientific, 22˚C, 16h:8h). Dishes were observed until the first full leaf was visible. At this point, the seedling was dissected, removing the coleoptile to reach the developing leaves beneath. Leaf 2 was excised

before being fixed and bleached as in Chapter 2. Staining with 0.01% propidium iodide (PI) for 4 hours and clearing with a solution of 200 g chloral hydrate, 20 ml glycerol and 30 ml water (6 hours) was carried out prior to mounting and imaging using an Olympus FV1000 CLSM and Fluoview software (Tokyo, Japan). PI was excited using a 561nm HeNe561 diode laser (10-20% laser power). Stomatal complexes and stomatal precursors were imaged using a 20x objective (UPLSAPO 20x, NA: 0.75) to a depth of 10 µm (step size 0.3 µm) underneath the guard cells in order to identify the presence of substomatal cavities and observe mesophyll cell separation. Samples were imaged at 12.5 µs/pixel with an aspect ratio of 800 x 800 pixels. Micrographs of fully differentiated stomata and the subtending mesophyll layer were collected from the tip of the leaf primordia, whilst immature stomatal complexes and the sub-epidermal mesophyll cells below them were imaged from regions towards the base of the leaf. Stacks were collected as TIFF images and exported to ImageJ for processing.

3.2.8. Data analysis

Statistical analyses of the datasets were carried out using GraphPad Prism 8 (Graphpad Software Inc.). Datasets were assessed for normality and significant differences between lines were identified using one-way analysis of variance (ANOVA). When individual lines were compared with each other, significance was determined if $P = <0.01$. When grouped by ploidy level, significance was determined if $P = <0.05$. When detected, Tukey's HSD was used as a multiple comparisons test to determine significance in the differences in means between lines (to 99% or 95% confidence respectively). Comparisons between 4n wild and domesticated lines were carried out via the use of an unpaired, two-tailed *t* test ($P = <0.05$). When assessing the relationships between parameters, Pearson correlations were used ($P = 0.05$). All error bars on graphs indicate +/- one standard error of the mean (S.E.M.).

3.3. Results

3.3.1. Mesophyll porosity is positively correlated with stomatal density

In order to explore how ploidy level and/or associated changes in stomatal characteristics affected the amount of intercellular airspace within the leaf, I carried out analysis on mesophyll porosity (% airspace) values extracted from X-ray µCT datasets for a range of accessions representing 2n, 4n and 6n species of the Triticeae (summarised in Table 2.2). 3D reconstructions of leaf sections and 2D slices (transverse, longitudinal and paradermal sections) through µCT stacks of *T. urartu* (2n), *T. araraticum* (4n), and *T. aestivum* (6n) are shown in Figure 3.2. These images and reconstructions were provided by Craig Sturrock, Hounsfield Facility (University of Nottingham). From these images it is clear that whilst the mesophyll tissue (shown in green) is surrounded by a regular pattern of airspaces (yellow) in each ploidy level, there are differences in the size, distribution and amount of airspace between 2n, 4n and 6n leaves. From the numerical data extracted from these scans, it was apparent that there was significant variation between the wheat lines (Figure 3.3A) (ANOVA, $F_{(10,37)}$= 6.021, P= <0.0001). Details of the multiple comparisons tests for this figure, and for all subsequent figures presenting data from the full range of accessions in this chapter, are available in Appendix 2. When grouped by ploidy (Figure 3.3B), it was shown that ploidy level had a significant impact upon the mesophyll porosity of the leaf (ANOVA, $F_{(2,8)}$= 11.24, P= 0.0047). Whilst 2n and 4n lines could not be distinguished from one another at the 95% confidence interval, 2n leaves were found to have a significantly greater proportion of airspace (27.55%) than the leaves of hexaploid plants (20.89%). The mean mesophyll porosity of 4n plants, at 26.21%, was also found to be significantly different to that in the 6n leaves. Levels of mesophyll porosity between wild (26.54%) and domesticated (25.99%) tetraploid lines were found not to be statistically significantly different from one another (unpaired *t* test, $t_{(3)}$= 0.8870, P= 0.4404).

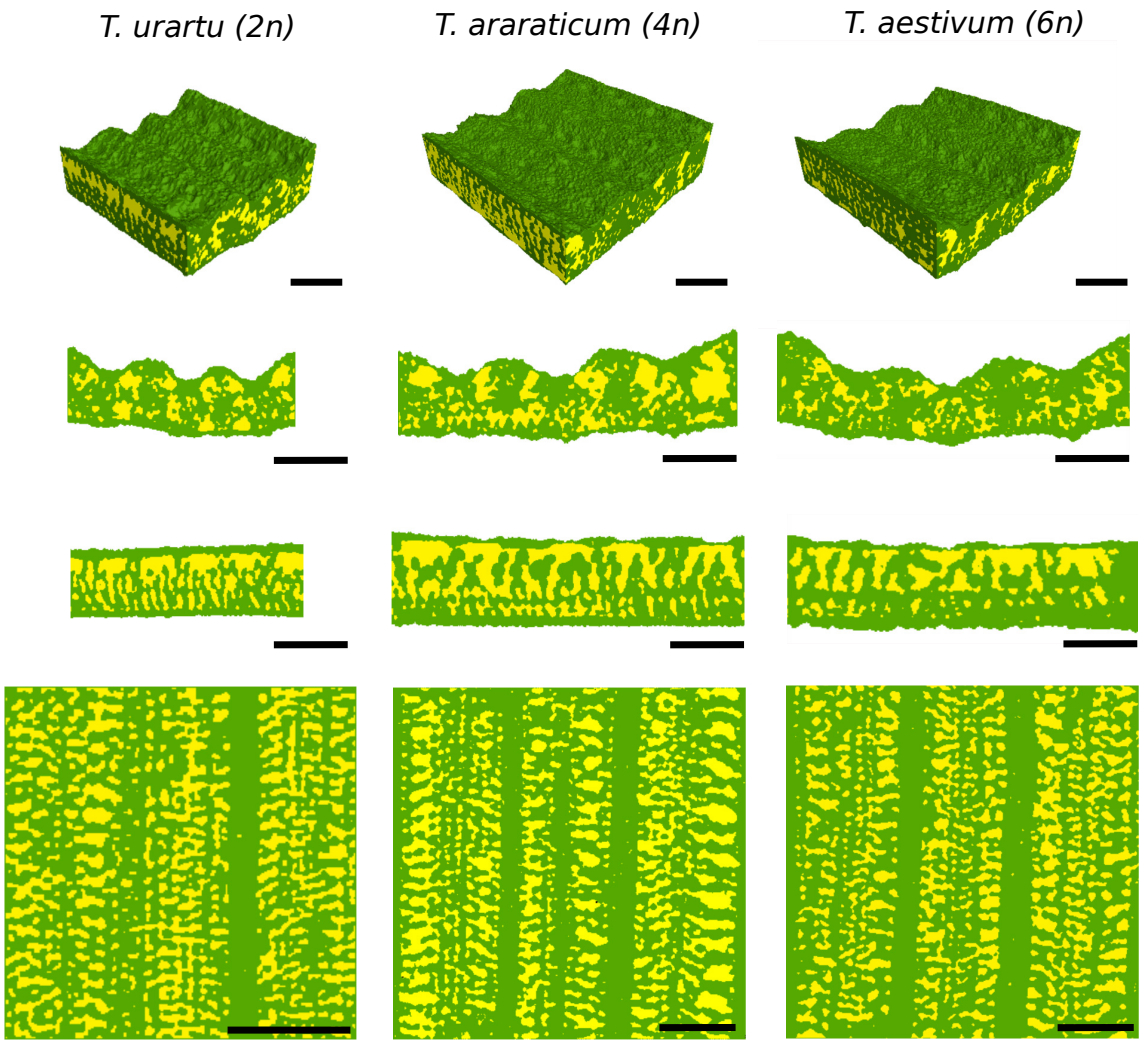

Figure 3.2. µCT reveals variation in leaf airspace between 2n, 4n and 6n genotypes
Sample images of *T. urartu* (2n), *T. araraticum* (4n) and *T. aestivum* cv. Cougar (6n). **A–C)** 3D renderings of tissue stacks. **D–F)** Transverse sections through the leaf sample. **G–I)** Longitudinal sections through the leaf sample. **J–L)** Paradermal sections through the leaf sample. Solid tissue is indicated by green and airspace by yellow. Scale bars = 200 µm.

In order to investigate the effect that changes in mesophyll porosity may have upon leaf level gas exchange, a correlation analysis between leaf airspace and stomatal conductance was carried out. (Figure 3.4A). It was found that there was a positive correlation between the amount of airspace in the leaf and g_s (Pearson correlation, r^2= 0.5293, P= 0.0112). Diploid genotypes typically had relatively high levels of both mesophyll porosity and g_s and 6n lines had lower amounts of porosity and stomatal conductance, with tetraploid lines being intermediate for both parameters. When lines were grouped into their respective ploidy levels (Figure 3.4B), this positive relationship remained, although the P value suggested that this was not statistically significant (Pearson correlation, r^2= 0.9803, P= 0.0897).

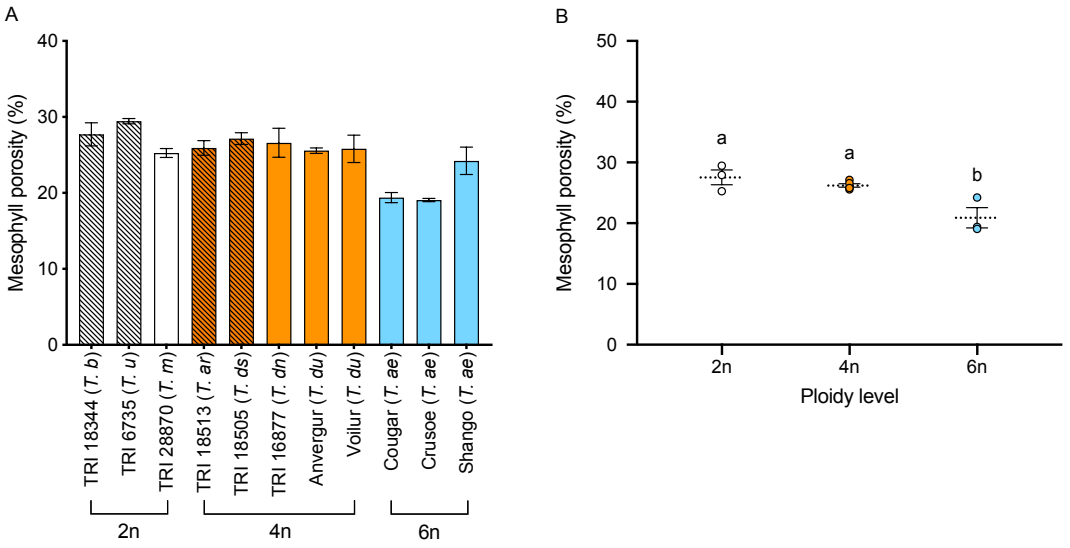

Figure 3.3. There is variation in mesophyll porosity between 2n, 4n and 6n wheat lines
A) Mean mesophyll porosity (%age airspace per volume) of the range of lines, including 2n, 4n and 6n species as indicated. Hatched bars indicate wild lines, solid bars are domesticated cultivars. A summary of lines is shown in Table 2.2. **B)** Mean mesophyll porosity of 2n, 4n and 6n wheat accessions, with data grouped from those shown in (A). Samples indicated with the same letter cannot be distinguished from one another (P= <0.05) (Tukey HSD post one-way ANOVA). Error bars = S.E.M. n = minimum of 3 per line.

Another important structural parameter of the mesophyll that can influence gas exchange is the amount of mesophyll surface area exposed to the intercellular airspaces. X-Ray µCT analysis also allows for quantitative data on this parameter to be extracted from 3D stacks of leaf tissue. Although it might be expected that the changes in leaf porosity associated with shifts in ploidy level described above would result in changes in S_{mes}, this parameter did not vary significantly across the range of 2n, 4n and 6n lines that were scanned (ANOVA, $F_{(10,44)}$= 1.896, P=0.0716)(see Figure 3.5A). When means were grouped by ploidy level (Figure 3.5B), it was found that diploid lines had the highest exposed mesophyll surface area per tissue volume (69.06 mm^{-1}), hexaploids the lowest S_{mes} (55.955 mm^{-1}), whilst tetraploid lines were intermediate (62.77 mm^{-1}), although these were again not found to be significantly different from one another although the P value was close to 95% confidence level (ANOVA, $F_{(2,8)}$= 4.282, P= 0.0544). When differences between 4n wild and 4n cultivated varieties were investigated, it was found that domestication has not resulted in significant changes in S_{mes} within the tetraploids (unpaired t test, $t_{(3)}$= 0.9632, P= 0.4065).

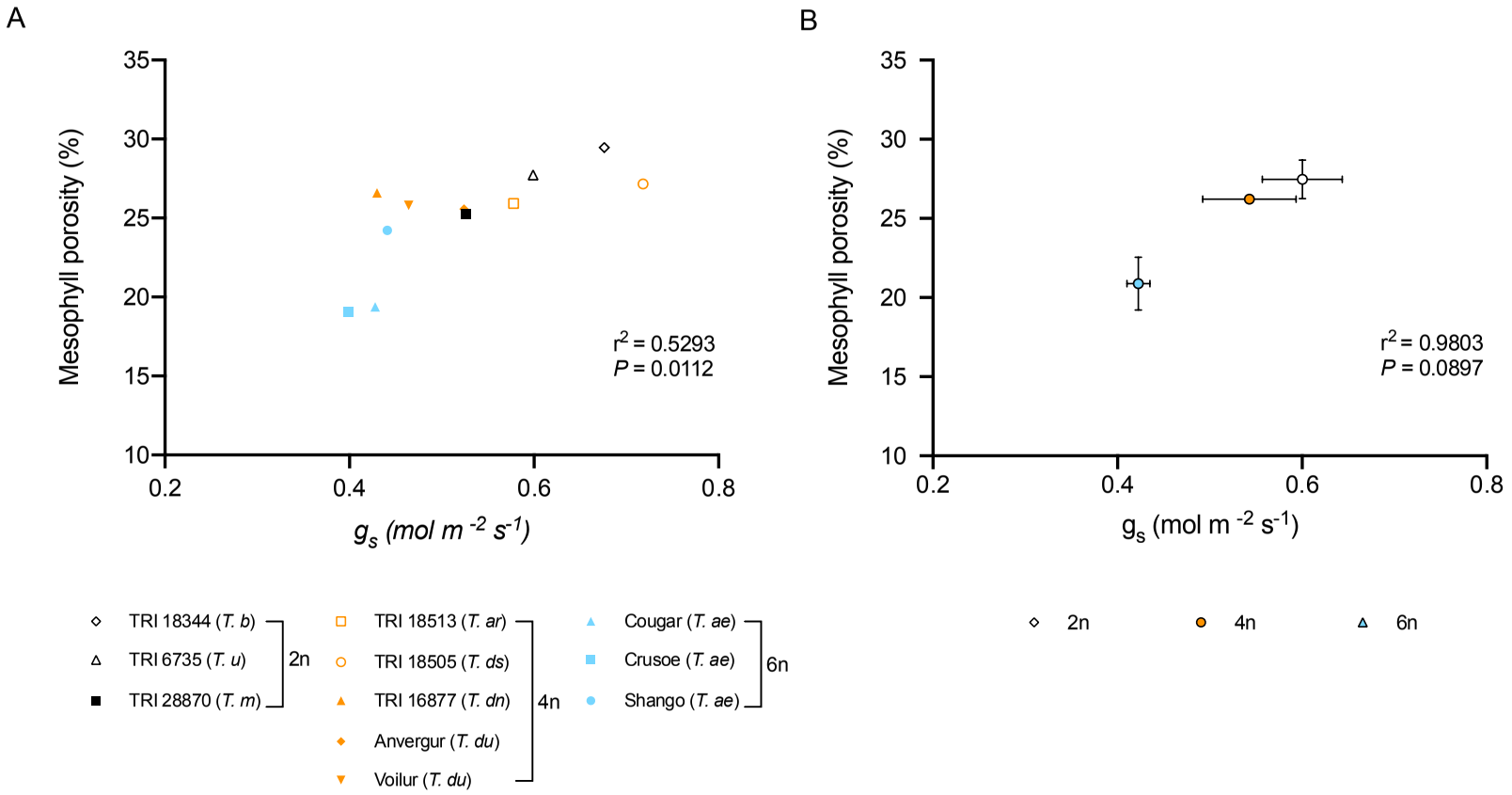

Figure 3.4. There is a positive correlation between mesophyll porosity and stomatal conductance (g_s) in the Triticeae with varying ploidy level
A) Mean mesophyll porosity plotted against mean stomatal conductance for each of the lines investigated – as summarised in Table 2.2. Symbols with no fill indicate wild lines, solid symbols are domesticated cultivars. **B)** Mean mesophyll porosity plotted against mean stomatal conductance with data from (A) grouped into their respective ploidy levels. Results of correlation analyses are presented (Pearson r^2 value). Error bars = S.E.M. n = minimum of 3 per line.

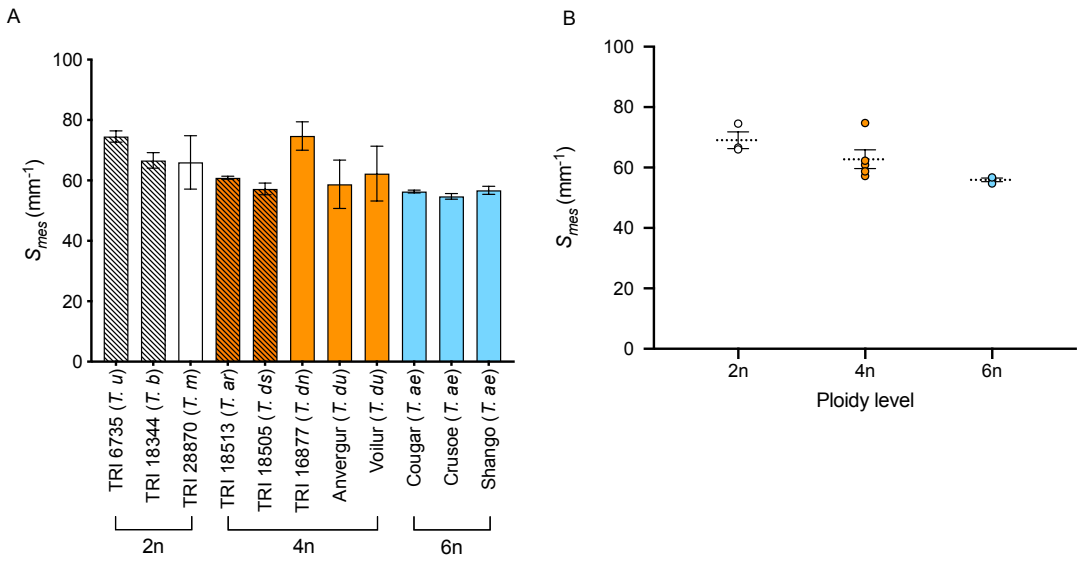

Figure 3.5. Exposed mesophyll surface area does not vary significantly between 2n, 4n and 6n *Triticum* lines
A) Mean S_{mes} (per tissue volume) for a range of 2n, 4n and 6n wheat accessions as indicated in Table 2.2. Hatched bars indicate wild lines, solid bars are domesticated cultivars. **B)** Mean S_{mes} when wheat lines from (A) are grouped into 2n, 4n and 6n, ploidy levels. Error bars = S.E.M. n= minimum of 3 per line.

3.3.2. Photosynthetic responses to changing levels of irradiance do not change significantly with ploidy level

In order to further investigate whether differences in ploidy level and the associated variation in leaf structural parameters has an effect on the response of photosynthesis to changing light intensity, light response curves were analysed for a range of lines of 2n, 4n and 6n wheat species (Table 2.2). These curves are shown in Figure 3.6. Initial observations of the curves suggest that there are clear differences in the responses to irradiance. This potential variation was further explored via a curve fitting approach. Light response curves also indicate the appropriate light intensity to be set when carrying out CO_2 response curves to further elucidate any differences in photosynthesis.

When the light saturated photosynthetic rate for each of the genotypes was plotted (Figure 3.7A), it was found that there was no significant variation between lines in A_{sat} (ANOVA, $F_{(10,58)}$= 1.841, P= 0.0733). However, when genotypes were grouped by ploidy level (Figure 3.7B), it was shown that ploidy level had a significant effect upon CO_2 assimilation under saturating light (ANOVA, $F_{(2,8)}$= 9.083, P= 0.0087). Hexaploid cultivars had

the lowest A_{sat} (33.59 µmol m^{-2} s^{-1}), whilst this was highest in diploid accessions (37.02 µmol m^{-2} s^{-1}) and middling for tetraploid genotypes (34.08 µmol m^{-2} s^{-1}), and the 2n group was found to have a significantly higher mean A_{sat} than 4n and 6n lines. When the differences in A_{sat} between wild and domesticated tetraploid lines were investigated, it was found that domestication status did not have a significant effect upon light-saturated photosynthesis (unpaired *t* test, $t_{(3)}$= 0.1202, *P*= 0.9119), with wild varieties having a mean A_{sat} of 34.17 µmol m^{-2} s^{-1}, in comparison to 34.02 µmol m^{-2} s^{-1} in cultivated accessions.

In addition to determining $A_{sat,}$ light response curves can also inform of differences in other photosynthetic parameters. One such parameter is the apparent quantum yield of photosynthesis (Φ), estimated from the linear portion of the curve. Figure 3.7C shows that there was significant variation in this parameter amongst all of the lines under investigation (ANOVA, $F_{(10,55)}$= 5.500, *P*= <0.0001). When varieties were grouped into their respective ploidy levels (Figure 3.7D), the only significant differences in Φ were found between the 4n (0.2570 µmol $µmol^{-1}$) and 6n groups (0.3414 µmol $µmol^{-1}$) (ANOVA, $F_{(2,8)}$=8.129, *P*= 0.0118). 2n lines (0.2996 µmol $µmol^{-1}$) could not be distinguished from either of the other ploidy groups. Similarly to A_{sat}, domestication was not found to have a significant effect upon the apparent quantum yield of tetraploid wheat (unpaired *t* test, $t_{(3)}$= 0.7015, *P*= 0.5335), with wild lines having a similar Φ (0.2446 µmol $µmol^{-1}$) to lines of the domesticated species.

3.3.1. Plants of different ploidy levels vary in their response to changes in CO_2 concentration

In order to observe any differences in photosynthetic responses to changing CO_2 concentrations with change in ploidy level, A/C_i curves were carried out for each of the lines under investigation. The fitting of curves generated using this technique allowed for a spectrum of parameters to be elucidated.

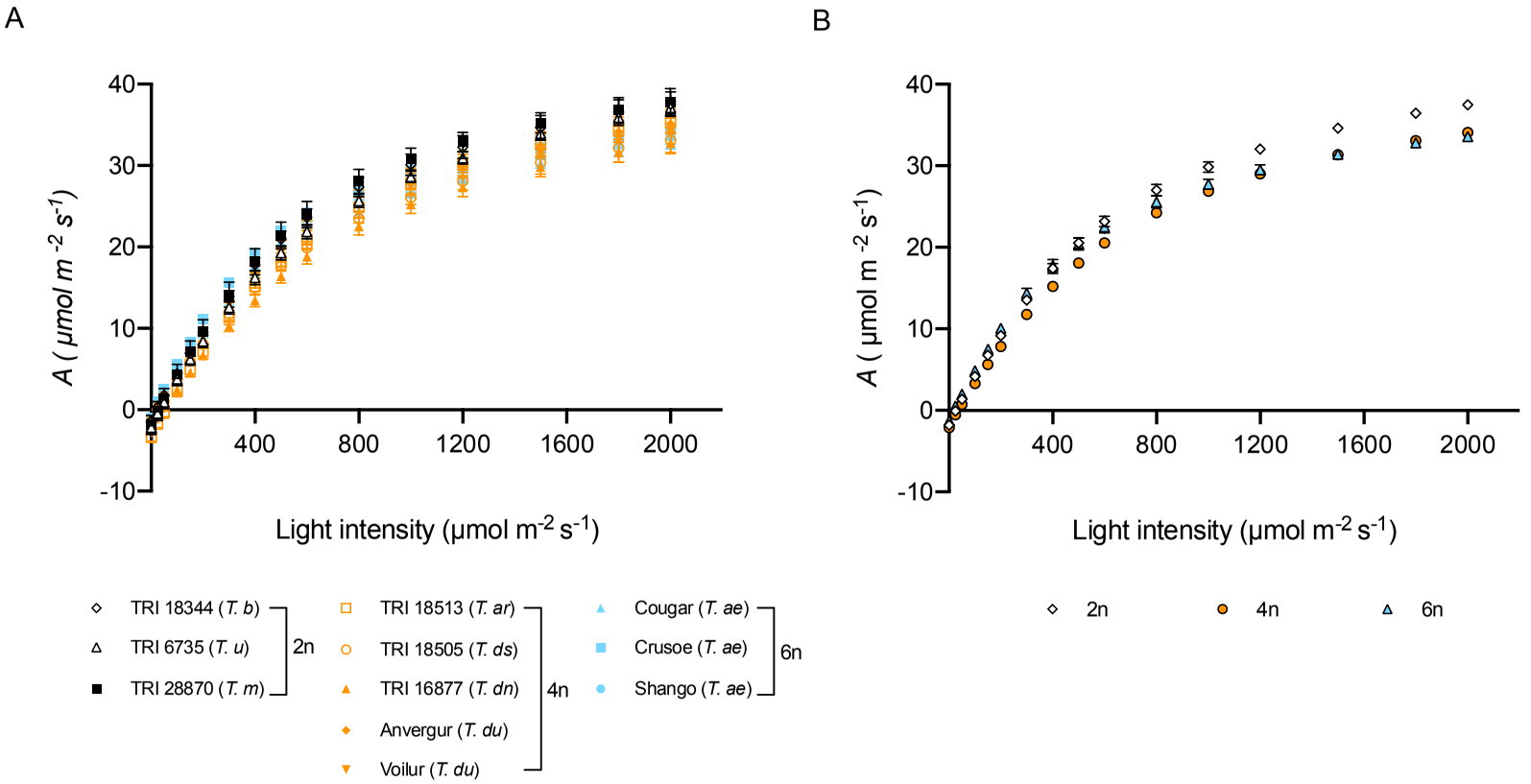

Figure 3.6. CO_2 assimilation response to changing irradiance levels in 2n, 4n and 6n accessions of the Triticeae
A) Mean light response curves for a range of 2n, 4n and 6n wheat lines as indicated in Table 2.2. Mean values of *A* are shown for each light level. Symbols with no fill indicate wild lines, solid symbols are domesticated cultivars. **B)** Mean light response curves when lines from (A) are grouped by their respective ploidy levels. Error bars = S.E.M. n= minimum of 5 per line.

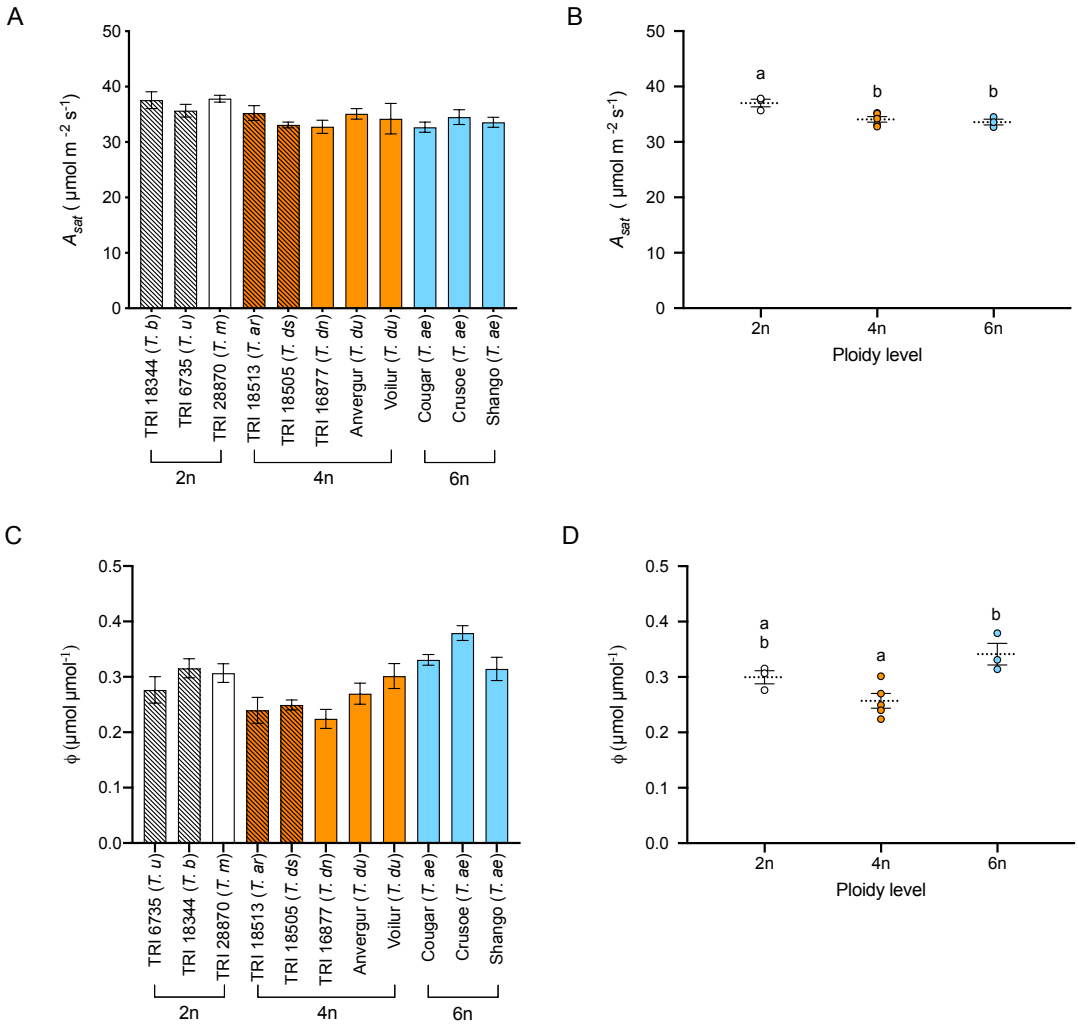

Figure 3.7. A_{sat} and apparent quantum yield values extracted from light response curves vary amongst the Triticeae
A) Mean A_{sat} values for a range of 2n, 4n and 6n wheat varieties as indicated in Table 2.2. Hatched bars indicate wild lines, solid bars are domesticated cultivars.**B)** Mean A_{sat} when lines from (A) are grouped into 2n, 4n and 6n ploidy level. **C)** Mean Φ (apparent quantum yield) values for each of the 2n, 4n and 6n accessions of the Triticeae under investigation – see Table 2.2. for an overview of the lines used. Hatched bars indicate wild lines, solid bars are domesticated cultivars. **D)** Mean Φ when data from (C) are grouped by ploidy level. Samples indicated with the same letter cannot be distinguished from one another (P= <0.05) (Tukey HSD post one-way ANOVA). Error bars = S.E.M. n= minimum of 5 per line.

The A/C_i curves indicate that, for hexaploid cultivars, assimilation saturates at a lower C_i than their diploid counterparts, with tetraploid lines once again being shown to be intermediate (Figure 3.8). The 4n accessions were also seen to display higher variation than the other ploidy levels. These differences are more easily identifiable when lines are grouped and means of each ploidy level are plotted (Figure 3.8B). In addition to saturating at a lower C_i, the A_{max} can be seen to be lower in 6n lines, intermediate in 4n plants and highest in 2n plants. Once again there appeared to be greater variation in the 4n lines for this parameter.

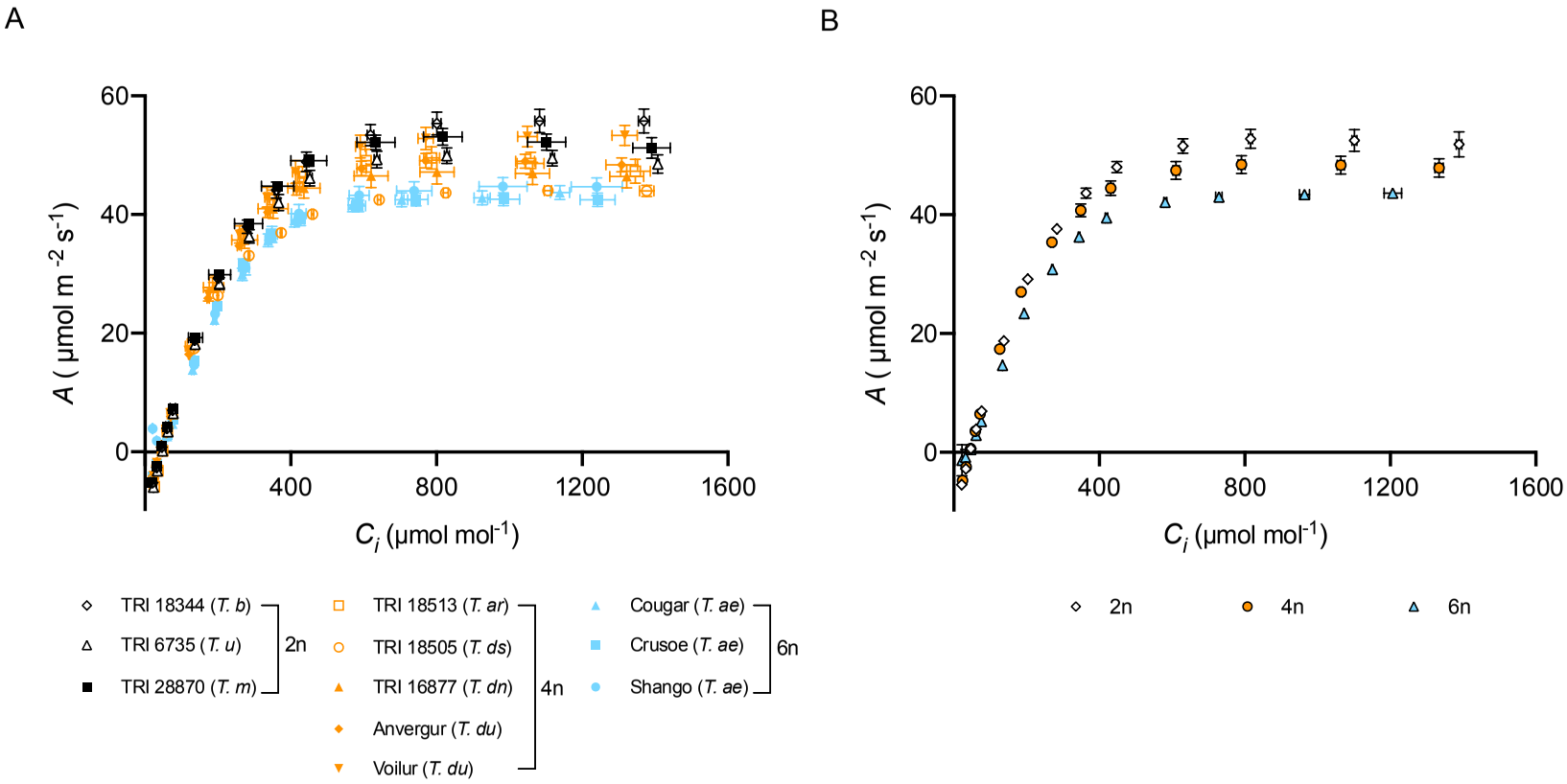

Figure 3.8. The response of CO_2 assimilation to shifts in C_i varies between 2n, 4n and 6n wheat lines
A) *A/Ci* curves for each of the wheat genotypes of varying ploidy levels, 2n, 4n and 6n (as indicated – lines used summarised in Table 2.2). Symbols with no fill indicate wild lines, solid symbols are domesticated cultivars. **B)** Mean *A/Ci* curves when data from (A) are grouped by ploidy level. Error bars = S.E.M. n = minimum of 5 per line.

When mean C_i at a reference CO_2 concentration of 1600 µmol mol^{-1} was graphed for each line under investigation (Figure 3.9A), it was shown that there was significant variation in the maximum C_i (ANOVA, $F_{(10,57)}$=4.144, P= 0.0003). When grouped by ploidy level (Figure 3.9B), it was found that 2n plants reached a significantly higher C_i (1389 µmol mol^{-1}) than 6n leaves (1207 µmol mol^{-1}) at a reference CO_2 value of 1600 µmol mol^{-1} (ANOVA, $F_{(2,8)}$= 19.80, P= 0.0008). Tetraploid varieties were also found to have a significantly higher C_i (1389 µmol mol^{-1}) than 6n cultivars, but this was not statistically distinguishable from that of 2n accessions. When the impact of domestication upon the C_i of tetraploids was further explored, it was found that here was no significant difference between wild and cultivated varieties (unpaired t test, $t_{(3)}$= 0.005941, P= 0.9996). In fact, the mean C_i was shown to be almost the same for wild and domesticated accessions (1334.31 µmol mol^{-1} and 1334.30 µmol mol^{-1} respectively).

Likewise, plotting A_{max} values (assimilation rate at a reference CO_2 concentration of 1600 µmol mol^{-1}) (Figure 3.9C) showed that there is significant variation in photosynthetic capacity within the 11 lines of the Triticeae under investigation (ANOVA, $F_{(10,57)}$=9.423, P= <0.0001). Once again, when grouped by ploidy level, it was also found that ploidy level (Figure 3.9D) had a significant effect upon A_{max} (ANOVA, $F_{(2,8)}$= 5.285, P= 0.0344). Diploid accessions were found to have a higher A_{max} (51.85 µmol m^{-2} s^{-1}), than 6n lines (43.62 µmol m^{-2} s^{-1}) at the 95% confidence limit. It was not possible to distinguish differences between 2n and 4n (47.89 µmol m^{-2} s^{-1}) groups or the 4n and 6n groups post-hoc Tukey test. Again, when the effect of domestication status in tetraploid accessions of the Triticeae was investigated, it was observed that there was no significant difference in photosynthetic capacity between lines of wild (*T. araraticum* and *T. diccocoides*) and domesticated (*T. diccocon* and *T. durum*) species, which had A_{max} values of 45.65 µmol m^{-2} s^{-1} and 49.38 µmol m^{-2} s^{-1} correspondingly (unpaired t test, $t_{(3)}$= 0.005941, P= 0.9996).

Fitting CO_2 response curves also allows for photosynthetic biochemistry parameters to be estimated. For example, it appears that the initial slopes of the A/C_i curves are steepest for the diploid lines (Figure 3.8), suggesting differences in the carboxylation efficiency of Rubisco between lines (which can be derived from this slope). When V_{cmax} was fitted from

the CO_2 response curves, it was found that this varied significantly across the genotypes under investigation ($F_{(10,60)}$= 8.781, P= <0.0001) – see Figure 3.10A.

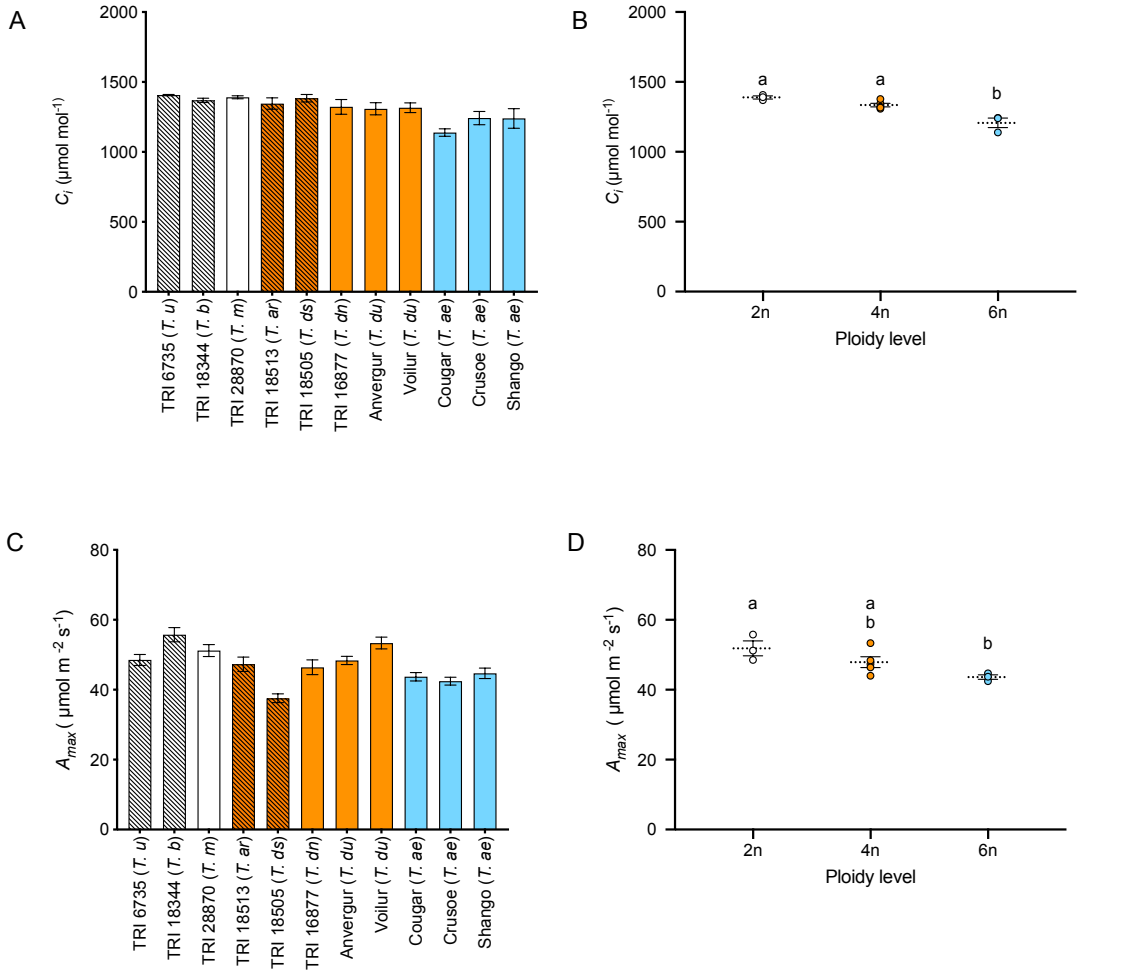

Figure 3.9. Variation in C_i and A_{max} values at high CO_2 concentrations between 2n, 4n and 6n members of the Triticeae
A) Mean C_i at a reference CO_2 value of 1600 µmol mol^{-1} for lines across the three ploidy levels (2n, 4n ,6n), as indicated. See Table 2.2 for key to accession data. Hatched bars indicate wild lines, solid bars are domesticated cultivars. **B)** Mean C_i at a CO_2R value of 1600 µmol mol^{-1}, data grouped from those shown in (A). **C)** Mean A_{max} across a range of 2n, 4n and 6n wheat accessions – as indicated. The lines used are summarised in Table 2.2. Hatched bars indicate wild lines, solid bars are domesticated cultivars. **D)** A_{max} grouped by ploidy level, data grouped from those shown in (C). Samples indicated with the same letter cannot be distinguished from one another (P= <0.05). (Tukey HSD post one-way ANOVA). Error bars= S.E.M. n = minimum of 5 per line.

Once again, trends were more clearly visible when the accessions were grouped by ploidy level (Figure 3.10B). It was shown (ANOVA, $F_{(2,8)}$= 11.36, P= 0.0046) that V_{cmax} was significantly higher in 2n plants (243.57 µmol m^{-2} s^{-1}) than 6n accessions (160.968 µmol m^{-2} s^{-1}). Tetraploid lines had a V_{cmax} (212.692 µmol m^{-2} s^{-1}) that was not distinguishable from that of 2n lines,

but was significantly different in comparison to the V_{cmax} of 6n genotypes). Fitted values of V_{cmax} were found not be significantly impacted by domestication, with wild 4n (205.9 µmol m^{-2} s^{-1}) and domesticated 4n (217.2 µmol m^{-2} s^{-1}) lines having similar carboxylation efficiency (unpaired *t* test, $t_{(3)}$= 0.3775, *P*= 0.7309).

The electron transport rate, *J*, was also fitted from the A/C_i curves (Figure 3.10C). Whilst the lines were once again shown to contain significant variation for this parameter ($F_{(10,60)}$= 7.907, *P*= <0.0001). When grouped by ploidy level (Figure 3.10D), an ANOVA followed by a post-hoc Tukey's HSD ($F_{(2,8)}$= 11.36, *P*= 0.0046) showed that 2n lines had a higher rate of electron transport (288.874 µmol m^{-2} s^{-1}) than 4n (264.705 µmol m^{-2} s^{-1}) and 6n lines (237.152 µmol m^{-2} s^{-1}). The only significant difference in *J* between groups was found between the means of the 2n and 6n ploidy levels. As with the previous parameters extracted from the CO_2 response curves, *J* was also shown not be significantly affected by domestication within the tetraploid group of lines (unpaired *t* test, $t_{(3)}$= 0.5110, *P*= 0.6446). Wild accessions were shown to have a mean fitted electron transport rate of 254.6 µmol m^{-2} s^{-1}, whilst this was 267.7 µmol m^{-2} s^{-1} in the cultivated lines.

3.3.2. There are no clear trends between ploidy level and mesophyll conductance

Mesophyll conductance (g_m) has been hypothesised to have a significant limiting effect upon photosynthesis. It would be expected that the changes in internal architecture, i.e, the amount of airspace shown previously, could have a significant effect upon this parameter. Fitting the A/C_i curves to the FvCB model of photosynthesis, as described above, allowed for estimates of g_m to be made. Once again, it was shown (Figure 3.11A) that g_m varied significantly between the 11 lines investigated ($F_{(10,60)}$= 3.554, *P*= 0.0010). When lines were grouped by ploidy level (Figure 3.11B), it was found that there was significant variation in the rate of g_m (ANOVA, $F_{(2,8)}$= 4.666, *P*= 0.0454), although a post-hoc Tukey test was unable to distinguish which of the groups were contributing to the observed variation. Tetraploid plants were found to have the highest fitted g_m (4.836 µmol m^{-2} s^{-1} Pa^{-1}), whilst this was lower for diploid and

hexaploid genotypes (3.984 µmol m^{-2} s^{-1} Pa^{-1} and 4.029 µmol m^{-2} s^{-1} Pa^{-1} respectively). Once again it was found that domestication status did not have a significant effect upon g_m within the 4n ploidy level (unpaired *t* test, $t_{(3)}$= 0.3504, *P*= 0.7492), although wild lines had a slightly higher mesophyll conductance (4.940 µmol m^{-2} s^{-1} Pa^{-1}) in comparison to the domesticated wheat varieties (4.766 µmol m^{-2} s^{-1} Pa^{-1}).

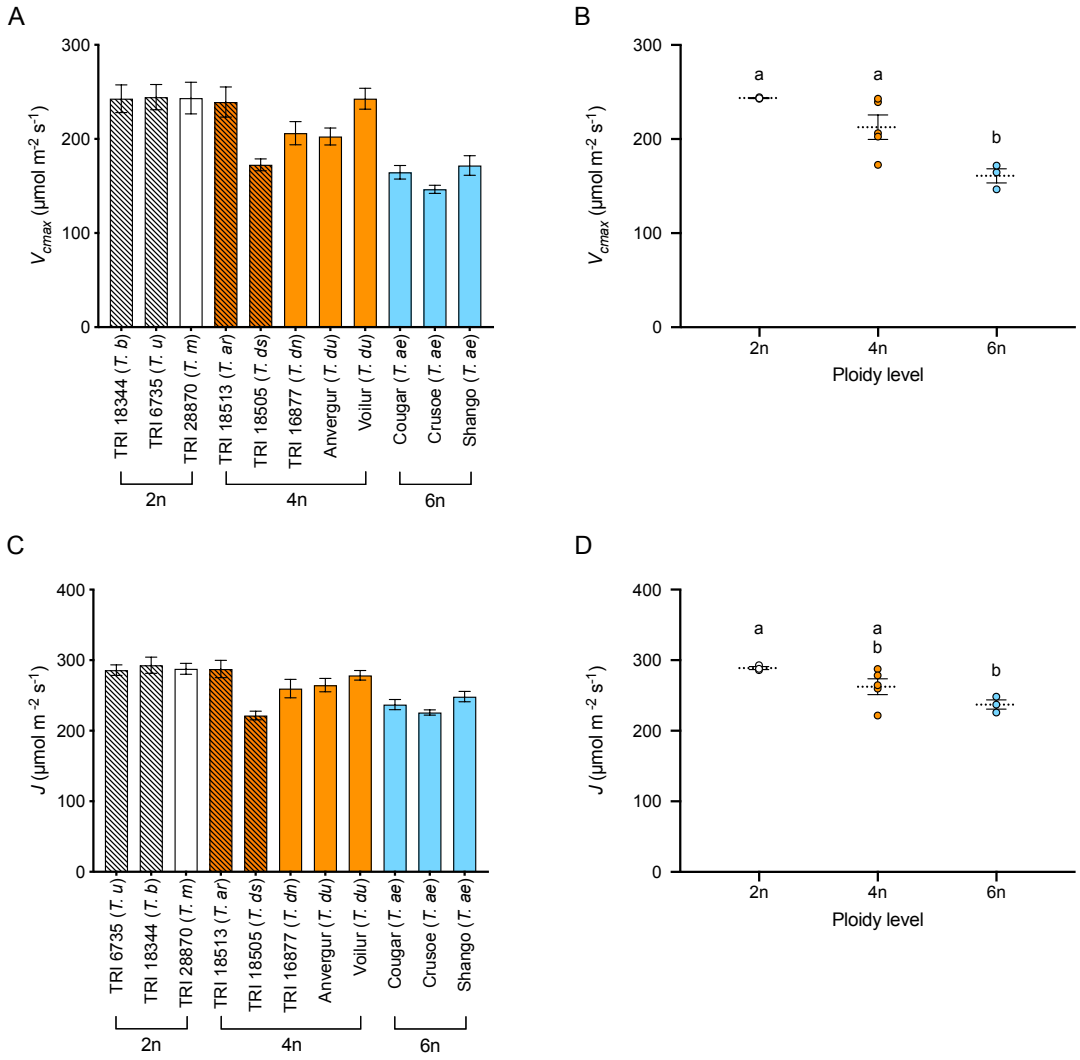

Figure 3.10. There is variation in photosynthetic biochemistry between 2n, 4n and 6n lines of the Triticeae
A) Mean fitted V_{cmax} values for the lines under investigation, including 2n, 4n and 6n species – as summarised in Table 2.2. Hatched bars indicate wild lines, solid bars are domesticated cultivars. **B)** Mean V_{cmax} values from (A) grouped into their respective ploidy levels: 2n, 4n and 6n. **C)** Mean fitted *J* for a range 2n, 4n and 6n varieties – as indicated, see Table 2.2. for key to accession data. Hatched bars indicate wild lines, solid bars are domesticated cultivars. **D)** Mean *J* values of 2n, 4n and 6n wheat lines taken from (A), grouped into each ploidy level. Datapoints indicated with the same letter (where shown) cannot be distinguished from each other (*P*= <0.05) (Tukey HSD post one-way ANOVA). Error bars = S.E.M. n = minimum of 5 per line.

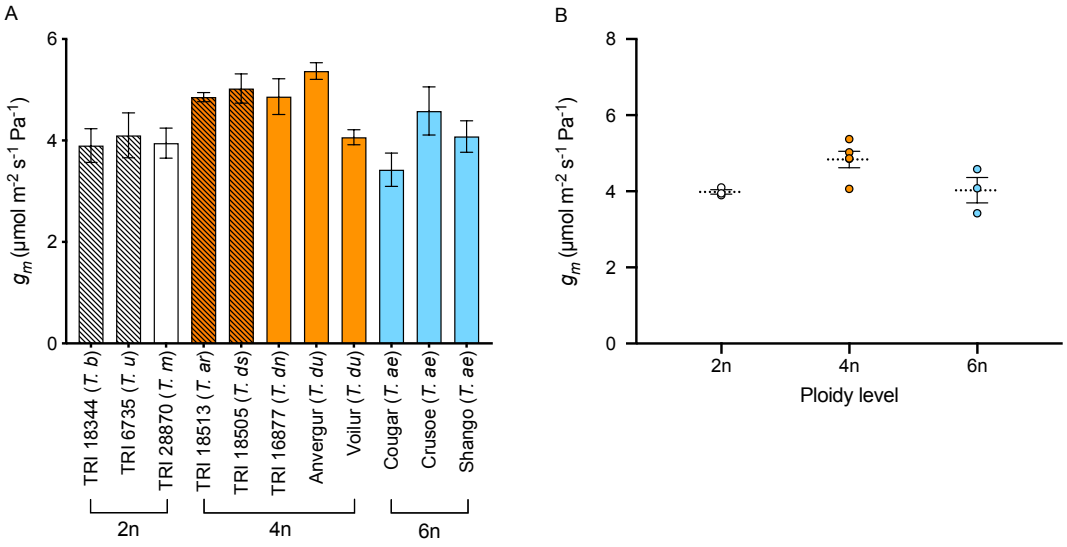

Figure 3.11. Variation in mesophyll conductance in wheat lines of different ploidy
A) Mean fitted g_m values for each of the *Triticum* lines selected, including 2n, 4n and 6n species – as summarised in Table 2.2. Hatched bars indicate wild lines, solid bars signify domesticated cultivars. **B)** Fitted g_m from (A) grouped by ploidy level; 2n, 4n and 6n. Error bars = S.E.M. n = minimum of 5 per line.

3.3.3. There is variation in chlorophyll and total soluble protein content in the Triticeae

Whilst leaf structure plays an important role in determining the photosynthetic rate, it is also important to collect information regarding pigment content and protein content (used as a proxy for the Rubisco content of the leaf) in order to fully explore any differences in photosynthesis since these can also clearly have an impact. When leaf chlorophyll was extracted, it was shown that there was significant variation amongst the wheat lines (Figure 3.12A) in the mean chlorophyll $a + b$ content per leaf area (ANOVA, $F_{(10,53)}$= 3.283, P= 0.0023). However, when genotypes were grouped by ploidy level (Figure 3.12B) it was found that, whilst the chlorophyll content per leaf area was highest in 6n lines (1.004 mg mm^{-2}), this was not significantly different (ANOVA, $F_{(2,8)}$= 1.094, P= 0.3803) to values extracted from 2n (0.866 mg mm^{-2}) and 4n plants (0.868 mg mm^{-2}). Despite the apparent trend of higher chlorophyll content in 6n leaves being visible by eye, the limited number of sample points makes statistical interpretation more difficult. When chlorophyll content was compared between wild and domesticated accessions of the tetraploid group, it was observed that domestication status had no

significant impact upon chlorophyll content per leaf area (unpaired *t* test, $t_{(3)}$= 0.3059, *P*= 0.7797). Lines of *T. diccocoides* and *T. araraticum* (0.844 mg mm^{-2}) were shown to have a similar mean chlorophyll content to that recorded in the leaves of *T. dicoccon* and *T. durum* cultivars (0.885 mg mm^{-2}).

Analysis of protein extracts indicated similar results (Figure 3.12C), with significant differences in total soluble protein per leaf fresh weight being observed when all of the varieties were compared to one another (ANOVA, $F_{(10,53)}$=2.719, *P*= 0.0093). However, when these were grouped into their respective ploidy levels (Figure 3.12D), there appeared to be a visible trend with genome size and protein content. Diploid plants had the highest protein content (7.308 µg mg^{-1}) whilst this was lower in the tetraploid and hexaploid accessions, which were similar to one another (5.582 µg mg^{-1} and 5.484 µg mg^{-1} respectively). Despite this, the limited number of sample points once again made statistical interpretation difficult, and was shown that there were no significant differences in the amount of protein (ANOVA, $F_{(2,8)}$= 4.134, *P*= 0.0585) between 2n, 4n and 6n lines. Nevertheless, as with chlorophyll content, mean leaf total soluble protein of tetraploid lines was shown to not be significantly different from one another in 4n wild (6.027 µg mg^{-1}) and 4n cultivated lines (5.286 µg mg^{-1}) (unpaired *t* test, $t_{(3)}$= 0.3059, *P*= 0.7797).

3.3.4. There are no significant differences in $\Delta^{13}C$ with ploidy level

In order to estimate lifetime water use efficiency, carbon isotope discrimination values ($\Delta^{13}C$) were calculated for a range of 2n, 4n and 6n genotypes of the Triticeae. Statistical analysis showed that although there was a trend with higher ploidy levels having a lower $\Delta^{13}C$, the limited sample number made statistical interpretation tricky, and as such no significant variation was in $\Delta^{13}C$ amongst the lines under investigation, although this was close to the 95% confidence limit (ANOVA, $F_{(10,11)}$= 2.794, *P*= 0.0534) (Figure 3.13A). However, when grouped by ploidy level (Figure 3.13B), it was found that carbon isotope discrimination was significantly lower (‰ difference from the standard) in hexaploid lines (29.74‰) than tetraploid (31.23‰) and diploid varieties (32.17‰), which could not be distinguished from one another via a post-hoc Tukey test (ANOVA, $F_{(2,8)}$= 13.05, *P*= 0.0030). When wild (31.29‰) and domesticated tetraploid lines

(31.18‰) were compared, it was shown that there was no significant difference in $\Delta^{13}C$ between these groups (unpaired *t* test, $t_{(3)}$= 0.8976, *P*= 0.8976).

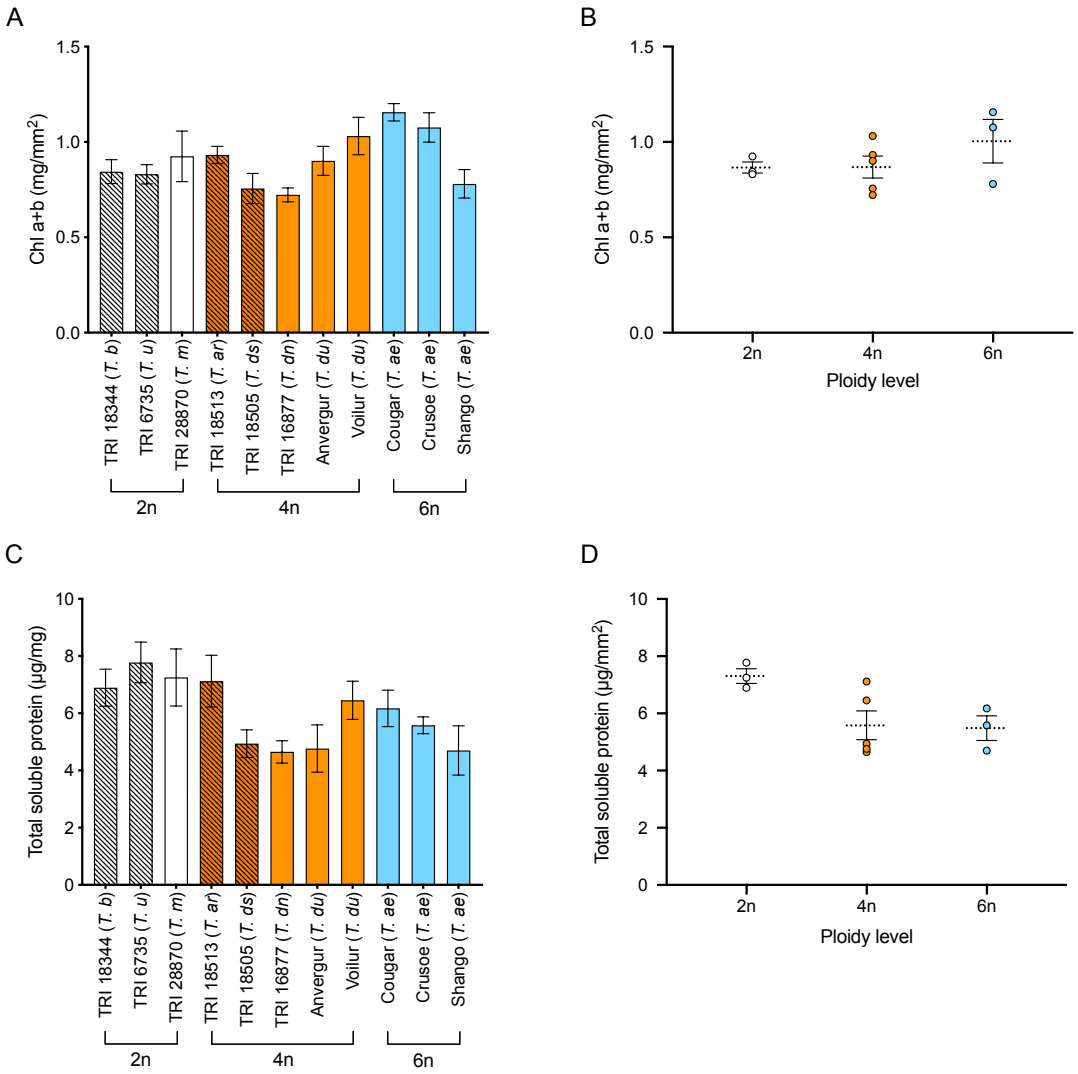

Figure 3.12. There is variation in leaf chlorophyll and total soluble protein
A) Mean chlorophyll content per leaf area for each of the 2n, 4n and 6n lines under investigation (see Table 2.2 for a summary). Hatched bars indicate wild lines, solid bars are domesticated cultivars. **B)** Leaf chlorophyll content per unit area from (A) grouped by ploidy level as indicated. **C)** Mean total soluble protein per leaf fresh weight for each of the 2n, 4n and 6n lines under investigation (see Table 2.2 for a summary). Hatched bars indicate wild lines, solid bars are domesticated cultivars. **D)** Total soluble protein levels when lines from (C) categorised into their respective ploidy levels. Error bars = S.E.M. n = minimum of 5 per line.

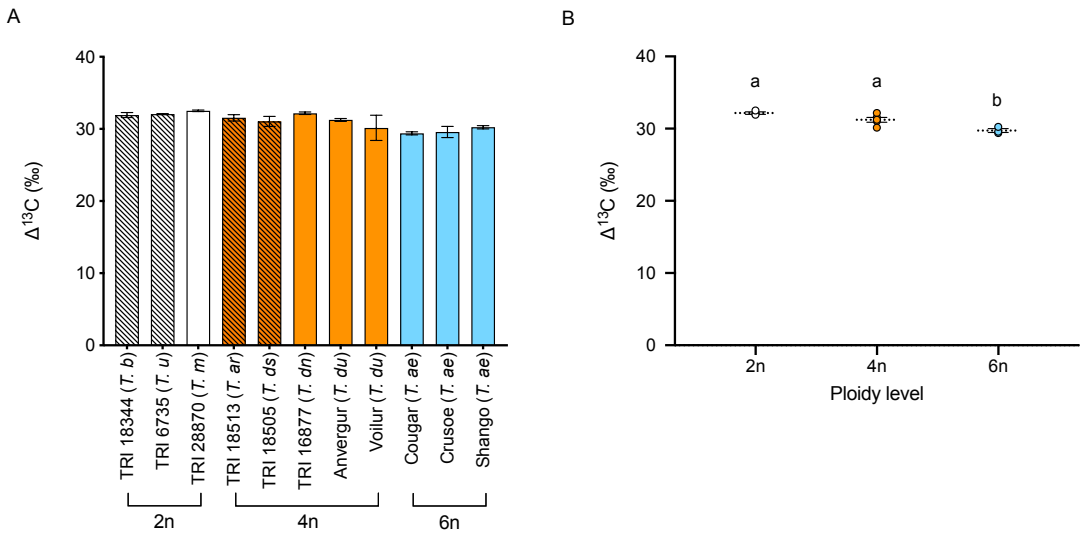

Figure 3.13. Carbon isotope discrimination ($\Delta^{13}C$) values for a range of 2n, 4n and 6n wheat lines
A) Mean $\Delta^{13}C$ for leaf material of each of the lines under investigation (2n, 4n or 6n as indicated). See Table 2.2 for accession data. Hatched bars indicate wild lines, solid bars are domesticated cultivars. **B)** Mean $\Delta^{13}C$ grouped by ploidy level, data taken from (A). Datapoints indicated with the same letter cannot be distinguished from each other (P= <0.05) (Tukey HSD post one-way ANOVA). Error bars = S.E.M. n = minimum of 2 per line.

When a correlation analysis was performed of $\Delta^{13}C$ values against the mean iWUE values as calculated in the previous chapter (Figure 3.14A), it was found that there was a significant negative correlation (Pearson correlation, r^2= 0.429, P= 0.0287), with plants having a lower $\Delta^{13}C$ being found to have a higher iWUE. When grouped into 2n, 4n and 6n ploidy levels (Figure 3.13B), this negative correlation was found to be even stronger (Pearson correlation, r^2= 0.995, P= 0.0474).

3.3.5. Sub-stomatal cavities and intercellular airspaces form after the stomata have gained full function

The correlation between porosity and g_s shown above suggests a potential relationship between stomatal formation and the formation of leaf airspace. I investigated this further with a series of experiments to test the hypothesis that functional stomata are required for the formation of airspaces beneath the epidermis.

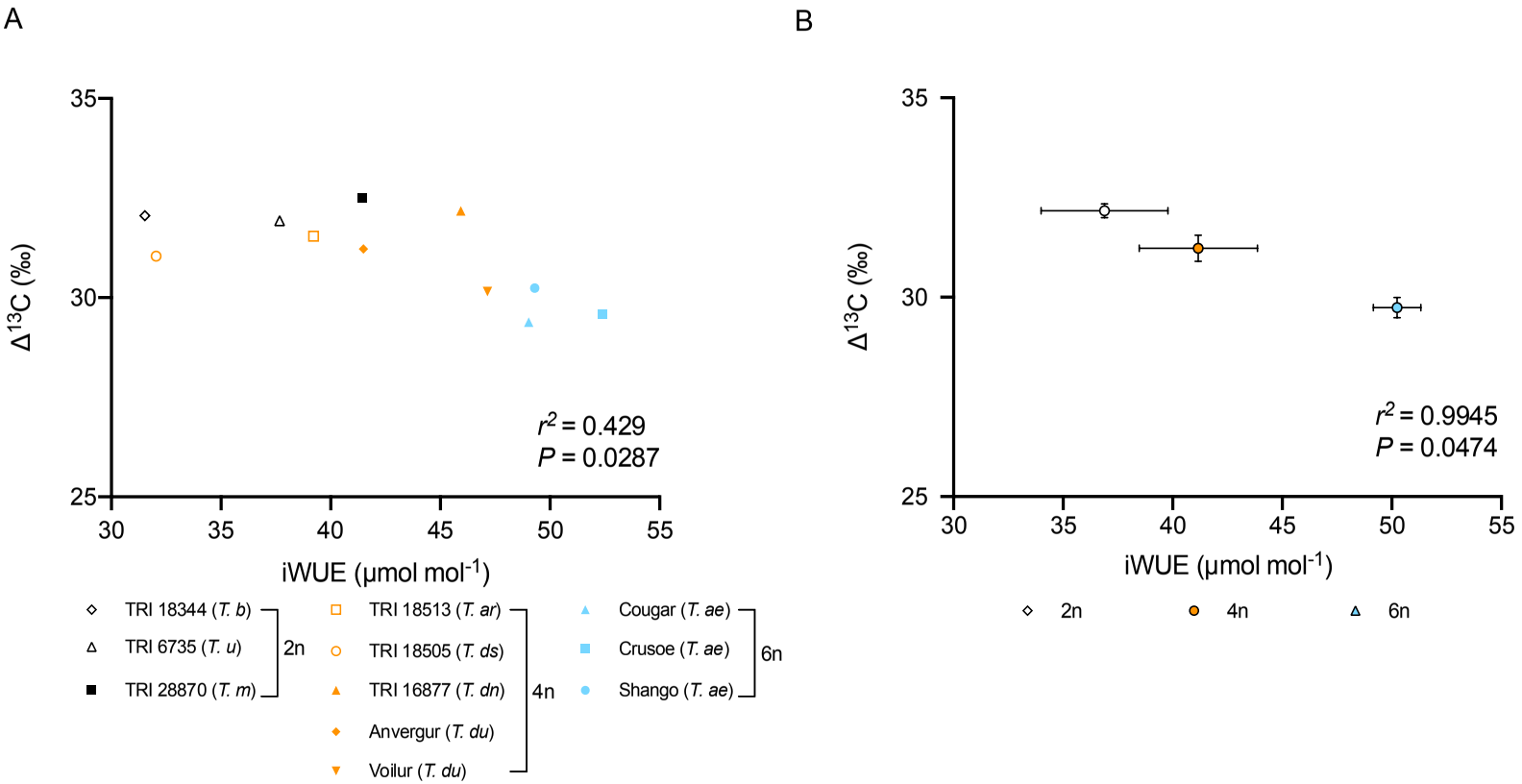

Figure 3.14. There is a negative correlation between Δ¹³C and iWUE for 2n, 4n and 6n members of the Triticeae
A) Mean Δ¹³C is plotted against mean iWUE for each of the lines investigated – as summarised in Table 2.2. Symbols with no fill indicate wild lines, solid symbols are domesticated cultivars. **B)** Mean Δ¹³C plotted against mean iWUE with data from (A) grouped into their respective ploidy levels. Results of correlation analyses are presented (Pearson r^2 value). Error bars = S.E.M. n = minimum of 2 per line.

As is well established, grasses have a developmental gradient from the base to the tip of the leaf blade, with the basal region being the youngest and the distal region the most mature (Lewis & Hake, 2016; Raissig *et al.*, 2016; Hepworth *et al.*, 2018). This gradient provides a useful tool by which any potential link between stomatal differentiation and mesophyll cell separation can be tested. Additionally, the availability of transgenic *TaEPF1-OE* wheat, which have a reduced leaf stomatal density (Dunn *et al.*, 2019) provided a further tool for testing this hypothesis.

Firstly, I investigated if there was a gradient of stomatal density associated with the leaf developmental gradient along the blade long axis. Analysis of the Fielder control line (the untransformed parent of *TaEPF1-OE* plants) showed that there was no significant change in stomatal density when measured at the tip, middle and base of the leaf lamina ($F_{(2,87)}$= 2.812 , P= 0.0656) (Figure 3.15A). However, in *TaEPF1-OE* (Figure 3.15B) plants it was found, via an ANOVA followed by a post-hoc Tukey test, that the basal region of the leaf blade had a significantly lower density of stomata than the distal and medial regions (ANOVA $F_{(2,87)}$= 3.283, P= 0.0019). There was no significant difference in mesophyll porosity with leaf region in the control plants (Figure 3.15C) (ANOVA, $F_{(2,3)}$= 0.2329, P= 0.8054). The reduction in stomatal density towards the base of the leaf blade shown in *TaEPF1-OE* plants was reflected by a corresponding significant decrease in mesophyll porosity in this region in comparison to that at the tip of the leaf blade, as revealed via X-ray µCT analysis (Figure 3.15D) (ANOVA, $F_{(2,15)}$= 3.283, P= 0.0023). The middle region of the leaf did not contain a significantly different amount of airspace (22.77%) compared to either the tip (24.16%) or base (21.68%) of the leaf but was intermediate to these two values. When all three regions of the leaf from which data was collected were grouped it was found that, as expected, *TaEPF1-OE* plants had a significantly reduced frequency of stomata (51.27 mm^{-2}) on the leaf epidermis compared to wild-type plants (77.07 mm^{-2}) (unpaired *t* test, $t_{(4)}$= 0.7990, P= 0.0013) (Figure 3.16A). For each of the regions of the leaf from which measurements were taken (tip, middle, base), stomatal density was found to be lower in the *TaEPF1-OE* line than the control. The observed reduction in mean stomatal density was mirrored by a decrease in the amount of mean leaf airspace (22.87% compared to 24.01% in the control), although this reduction in mesophyll porosity was not found to be statistically significant (unpaired *t* test, $t_{(6)}$= 1.464, P= 0.1936) – see Figure 3.16B.

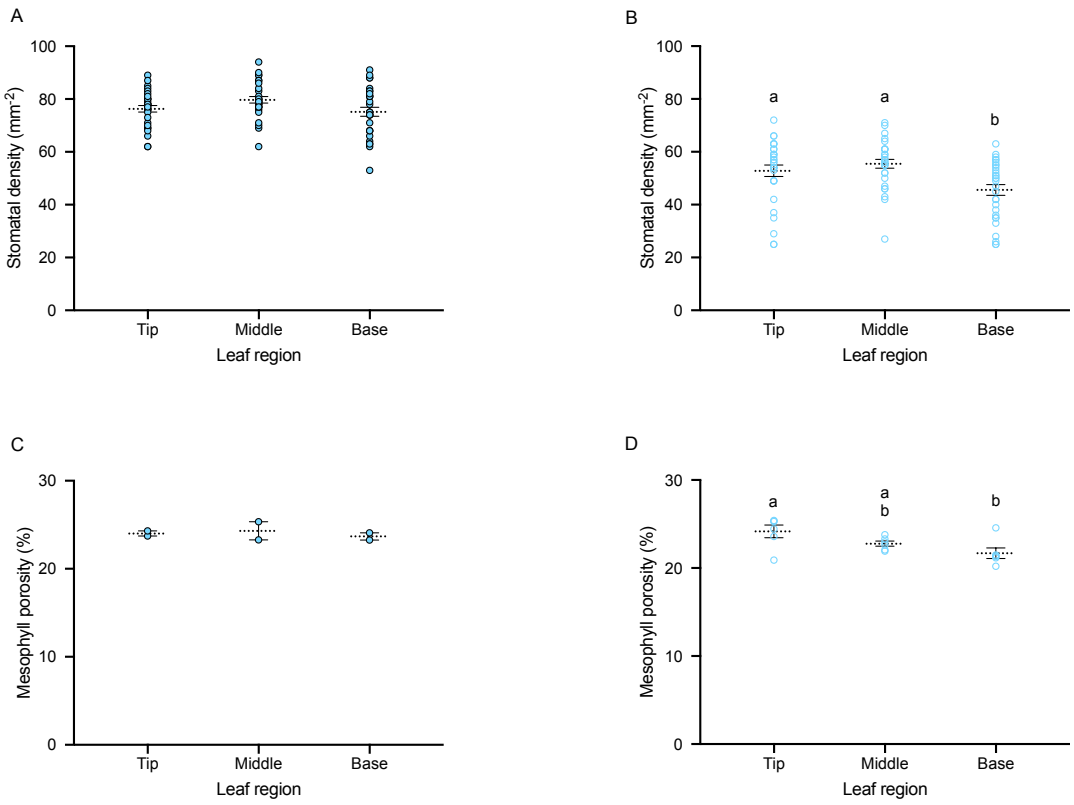

Figure 3.15. There are gradients in stomatal density and mesophyll porosity along mature wheat leaves
A) Mean stomatal density at tip, middle and basal regions of mature leaf 5 of *T. aestivum* cv. Fielder (solid symbols). **B)** Mean stomatal density at the tip, middle and base of mature leaf 5 of *TaEPF1 OE* plants (no-fill symbols). **C)** Mesophyll porosity (%) at the tip, middle and base of the leaf blade in mature leaf 5 of *T. aestivum* cv. Fielder. **D)** Mesophyll porosity (%) at the tip, middle and base of the leaf blade in mature leaf 5 of *TaEPF1* OE lines. Datapoints indicated with the same letter cannot be distinguished from each other (P= <0.05) (Tukey HSD post one-way ANOVA). Error bars = S.E.M. n = minimum of 5 per line.

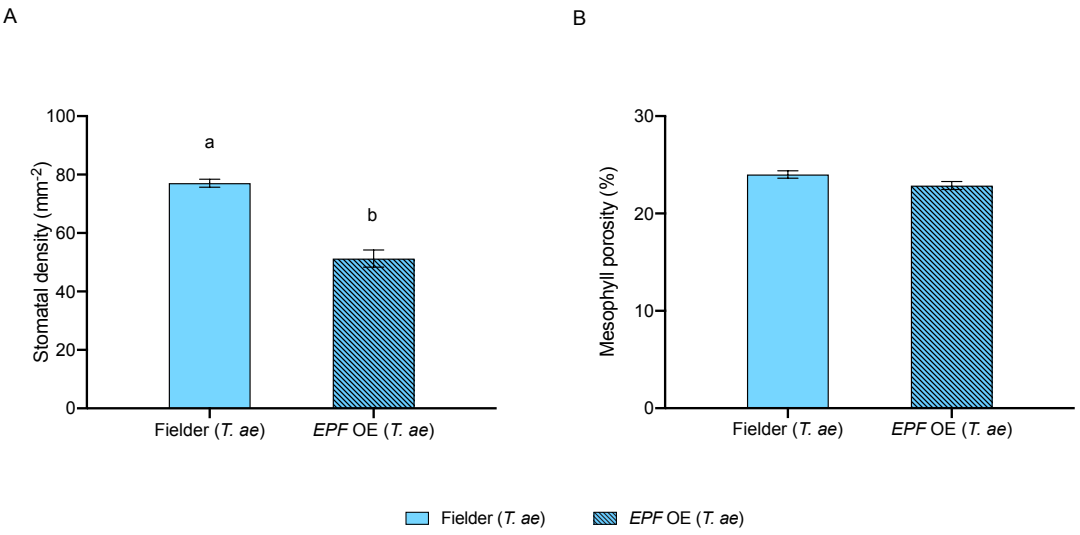

Figure 3.16. *TaEPF1-OE* plants have a lower whole-leaf mean stomatal density and mesophyll porosity than wild-type Fielder plants
A) Mean stomatal density across all regions of leaf 2 of Fielder and the *EPF-OE* line. **B)** Mean mesophyll porosity across all regions of leaf 2 of control and transgenic plants. Datapoints indicated with the same letter cannot be distinguished from each other (P= <0.05) (unpaired *t* test). Error bars = S.E.M. n = minimum of 5 per line.

The data in Figure 3.15 confirm a relationship between stomatal density and mesophyll airspace but do not allow judgement of which comes first during development. To address this question, I used confocal microscopy imaging of young leaves in wheat seedings to see if it was possible to identify the earliest stages of stomatal differentiation and, if so, to characterise the process of mesophyll cell separation in the leaves at that stage of development. When young leaves in germinating wheat seedlings were imaged, it was found that towards the distal tip regions of the lamina the stomata were mature and fully developed. As can be seen in Figure 3.17 (A-C), these fully differentiated pores had large airspaces beneath them. Conversely, when still developing basal areas of the leaf blade were observed (Figure 3.17D-F), it was possible to see epidermal cells still undergoing stomatal differentiation, i.e., with no pore. Although there were occasional airspaces present at points where mesophyll cells were joined to one another, these were not only much smaller than those found beneath the fully developed stomata near the leaf tip, they also showed no clear pattern with regard to the overlying cells undergoing differentiation into stomata. Rather than the stereotypical lobed mesophyll cells seen in mature leaf blades, the mesophyll cells of these basal leaf regions were arranged in a regular 'brickwork' pattern. These images support the hypothesis that the development of mature stomata on the epidermis is required for the formation of subtending airspace in wheat leaves.

3.4. Discussion:

The arrangement and quantity of intercellular airspaces within the mesophyll of wheat leaves is thought to be important for physiological function, but the functional mechanistic relationship of airspace to physiological performance remains open to discussion (Lehmeier *et al.*, 2017b; Lundgren *et al.*, 2019). Moreover, the control of mesophyll airspace formation remains largely unexplored. Using X-Ray µCT imaging to extract quantitative 3D data, this chapter investigated the relationship between mesophyll porosity and stomatal conductance, as well as providing in depth analysis of photosynthesis and leaf physiology in a range of ploidy levels (2n, 4n and 6n) available in *Triticum* species.

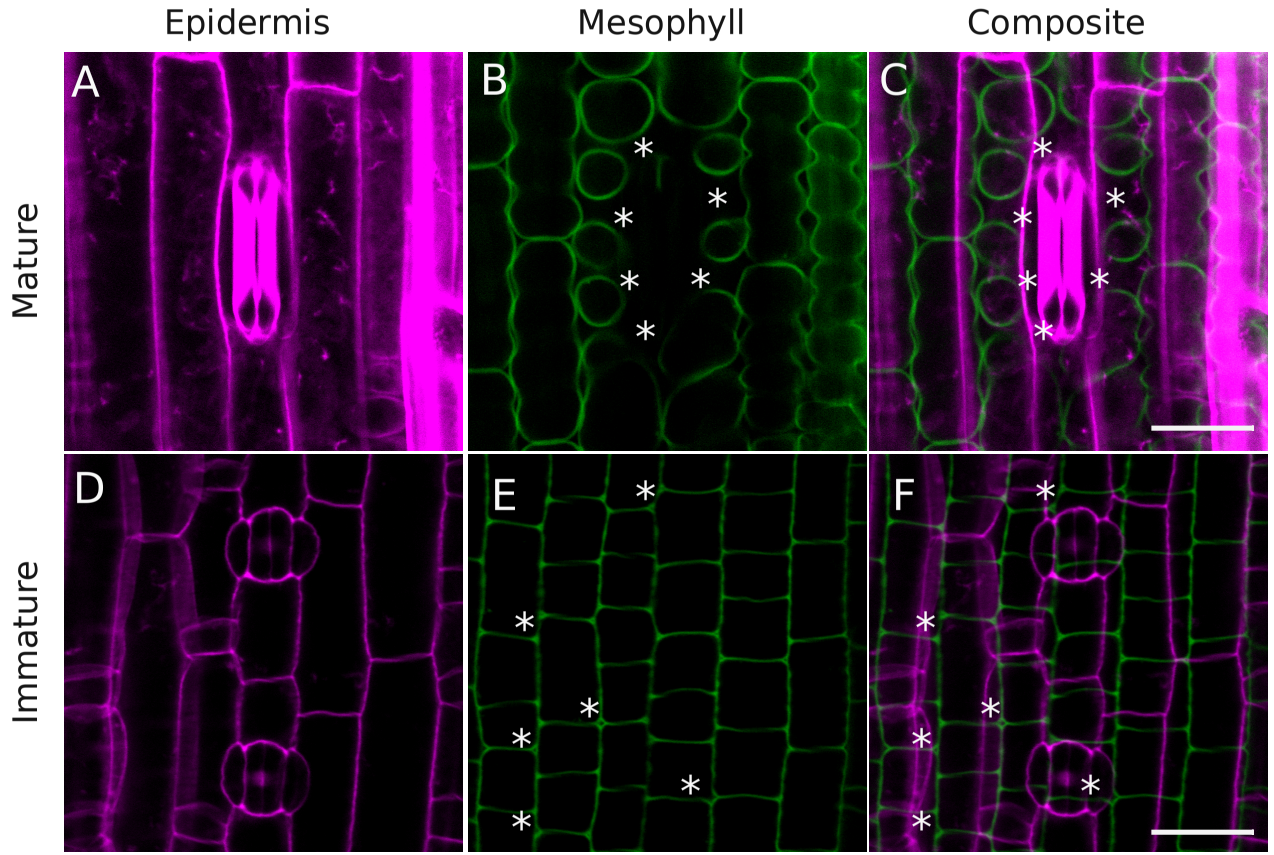

Figure 3.17. Mesophyll airspace formation is linked to the presence of fully differentiated stomata
A–C) Confocal micrographs taken at the distal tip region of the leaf 3 of a wheat seedling (c.v. Fielder). **D–F)** Confocal images taken at the proximal base region of the leaf. Slices were taken from the epidermis (A,D) and the mesophyll layer (B,E). Cell walls are false-coloured magenta (A,D) and green (B,E) and overlaid in (C,F). A single mature stomata is visible in A, whilst two immature stomata can be observed in D,F. In (A), the presence of a large airspace subtending the stomatal complex is visible (indicated by asterisks in B,C). Smaller airspaces (highlighted with asterisks) are visible in E,F at cell junctions only. Scale bars = 20 μm.

This allowed the investigation of the hypothesis that leaf airspace is affected by genome size, and that this is linked to the stomatal characteristics. Additionally, the potential causal link between stomatal and airspace differentiation was explored via both a novel three-dimensional imaging approach combined with more traditional confocal analysis of transgenic wheat engineered to have fewer stomata.

3.4.1. The patterning of intercellular airspaces in wheat leaves is positively correlated with stomatal conductance.

Previous studies have indicated both that the mesophyll porosity of leaves was significantly impacted by ploidy level in flag leaves of the Triticeae (Austin *et al.*, 1982), and also that ploidy has no significant effect upon leaf intercellular airspaces in younger leaves (Jellings & Leech, 1984). My results suggested that diploid leaves had a higher mesophyll porosity than hexaploid plant material, whilst tetraploids contained intermediate levels of airspace. In addition to investigating a wider range of more modern varieties, a further advantage over these more historical studies is the novel use of X-Ray µCT imaging to quantify leaf airspace in three-dimensions. Estimating a 3D parameter (leaf airspace) from 2D sections is not only tedious, it relies on several assumptions. It has been shown that 3D imaging techniques can quantify mesophyll porosity more accurately, with traditional 2D techniques prone to providing underestimates of this value (Théroux-Rancourt *et al.*, 2017; Mathers *et al.*, 2018).

A previous study by colleagues in Sheffield investigated airspace formation in Arabidopsis mutants with altered stomatal phenotypes. Plants overexpressing the negative stomatal regulator *EPF2* were shown to have lower stomatal conductance and correspondingly decreased airspace quantities and distributions in comparison to the Col-0 wild type. Likewise, *focl1* (Fused Outer Cuticular Ledge1) plants (which have a defect in stomatal development and have disrupted formation of the cuticular ledge of the guard cell which acts to limit gas exchange into the leaf) have lower mesophyll porosity and lower g_s than the wild type. An *epf1/epf2* double knockout line with a higher stomatal density and g_s was also scanned, and this line was also shown to have a greater level of airspace. The results presented in this chapter confirm that this positive

correlation between mesophyll porosity and g_s is also present in wheat across the three ploidy levels investigated (2n, 4n and 6n), suggesting that this relationship is common to both eudicot and monocot leaves. This suggests that there is potentially a causal link between stomatal function (gas exchange) and intercellular airspace formation in the mesophyll.

Furthermore, more accurate estimations of S_{mes} were also provided using this imaging technique. It was found that despite relative airspace levels changing within leaves of different ploidy, the exposed surface area of the mesophyll cells did not change significantly with ploidy level, suggesting that S_{mes} and porosity are not absolutely dependent upon one another. One possibility to explain this apparent discrepancy is that mesophyll cell size, shape and packing are altered between genotypes of different ploidy levels. Changes in mesophyll size and shape (i.e., lobe number) with wheat evolution are further explored in the following chapter.

Despite providing greater accuracy than 2D sections, X-ray µCT does have some limitations (Pajor *et al.*, 2013). Firstly, the instruments and software required to scan and process samples are highly specialised, and thus expensive – limiting access. Additionally, errors may be associated with user selection of regions of interest and the subjective manner of the processing steps which require manual inputs (Mathers *et al.*, 2018). Furthermore, there is a trade-off between scan time, sample size and scan resolution. Resolution is impaired by sample size, and as such larger samples cannot be imaged at high quality. Additionally higher resolution images also bring with them the caveat of being more data-intensive, increasing both scan and processing times (Dhondt *et al.*, 2010; Pajor *et al.*, 2013). As a result of this balance between sample size, scan time and resolution, it was not possible to take images of cellular resolution from which individual cell geometries could be extracted. Despite this, as a method for quantifying airspace in 3D, X-Ray µCT analysis is preferable to traditional histology. An alternative method which may allow for cellular resolution would be via synchrotron radiation computed tomography (SR-CT), which enables enough contrast to be able to observe individual cells within a tissue and potentially allows for image resolution below one micron (Verboven *et al.*, 2014). However, access to such

systems is even more limited, greatly restricting sample number and, consequently, statistical analysis. As such, an alternative route to this information was sought and is discussed in the following chapter.

Overall, the data extracted from µCT analysis of wheat leaves of varying ploidy levels (2n, 4n and 6n) indicated that the greater allocation of the leaf volume to airspace in diploid lines facilitated increased rates of gas exchange to and from the mesophyll cells, and suggested that this may also be associated with a higher exposed surface area, although this data was not conclusive, and a greater number of replicates may help to confirm trends.

3.4.2. A more in-depth analysis reveals variation in photosynthetic parameters in the Triticeae

The variation in leaf internal structure found in the Triticeae suggests that there may be physiological differences between ploidy levels that cannot be determined from steady-state measurements alone (as described in the previous chapter). Earlier studies found that tetraploid members of the Triticeae had a higher light-saturated rate of CO_2 assimilation than hexaploid plants (Biswas & Jiang, 2011). However, my results showed that there was no statistically significant difference in A_{sat} between the 4n and 6n ploidy levels, although diploid accessions were observed to have a higher light-saturated rate of photosynthesis as per previous studies (Dunstone & Evans, 1974; Biswas & Jiang, 2011). My data also suggests that the inter- and intra-ploidy level variation in A_{sat} in the Triticeae noted by previous authors was present for the lines examined (Dunstone & Evans, 1974; Sadras *et al.*, 2012), but trends between ploidy level were weaker than intra-ploidy variation. Analysis of further parameters that can be fitted from light response curves, such as the light compensation point and convexity of the curve, may further inform of differences in photosynthetic responses of different ploidy levels to changing levels of irradiance.

Furthermore, when the maximum rate of CO_2 carboxylation (A_{max}) was measured using A/C_i curves, it was found that diploid accessions had higher rates of A_{max} and that hexaploid varieties had lower rates of A_{max}, as noticed by previous authors (Austin *et al.*, 1982; Jellings & Leech, 1984;

Warner & Edwards, 1993), with tetraploid accessions being intermediate. Comparisons of fitted values of V_{cmax} and J which informing on photosynthetic biochemistry, have not previously been carried out on a wide range of lines of varying ploidy levels (2n, 4n, 6n) in *Triticum* species. My results indicate that diploid plants had a significantly higher V_{cmax} than hexaploid accessions. Tetraploid lines were shown to be intermediate, but the carboxylation rate of Rubisco was not significantly different to that of the 2n ploidy level. Biswas & Jiang (2011), have also previously found that a 4n durum wheat had a higher rate of V_{cmax} than 6n bread wheat, although only one line of each ploidy level was investigated. This study also found the same trend was present for *J*. My results indicated that whilst *J* was higher in diploid plants, it was only found to vary significantly from that of hexaploid plants. Tetraploid genotypes were statistically indistinguishable from either of the other two ploidy levels. This significant variation in photosynthetic biochemistry with ploidy intimates that differences in photosynthetic capacity may result from the observed variation in these parameters, as well being a consequence of differences in leaf structure.

The values for V_{cmax} and J are estimates and dependent upon correct use of a fitting tool. Whilst fitting tools allow for rapid generation of data, it is essential that they be used correctly. This requires the correct categorisation of points to the rate limiting step of photosynthesis (Sharkey, 2016). Estimations of V_{cmax} are highly sensitive to values of g_m (Sharkey *et al.*, 2007), and as such, in the future more accurate estimations of V_{cmax} may be made if g_m is constrained or an independent value of g_m is used (Sharkey, 2016). Whilst the Sharkey tool used in this investigation provides a good balance between detailed outputs and simplicity of use, it may also be of interest in future experiments to use the tool presented by Bellasio *et al.*, (2015), as it is possible to extract a greater number of parameters.

3.4.3. There is no trend with ploidy level and mesophyll conductance in wheat

Diffusion of CO_2 across the mesophyll can be limiting for photosynthesis (Tholen, Ethier, *et al.*, 2012; Griffiths & Helliker, 2013), and can have a large impact upon WUE (Barbour *et al.*, 2016). The potential impact of g_m

is therefore of interest, and varieties with higher g_m should be, in theory, more water use efficient (Barbour *et al.*, 2016). The data shown in this chapter demonstrated that leaf mesophyll porosity value was correlated with changing ploidy level and, thus, could potentially have an impact upon mesophyll conductance in the Triticeae. Previous results have suggested that there is significant variation in mesophyll conductance in *T. aestivum* (Driever *et al.*, 2014; Jahan *et al.*, 2014; Barbour *et al.*, 2016; Olsovska *et al.*, 2016; Ouyang *et al.*, 2017), and my results confirm both intra- and inter-ploidy level variation in g_m for *Triticum* species. However, my results do not suggest any significant trend between mesophyll conductance and ploidy level in wheat species, despite these having varying levels of leaf airspace (porosity). The lack of variation in S_{mes} in leaf 5 of the plants under investigation may help to explain the absence of variation in g_m. However, g_m is a complex trait which is influenced by a range of structural and biochemical factors, not just S_{mes}. For example, mesophyll conductance is also influenced by aquaporins facilitating CO_2 transport (Griffiths & Helliker, 2013) and cell wall thickness (Tomas *et al.*, 2013), and these other factors have clearly not been investigated in this study. Nevertheless, the finding that S_{mes} does not seem to change significantly with ploidy level, whereas porosity does, suggests changes must be occurring in internal cell geometry. This point is explored further in the next chapter.

Whilst mesophyll conductance values can be fitted from gas exchange curves alone, this method does have limitations (Pons *et al.*, 2009; Flexas *et al.*, 2013). Using chlorophyll fluorescence data (variable/constant J method) could have improved the accuracy of these estimations (Pons *et al.*, 2009; Flexas *et al.*, 2012), but unfortunately, due to technical issues, not all of the curves had the full datasets required for fitting g_m using the Bellasio fitting tool (Bellasio *et al.*, 2015) as initially planned. Nevertheless, despite the Sharkey calculator assuming constant g_m with changes in CO_2 and its generation of assimilation-weighted values, the values generated are still considered to be reasonable estimates (Sharkey, 2016). Alternative methods for measuring g_m require the use of more specialist equipment (Pons *et al.*, 2009). Using combined chlorophyll fluorescence and gas exchange analysis to determine mesophyll conductance requires the calculation of leaf absorptance via the use of an

integrating sphere, which was not available. A further method by which g_m can be recorded is via the use of mass spectrometry to carrying out 'online' measurements (Pons *et al.*, 2009; Barbour *et al.*, 2016), which could also be considered in future experiments to generate g_m estimates of higher accuracy.

3.4.4. Chlorophyll and protein content

In addition to the physiological parameters previously mentioned, leaf chlorophyll content and levels of Rubisco can also influence photosynthesis, even if in reality, the contribution of variance in levels in Rubisco to variance in photosynthetic capacity is minor compared to leaf structural components (Driever *et al.*, 2014). My results suggest that, despite a visible trend, there is no significant difference in chlorophyll content per leaf area with ploidy, unlike Watanabe *et al.*, (1994) or Kaminski *et al.*, (1990). Despite not being significantly different, higher chlorophyll contents were found in hexaploid lines, similarly to those reported by Kaminski *et al.*, (1990). The genotypic variation in chlorophyll level found within ploidy levels concurs with that found in previous studies (Babar *et al.*, 2006; Gaju *et al.*, 2016; Hamblin *et al.*, 2014; Sid'ko *et al.*, 2017). The low sample number may be responsible for this difficulty in the statistical interpretation of this data.

Total soluble protein levels were used as a proxy for determining Rubisco content, as has previously been demonstrated in hexaploid wheat (Carmo-Silva *et al.*, 2017). Despite finding variation amongst the accessions for total soluble protein per leaf volume, my results indicate that changes in ploidy level do not result in significant differences in total soluble protein, despite a visible trend showing a slightly higher protein content in diploid lines. This contradicts the results found by Dean and Leech, (1982a), and is more similar to those observed by Evans and Seeman, (1984).

Overall, my results suggest that whilst the leaf structure of the Triticeae is significantly altered by changes in ploidy level, this does not manifest in major alterations in photosynthetic pigment and protein contents per leaf area or volume, supporting the idea that any differences in

photosynthesis may primarily result from changes in leaf structure. It is possible that any increases or decreases in chlorophyll and/or Rubisco content are less pronounced when presented on a leaf volume or area basis as a result of potential differences in leaf or mesophyll cell size, which influences the number of cells per area or volume. In the future, measuring the number of chloroplasts and the amount of Rubisco per cell may help to eliminate any potential masking effects of the leaf structural changes associated with shifts in ploidy level. Additionally, direct measurements of leaf Rubisco content and its catalytic properties could provide further information regarding how wheat leaf photosynthetic biochemistry is influenced by changes in ploidy level (Prins, *et al.*, 2016).

3.4.3. iWUE is correlated with $\Delta^{13}C$ values in the Triticeae

In both hexaploid and tetraploid wheat, $\Delta^{13}C$ has been shown to correlate with water use efficiency (Farquhar & Richards, 1984; Araus *et al.*, 1997; Misra *et al.*, 2010; Rizza *et al.*, 2012). I found that in the Triticeae, ploidy level had a significant effect upon $\Delta^{13}C$, being lower in hexaploid lines than diploids and tetraploids. Additionally, my results confirm the negative relationship between carbon isotope discrimination and iWUE across *Triticum* species identified by previous authors (Farquhar & Richards, 1984; Araus *et al.*, 1997; Misra *et al.*, 2010; Rizza *et al.*, 2012).

Lower $\Delta^{13}C$ values are associated with lower rates of g_s, thus the data presented in this chapter supports the iWUE analysis presented in the previous chapter. This suggests that the reduced stomatal conductance/density and associated reduction in leaf airspace observed in hexaploid wheat compared to leaves of lower ploidy level results in higher water use efficiency. I hypothesise that this may have played a potentially important role in the selection/domestication of modern bread wheat from its wild ancestors. This point is expanded upon in the General Discussion chapter. In the future, it may be interesting to investigate different indicators of water use efficiency, such as dry matter per water use.

3.4.5. Sub-stomatal cavities and intercellular airspaces form after the stomata have gained function

The relationship reported here between mesophyll porosity and stomatal conductance suggests a potential link between stomatal function and airspace formation. Analysis of stomatal development on the epidermis and the underlying mesophyll in wild-type wheat plants, along with the use of mutants with decreased stomatal density, supports the hypothesis that fully differentiated, functionally operative stomata are required for cell separation in the mesophyll and the genesis of intercellular airspaces in wheat leaves. Interestingly, despite different stomatal development pathways, this pattern mirrors that discovered in the eudicot *Arabidopsis thaliana*, suggesting that this may be common for all angiosperms (Lundgren *et al.*, 2019). My data indicates that airspace formation is likely not simply a direct result of guard cell differentiation, as previously postulated (Dow *et al.*, 2017). Rather, the results suggest that it is the functioning of the developed stomata to enable gas flux that is a major driver of mesophyll separation in sub-adjacent mesophyll cells and, thus, the establishment of leaf airspace.

If mesophyll patterning is conductance-driven, this could enable leaves to adjust the differentiation of the mesophyll to match actual photosynthetic functioning, and as such would provide a mechanism explaining how leaves become anatomically specialised to their environment (Terashima *et al.*, 2011). The identity of this potential signal is unknown and open to debate. One suggestion is that the CO_2 concentration to which the mesophyll is exposed (C_i) could directly influence mesophyll porosity once stomata allow gas flux. An alternative hypothesis is that the opening of stomata affects the vapour pressure deficit (VPD) adjacent to mesophyll cells, and associated water vapour losses may be allied to cell separation. The molecular events that coordinate cell separation and growth in wheat leaves area yet to be elucidated, thus identifying the mechanistic link remains a major challenge. The potential link between mesophyll airspace formation and stomata also allows for the speculation that restricting water loss was a major driver for the changes in leaf structure and airspace associated with ploidy level increases. This point is returned to in the General Discussion.

3.5. Conclusion

In this chapter I have found that mesophyll porosity varies with ploidy level in the Triticeae, and that leaf airspace is positively correlated with stomatal conductance. Despite this, the amount of exposed mesophyll surface area did not appear to be significantly impacted by changes in ploidy. More in depth observations of photosynthesis and photosynthetic biochemistry showed that several parameters, including A_{sat}, the apparent quantum yield of photosynthesis, A_{max}, V_{cmax} and J are affected by shifts in ploidy level, others (including chlorophyll and protein content) are not significantly altered. My results suggest that mesophyll conductance, a potentially important limit upon photosynthesis (with knock-on impacts upon water use efficiency) had no significant trend with changes in ploidy, despite the altered intercellular airspace arrangements associated with alterations in genome size. Finally, the idea that fully operative stomata are required for the formation of mesophyll airspace was tested, leading to data supporting the hypothesis of a mechanistic link between stomatal function and leaf porosity. Whilst this chapter focussed upon leaf intercellular airspace, mesophyll cell size and shape are both likely to vary with changes in ploidy and may influence photosynthesis. The changes in mesophyll cell size and shape associated with wheat evolution and domestication are the subject of the next chapter.

Chapter 4. 3D imaging at cellular resolution: size and shape changes of mesophyll cells throughout wheat evolution

4.1. Introduction

The internal anatomy of leaves is made up of a highly complex 3D structure. It was shown in the first chapter that ploidy level has a significant effect upon guard cell and epidermal cell size in the Triticeae. It may therefore be expected that the mesophyll cells would follow suit, contributing to the altered size and arrangement of leaf intercellular airspaces reported in the previous chapter. Whilst techniques such as X-ray µCT offer a method to generate quantitative data on overall mesophyll structure, they offer limited cellular resolution and it is not possible to collect numerical information about individual mesophyll cell geometries. Using the technique and equipment described in the previous chapter, it is impossible to collect information about individual mesophyll cells such as surface area, volume and the number of lobes – all of which will have an impact upon the diffusion of gas to the site of CO_2 fixation in the leaf. Therefore, I sought to generate 3D images of the wheat parenchyma at cellular resolution to observe the effects of changes in ploidy upon the mesophyll cells. To achieve this a confocal microscopy approach, adapted from (Wuyts *et al.*, 2010), for imaging wheat leaves was taken.

4.1.1. Changes in ploidy level have previously been associated with changes in mesophyll cell size and shape

In addition to the differences in mesophyll porosity discussed in Chapter 3, it has also been observed that mesophyll cell size and shape in wheat leaves varies with ploidy level (Parker & Ford, 1982). As mentioned earlier, the chlorenchyma tissue of *Triticum* leaves is not clearly differentiated into spongy and palisade layers, instead being comprised of indistinct, stereotypically lobed mesophyll cells (Jung & Wernicke, 1990). Historically, wheat mesophyll cells have been observed using classical histology techniques. These only provide two-dimensional information that will be a source of error as 2D surface areas and 3D volumes must be estimated rather than directly measured (Parker & Ford, 1982; Jellings

& Leech, 1984; Pyke *et al.*, 1990). In addition, the techniques required to generate sections containing mesophyll cells are time-consuming and a large sample size is required to generate accurate data (Truernit *et al.*, 2008; Pajor *et al.*, 2013; Kurihara *et al.*, 2015). It would be expected that 2D methods would result in inaccurate estimations of cell surface area and volume in comparison to images acquired in 3D (Théroux-Rancourt *et al.*, 2017). Three dimensional imaging and analyses are able to provide far more accurate datasets of complex structural information (Buda *et al.*, 2009; Earles *et al.*, 2019).

In a similar fashion to guard cells and epidermal cells, polyploidy has been associated with increases in mesophyll cell size in several species. In Arabidopsis, a doubling of genome size has been shown to result in increased mesophyll cell relative volume (Tsukaya, 2013; 2019), although this has been observed to occur to different degrees in palisade and spongy mesophyll tissue (Katagiri *et al.*, 2016; Tsukaya, 2019), suggesting that, in Arabidopsis, the relationship between ploidy and cell size may also be influenced by cell identity (Katagiri *et al.*, 2016). In the grass genus *Lolium*, it has been shown that tetraploid varieties have significantly larger mesophyll cells than diploid lines (Sugiyama, 2005). Additionally, mesophyll cell cross-sectional area in *Lolium* has previously been negatively associated with light-saturated photosynthesis, with plants with larger cells having reduced assimilation rates (Wilson & Cooper, 1970).

Several investigations have been made on how cell size has changed during wheat evolution. Dunstone & Evans (1974) found that the projected area of mesophyll cells was around one and a half to two times larger in domesticated tetraploid and hexaploid species than that observed in diploid accessions and the wild tetraploid *T. dicoccoides*. The authors indicated that there was a significant negative relationship between mesophyll cell area and the rate of photosynthesis, and also noticed that the larger mesophyll cells found in hexaploid plants had a greater degree of lobing than diploid cells (Dunstone & Evans, 1974).

Parker & Ford (1982), also observed that hexaploid wheat lines had cells that were significantly larger than those in two diploid species. Mesophyll cells were found to be on average significantly longer and taller, with isolated cells from 6n flag leaves having a larger mean plan area than their 2n counterparts. Estimations of cell surface area and volume suggested that the mesophyll cells of *T. aestivum* were over double the size of those found in *T. urartu* and *T. monococcum* leaves. Despite this, the mean surface to area volume ratio was discovered to be similar across all three genotypes used in this investigation, despite differences in ploidy. This suggested that there was a shape change also associated with increased genome size. When the average number of lobes per cell was investigated, it was observed that, whilst both of the diploid lines had similar levels of the cell lobing stereotypical of the wheat mesophyll, the hexaploid line contained mesophyll cells with around double the number of lobes than their diploid counterparts. The above changes in mesophyll cell geometry were hypothesised to be associated with the observed increases in exposed mesophyll cell surface area and higher levels of photosynthetic capacity observed in diploid *T. urartu*, in addition to changes in vascular patterning within the leaf (Austin *et al.*, 1982; Parker & Ford, 1982).

A later study also investigated the differences in the internal structure of members of the Triticeae associated with shifts in ploidy level, and also included analysis of tetraploid lines (Jellings & Leech, 1984). The authors found that mesophyll cell area was lowest in diploid lines, whilst 4n genotypes were found to have intermediate values of mesophyll cell area. Hexaploid bread wheat varieties were found to have the largest mesophyll cell area in comparison to other *Triticum* species and cell size was shown to correlate strongly with genome size. This study however found no correlation between the exposed mesophyll cell surface area and photosynthetic area for the accessions under investigation (Jellings & Leech, 1984). When a wider panel of *Triticum* species of varying ploidy levels was investigated, it was again found that mesophyll plan area was larger in 6n varieties, middling in 4n lines and lowest in diploid accessions (Pyke *et al.*, 1990). Additionally, it was shown that mesophyll cells are subject to a reduction in size as the plant develops, with later leaves being shown to have smaller cells (Pyke *et al.*, 1990).

It is expected that cell size will impact upon photosynthesis by not only influencing gas diffusion rates, but also by affecting wider leaf anatomy. The heavily lobed nature of mesophyll cells found in rice leaves (Sage & Sage, 2009) has been suggested to greatly increase their surface area to volume ratio (Tholen *et al.*, 2012). Furthermore, the small size of rice mesophyll cells has been theorised to enable a further relative increase in the surface area of the cell available for CO_2 diffusion (Tholen *et al.*, 2012). Increased lobing has also been hypothesised to increase the chloroplast area exposed to intercellular airspaces (S_c) (Sage & Sage, 2009), which is associated with higher rates of CO_2 assimilation (Terashima *et al.*, 2011; Ren *et al.*, 2019). Additionally, smaller cells are hypothesised to allow for a tighter arrangement of leaf vasculature in rice, with mesophyll cell size (rather than the number of cells) being shown to be significantly correlated with interveinal distance (Smillie *et al.*, 2012). Reductions in mesophyll cell size and associated increases in vein density in rice have been shown to result in higher photosynthetic rates (Feldman *et al.*, 2017).

Shifts in cell size may also be associated with changes in mesophyll porosity, for example those identified in the previous chapter. In Arabidopsis, cell cycle mutants have been used to investigate the effects of altered cell size upon leaf airspace. Dorca-Fornell *et al.*, (2013) observed a higher relative frequency of smaller palisade cells compared to controls leaves when RBR (a negative regulator of the cell cycle) was silenced, alongside a slight increase in mesophyll porosity, although smaller mesophyll cells have also been associated with tighter cell packing and reduced leaf airspace, resulting in higher rates of g_m and photosynthetic capacity (Lehmeier *et al.*, 2017). This second study also found that increasing cell size via the overexpression of *KIP-RELATED PROTEIN 1* (*KRP1*) resulted in a slight reduction in mesophyll porosity (Lehmeier *et al.*, 2017).

4.1.2. Using confocal laser scanning microscopy to generate 3D image stacks of plant tissues

Confocal laser scanning microscopy (CLSM) is an imaging technique which allows for the generation of high-resolution 3D images of the mesophyll from which it is possible to extract numerical data at a cellular resolution (Wuyts *et al.*, 2010). Confocal microscopy provides an advantage over conventional widefield fluorescence microscopy, as via the use of confocal pinholes, light that is not on the desired focal plane can be excluded from detection (Paddock, 2000). This reduces the glare associated with out of focus light, which would otherwise impair image quality (Hepler & Gunning, 1998; Amos & White, 2003). This is especially relevant to thick samples, as fluorescence is emitted throughout the sample and thus reduces the resolution of structures on the preferred focal plane. Therefore, the use of CLSM to image thick samples, such as wheat leaves, in high resolution is highly attractive (Paddock, 2000). Such samples must be fixed, cleared and stained using a fluorescent dye prior to imaging (Bassel *et al.*, 2014).

The sample is illuminated by a focused beam of light, emitted from a laser excitation source, which passes through a pinhole before being reflected by a dichroic mirror and scanned across the desired focal plane (Figure 4.1A). Fluorescence emitted from the sample passes back through the dichroic mirror and through a second pinhole that is confocal with the first aperture, after which it strikes a detector. Light that is not on the chosen plane of focus is prevented from reaching this by the presence of the second pinhole (Figure 4.1A), thus eliminating the potential for flare by operating as a spatial filter (Paddock, 2000). Scanning across the sample enables the generation of thin high-resolution optical sections (Paddock, 2000) with improved signal-to-noise ratios in comparison to those imaged using widefield systems (Hepler & Gunning, 1998). Building up a series of 2D optical sections (or slices) into a z-stack allows for a 3D image to be rendered (Figure 4.1B) (Truernit *et al.*, 2008; Buda *et al.*, 2009; Wuyts *et al.*, 2010). From these reconstructions, it is possible to segment tissues into individual cells and to thus deduce quantitative measures of cell geometry.

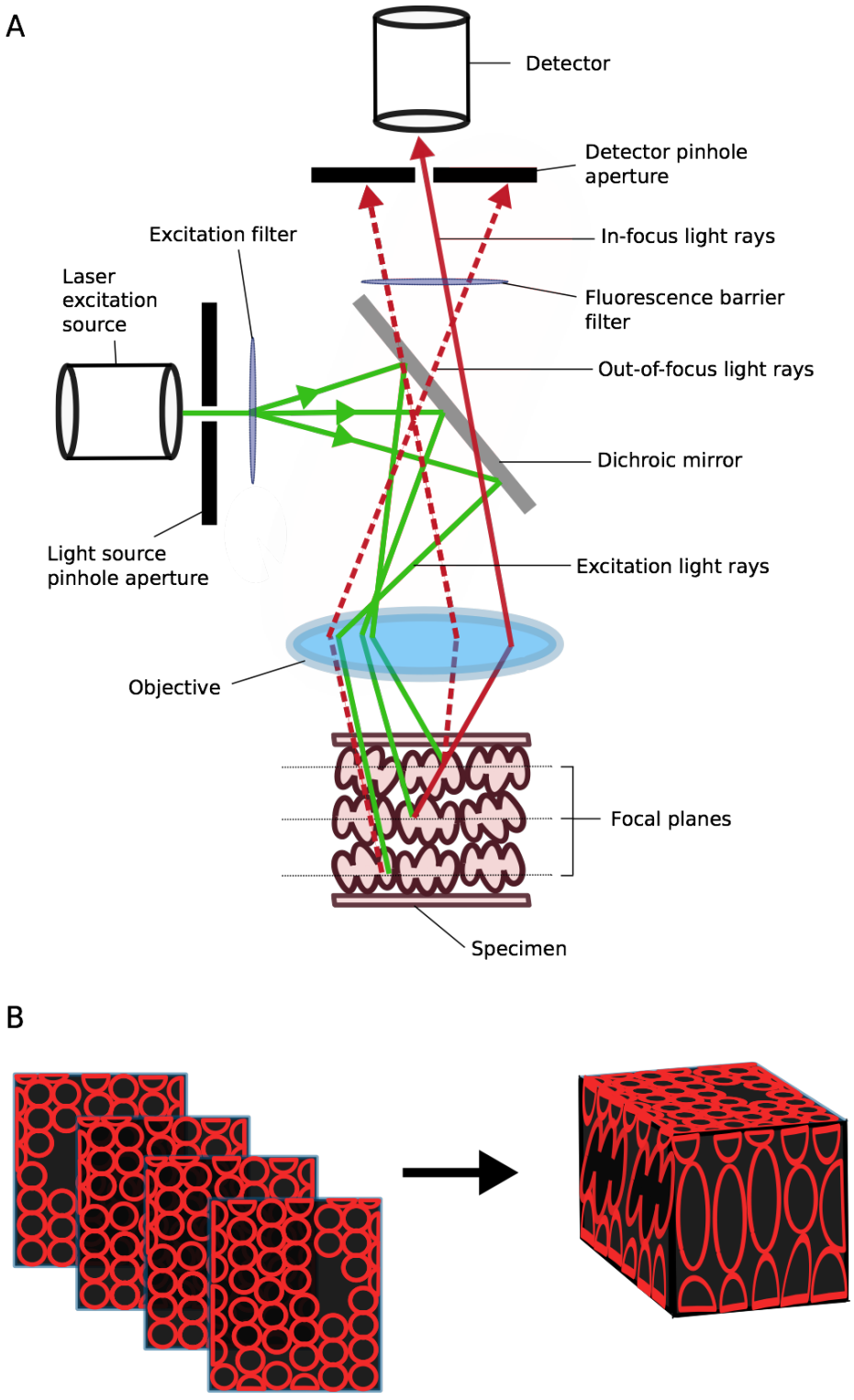

Figure 4.1. Confocal microscopy can be used to generate high-resolution images of the leaf mesophyll
A) A schematic of the light path inside a confocal microscope. Via the use of confocal pinholes, the detector can only receive light from the desired focal plane. **B)** A series of 2D optical sections can be combined to create a 3D z-stack of the leaf.

Confocal microscopy has frequently been used on plant tissues for the imaging of a wide variety of structures and compounds, such as phenolic compounds (Hutzler, 1998), phloem development (Truernit *et al.*, 2008), chloroplasts (Omasa *et al.*, 2009), fruit cuticle architecture (Buda *et al.*, 2009), and plant meristems in 3D (Yoshida *et al.*, 2014). It has also previously been used to image Arabidopsis mesophyll cells (Wuyts *et al.*, 2010; Dow *et al.*, 2017). Unlike most other μCT and other 3D imaging techniques, a confocal approach allows for individual cells to be imaged. Additionally, CLSM systems require less specialist equipment and are far more accessible than other imaging systems, being present in most universities and research institutes (Wuyts *et al.*, 2010). Leaves are by their nature difficult to image due to limited light penetration, (as a result of cuticle opacity) and the light scattering nature of the tissue (Wuyts *et al.*, 2010; Littlejohn *et al.*, 2014). With increasing depth through samples, laser intensity is reduced, thus deeper parts of the tissue have reduced signal intensity (Truernit *et al.*, 2008; Littlejohn *et al.*, 2010). This can be corrected for, but this tends to increase noise and thus reduces image quality, which has a negative impact upon ease of subsequent segmentation and the quantification of geometrical parameters. It has previously been noted that the use of cleared tissue allows for optical sectioning to be carried out to a greater depth than if non-cleared tissue is used (Wuyts *et al.*, 2010). Despite these limitations, it is generally possible to generate image stacks with the required level of resolution and contrast, which allows for quantitative data to be extracted via image analysis pathways, though this is highly dependent on the exact species/organ/tissue being analysed.

In order to generate suitable images, correct application of clearing and staining protocols is vital. The leaf cuticle is hydrophobic, and therefore non water-based treatments must be used. The method used to clear the leaf tissue is important, as some techniques (Truernit *et al.*, 2008) can lack reliability and may even lead to the excessive shrinkage and wrinkling of mesophyll cells, thus reducing the accuracy of any data extracted from these images (Wuyts *et al.*, 2010). Clearing samples also mitigates for the auto-fluorescent nature of plant tissues. Clearing and staining is improved towards the cut edges of samples, as it is easier for solutions to diffuse into these regions (Wuyts *et al.*, 2010). Fixing samples

also allows for them to be stored for periods before imaging, in addition to increasing the permeability of tissue to other later treatment steps. A reliable, rapid clearing step is required, and it is often also essential to treat the sample with alpha-amylase in order to digest starch granules, which are not normally removed in the clearing process, as these have a negative impact upon cell segmentation accuracy (Wuyts *et al.*, 2010). Samples should also be stained with a cell wall specific stain, in order to generate a high signal-to-noise ratio at cell boundaries (Truernit *et al.*, 2008; Bassel, 2015). Leaves must then be mounted and imaged soon afterwards to reduce tissue compression as the mountant dries (Wuyts *et al.*, 2010).

In order to aid cell segmentation, it is essential that complete cells are imaged, and that cell walls are unbroken and have high contrast with the surrounding areas of the image stack. This is aided by using a small z-slice size. For thinner samples, i.e. Arabidopsis, it is possible to take optical sections of the entire leaf thickness, but in thicker samples light penetration is the limiting factor, so only a proportion of the leaf depth can be reliably captured (Wuyts *et al.*, 2010).

4.1.3. Image processing using LithoGraphX

LithoGraphX (LGX) is an open-source software package that can be used to process 3D images. Using this software, it is possible to reconstruct, segment and generate quantitative data on cell volume and surface area. It was originally developed as MorphoGraphX as a tool for investigating morphogenesis and the cell geometry changes associated with this process (Barbier de Reuille *et al.*, 2015). Whilst able to process other 3D image types including SEM (scanning electron microscopy) images, it is most commonly used on confocal stacks.

Extraction of 3D shapes using this software requires cell outlines to be distinct from all angles. The auto-fluorescent nature of plant tissues means that fixed, cleared samples are often used when segmenting confocal stacks at depth (Bassel *et al.*, 2014; Barbier de Reuille *et al.*, 2015). LGX carries out 3D segmentation by making use of an auto-seeded, morphological watershed algorithm that is available in the ITK (Insight

Segmentation and Registration Toolkit) toolkit, followed by manual input to correct any errors resulting from this auto-segmentation. Post-segmentation, the surface is extracted using marching cubes and labelled. This mesh is representative of the boundaries of each object (i.e. a cell), and contains further information regarding this, such as the cell label or signal value (Barbier de Reuille *et al.*, 2015; Bassel, 2015).

With LGX, it is then possible to quantify cell area and volume from this surface data and this can easily be exported in spreadsheet format. Additionally, it is also possible to quantify fluorescence signal, although in this chapter I restrict the use of LGX to extracting geometrical values of cell size and shape alone. Validation of LGX has previously been carried out and showed that errors as a result of viewing angle and automatic segmentation were minimalized (Barbier de Reuille *et al.*, 2015). Furthermore, it is also possible to remove objects from the stack that are not of interest, such as leaf vasculature, leaf hairs and the epidermis. LGX also contains many pre-processing tools that are useful prior to segmentation, such as a Gaussian blur function (Montenegro-Johnson *et al.*, 2015; Bassel & Smith, 2016).

The precursor of LGX, MorphoGraphX, has previously been used to investigate cell size in the wings of drosophila (Aegerter-Wilmsen *et al.*, 2012) as well as to investigate cell growth and (Kierzkowski *et al.*, 2012; Vlad *et al.*, 2014) and for quantification of 3D properties in plants, including Arabidopsis (Montenegro-Johnson *et al.*, 2019) and soybean (Souza *et al.*, 2017). In this chapter, this software was selected to quantify image stacks generated from analysis of wheat leaf tissue.

4.1.4. Aims

In this chapter, I aim to determine how leaf mesophyll size and shape vary with ploidy level for a range of 2n, 4n and 6n wheat genotypes. In contrast to previous investigations, a three-dimensional approach allows for more accurate collation of the differences in mesophyll geometry associated with changes in ploidy. How potential differences in mesophyll surface area, volume, surface area to volume ratio and shape

affect the extent of intercellular airspace within the leaf, which was shown to be significantly correlated with crop water use, is also explored.

4.2. Methods

4.2.1. Plant material and growth conditions

All plant material used in this chapter was grown as per section 2.2.1. A summary of the 2n, 4n and 6n wheat lines used for 3D imaging of the mesophyll cells is available in Table 2.2.

4.2.2. Sample collection, fixation and storage

Once leaf 5 was fully expanded, three sections approximately 1cm^2 in size were removed from each plant and immediately placed into a fixative comprising of room-temperature 3:1 ethanol:acetic anhydride (v/v) in glass vials. These samples were then placed into a vacuum pump for one hour to vacuum infiltrate them, before they were stored in the fridge at 4˚C for a minimum of 48 hours. This fixative forms ethyl acetate, which aids permeability of the sample. After this time, samples were washed with a 50% ethanol solution for 15 minutes, before being rinsed in 70% ethanol and left in this solution at 4˚C until imaged.

4.2.3. Sample preparation for confocal microscopy

When required, one leaf section was transferred into a new vial, where it was initially treated with chloroform for a period of 10 minutes to remove leaf cuticular waxes (Wuyts *et al.*, 2010). The chloroform was then removed from the vial and replaced with a solution of 70% ethanol for 15 minutes - the first step of a progressive rehydration. This was followed by 50% ethanol and a wash in dH_2O (15 minutes per step).

The next step was to add 0.2 M NaOH containing 1% Sodium dodecyl sulphate (w/v) (SDS) to the sample for 15 minutes before rinsing three times with distilled water. Next, leaf tissue was treated with a starch digester solution consisting of phosphate buffered saline (PBS), 0.1% Tween-20 and 0.01% (w/v) alpha-amylase (Sigma-Aldrich, UK) and placed in an incubator at 37˚C overnight. This removed starch grains from the

sample to ensure that these did not affect image quality and any downstream processing required.

After removal from the incubator, samples were next treated with a solution of freshly prepared 1% (v/v) periodic acid (Sigma-Aldrich, UK) for 40 minutes. After a further wash in water, samples were stained using the fluorescent dye propidium iodide (PI, Sigma-Aldrich, UK) to stain the cell walls. Leaf sections were left in a pseudo-schiff PI solution consisting of 0.1 M $Na_2S_2O_5$, 0.15 N HCl, 0.01% PI for 4 hours. Periodic acid treatment leads to the formation of aldehyde groups at cell walls, which react with the PI and strongly label the cell walls with this fluorescent dye (Truernit *et al.*, 2008). This step must be carried out in the dark to avoid decay of the PI fluorophore, which is light labile. After this staining period, samples were washed three times in water and left overnight in the third rinse at 4˚C. If the staining is successful, sections should now be pink in colour, with more intense staining along leaf vasculature and at the edges of the sample.

The next step of sample preparation was clearing. A few drops of a clearing solution consisting of 200 g chloral hydrate (Sigma-Aldrich, UK), 20 ml glycerol and 30 ml distilled water were added to the vials containing the leaf sections and left for 6 hours. After the clearing step, leaf sections were blotted using a tissue to remove excess liquid before being dissected along the midrib to allow for the preparation of flatter samples. One piece of the dissected sample was then flipped so that the adaxial side was facing up and placed directly onto coverslip using a few drops of mountant made of 3 g 20% (v/v) Arabic gum, 10 g chloral hydrate and 1 g glycerol and mounted onto microscope slides. This reduced the distance between the sample and the coverslip. Coverslips were secured using clear nail varnish. The other half was left with the abaxial side upwards and mounted in the same manner. Once mounted on slides, samples were kept at 4˚C in the dark to prevent the sample bleaching and imaged within one week.

4.2.4. Imaging leaf sections using confocal microscopy:

During method development, three different CLSM systems were used. Best results were seen using an Olympus FLUOVIEW FV1000 confocal microscope. The PI stain was excited using the 561 nm HeNe561 diode laser (laser power of 10-15%). Kalman averaging was not used and scans were carried out in a bidirectional manner in order to reduce the image collection time and any potential for sample bleaching. Specimens were imaged between veins to avoid leaf vasculature as much as possible. Samples were scanned with either the abaxial or adaxial surface uppermost, due to the lack of distinct palisade and spongy layers in the wheat chlorenchyma. Initial scans were performed at a resolution of 512 x 512 pixels, with a pixel time of 8 µs/pixel and with a z-step size of 1.14 µm per slice. Both 20x (UPlanSApo 20x, NA: 0.75) and 40x dry objectives (LUMPlanFl 40x, NA: 0.8) were used to complete initial z-stacks of the entire leaf thickness, but the resolution of these stacks was such that individual cells in the resultant 3D stacks could not be easily seeded, and were often over- or under-segmented.

It was discovered that for optimal image collection using this setup, the 40x oil immersion lens of this microscope should be used (UPlanApo 40x, NA: 1.0). Once the imaging protocol had been improved, scans were performed at a resolution of 640 x 640 pixels, with the pixel time increased to 12 µs/pixel and the Z-step reduced to 0.3 µm. This produced stacks with a final voxel size of 0.497 x 0.497 x 0.3 µm (xyz). Additionally, as opposed to trying to scan through the entire leaf thickness (from epidermis to epidermis), a reduced z-depth was used to produce images suitable for segmentation. A mean number of 502 slices, producing a stack size of around 150 µm, were collected from each sample, with scans taking up to 50 minutes. Initiating the stack partway through the sub-epidermal layer of mesophyll cells ensured that one complete layer of mesophyll cells could be imaged in the z-axis. This allowed for the middle layers of mesophyll cells to be reconstructed and reduced stretching of the sample, whilst also mitigating the light decay seen in thicker samples.

4.2.5. Image processing and reconstruction/segmentation using LithoGraphX

3D reconstruction and segmentation of leaf mesophyll cells was carried out using freely available LithoGraphX (LGX) software (Barbier de Reuille *et al.*, 2015). Figure 4.2 summarises the steps required for processing images. Stacks were first converted into the TIFF format using the bioformats plugin for FIJI/ImageJ (Linkert *et al.*, 2010). TIFF image files (16-bit images are required) were then dragged into the user interface to open the stack. The correct voxel size was inputted into the programme and the stack subjected to several stages of processing prior to segmentation and mesh creation. First the stack was autoscaled, before using the sieve algorithm (sieve size: 100 μm^2) to reduce the number of artefacts within the stack. At this stage, the image was also cleaned up, removing leaf vasculature, epidermis and leaf hairs/trichomes if present, as this vastly decreased the computer processing time required to seed the stack. The final step before segmentation was to carry out a Gaussian blur on the stack, with a radius of 0.5 µm. Before optimisation, the blur radius was set at 0.3 µm, but increasing this value to 0.5 µm resulted in a vastly increased accuracy of the segmentation process. An example of a processed stack is shown in Figure 4.2A,B.

Segmentation of the sample was carried out using the ITK Autoseeded Watershed function with a threshold of 1500. If the stack was extremely under- or over-segmented then this value was changed accordingly. In order to ensure that cells were correctly seeded, a certain level of manual input was required. Seeding was examined using a combination of clipping planes and when cells were found to be over-segmented, the labels were fused and reseeded as appropriate, which was often time-consuming. If cells were not completely within the field of view or fully seeded then they were deleted at this stage of processing. Additionally, labelled intercellular airspaces and regions that were under segmented were also removed prior to the creation of the mesh from which geometric data could be extracted. A segmented stack is shown in Figure 4.2C,D.

The mesh was generated using the 3D marching cubes algorithm, with a cube spacing of 1 µm, with three smooth passes. Once this mesh had been

created, final cleaning up of the sample was carried out so that just the middle layer (in z) of mesophyll cells remained. Any remaining artefacts were removed along with other cell types such as guard cells and epidermal cells that remained (process shown in Figure 4.3.) An example of a cleaned mesh is shown in Figure 4.2E,F. A heat map was created for the remaining cells to indicate both cell (mesh) surface area and the volumetric data paired to cell labels – as shown in Figure 4.2G,H. In order to measure the level of mesophyll cell lobing, longitudinal sections of each cell file were taken using clipping planes and lobes counted. This was repeated for three biological replicates per line.

4.2.6. Data analysis

Statistical analyses of the datasets were carried out using GraphPad Prism 8 (Graphpad Software Inc.). Datasets were assessed for normality and significant differences between lines were identified using one-way analysis of variance (ANOVA). When data was not found to be normally distributed, non-parametric analyses (Kruskal-Wallis) to assess variation between genotypes. When individual lines were compared with each other, significance was determined if P= <0.01. When grouped by ploidy level, significance was determined if P= <0.05. When detected, Tukey's HSD was used as a multiple comparisons test to determine significance in the differences in means between lines (to 99% or 95% confidence respectively). Dunn's multiple comparisons test was used on non-parametric datasets to distinguish groups. Comparisons between 4n wild and domesticated lines were carried out via the use of an unpaired, two-tailed t test (P = <0.05). Again, when data was not normally distributed, non-parametric tests were used to analyse differences in ploidy level (Mann-Whitney). When assessing the relationships between parameters, Pearson correlations were used (P= 0.05), unless data was not normally distributed, in which case Spearman correlation analyses were carried out (P= 0.05). All error bars on graphs indicate +/- one standard error of the mean (S.E.M.).

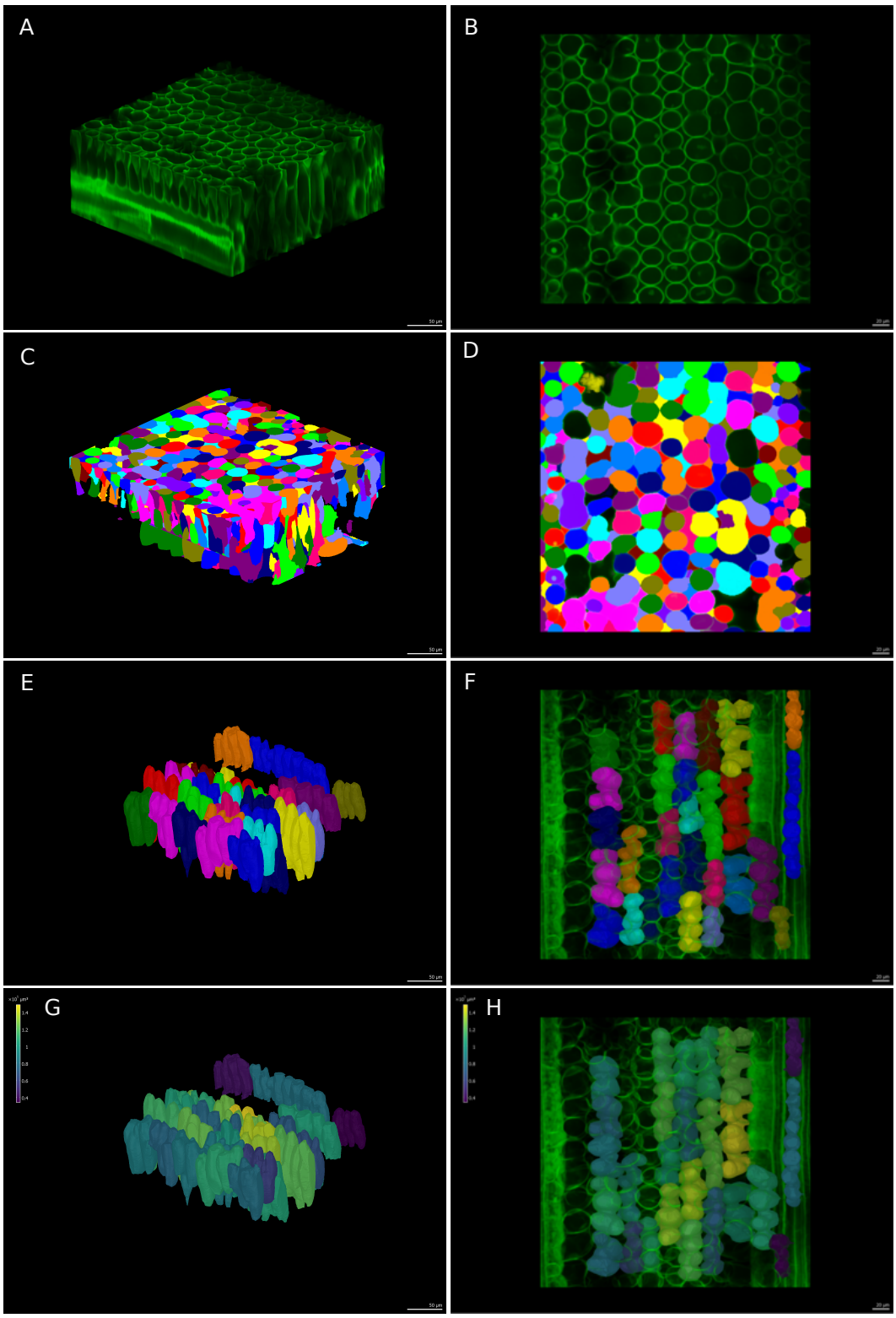

Figure 4.2. LithoGraphX software allows for the reconstruction and segmentation of individual mesophyll cells
Panels A, C, E, G show image stacks, whilst a paradermal slice is shown in panels B, D, F, H. **A, B)** Confocal stacks are converted to tiff files and imported into LGX, where initial cleaning and processing is carried out. **C, D)** Stacks are segmented using the ITK Autoseeded Watershed function. Each cell is designated a different colour (16-bit). Cell seeding is manually checked and corrected as appropriate. **E, F)** A 3D cell mesh is created and cleaned further if required**. G, H)** Quantitative data such as cell surface area and volume are extracted from the mesh and heat maps can be created. In (C, D) and (E, F) individual cells are assigned different colours. In (G, H), purple cells have the smallest volume, whilst those with the greatest volume are yellow in colour. For A, C, E, G scale bars = 50 μm. In B, D, F, H scale bars = 20 μm.

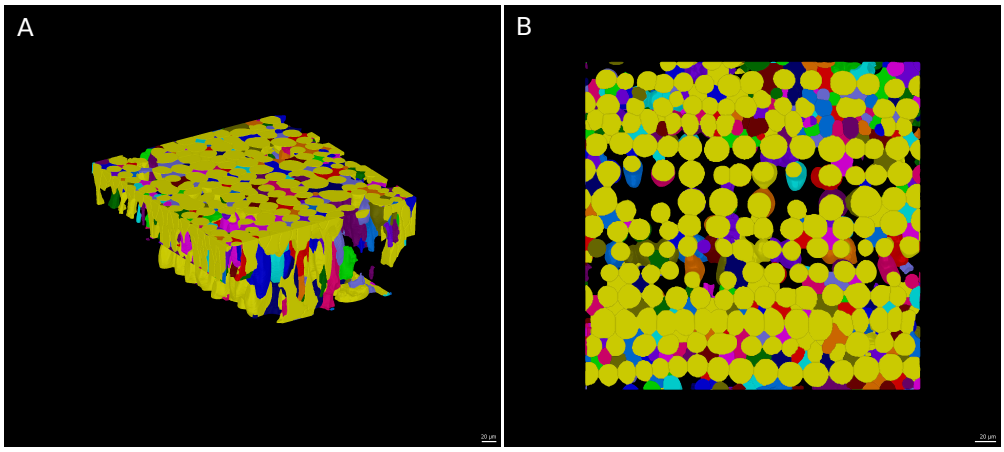

Figure 4.3. Manual mesh cleaning in LGX
Cell meshes are cleaned manually in LGX to remove unwanted epidermal cells and mesophyll cells. **A)** 3D image stack. **B)** Paradermal view of the stack. Cells labelled yellow are those that are to be deleted from the mesh. Scale bars = 20 μm.

4.3. Results

4.3.1. Increases in ploidy level in wheat result in changes in mesophyll cell size and shape

Following the previously observed changes in stomatal and epidermal cell size with changes in ploidy level, and the altered levels of mesophyll porosity that also result from this, it was expected that mesophyll cell size would be affected in a similar manner. Therefore, I explored how ploidy level changes affected mesophyll cell size using a confocal microscopy protocol to image a range of Triticeae varieties representing 2n, 4n and 6n ploidy levels – as summarised in Table 2.2. Initial observations indicated that cells of 2n varieties appeared smaller than those of 4n accessions, whilst 6n cultivars had the largest mesophyll cells in comparison to those of lower ploidy levels (Figure 4.4).

The first geometrical parameter that was investigated was mesophyll cell surface area. It was apparent that there was significant variation in the surface area of the mesophyll cells amongst the 2n, 4n and 6n lines imaged, with a trend towards leaves with a smaller genome size containing mesophyll cells with a smaller mean surface area, similar to the phenotype shown by epidermal and guard cells (Figure 4.5A) (ANOVA, $F_{(10,22)}$= 9.411, P= <0.0001). Details of the multiple comparisons tests for this figure, and for all subsequent figures presenting data from the full range of accessions in this chapter, are available in Appendix 3.

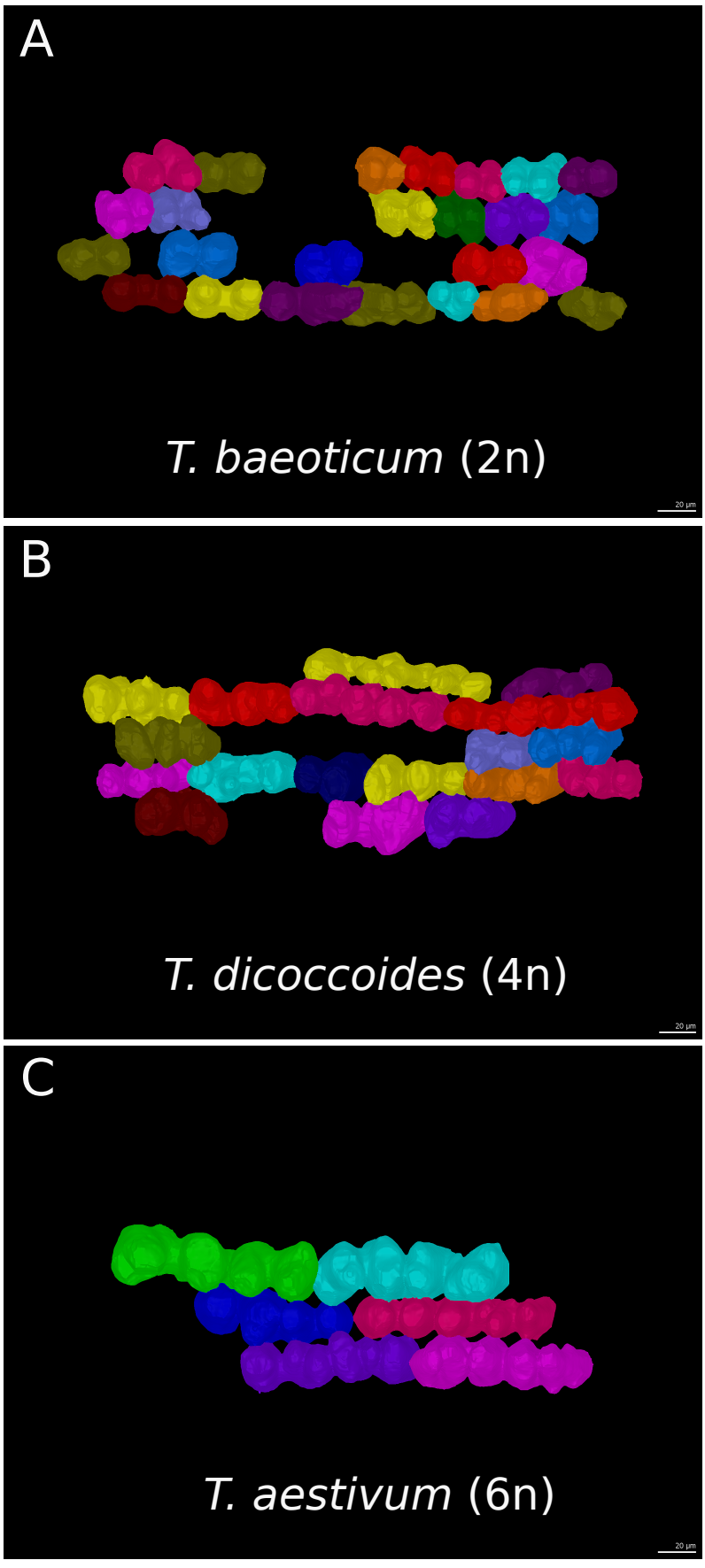

Figure 4.4. Mesophyll cells appear smallest in diploid plants, intermediate in 4n lines and largest in hexaploid accessions
A) Representative image of seeded 2n mesophyll cells. **B)** Seeded cells from a 4n leaf section. **C)** Example mesophyll cells from a 6n wheat leaf. Individual mesophyll cells are assigned a different 16-bit colour. Scale bar = 20 µm.

When the accessions were grouped into their 2n, 4n and 6n ploidy levels (Figure 4.5B), it was apparent that hexaploid mesophyll cells had the highest mean surface area (18966 µm^2), which as significantly higher than the tetraploid samples (13747 µm^2), which in turn had a mean mesophyll cell surface significantly higher than that observed in 2n leaves (8324 µm^2) (ANOVA, $F_{(2,8)}$= 31.12, P= 0.0002). When the role of domestication upon mean mesophyll cell surface area was explored in tetraploid accessions, it was found that there was no significant difference in surface area between 4n wild (13744 µm^2) or domesticated lines (13749 µm^2), which were very similar to one another (unpaired *t* test, $t_{(3)}$= 0.002638, P= 0.9981).

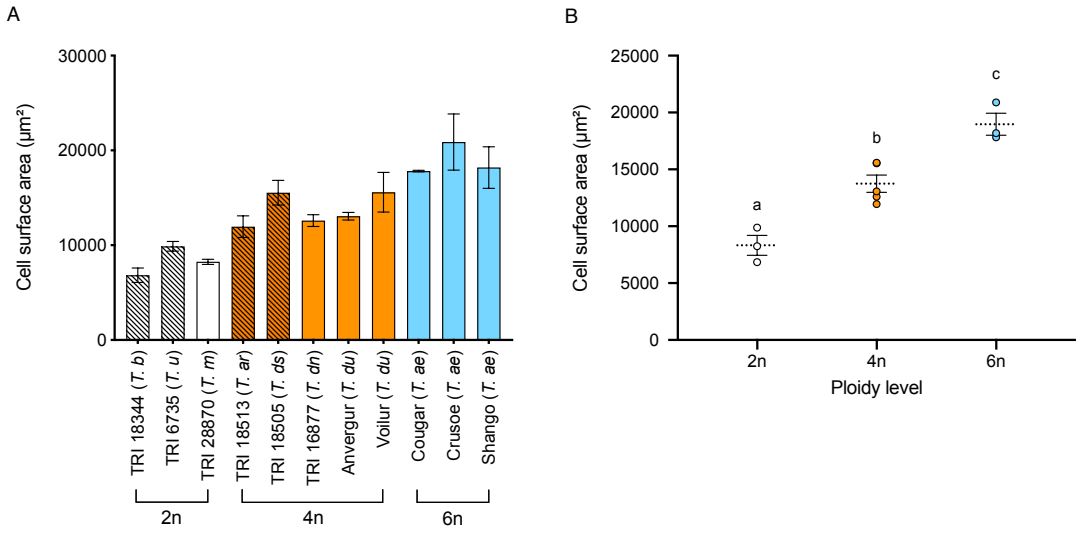

Figure 4.5. There is variation in mesophyll cell surface area between 2n, 4n and 6n lines
A) Mean mesophyll cell surface area of the range of lines, including 2n, 4n and 6n species as indicated. A summary of lines is shown in Table 2.2. **B)** Mean mesophyll cell surface area of 2n, 4n and 6n wheat accessions, with data grouped from those shown in (A). Samples indicated with the same letter cannot be distinguished from one another (P= <0.05) (Tukey HSD post one-way ANOVA). Error bars = S.E.M. n = minimum of 3 per line.

Secondly, differences in mean mesophyll cell volume were examined. Analysis of cell volume data extracted from 3D images using the heat map function of LithoGraphX indicated that, similarly to observed changes in stomatal and epidermal cell size, there was significant variation in mesophyll cell volume across the range of lines under investigation, and that there appeared to be a trend with ploidy level (Figure 4.6A) (ANOVA, $F_{(10,22)}$= 9.411, P= <0.0001). Splitting wheat genotypes into their appropriate ploidy levels, allowed for this trend to be more easily observed (Figure 4.6B), and it was shown that increases in

ploidy level resulted in a significant increase in mesophyll cell volume (ANOVA, $F_{(2,8)}$= 31.12, P= 0.0002). The mean mesophyll cell volume of 2n genotypes was 37413 µm^3, whilst 4n lines had larger cells (65401 µm^3). 6n lines were found to have mesophyll cells with a significantly higher mean volume than both diploid and tetraploid leaves (100726 µm^3). As with mesophyll surface area, domestication was not found to have a significant impact upon mesophyll cell volume in tetraploid plants, with both wild and domesticated species being found to have mesophyll cells of similar mean volume (68113 µm^3 and 63593 µm^3 respectively) (unpaired t test, $t_{(3)}$= 0.4086, P= 0.7103).

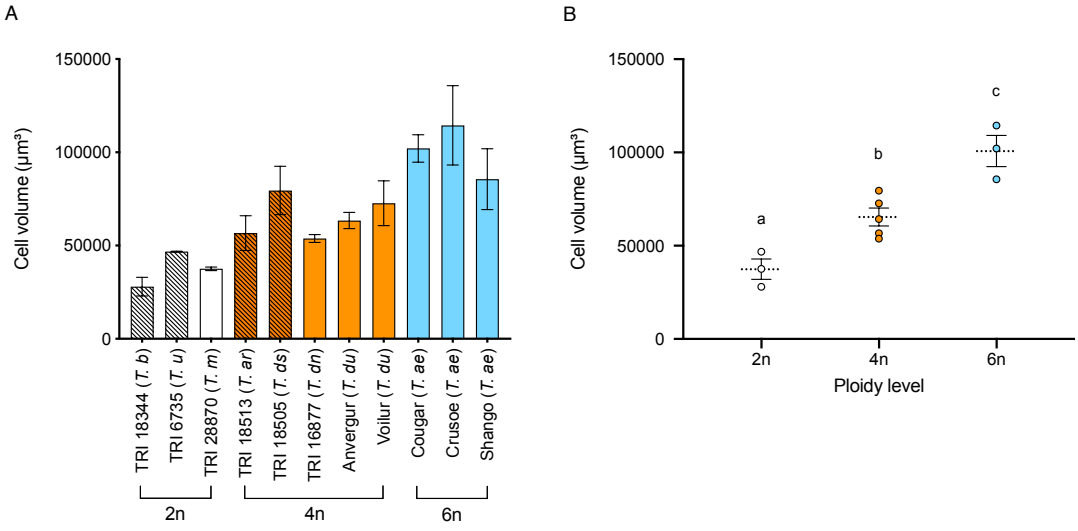

Figure 4.6. There is variation in mesophyll cell volume between 2n, 4n and 6n lines
A) Mean mesophyll cell volume of a range of wheat genotypes, including 2n, 4n and 6n species as indicated. Accession data is available in Table 2.2. **B)** Mean mesophyll cell surface area of 2n, 4n and 6n *Triticum* lines, with data grouped from those shown in (A). Samples indicated with the same letter cannot be distinguished from one another (P= <0.05) (Tukey HSD post one-way ANOVA). Error bars = S.E.M. n = minimum of 3 per line.

In order to investigate the relationship between surface area and volume of mesophyll cells in the Triticeae and how this may or may not change with shifts in ploidy, a correlation analysis between mesophyll cell surface area and mesophyll cell volume was undertaken (Figure 4.7A). It was found that there was a striking positive, linear correlation between surface area and volume (Pearson correlation, r^2= 0.9585, P= <0.0001). Mathematically, surface area should not increase at the same rate as volume increases if the shape remains the same (increases in surface area are squared (x^2), whilst increases in volume are cubed (x^3), see Figure 4.7B), thus suggesting that in addition to the observed size changes associated

with ploidy level, mesophyll cells are also shaped differently in plants of higher levels of ploidy.

Following this discovery, the differences in mesophyll cell shape associated with changes in ploidy level were characterised. Analysis of the surface area to volume ratio (surface area/volume, SA/V) of the mesophyll cells showed that, despite the changes in surface area and volume which occur with changes in ploidy level in *Triticum* species, the surface area to volume ratio does not vary significantly with ploidy at the 99% confidence limit (Figure 4.8A) (ANOVA, $F_{(10,22)}$=2.5, P= 0.0351). When lines were grouped into their respective 2n, 4n and 6n ploidy levels (Figure 4.8B), it was found that, despite a trend towards leaves of higher ploidy level having a lower surface area to volume ratio, there was no significant difference in this parameter between ploidy levels at the 0.05 confidence limit (ANOVA, $F_{(2,8)}$=3.388, P= 0.0859). Any differences in the surface area to volume ratio of the mesophyll cells resulting from domestication within the tetraploid group of accessions were not found to be statistically significant (unpaired t test, $t_{(3)}$= 0.4086, P= 0.7103).

With a view to further investigating this shape change, the number of lobes of individual mesophyll cells was counted (Figure 4.9A). It was found that there was significant variation between the lines under investigation (Kruskal-Wallis, H = 26.24, n = 3,6,3, P= 0.0034). When grouped by ploidy level (Figure 4.9B), it was shown that ploidy level had a significant effect upon mesophyll cell lobe number (Kruskal-Wallis, H = 8.727, n = 3,6,3, P= 0.0006). Dunn's multiple comparisons test was used to identify significant differences between groups. There was a trend towards mesophyll cells of higher ploidy levels having a higher mean number of cell lobes (8.96) than intermediate diploid lines (6.59), with diploid genotypes having on average the lowest mean number of lobes per cell (4.55), and this was easily visually observed (Figure 4.10). Only the 2n and 6n groups were found to be significantly different from one another. Domestication was not found to have a significant effect upon mesophyll cell lobe number within the group of 4n lines (Mann-Whitney, U = 2, n = 2,3, P= 0.800).

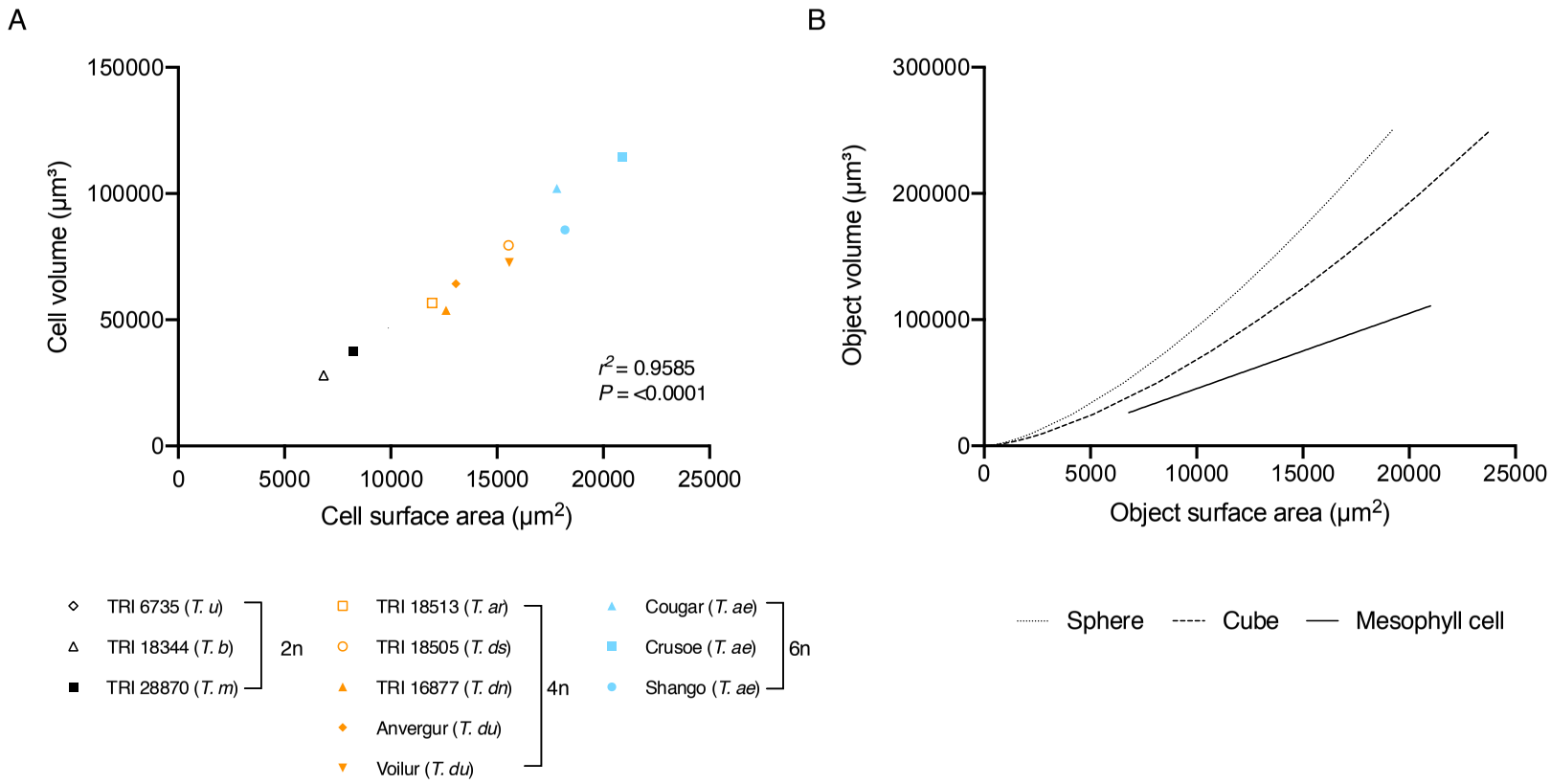

Figure 4.7. Relationships between mesophyll cell surface area and volume

A) There is a strong, linear positive correlation between mean mesophyll cell surface area and mean mesophyll cell volume in 2n, 4n and 6n members of the Triticeae (as indicated – see Table 2.2 for accession data). Results of the correlation analysis are presented (Pearson r^2 value). n = minimum of 3 per line. **B)** The theoretical curvilinear relationships between surface area and volume for a sphere and a cube (dashed lines as indicated) compared to the linear relationship observed in wheat mesophyll cells of varying ploidy levels (solid line).

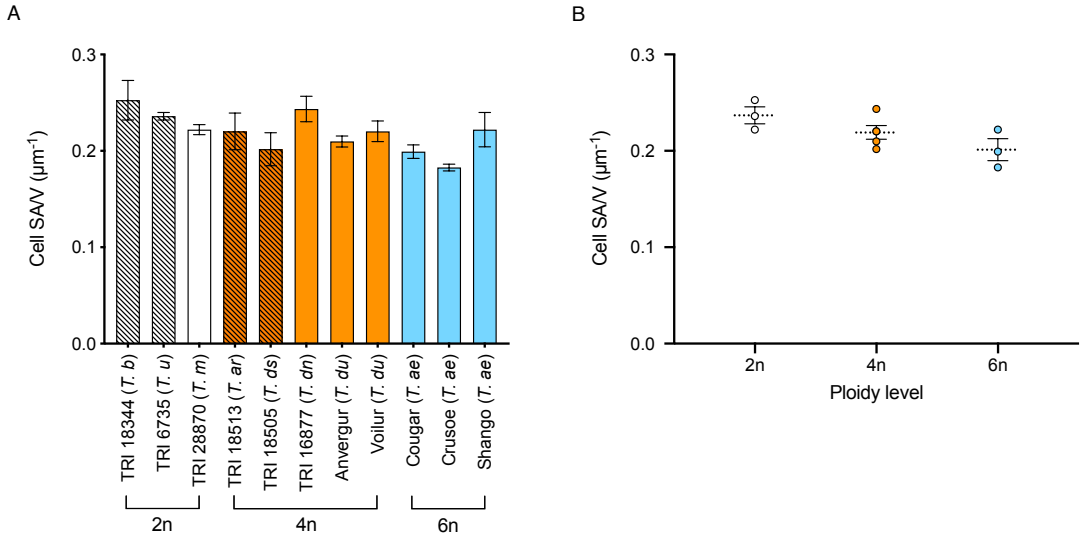

Figure 4.8. There is no significant variation in the surface area to volume ratio of wheat mesophyll cells for wheat lines of ranging ploidy level (2n, 4n, 6n)
A) Mean mesophyll cell surface area to volume ratio of a series of wheat genotypes, including 2n, 4n and 6n accessions as indicated. Accession data is summarised in Table 2.2. **B)** Mean mesophyll cell surface area to volume ratio of 2n, 4n and 6n wheat varieties, with data grouped from those shown in (A). Error bars = S.E.M. n = minimum of 3 per line.

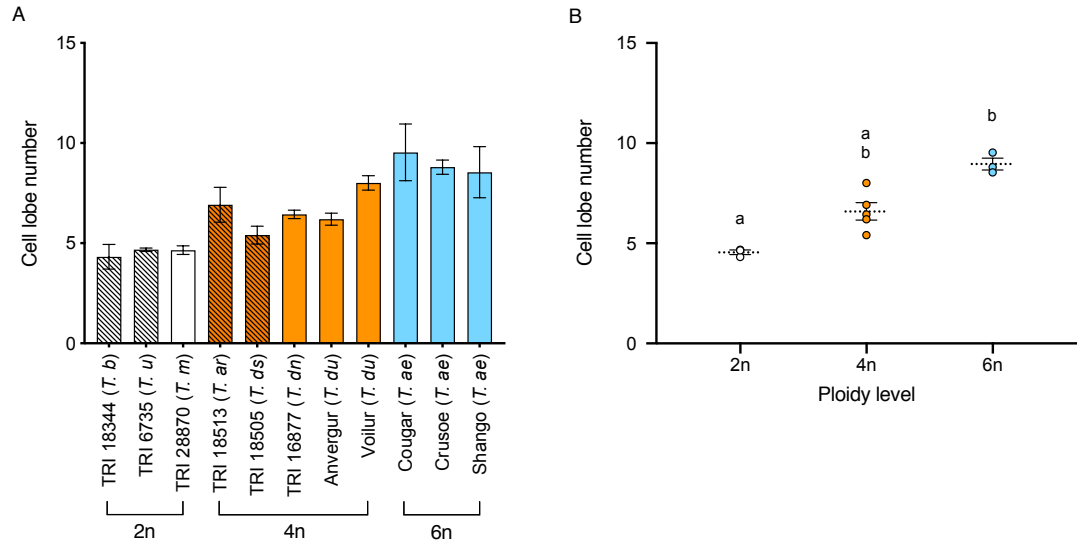

Figure 4.9. There is significant variation in the mesophyll cell lobe number of wheat genotypes of ranging ploidy level (2n, 4n, 6n)
A) Mean mesophyll cell lobe number of a range of wheat lines, including 2n, 4n and 6n accessions as indicated. A summary of lines is available in Table 2.2. **B)** Mean mesophyll cell lobe number of 2n, 4n and 6n wheat varieties, with data grouped from those shown in (A). Lobe number changes significantly with changes in ploidy level. Samples indicated with the same letter cannot be distinguished from one another (P= <0.05) (Kruskal–Wallis). Error bars = S.E.M. n = minimum of 3 per line.

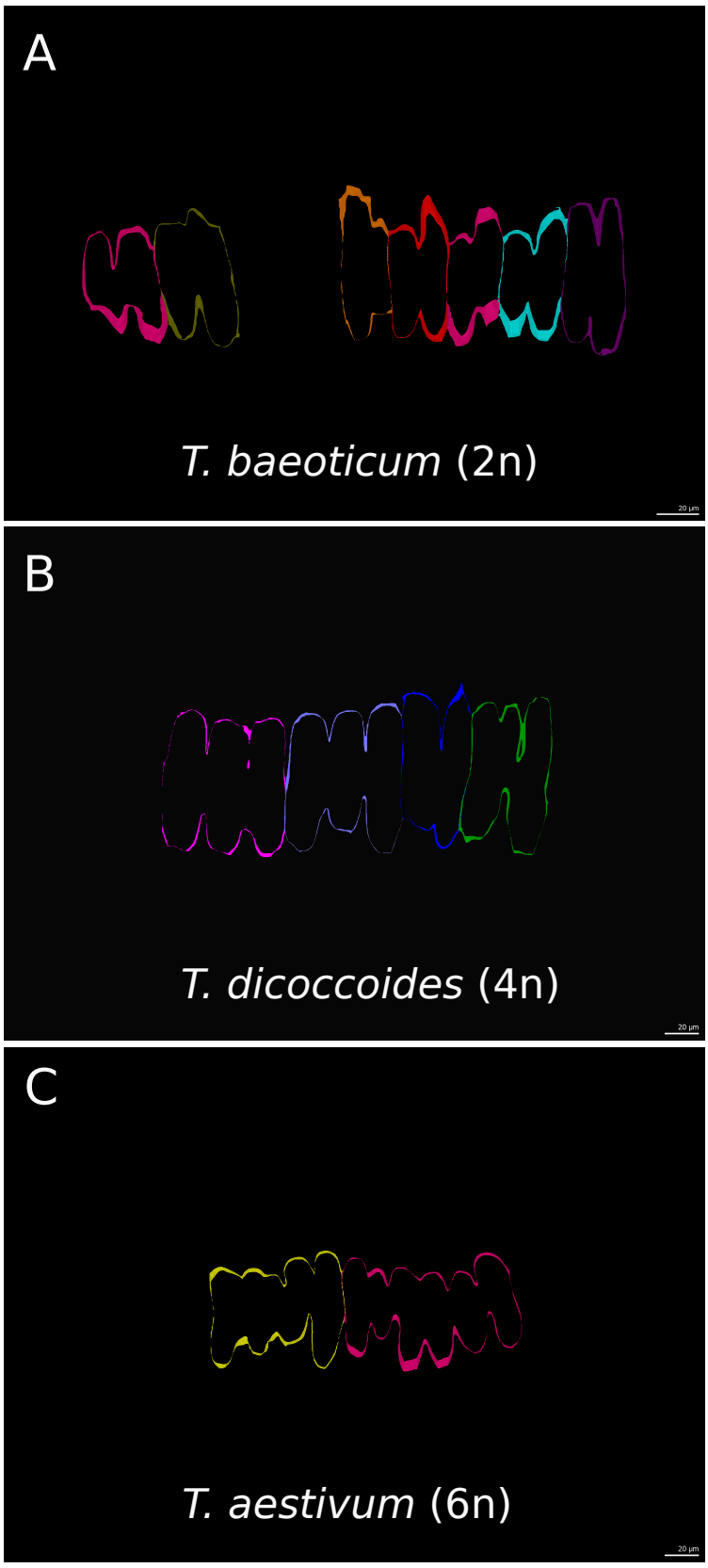

Figure 4.10. Variation in mesophyll cell lobing
Mesophyll cells have the smallest number of lobes in diploid plants. Lobing is intermediate in 4n lines and hexaploid accessions have cells with the greatest number of cell lobes. **A)** Representative slice through a file of seeded 2n mesophyll cells showing the degree of lobing. **B)** A slice through seeded cells from a 4n leaf section showing cell lobing. **C)** Example slice through mesophyll cells from a 6n wheat leaf from which cell lobes can be counted. Individual mesophyll cells are assigned a different 16-bit colour. Scale bar = 20 µm.

In order to explore how the observed changes in mesophyll cell lobe number that occur with shifts in ploidy level may relate to changes in cell size, a number of correlations between lobe number and cell geometrical parameters were carried out. When lobe number and mesophyll cell surface area were analysed, it was found that these parameters were positively correlated (Figure 4.11A), with mesophyll cells having a higher number of cell lobes showing a concurrent increase in surface area (Spearman correlation, r_s= 0.8818, P= 0.0007. A similar relationship was observed when the correlation between lobe number and mesophyll cell volume was investigated (Figure 4.11B) (Spearman correlation, r_s= 0.8727, P= 0.0009). When the relationship of cell lobing with surface area to volume ratio was explored, despite the presence of a negative trend (Figure 4.11C) (a decreased number of cell lobes being associated with a higher surface area to volume ratio), this relationship was not found to be significant (Spearman correlation, r_s= -0.5909, P= 0.0609).

4.3.2. Mesophyll cell geometry is correlated with mesophyll airspace levels and exposed mesophyll surface area

The different mesophyll cell geometries found in wheat leaves of different ploidy levels might be expected to have a relationship with the levels of leaf airspace discussed in the previous chapter. Investigations of the relationship of mesophyll cell surface area with mesophyll porosity values taken from the previous chapter (Figure 4.12A) indicated that mesophyll cells which have a larger surface area are associated with lower levels of leaf airspace as they are inversely correlated (Pearson correlation, (r^2= 0.6097, P= 0.0046). Likewise, a similar negative relationship was indicated between mesophyll cell volume and mesophyll porosity (Figure 4.12B) (Pearson correlation, r^2= 0.7262, P= 0.0009).

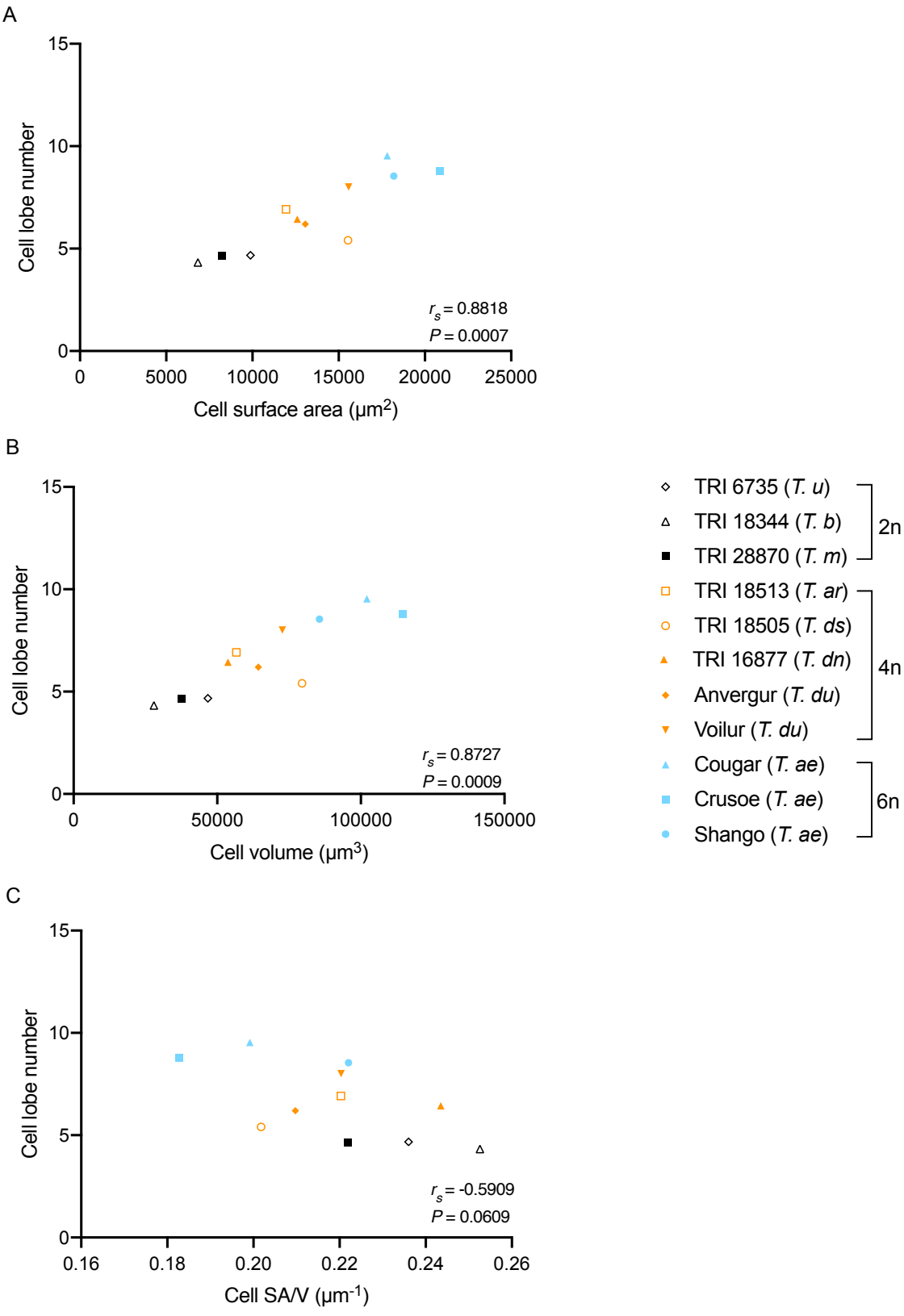

Figure 4.11. Mesophyll cell lobe number is correlated with other mesophyll cell geometric parameters in wheat leaves of varying ploidy levels
A) Mean cell lobe number is plotted against mean cell surface area for each of the lines described in Table 2.2. **B)** Mean cell lobe number plotted against mean cell volume for the same *Triticum* varieties as in (A). **C)** Mean cell lobe number plotted against mean cell surface area to volume ratio for the same range of wheat accessions as in (A) and (B). Results of correlation analyses are presented (Pearson r^2 value or Spearman r_s value as appropriate). n = minimum of 3 per line.

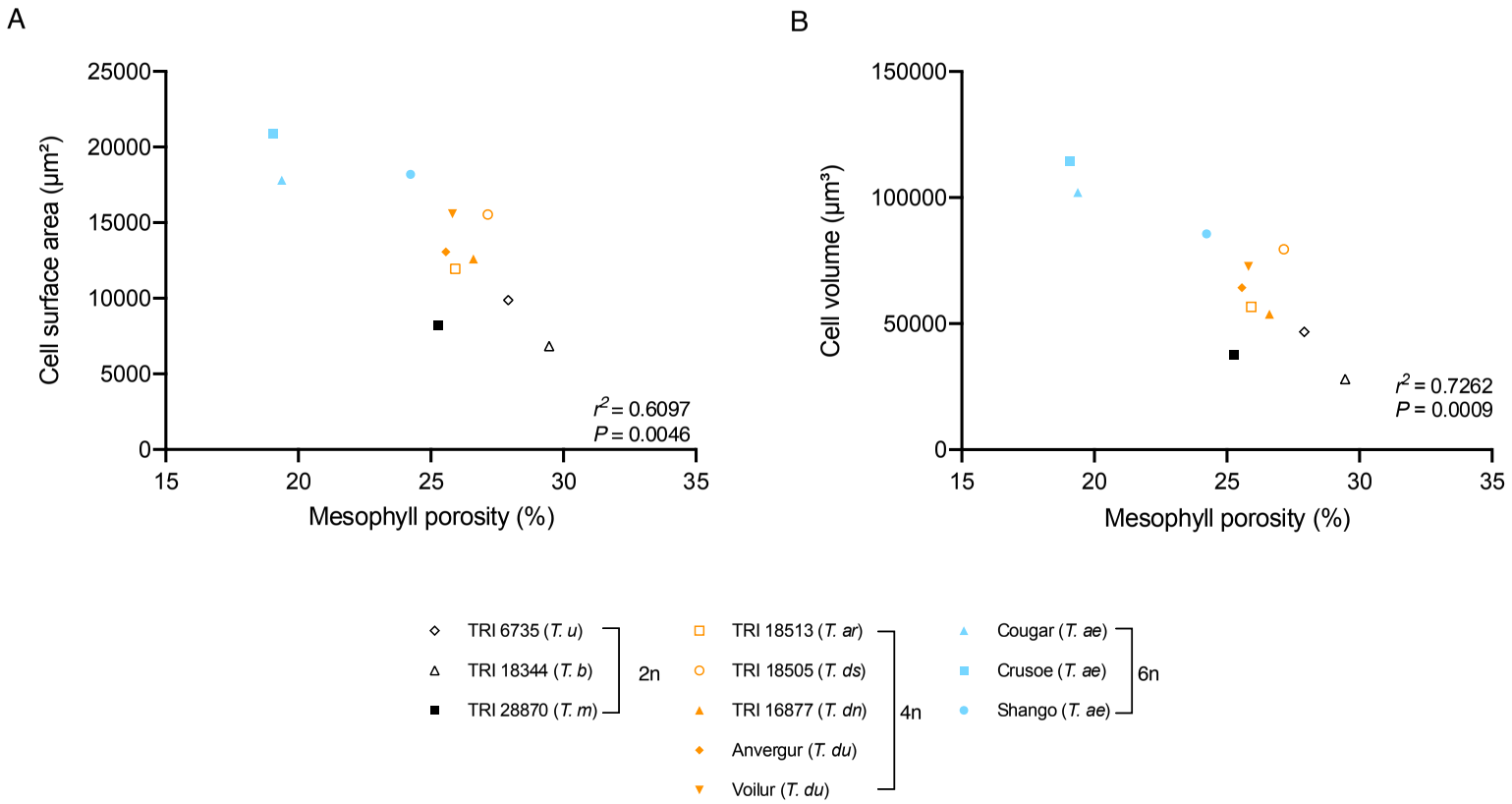

Figure 4.12. Mesophyll cell size parameters are inversely correlated with mesophyll porosity (%airpace/volume) in 2n, 4n and 6n *Triticum* lines
A) Mean mesophyll cell surface area plotted against mean mesophyll porosity for wheat lines of varying ploidy level as indicated. See Table 2.2. For a list of genotypes used. **B)** Mean mesophyll cell volume plotted against mean mesophyll porosity for the same varieties as in (A). Results of correlation analyses are presented (Pearson r^2 value). n = minimum of 3 per line.

In addition to mesophyll cell size parameters, how mesophyll cell shape affects intercellular airspace levels in the Triticeae across the three ploidy levels was also investigated. When the relationship between mean mesophyll cell surface area to volume ratio and mesophyll porosity was explored (Figure 4.13A), it was found that there was a positive correlation between these parameters (Pearson correlation, r^2= 0.6339, P= 0.0034). Mesophyll cell lobe number was significantly negatively correlated with leaf airspace (Figure 4.13B), with an increased level of cell lobing being associated with lower levels of mesophyll porosity (Spearman correlation, r_s= -0.7455, P= 0.0112).

To investigate if there was a relationship between individual mean mesophyll cell size and the total amount of exposed mesophyll surface area per volume of leaf (S_{mes}), I performed a correlation analysis across the *Triticum* genotypes of varying ploidy levels (2n, 4n, 6n). The results showed that there was a significant negative correlation of individual mean cell surface area and S_{mes} (Figure 4.14A) (Pearson correlation, r^2= 0.4995, P= 0.015). Additionally, when the relationship between individual mesophyll cell volume and S_{mes} was explored, a similar pattern was observed (Figure 4.14B) (Pearson correlation, r^2= 0.5540, P= 0.056).

When mesophyll cell shape parameters, i.e. the mesophyll cell surface area to volume ratio and the number of cell lobes, were investigated, it was found that mesophyll cell surface area to volume ratio had a significant positive correlation with S_{mes} in wheat species (Figure 4.15A) (Pearson correlation, r^2= 0.6545, P= 0.0026). Conversely, and similarly to cell size variables, it was shown that S_{mes} and mesophyll cell lobe number were moderately negatively correlated (Figure 4.15B) (Spearman correlation, r_s= -0.7000, P= 0.0204).

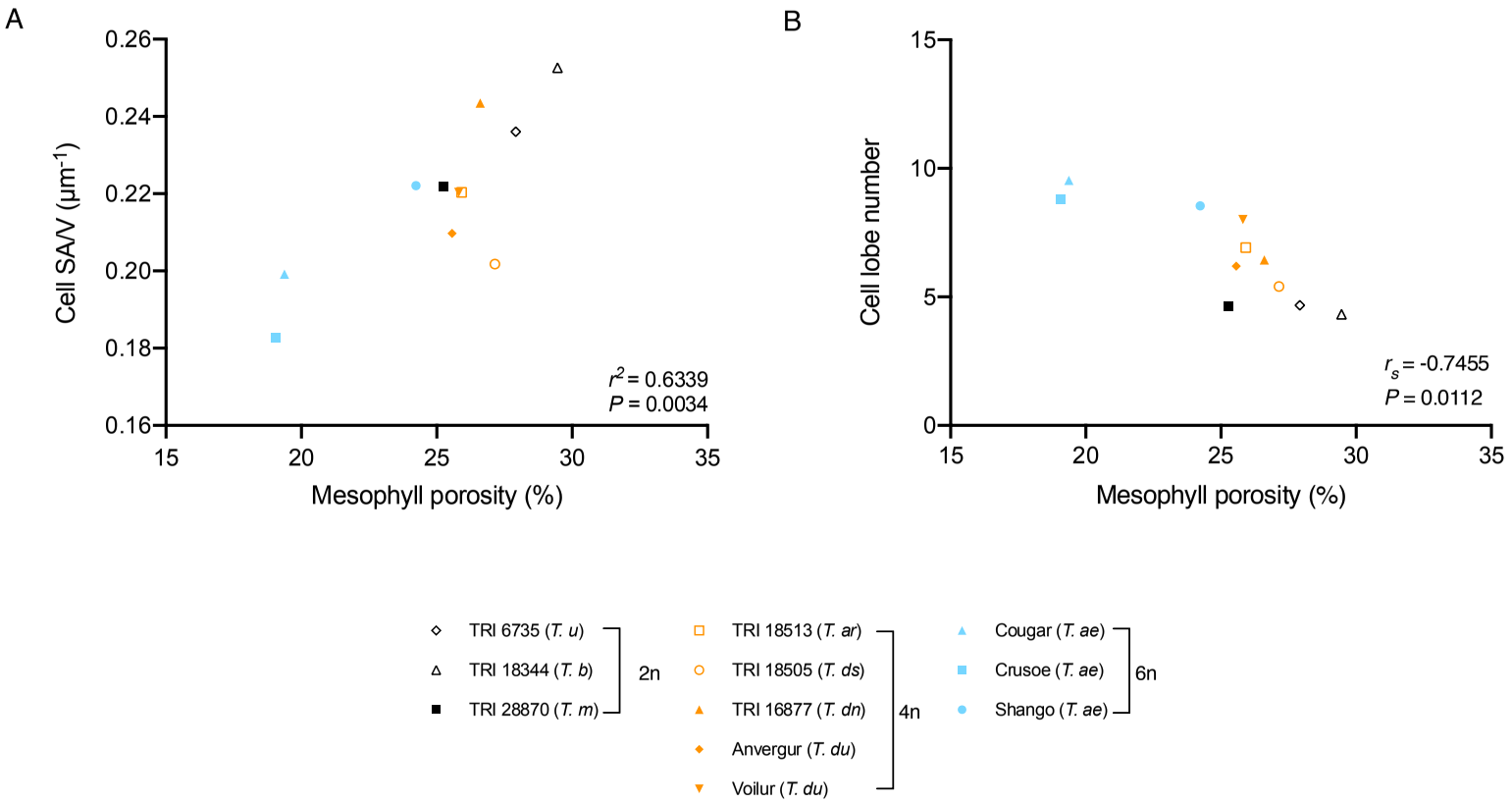

Figure 4.13. Mesophyll cell shape parameters are correlated with mesophyll porosity (%airspace/volume) in 2n, 4n and 6n wheat genotypes
A) Mean mesophyll cell surface area to volume ratio (SA/V) plotted against mean mesophyll porosity for lines of the Triticeae of varying ploidy level as indicated. See Table 2.2 For a list of genotypes used. **B)** Mean mesophyll cell lobe number plotted against mean mesophyll porosity for the same genotypes as (A). Results of correlation analyses are presented (Pearson r^2 value or Spearman r_s value as appropriate). n = minimum of 3 per line.

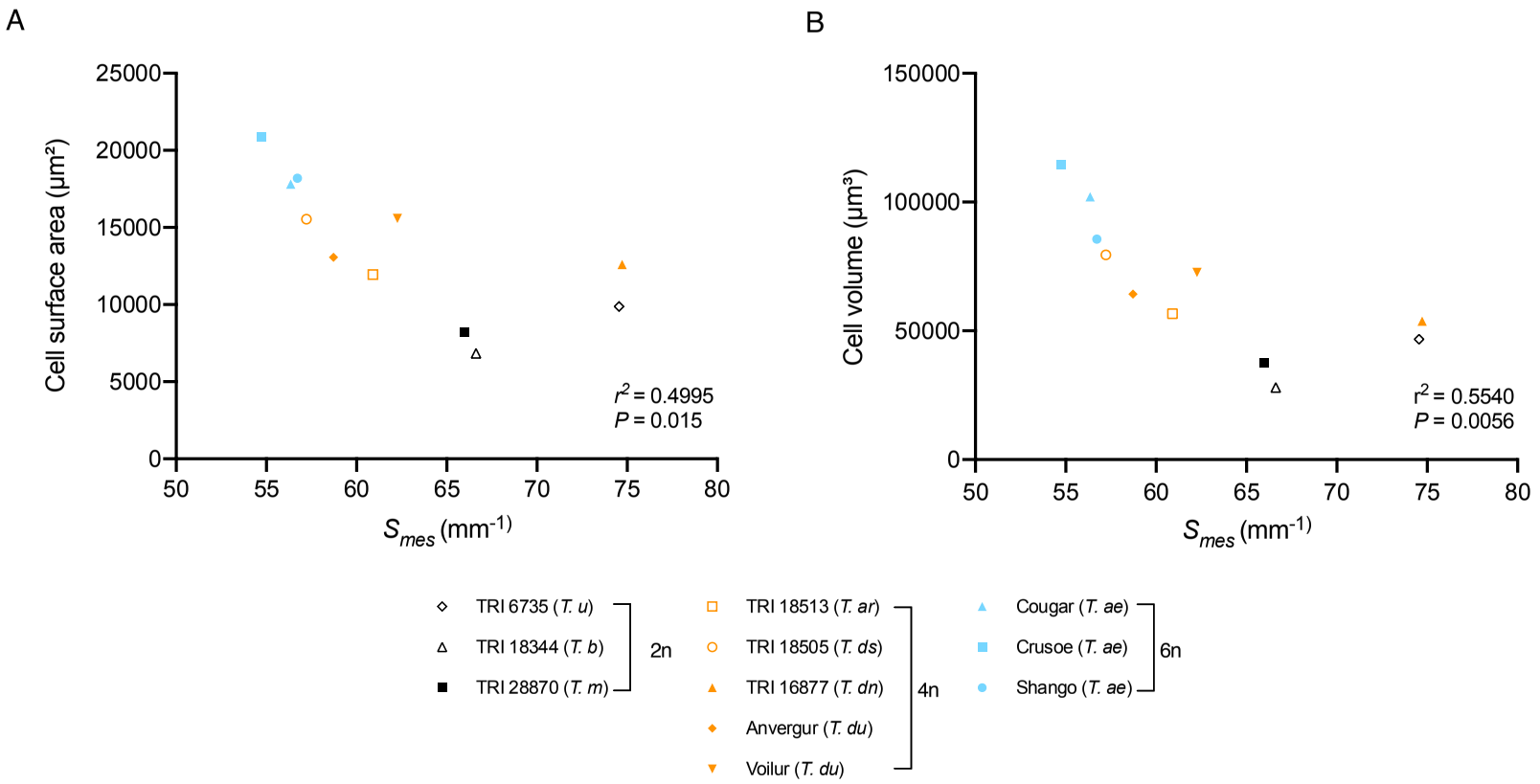

Figure 4.14. Mesophyll cell size parameters are correlated with exposed mesophyll surface area (S_{mes}) in 2n, 4n and 6n wheat genotypes
A) Mean mesophyll cell surface area plotted against mean S_{mes} for lines of the Triticeae of varying ploidy level as indicated. See Table 2.2 for a summary of accessions. **B)** Mean mesophyll cell volume plotted against mean S_{mes} for the same genotypes as (A). Results of correlation analyses are presented (Pearson r^2 value). n = minimum of 3 per line.

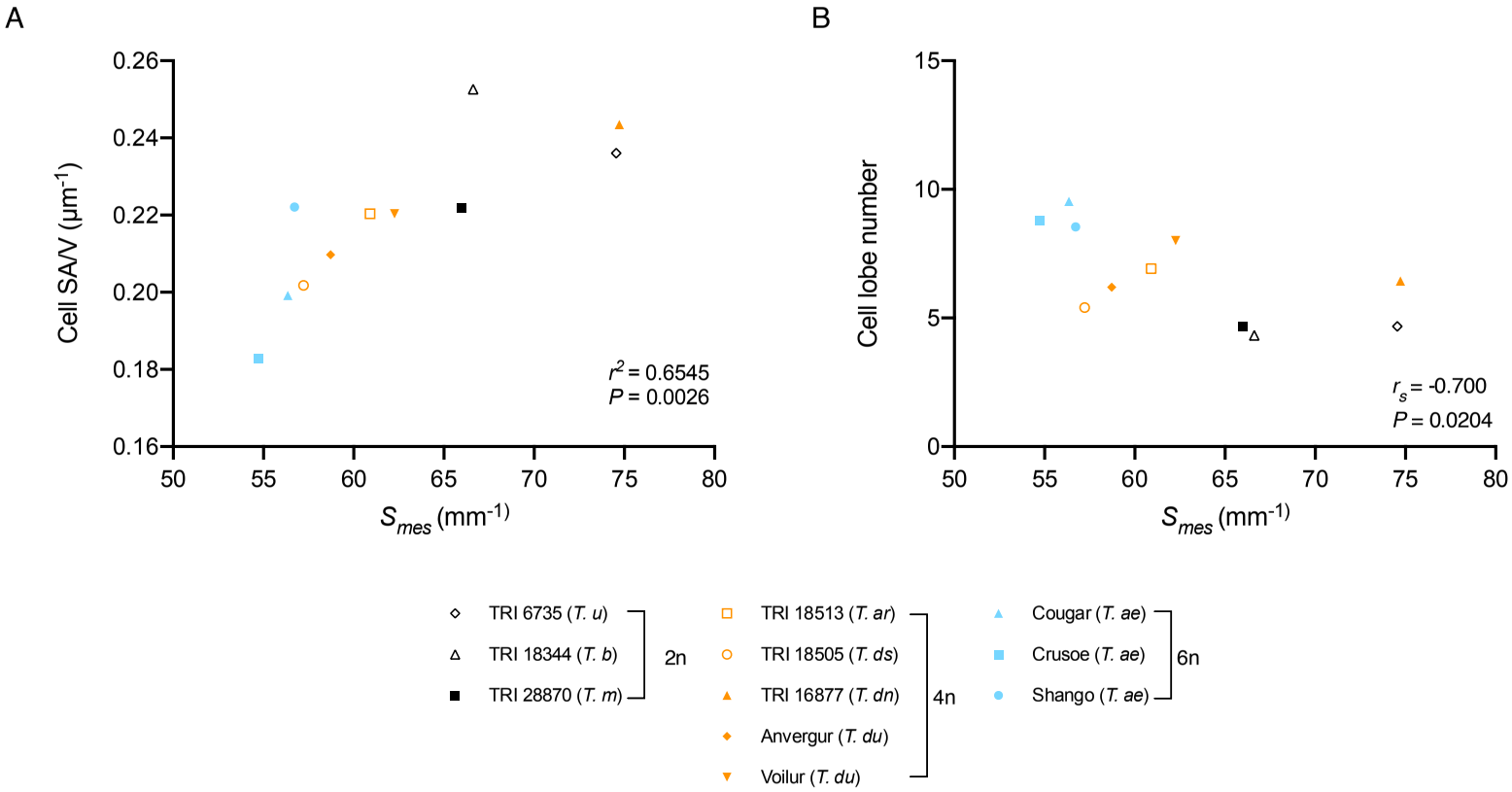

Figure 4.15. Mesophyll cell shape parameters are correlated with *S*$_{mes}$ in 2n, 4n and 6n wheat genotypes
A) Mean mesophyll cell surface area to volume ratio (SA/V) plotted against mean *S*$_{mes}$ for lines of the Triticeae of varying ploidy level – as indicated. See Table 2.2 for a summary of lines used. **B)** Mean mesophyll cell lobe number plotted against *S*$_{mes}$ for the same accessions as (A). Results of correlation analyses are presented (Pearson r^2 value or Spearman r_s value as appropriate). n = minimum of 3 per line.

4.4. Discussion

The interactions between ploidy level and mesophyll cell size and shape in the Triticeae have previously been characterised (Dunstone & Evans, 1974; Parker & Ford, 1982; Jellings & Leech, 1984; Pyke *et al.*, 1990). However, these studies rely upon the intrinsically indirect assay of 2D geometric datasets using traditional histological sectioning methods to estimate 3D properties (surface area and volume). The decades since these papers were published have witnessed the advent of high-resolution 3D imaging techniques. This chapter takes advantage of the capability of confocal microscopy to produce 3D z-stacks of thick tissues to cellular resolution in order to generate more accurate estimations of the cell size and shape differences that result from differential genome size that occurred during the domestication/evolution of wheat from its wild relatives. Furthermore, the impact of any changes in mesophyll cell geometry upon the arrangement of leaf intercellular airspace is also investigated, as this provides the interface between cell form and function.

4.4.1. Mesophyll cell size and shape is influenced by ploidy level in *Triticum* species

Previous studies using 2D estimations of mesophyll geometry indicated that increases in ploidy level in the Triticeae were accompanied by a concurrent rise in mesophyll cell size (Dunstone & Evans, 1974; Parker & Ford, 1982; Jellings & Leech, 1984; Pyke *et al.*, 1990). The more accurate 3D datasets produced in this chapter confirm this pattern, with diploid plants being shown to have the lowest mean mesophyll cell surface area and volume, tetraploid leaves containing mesophyll cells of intermediate size and hexaploid lines having the biggest mesophyll cells. Despite the differing varieties and growth conditions used, leaf 5 mesophyll cell volumes for each of the ploidy levels used in this study were bigger than those measured in flag leaves by Parker and Ford (1982), similarly to observations by Pyke *et al.* 1990.

In addition to the observed changes in mesophyll cell size in *Triticum* species, it was previously found that mesophyll cells of different ploidy levels had differing shapes - specifically in the degree of lobing (Dunstone

& Evans, 1974; Parker & Ford, 1982). When measured surface area and volume values were plotted against one another, it could be seen that these had an almost linear positive relationship. When volume increases, it is not mathematically expected that the surface area of a shape will increase linearly if the shape remains the same. This is because surface area scales to the power of two (x^2), whilst volume scales to the power of three (x^3). If a linear relationship is observed, this implies that there must be a concomitant shape change (e.g., the number of lobes) associated with size change in wheat mesophyll cells. If such a linear relationship is observed, this also raises the question of the functional driver for any shape change. It has been hypothesised that increases in the number of lobes has the effect of increasing the surface area to volume ratio of the mesophyll cells and thus available area for CO_2 diffusion (Tholen *et al.*, 2012). My results suggest that whilst increased levels of lobing in 6n mesophyll cells did not increase the surface area to volume ratio compared with lower ploidy level cells, this parameter did not decrease significantly (as would be expected if there was a simple increase in volume without shape change). This indicates that the increased lobing observed in larger, higher ploidy cells may act to maintain an optimum mesophyll cell surface area to volume ratio for gas exchange in the Triticeae. In this perspective, cell lobing may be seen more as a way to cope with increased cell size linked to increased ploidy rather than a mechanism of increasing cell area for gas exchange.

4.4.2. Mesophyll cell geometry is correlated with leaf airspace and the amount of exposed mesophyll surface

These findings led to questions regarding the relationships of mesophyll cell size and shape to other leaf internal parameters that may influence gas flux such as mesophyll porosity and S_{mes}. Previous work in Arabidopsis has investigated how changes in cell size may affect the intercellular airspaces in the chorenchyma and resultant impacts upon leaf gas exchange and physiology (Dorca-Fornell *et al.*, 2013; Lehmeier *et al.*, 2017). In the first of these studies, the authors found that alterations to the cell cycle that caused a reduction in mesophyll cell size were linked with an increase of mesophyll porosity (Dorca-Fornell *et al.*, 2013). Lehmeier *et al.* (2017) also noticed that manipulation of the cell cycle to produce larger cells resulted in a decrease in leaf porosity. This negative

relationship between leaf intercellular airspaces and mesophyll cell size was mirrored in the Triticeae, with 2n lines having smaller cells and a more porous chlorenchymatous tissue than 4n and 6n varieties (which had larger cells). Contrasting consequences of changes in mesophyll geometry have also been shown in Arabidopsis, with a diminution in cell size being associated with more dense packing of mesophyll cells and a lower volume of leaf airspace (Lehmeier *et al.*, 2017). The effects of mesophyll cell shape upon mesophyll porosity have not previously been investigated. My results suggest that surface area to volume ratio has a positive relationship with leaf airspace and that lobe number is negatively correlated with mesophyll porosity.

Whilst increasing lobing has been hypothesised to increase surface area, a more important parameter for photosynthetic gas exchange is the S_{mes}, or how much of the mesophyll surface area is exposed to the intercellular airspace. It has previously been suggested that the increased lobing of mesophyll cells in hexaploid leaves increases S_{mes} (Austin *et al.*, 1982; Parker & Ford, 1982), however my results suggest that S_{mes} is negatively related with the degree of cell lobing. Although a reduction in cell surface area for the diffusion of gases might limit CO_2 entry, it will also mitigate water vapour egress thus playing an important role in balancing assimilation and water use and as such may improve plant WUE. Different cell shapes will influence potential cell packing within a leaf, thus influencing how much of a cell surface is free for gas exchange, which is a topic for further investigation. Alternative packing patterns may also explain the lack of an effect of ploidy level (and thus cell size) upon leaf thickness (as found in Chapter 2) and may also illuminate discrepancies in leaf size. Differential cell packing may also impact upon leaf airspace levels, for example if cells are more tightly packed this may reduce mesophyll porosity (Lehmeier *et al.*, 2017). Although it has not been possible to image two mesophyll cell layers in their entirety, it is possible to perceive how cell layers may interact. Observations of the packing of adjacent mesophyll cell layers allow me to postulate that the larger lobes of hexaploid mesophyll cells may be able to 'interlock' in a tighter fashion, although this should be explored further.

Furthermore, changes in the size, shape and distribution of mesophyll cells and intercellular airspaces may also have an effect on the light environment in the leaf (Tholen *et al.*, 2012; Ren *et al.*, 2019). It is expected that different mesophyll geometries will result in alternative light scattering and focussing patterns, which may have knock-on effects on light absorption and photosynthetic electron transport (Xiao *et al.*, 2016). Analysis of how light absorption is influenced by leaf anatomy – possibly via a chlorophyll fluorescence approach (Takahashi *et al.*, 1994; Vogelmann & Evans, 2002; Brodersen & Vogelmann, 2010; Ichiro *et al.*, 2016), would be useful to further understand the effects that variations in cell size and shape have upon photosynthesis.

Using wheat transgenics targeting the cell cycle, it may be possible to achieve similar changes in mesophyll cell size as previously utilised in Arabidopsis. This will allow for cell size and shape changes in leaves to be made independent of ploidy, which may enable a more complete picture of the relationships between cell size, leaf internal structure and physiology to be elucidated. Additionally, it may also be possible to alter the amount of mesophyll lobing via a transgenic approach (Wang *et al.*, 2017), allowing the importance of cell lobing for optimum gas exchange to be determined. Changes in cell size in wheat may also have knock-on effects upon leaf vasculature patterning, as in rice (Smillie *et al.*, 2012; Feldman *et al.*, 2017), which could also impact upon photosynthesis and water use (although, unlike in wheat leaves, rice mesophyll cells are arranged perpendicular to veins, and such changes in cell size may have a greater effect upon vein density characteristics in this species). The observed changes in mesophyll cell size reported here in wheat may explain the differences seen in leaf vasculature with ploidy in Chapter 2.

4.4.3. Method development and future prospects of using a confocal microscopy approach to quantify mesophyll cell geometric parameters

Whilst confocal microscopy provides advantages over traditional histology techniques for the extraction of 3D structural data from leaf tissue, this method does however have some limitations. Although more accurate and still faster than the 2D sectioning techniques, it requires a large amount of manual input for correct cell seeding during image

processing. In the future, it may be possible to further improve image acquisition or to introduce automation of this procedure. Now that I have successfully developed a protocol for imaging thicker leaf samples, it would also be of interest to expand the use of this technique for the 3D imaging of mesophyll cells in other crop species, such as rice.

A requirement of the stacks used to reconstruct and segment plant cells in 3D in this manner is that they must have a high contrast between the stained cell wall boundary and surrounding areas of the image (Bassel, 2015). Without this high signal/noise ratio, it becomes trickier to seed individual cells accurately. In order to generate appropriate image stacks, it is necessary during image acquisition to ensure that cell boundaries are near saturation and that there is an absence of signal adjacent to these borders. This can be achieved by altering the HV (detector voltage), gain and offset directly on the microscope, but can also be achieved via improved sample preparation and clearing (Truernit *et al.*, 2008; Bassel, 2015). Furthermore, some detectors on confocal microscopes are more sensitive and may be better at providing a higher contrast between cell wall signal and other areas of the stack (Bassel, 2015). If boundaries between objects are not clear and complete, this can lead to accuracy issues with cell segmentation, and cells may bleed into each other and be incorrectly seeded. Oversaturation of samples may also lead to segmentation difficulties (Bassel, 2015).

The use of alternative clearing protocols may improve this process, thus enabling high-resolution, high contrast imaging deeper into the tissue (Kurihara *et al.*, 2015). It is also possible that image resolution could be improved via the use of perfluorodecalin as a mountant, as this has previously been shown to improve contrast and the depth to which Arabidopsis leaves can be imaged successfully (Littlejohn *et al.*, 2010; Littlejohn *et al.*, 2014). Furthermore, using CLARITY techniques assisted by enzyme degradation to increase the permeability of cell walls may further improve clearing (Palmer *et al.*, 2015). A further advantage of this technique is that proteins and nucleic acids are not removed, unlike when PS-PI stain is used.

Several attempts were made to improve the signal-to-noise ratio of stacks throughout the project. A reduction in step size from the system derived optimum of 1.4 µm to 0.3 µm ensured that axial resolution of cell walls was maintained. Whilst this amounted to over-sampling, and increased scan time, the improvements in stack segmentation outweighed this. The detectors on the Olympus FV100 used for image acquisition were upgraded from PMT (photomultiplier tube) to more sensitive GaAsP (gallium arsenide phosphide) detectors part way through the project, and this led to significant improvements in the signal to noise ratio and thus ease of segmentation. Furthermore, whilst having a shorter working distance – and thus not being able to image as deep into the tissue as non-immersion lenses – the 40x oil immersion lens used resulted in images having cell boundaries that were far clearer than those seen when stacks were taken using the 40x dry or 20x dry lenses. This lens had a far greater numerical aperture value (NA – the measure of an objective's ability to gather light and resolve detail at a set distance) than the other objectives used, and viewing through immersion oil ensured that the refractive index was more similar to that of the mountant, further increasing the quality of the images taken. As a result of this, segmentation of these stacks was far less prone to error than those collected using the alternative objectives.

Boundary clarity can also be improved post-acquisition during image processing. Increasing the Gaussian blur from the initially recommended value of 0.3 µm to a blur of 0.5 µm vastly improved the continuity of cell boundaries and led to far greater segmentation accuracy and consistency. It may be possible to further increase this contrast of the cell boundary using alternative imaging techniques: either by acquiring images from multiple angles (particularly useful for increasing signal to noise in the z-direction) or using multiphoton systems (Wuyts *et al.*, 2010; Kurihara *et al.*, 2015), which can produce images with a higher signal-to-noise-ratio. Additionally, multiphoton microscopy allows for deeper penetration than traditional confocal microscopes, but these systems are not as easily accessible as confocal microscopes (Wuyts *et al.*, 2010). An alternative system that could also be adopted for volumetric imaging of wheat leaves is light sheet microscopy, although the sample size although light-

scattering within the mesophyll may reduce the utility of such systems (Ovečka *et al.*, 2018).

Whilst improving image quality and, thus, segmentation accuracy, the 40x oil immersion objective used for image acquisition brought with it a couple of limitations. Firstly, the field of view area was reduced compared to a lower magnification lens, meaning that fewer cells could be reconstructed per stack. Not only did the stack contain a lower number of mesophyll cells; in images containing larger, longer cells (i.e. those of 6n and 4n samples) these were more likely to be not completely in the field of view and were therefore deleted. This meant that often fewer cells were successfully reconstructed for the higher ploidy levels.

Secondly, as an immersion lens, this objective had a lower working distance than the air objectives. This meant that it was not possible to image all the way through the sample, which was often around 250-300 µm thick. As such, the middle layer of cells alone was imaged. A second limitation of the immersion lens and its reduced working distance was that the objective had to be in contact with the sample throughout the scan time. As each stack took over 45 minutes to collect, this meant that the sample could move underneath any pressure exerted by the lens. As a result of this - primarily due to shifts in the z-direction - on occasions, cells within stacks could be either stretched or squashed, and often it was not possible to tell until images had been fully processed in LGX to inform of cell geometrical values. This inconsistency in stack quality and the time-intensive nature of both image acquisition and segmentation is the primary reason why only three biological replicates per line were chosen for analysis. If any stacks were stretched or squashed, altering their size, it was unlikely to be to the magnitude of the changes associated with ploidy level. Additionally, stretching and squashing occurred to similar degrees between lines, and it is expected that relative differences in cell geometries would remain the same. Although not carried out in this study due to time constraints, it would be useful to validate the geometrical parameters acquired in this manner via traditional 2D methods. Technovit embedding (Kalve *et al.*, 2015) and the collection of both transverse and longitudinal sections of the same region of the leaf would allow for estimates of surface area and volume to be made, which can

then be compared to the values generated via confocal microscopy. Whilst the absolute values may differ, I suggest that the relative differences in cell size and shape between ploidy levels in *Triticum* species would remain obvious.

One way in which this problem could be averted in the future would be to use a different objective with a much higher working distance. The Olympus FV1000 in the Wolfson Light Microscopy Facility at the University of Sheffield does not have such an objective, but these are available for this system. The Zeiss Airyscan system within the facility allows for images to be collected at far higher resolution at the lower magnification (and thus higher working distance) of 20x. However, this is not an immersion lens, and as such the NA value is not sufficient for accurate segmentation, despite it being possible to image all the way through the leaf tissue.

The Nikon system also available in the Sheffield facility does have a 20x multi-immersion lens, which has both the desired working distance and NA to acquire image stacks that can be easily segmented. As a large proportion of the dataset had already been collected it was decided to continue using the Olympus system. This microscope also allows for laser intensity to be increased with sample depth, although this can lead to banding on the stack as a result of differences in contrast, and thus segmentation issues. Additionally, increasing the laser power can also bleach samples, and as such laser power should be used sparingly (Wuyts *et al.*, 2010).

A further way in which data collection could be improved would be to carry out surface smoothing on the image stacks, as recommended by Bassel (2015), although this should be undertaken with care as it can lead to mesh shrinkage, although it may be better at representing the curved nature of cell surfaces. In order to reduce the level of image processing and the potential for error that comes with this, smoothing was not carried out. I have assumed that any error in the sample as a result a lack of smoothing was equivalent for each genotype.

Another interesting future line of research would be to investigate differences in chloroplasts between ploidy levels. Previous experiments have found that plastid number per cell is increased with ploidy level, (Dean & Leech, 1982b; Jellings & Leech, 1984), and it has been suggested that chloroplast replication results in a constant proportion of mesophyll cell surface coverage by the plastids (Warner & Edwards, 1993a). In addition to making comparisons of chloroplast size and number per cell, and also chloroplast surface area exposed to airspace (S_c), it would be interesting if the position of chloroplasts on the mesophyll cells could be imaged within the 3D leaf environment. However, this is likely to be tricky using this technique in its current format as it requires tissue to be fixed and cleared in order to image cells at depth. It has been achieved in rice mesophyll cells using a more complex focused ion beam scanning electron microscopy (FIB-SEM) approach (Oi *et al.*, 2017), which may prove more appropriate for imaging the distribution and size of chloroplasts in 3D.

A colleague in Sheffield (Ellie Healicon) has also recently used LGX to investigate guard cell shape changes upon opening and closing in Arabidopsis tagged with a YFP (yellow fluorescent protein) fluorochrome. Currently, wheat guard cells take up the PI stain better than mesophyll cell walls – possibly due to cell wall compositional changes or because they are thicker – resulting in the emission of a saturated signal. As such, using the current protocol, it is not possible to quantify guard cell volume in wheat and its wild relatives. Using an alternative cell wall stain such as calcofluor white (Kurihara *et al.*, 2015) may be more suitable for this and should be investigated further. The interest in the generation of 3D reconstructions of mesophyll cells is not limited just to wheat. 3D geometrical information would also prove to be useful in rice and other crop species. Additionally, using 3D structural data for photosynthetic modelling improves insights into the distribution of photosynthesis (Ho *et al.*, 2016; Earles *et al.*, 2019). For example, colleagues have created a photosynthetic model, (Xiao *et al.* in preparation), which requires cell geometrical data, for which the use of 3D datasets would provide more accurate values.

Finally, the above protocol does not allow for the measurement of cell wall characteristics. Cell wall thickness is known to provide a major barrier to gas diffusion (Terashima *et al.*, 2011; Tholen *et al.*, 2012), and increases in the width of the cell wall have been associated with decreases in g_m (Flexas *et al.*, 2012; Tomas *et al.*, 2013). It may be that cell wall thickness scales with ploidy level in wheat leaves since it has previously been observed that cell wall thickness scales with mesophyll cell cross-sectional area for a range of species (John *et al.*, 2013). Whilst it may be possible to measure cell wall thickness from individual slices pre-processing, a more appropriate method would be via transmission electron microscopy (TEM) (Tosens *et al.*, 2012; Giuliani *et al.*, 2013; Tomas *et al.*, 2013; Lehmeier *et al.*, 2017). Cell wall composition differences may also be of interest, including the question as to whether lobes are formed in the same manner for each ploidy level as repeated units. A colleague (Sarah Carroll) has carried out some initial immunolabelling imaging of wheat leaves (as per Giannoutsou *et al.*, (2013)) and characterising any differences in cell wall composition or mesophyll cell morphogenesis associated with changes in ploidy level in *Triticum* species should be prioritised as a future research area.

4.5. Conclusion

In this chapter I have successfully adapted a confocal microscopy protocol to image wheat mesophyll cell geometry in three dimensions. Utilising this technique has allowed me to observe that mesophyll cell surface area and volume are increased in higher ploidy levels, and that, in addition to this, mesophyll cell shape also significantly varies with genome size. The relationships of these traits to leaf intercellular airspace provide a link between mesophyll cell geometry and photosynthetic gas exchange. They also highlight the delicate balancing act between CO_2 uptake and water loss that is responsible for influencing wheat leaf form, and which may have been at least partly responsible for the selection of more water use efficient bread wheat.

Chapter 5. General Discussion

5.1 Wheat leaf form is responsible for function

Photosynthesis is dependent upon the flux of atmospheric CO_2 into the leaf and the diffusion of H_2O out of the leaf. This gas exchange pathway is subject to stomatal and mesophyll resistances, and therefore leaf structure can directly influence rates of gas flux (Terashima *et al.*, 2011; Griffiths & Helliker, 2013). As with many biological processes, the advantages conferred by increasing conductance to CO_2 must be balanced against the associated amplified potential for water loss. The research in this thesis investigated how the changes in leaf structure associated with the evolution of modern hexaploid bread wheat (*T. aestivum*) have impacted leaf gas exchange and water use efficiency.

As the primary photosynthetic organs of plants, leaves are highly specialised and their form is directly related to their function (Terashima *et al.*, 2011; Tholen *et al.*, 2012). Previous analyses of leaf structure in the Triticeae have identified relationships between ploidy level and wheat leaf structure, with associated variation in leaf gas exchange parameters (Dunstone & Evans, 1974; Austin *et al.*, 1982; Parker & Ford, 1982; Jellings & Leech, 1984; Pyke *et al.*, 1990). In Chapter 1 of this thesis, I investigated how stomatal characteristics (frequency and size) are impacted by shifts in ploidy for a wide range of *Triticum* species including diploid, tetraploid and hexaploid accessions. The results of this study confirmed that the well-established relationships between genome size and guard cell size and stomatal density (Masterson, 1994; Beaulieu *et al.*, 2008) were present in the Triticeae, with 2n plants having the highest frequency of small stomata and 6n varieties having the largest stomata but the lowest stomatal density. This chapter also explored how leaf size, thickness and vascular patterning are influenced by ploidy level in *Triticum* species. In addition, I investigated the impacts of these leaf form changes upon steady-state leaf gas exchange. It was observed that rates of stomatal conductance were found to be generally higher in 2n plants than 4n and 6n plants (despite no significant impact upon steady-state photosynthesis under standard growth conditions). As a result of this, modern hexaploid wheat varieties were found to have the highest iWUE

(A/g_s) in comparison to 2n and 4n relatives. It is possible that the higher iWUE associated with changes in stomatal characteristics may have been one factor that led to the preferential selection (either consciously or unconsciously) of 6n wheat by early adopters of agriculture in the Near East. WUE has also been identified as a future breeding target (Bertolino *et al.*, 2019; Leakey *et al.*, 2019). Developing wheat varieties with reduced stomatal density and stomatal conductance (whilst maintaining photosynthetic rates and grain yields) is therefore a priority for breeders. Recent work by colleagues in Sheffield has found that small reductions in stomatal density of wheat have no significant impact upon grain yield, but do confer higher water-use efficiency and resilience to drought (Dunn *et al.*, 2019).

Whilst stomatal characteristics have a significant impact upon CO_2 uptake and water loss, the internal structure of wheat leaves can also limit gas diffusion (Tholen *et al.*, 2012). Sub-stomatal cavities and the intercellular airspace network allow for gas to diffuse to and from mesophyll cells where CO_2 is fixed in the chloroplasts (Ren *et al.*, 2019). Chapter 3 investigated how wheat leaf airspace is influenced by changes in ploidy level via the novel use of the medical imaging technique X-ray µCT. These 3D datasets allow for a more accurate representation of the internal leaf structure to be determined (Earles *et al.*, 2019). It was observed that leaf porosity was highest in 2n lines, lowest in 6n cultivars and middling in the 4n accessions under investigation. When correlated with g_s values from the previous chapter, it became apparent that there was a significant positive correlation between mesophyll porosity and stomatal conductance in wheat, which suggests that the two may be mechanistically linked. Concurrent work in Arabidopsis showed a similar pattern, suggesting that this fundamental relationship between leaf airspace and gas exchange is common to both monocot and eudicot plants (Lundgren *et al.*, 2019). Differences in leaf airspace patterning and distribution have been suggested to impact upon mesophyll conductance, and the rate of gas diffusion across the mesophyll is also thought to significantly limit photosynthetic gas exchange (Flexas *et al.*, 2012; Griffiths & Helliker, 2013). g_m has also been suggested to be a target for improving plant iWUE (Flexas, 2016). However, when differences in this parameter were assessed it was shown that there was no clear trend

between ploidy and g_m, despite the observed changes in the quantity of leaf airspace. Mesophyll conductance is a complex trait, and many different anatomical parameters which were not investigated, such as cell wall thickness, contribute to the resistance to gas diffusion within the leaf (Tomas *et al.*, 2013). The hypothesis that leaf gas exchange is mechanistically linked with the generation of the leaf airspace network was further supported via the observation that fully differentiated, operative stomata are required to form airspaces in the subtending mesophyll. Whilst the signal for this process has not yet been elucidated, it is possible that gas flux (either CO_2 or water vapour) itself may initiate the formation of airspaces within the mesophyll. This potential link between stomatal function and mesophyll structure allows me to theorise that attempts to restrict water loss may be the driver for the observed changes in leaf airspace levels associated with wheat evolution. This also supports the suggestion that the increased water use efficiency shown by hexaploid wheat could have played a major role in its selection as an agricultural crop species.

Further leaf structural components, such as mesophyll cell size and shape, are also thought to affect the rates of photosynthetic gas exchange (Tholen *et al.*, 2012; Ren *et al.*, 2019). The changes in wheat mesophyll cell size and shape associated with changes in ploidy level during wheat evolution were explored in Chapter 4. Previous investigations have identified a relationship between genome size and mesophyll cell size in wheat, with hexaploid wheat leaves being found to have larger mesophyll cells (Dunstone & Evans, 1974; Parker & Ford, 1982). Using a newly-developed confocal imaging protocol adapted from one developed for imaging Arabidopsis cells (Wuyts *et al.*, 2010), I have been able to characterise the alternative cell geometries showcased by 2n, 4n and 6n wheat mesophyll cells. Previous investigations have relied upon 2D imaging techniques to estimate cell geometry, whilst the confocal imaging technique allows for more accurate data collection in three dimensions (Théroux-Rancourt *et al.*, 2017; Earles *et al.*, 2019). I confirmed the previously recorded relationship between ploidy level and size, and also established that mesophyll cell shape changes via an increase in cell lobe number alongside these size changes in order to sustain an appropriate surface area to volume ratio for gas exchange in larger cells. When the

relationships between cell geometry and the levels of leaf intercellular airspace were investigated, it was shown that the observed increases in cell size and in lobe number in hexaploid wheat were correlated with a reduction in leaf porosity and exposed mesophyll surface area. Whilst reductions in the surface area available for gas exchange hinder the diffusion of CO_2 from leaf airspaces to the chloroplasts, this acts in parallel to also reduce the loss of water out of cells. Therefore, this observed trend allows me to propose that balancing potential water vapour loss with CO_2 diffusion has driven the observed mesophyll shape changes with increasing ploidy level.

To summarise, it appears as though the changes in wheat leaf structure (both internal and external) resulting from changes in genome size during its evolution act to reduce the potential for leaf water loss. This has resulted in modern 6n bread wheat (*T. aestivum*) having a higher water use efficiency than other *Triticum* species of lower ploidy. It is therefore possible that increased tolerance of drought events may have been one of the potential drivers that led to the preferential selection of 6n wheat over its 2n and 4n relatives and, thus, its ubiquity in agriculture across a wide range of environmental conditions. Nevertheless, grain yield is a complex trait and has not been the only driver for the historical selection of 6n wheat over its 4n and 2n relatives (Peng *et al.*, 2011). As such improved WUE is just one factor that may have led to the conscious or unconscious preferential selection of hexaploid wheat. Additionally, alternate useful traits, such as disease tolerance, may be improved in wild ancestors in comparison to modern hexaploid cultivars (Grewal *et al.*, 2018), and as such, the role of wheat progenitors as a source of genetic variation to be used in future breeding programmes should not be ignored.

My research also addresses the question whether hexaploid wheat is 'better' at photosynthetic gas exchange than its diploid and tetraploid relatives, and this is still open for debate. Whilst previously being shown to have a lower photosynthetic capacity than tetraploid and diploid *Triticum* species (Austin *et al.*, 1982), under operating conditions, my results suggest that there is very little to separate CO_2 assimilation rates between ploidy levels. It has been suggested that improving operating

rates of photosynthesis are one method by which wheat grain yields could be increased (Carmo-Silva *et al.*, 2017). Whether this should be preferred to improvements in photosynthetic capacity is up for contention. Alongside the observed reduction in stomatal conductance, the lack of variation in operating *A* confers hexaploid wheat an advantage in terms of water use. Recent modelling approaches have proposed that, in the future, limitations of water availability would have particularly large impacts upon crop yields (Wu *et al.*, 2019) and, as such, striving to improve crop WUE should be of greater priority than efforts to improve photosynthetic capacity alone.

The research presented in thesis also allows for speculation as to the structural ideotype of a wheat leaf. The above findings, along with previous investigations in wheat (Dunn *et al.,* 2019), suggest that stomatal density has a major influence upon water loss, and thus leaf iWUE. We suggest that optimising stomatal density to reduce g_s whilst not compromising the rate of CO_2 assimilation, is one leaf structural component that is a potential target for increasing iWUE. Data in Chapter 3 highlighted the correlation between leaf mesophyll porosity and stomatal conductance in the Triticeae, and it may be that breeding for a reduced stomatal frequency may also result in leaves which have lower levels of leaf intercellular airspace (Lundgren *et al.*, 2019). The changes in cell size and shape observed with changes with ploidy level in *Triticum* species in Chapter 4 can also provide useful information with regards to the ideal wheat leaf structure. Larger mesophyll cells with more lobes are found in 6n genotypes, and it is possible that the reduced SA/V ratios associated with these cells allows for reduced cell water uptake from vascular tissue/neighbours and loss into intercellular airspaces. Optimising leaf size and shape is also likely to be of importance, as leaf area can be significant both in terms of light interception and photosynthesis, but larger leaves may also have a reduced whole leaf iWUE in comparison to smaller leaves.

Therefore, we suggest that the optimal structure for wheat leaves in terms of maximising iWUE would be to have reduced stomatal density and lower levels of mesophyll porosity – with the aim of limiting water loss through stomatal conductance. As leaf gas exchange is a trade-off

between water loss and CO_2 uptake (Lawson & Blatt, 2014), it is essential that reductions in stomatal density are not so extreme as to negatively affect *A*. Alongside this, increasing cell size and lobe number may also have a positive impact upon wheat iWUE, although this may be restricted by, or have knock-on effects upon, cell packing within the mesophyll which could influence leaf gas exchange (Lehmeier *et al.*, 2017).

5.2. Future research directions

The observations made in this thesis have enabled the identification of several future research avenues, which may help to further elucidate the leaf structure/function relationships in wheat (and other species). This section highlights potential experiments that directly follow the work presented in this thesis, in addition to discussing further uses of the 3D imaging techniques used.

This project collected data from the fifth leaf, as this not only increased the speed of experiments, but also allowed for more efficient use of the controlled environment growth facilities. Whilst this leaf is considered to be an adult leaf (and thus representative of the plant as a whole), one potential future experiment would be to investigate whether the differences in leaf structure with ploidy level observed remain in other leaves (i.e. flag leaves). Additionally, the datasets in this project were gathered from plants grown under favourable environmental conditions. In order to explore whether the improved leaf iWUE exhibited by hexaploid lines confers real-world drought tolerance, it would be of great interest to carry out a detailed drought experiment investigating water use. Smaller stomata, such as those in diploid accessions, have been suggested to open and close faster than larger stomata (Lawson & Blatt, 2014), and as such 2n lines may have a reduced disconnect between photosynthesis and stomatal conductance under changing environmental conditions (Lawson & Vialet-Chabrand, 2019). The impacts of this upon iWUE could be investigated in greater detail. Although ignored in this study, it is conceivable that potential differences in root structure or architecture resulting from differences in genome size may mitigate the increases in water vapour loss through stomata in 2n and 4n plants, i.e, they may be better at taking up water from the soil. Likewise, the effects of further changes in environmental conditions upon leaf physiology and

structure, such as elevated CO_2 or shifts in leaf temperature, may also be of interest.

Furthermore, whilst estimates of g_m were made as part of this research project using curve fitting tools, more accurate determination of how this parameter varies with ploidy should be a priority, potentially using an online carbon isotope discrimination approach (Pons *et al.*, 2009). Cell wall thickness has been suggested to have a large impact upon the diffusion of gas into mesophyll cells (Flexas *et al.*, 2012). Characterisation of how cell wall thickness is affected by ploidy may help to further explain the observed lack of variation in g_m with ploidy level. It is possible that the maintenance of an appropriate surface area to volume ratio via an increased number of lobes, as observed in this thesis, may act to allow similar rates of g_m and this should be explored further. Investigations of any differences in cell wall composition and lobe formation between ploidy levels via an immunolabelling approach should also be considered.

Additional prospective avenues of research include further testing of the hypothesis of the presence of a mechanistic link between mesophyll airspace formation and stomatal function, with the aim of identifying any potential gaseous signal. This may be non-trivial due to the fundamental role of gas exchange in all living cells. For example, physically blocking leaf gas exchange (i.e with petroleum jelly or similar) might be informative, but in practice might simply lead to death of the plant due to anoxia and the response to total lack of CO_2 for photosynthesis. Focussing efforts upon early leaf primordia or further use of stomatal mutants (Dunn *et al.*, 2019; Lundgren *et al.*, 2019) may prove a more appropriate technique by which this link can be further elucidated, although this is still likely to be technically challenging.

The relationships between wheat mesophyll cell size, shape and gas exchange should also be the focus of future experiments. The use of cell cycle mutants, in a similar manner to Dorca-Fornell *et al.* (2013) and Lehmeier *et al.* (2017), may prove a valid method by which cell size can be manipulated in the same ploidy level. How these manipulations of cell size will influence cell shape is unclear, as are the implications upon mesophyll porosity, cell packing and gas exchange. Likewise, the use of

transgenic lines with altered levels of lobing (Wang *et al.*, 2017) may allow further insights into the interactions between cell surface area and leaf gas flux. Furthermore, the impact of changes in wheat cell size and shape upon the internal light environment of the leaf blade has not previously been investigated, and this provides a further route of potential research. Another experiment that may further enlighten how ploidy affects leaf structure and function would be to carry out a more thorough investigation of how increases in genome size affect leaf vasculature patterning. Whilst differences in vein density and interveinal distance have been investigated in this thesis to some extent, any potential changes in vascular bundle size as a result of shifts in ploidy, and how this may affect leaf water transport, have not yet been characterised. The creation of wheat plants of even higher ploidy levels e.g, using colchicine (Sattler *et al.*, 2016) may allow for further testing of the wheat structure/function relationships, posing the question of whether a theoretical octoploid wheat line would have a greater water use efficiency than hexaploid cultivars.

Further improvements of the confocal imaging technique may also be desirable, for example the use of an alternative objective with a larger field of view and working distance (to allow for deeper imaging). This will allow for an increased number of cells to be segmented and may also enable potential differences in mesophyll cell packing to be explored. The use of alternative 3D imaging techniques (e.g., Laser Ablation Tomography, LAT (Strock *et al.*, 2019)) may provide an better methods via which extraction of quantitative structural data at cellular resolution could be achieved. The adoption of the confocal technique described in this thesis for the 3D imaging of other crop species, such as rice, will allow for the structure/function relationships of different species to be investigated in greater detail. In particular, these investigations would allow us to to see whether the findings reported here for wheat reflect more universal rules on leaf structure/function in grasses. Finally, the 3D geometric data exemplified in this thesis could be incorporated into new photosynthetic models (Ho *et al.*, 2012; 2016), improving their accuracy and the insights that they can provide on this fundamental aspect of plant biology.

Bibliography

Abbo, S. & Gopher, A., 2017. Near Eastern Plant Domestication: A History of Thought. *Trends in Plant Science*, 22(6), 491–511.

Adams, M.A. & Grierson, P.F., 2001. Stable isotopes at natural abundance in terrestrial plant ecology and ecophysiology: An update. *Plant Biology*, 3(4), 299–310.

Adiredjo, A.L., Navaud, O., Lamaze, T. & Grieu, P., 2014. Leaf carbon isotope discrimination as an accurate indicator of water-use efficiency in sunflower genotypes subjected to five stable soil water contents. *Journal of Agronomy and Crop Science*, 200(6), 416–424.

Aegerter-Wilmsen, T., Heimlicher, M. B., Smith, A. C., de Reuille, P. B., Smith, R. S., Aegerter, C. M. & Basler, K., 2012. Integrating force-sensing and signaling pathways in a model for the regulation of wing imaginal disc size. *Development*, 139(17), 3221–3231.

Allaby, R.G., Stevens, C., Lucas, L., Maeda, O. & Fuller, D.Q., 2017. Geographic mosaics and changing rates of cereal domestication. *Philosophical Transactions of the Royal Society B: Biological Sciences*, 372(1735), 20160429.

Allen, J.F. & Martin, W., 2007. Evolutionary biology: out of thin air. *Nature*, 445(7128), 610–612.

Amos, W.B. & White, J.G., 2003. How the Confocal Laser Scanning Microscope entered Biological Research. *Biology of the Cell*, 95(6), 335–342.

Araus, J.L., Amaro, T., Zuhair, Y. & Nachit, M.M., 1997. Effect of leaf structure and water status on carbon isotope discrimination in field-grown durum wheat. *Plant, Cell and Environment*, 20(12), 1484–1494.

Araus, J.L., Alegre, L., Tapia, L. & Calafell, R., 1986. Relationship between leaf structure and gas exchange in wheat leaves at different insertion levels. *Journal of Experimental Botany,* 37(9), 1323–1333.

Aryavand, A., Ehdaie, B., Tran, B. & Waines, J. G. 2003. Stomatal frequency and size differentiate ploidy levels in Aegilops neglecta. *Genetic Resources and Crop Evolution,* 50(2), 175–182.

Austin, R.B., Morgan, C. L., Ford, M.A. & Bhagwat, S.G., 1982. Flag leaf photosynthesis of *Triticum aestivum* and Related diploid and tetraploid species. *Annals of Botany*, 49(1973), 177–189.

Avni, R., Nave, M., Barad, O., Baruch, K., Twardziok, S.O., Gundlach, H., Hale, I., Mascher, M., Spannagl, M., Wiebe, K., Jordan, K.W., Golan, G., Deek., Ben-Zvi, B., Ben-Zvi, G, Himmelbach, A., MacLachlan, R.P>, Sharpe, A.G., Fritz, A., Ben-David, R., Budak, H., Fahima, T., Korol, A., Faris, J.D., Hernandez, A., Mikel, M.A., Levy, A.A., Steffensen, B., Maccaferri, M., Tuberosa, R., Cattivelli, L., Faccioli, P., Ceriotti, A., Kashkush, K., Pourkheiandish, M., Komatsuda, T., Eilam, T., Sela, H., Sharon, A., Ohad, N. Chamovitz, D.A., Mayer, K.F.X., Stein, N., Ronen, G., Peleg, Z., Pozniak, C.J., Akhunov, E.D. & Distelfeldm A. 2017. Wild emmer genome architecture and diversity elucidate wheat evolution and domestication. *Science,* 357(6346), 93–97.

Babar, M. A., Reynolds, M. P., Van Ginkel, M., Klatt, A. R., Raun, W. R. & Stone, M. L., 2006. Spectral Reflectance to Estimate Genetic Variation for In-Season Biomass, Leaf Chlorophyll, and Canopy Temperature in Wheat. *Crop Science*, 46(3), 1046–1057.

El Baidouri, M., Murat, F., Veyssiere, M., Molinier, M., Flores, R., Burlot, L., Alaux, M., Quesneville, H., Pont, C. & Salse, J. 2017. Reconciling the evolutionary origin of bread wheat (*Triticum aestivum*). *New Phytologist*, 213(3), 1477–1486.

Balfourier, F., Bouchet, S., Robert, S., De Oliveira, R., Rimbert, H., Kitt, J., Choulet, F., Paux, E., International Wheat Genome Sequencing Consortium, BreedWheat Consortium & Paux, E., 2019. Worldwide phylogeography and history of wheat genetic diversity. *Science Advances*, 5(5), eaav0536.

de Reuille, P.B., Routier-Kierzkowska, A.L., Kierzkowski, D., Bassel, G.W., Schüpbach, T., Tauriello, G., Bajpai, N., Strauss, S., Weber, A., Kiss, A., Burian, A., Hofhuis, H., Sapala, A., Lipowczan, Heimlicher, M.B., Robinson, S., Bayer, E.M., Basler, K., Koumoutsakos, P., Roeder, A.H.K., Aegerter-Wilmsen, T., Nakayama, N, Tsiantis, M, Hay, A., Kwiatowska, D., Xenarios, I., Kuhlemeier, C. & Smith, R.S., 2015. MorphoGraphX: A platform for quantifying morphogenesis in 4D. *eLife*, 4, 05864.

Barbour, M.M., Bachmann, S., Bansal, U., Bariana, H. and Sharp, P., 2016. Genetic control of mesophyll conductance in common wheat. *New Phytologist,* 209(2), 461–465.

Bassel, G.W., 2015. Accuracy in Quantitative 3D Image Analysis. *The Plant Cell*, 27(4), 950–953.

Bassel, G.W., Stamm, P., Mosca, G., de Reuille, P.B., Gibbs, D.J., Winter, R., Janka, A., Holdsworth, M.J. & Smith, R.S., 2014. Mechanical constraints imposed by 3D cellular geometry and arrangement modulate growth patterns in the Arabidopsis embryo. *PNAS*, 111(23), 8685–8690.

Bassel, G.W. & Smith, R.S., 2016. Quantifying morphogenesis in plants in 4D. *Current Opinion in Plant Biology*, 29, 87–94.

Beaulieu, J.M., Leitch, I. J., Patel, S., Pendharkar, A. & Knight, C.A., 2008. Genome size is a strong predictor of cell size and stomatal density in angiosperms. *New Phytologist*, 179(4), 975–986.

Bellasio, C., Beerling, D.J. & Griffiths, H., 2015. An Excel tool for deriving key photosynthetic parameters from combined gas exchange and chlorophyll fluorescence: theory and practice. *Plant, Cell & Environment*, 39(6), 1180–1197.

Bergmann, D.C., 2004. Integrating signals in stomatal development. *Current Opinion in Plant Biology*, 7(1), 26–32.

Bergmann, D.C. & Sack, F.D., 2007. Stomatal Development. *Annual Review of Plant Biology*, 58(1), 163–181.

Berkman, P.J., Visendi, P., Lee, H.C., Stiller, J., Manoli, S., Lorenc, M.T., Lai, K., Batley, J., Fleury, D., Šimková, H., Kubaláková, M., Weining, S., Dolezel, J. & Edwards, D., 2013. Dispersion and domestication shaped the genome of bread wheat. *Plant Biotechnology Journal*, 11(5), 564–571.

Bertolino, L.T., Caine, R.S. & Gray, J.E., 2019. Impact of Stomatal Density and Morphology on Water-Use Efficiency in a Changing World. *Frontiers in Plant Science*, 10, 225.

Biswas, D.K. & Jiang, G.M., 2011. Differential drought-induced modulation of ozone tolerance in winter wheat species. *Journal of Experimental Botany*, 62(12), 4153–4162.

de Boer, H.J., Price, C.A., Wagner-Cremer, F., Dekker, S.C., Franks, P.J. & Veneklaas, E.J., 2016. Optimal allocation of leaf epidermal area for gas exchange. *New Phytologist*, 210(4), 1219–1228.

Borrino, E.M. & Powell, W., 1988. Stomatal guard cell length as an indictor of ploidy in microspore-derived plants of barley. *Genome*, 30(2), 158–160.

Braybrook, S.A. & Kuhlemeier, C., 2010. How a Plant Builds Leaves. *The Plant Cell*, 22(4), 1006–1018.

Brodersen, C.R. & Vogelmann, T.C., 2010. Do changes in light direction affect absorption profiles in leaves? *Functional Plant Biology*, 37(5), 403.

Brodribb, T.J., Feild, T.S. & Jordan, G.J., 2007. Leaf Maximum Photosynthetic Rate and Venation Are Linked by Hydraulics. *Plant Physiology,* 144(4), 1890–1898.

Brodribb, T.J., Feild, T.S. & Sack, L., 2010. Viewing leaf structure and evolution from a hydraulic perspective. *Functional Plant Biology*, 37(6), 488–498.

Brodribb, T.J., Jordan, G.J. & Carpenter, R.J., 2013. Unified changes in cell size permit coordinated leaf evolution. *New Phytologist*, 199(2), 559–570.

Brown, T.A., Jones, M.K., Powell, W. & Allaby, R.G., 2009. The complex origins of domesticated crops in the Fertile Crescent. *Trends in Ecology & Evolution*, 24(2), 103–109.

Buckley, T.N., 2015. The contributions of apoplastic, symplastic and gas phase pathways for water transport outside the bundle sheath in leaves. *Plant, Cell and Environment*, 7–22.

Buckley, T.N. & Diaz-Espejo, A., 2015. Reporting estimates of maximum potential electron transport rate. *New Phytologist*, 205(1), 14–17.

Buckley, T.N. & Warren, C.R., 2014. The role of mesophyll conductance in the economics of nitrogen and water use in photosynthesis. *Photosynthesis Research*, 119(1–2), 77–88.

Buda, G.J., Isaacson, T., Matas, A.J., Paolillo, D.J. & Rose, J.K., 2009. Three-dimensional imaging of plant cuticle architecture using confocal scanning laser microscopy. *The Plant Journal*, 60(2), 378–385.

Busch, F.A., 2018. Photosynthetic gas exchange in land plants at the leaf level. In *Methods in Molecular Biology*. Humana Press, New York, NY, 25–44.

Buttery, B.R. & Buzzell, R.L., 1977. The relationship between chlorophyll content and rate of photosynthesis in soybeans. *Canadian Journal of Plant Science,* 57(1), 1–5.

Byrne, M.E., 2012. Making leaves. *Current Opinion in Plant Biology*, 15(1), 24–30.

von Caemmerer, S. & Evans, J.R., 2015. Temperature responses of mesophyll conductance differ greatly between species. *Plant, Cell & Environment*, 38(4), 629–637.

Caine, R.S., Yin, X., Sloan, J., Harrison, E.L., Mohammed, U., Fulton, T., Biswal, A.K., Dionora, J., Chater, C.C., Coe, R.A., Bandyopadhyay, A., Murchie, E.H., Swarup, R., Quick, W.P. & Gray, J.E., 2019. Rice with reduced stomatal density conserves water and has improved drought tolerance under future climate conditions. *New Phytologist*, 221(1), 371–384.

Cao, X., Jia, J.B., Li, H., Li, M.C., Luo, J., Liang, Z.S., Liu, T.X., Liu, W.G., Peng, C.H. & Luo, Z.B., 2012. Photosynthesis, water use efficiency and stable carbon isotope composition are associated with anatomical properties of leaf and xylem in six poplar species. *Plant Biology*, 14(4), 612–620.

Carmo-Silva, E., Andralojc, P.J., Scales, J.C., Driever, S.M., Mead, A., Lawson, T., Raines, C.A. & Parry, M.A., 2017. Phenotyping of field-grown wheat in the UK highlights contribution of light response of photosynthesis and flag leaf longevity to grain yield. *Journal of Experimental Botany*, 68(13), 3473–3486.

Cartelat, A., Cerovic, Z.G., Goulas, Y., Meyer, S., Lelarge, C., Prioul, J.L., Barbottin, A., Jeuffroy, M.H., Gate, P., Agati, G. & Moya, I., 2005. Optically assessed contents of leaf polyphenolics and chlorophyll as indicators of nitrogen deficiency in wheat (Triticum aestivum L.). *Field Crops Research*, 91(1), 35–49.

Casson, S. & Gray, J.E., 2008. Influence of environmental factors on stomatal development. *New Phytologist,* 178(1), 9–23.

Centritto, M., Lauteri, M., Monteverdi, M.C. & Serraj, R., 2009. Leaf gas exchange, carbon isotope discrimination, and grain yield in contrasting rice genotypes subjected to water deficits during the reproductive stage. *Journal of Experimental Botany*, 60(8), 2325–2339.

Cernusak, L.A., Ubierna, N., Winter, K., Holtum, J.A., Marshall, J.D. & Farquhar, G.D., 2013. Environmental and physiological determinants of carbon isotope discrimination in terrestrial plants. *New Phytologist*, 200(4), 950–965.

Choat, B., Badel, E., Burlett, R., Delzon, S., Cochard, H. & Jansen, S., 2016. Noninvasive Measurement of Vulnerability to Drought-Induced Embolism by X-Ray Microtomography. *Plant Physiology*, 170(1), 273–82.

Condon, A.G., Richards, R.A., Rebetzke, G.J. & Farquhar, G.D., 2004. Breeding for high water-use efficiency. *Journal of Experimental Botany*, 55(407), 2447–2460.

Condon, A.G., Reynolds, M.P., Rebetzke, G.J., Van Ginkel, M., Richards, R.A. & Farquhar, G.D., 2007. Using Stomatal Aperture-Related Traits to Select for High Yield Potential in Bread Wheat. In *Developments in Plant Breeding,* 617–624. Springer, Dordrecht.

Croft, H., Chen, J.M., Luo, X., Bartlett, P., Chen, B. & Staebler, R.M., 2017. Leaf chlorophyll content as a proxy for leaf photosynthetic capacity. *Global Change Biology*, 23(9), 3513–3524.

Dean, C. & Leech, R.M., 1982a. Genome Expression during Normal Leaf Development: I. Cellular and Chloroplast Numbers and DNA, RNA, and Protein Levels in Tissues of Different Ages Within a Seven-day-old Wheat Leaf. *Plant Physiology*, 69(4), 904–10.

Dean, C. & Leech, R.M., 1982b. Genome Expression during Normal Leaf Development: 2. Direct Correlation between Ribulose Bisphosphate Carboxylase Content and Nuclear Ploidy in a Polyploid Series of Wheat. *Plant Physiology*, 70(6), 1605–8.

Dhondt, S., Vanhaeren, H., Van Loo, D., Cnudde, V. & Inzé, D., 2010. Plant structure visualization by high-resolution X-ray computed tomography. *Trends in Plant Science*, 15(8), 419–422.

Doebley, J.F., Gaut, B.S. & Smith, B.D., 2006. The Molecular Genetics of Crop Domestication. *Cell*, 127, 1309–1321.

Doheny-Adams, T., Hunt, L., Franks, P.J., Beerling, D.J. & Gray, J.E., 2012. Genetic manipulation of stomatal density influences stomatal size, plant growth and tolerance to restricted water supply across a growth carbon dioxide gradient. *Philosophical Transactions of the Royal Society B: Biological Sciences*, 367(1588), 547–555.

Dorca-Fornell, C., Pajor, R., Lehmeier, C., Pérez-Bueno, M., Bauch, M., Sloan, J., Osborne, C., Rolfe, S., Sturrock, C., Mooney, S. & Fleming, A., 2013. Increased leaf mesophyll porosity following transient retinoblastoma-related protein silencing is revealed by microcomputed tomography imaging and leads to a system-level physiological response to the altered cell division pattern. *The Plant Journal*, 76(6), 914–929.

Dow, G.J., Bergmann, D.C. & Berry, J. A., 2014. An integrated model of stomatal development and leaf physiology. *New Phytologist*, 201(4), 1218–1226.

Dow, G.J., Berry, J.A. & Bergmann, D.C., 2017. Disruption of stomatal lineage signaling or transcriptional regulators has differential effects on mesophyll development, but maintains coordination of gas exchange. *The New Phytologist*, 216(1), 69–75.

Drake, P.L., de Boer, H.J., Schymanski, S.J. & Veneklaas, E.J., 2019. Two sides to every leaf: water and CO_2 transport in hypostomatous and amphistomatous leaves. *New Phytologist*. 222(3), 1179–1187.

Drake, P.L., Froend, R.H. & Franks, P.J., 2013. Smaller, faster stomata: scaling of stomatal size, rate of response, and stomatal conductance. *Journal of Experimental Botany*, 64(2), 495–505.

Driever, S.M., Lawson, T., Andralojc, P.J., Raines, C.A. & Parry, M.A.J., 2014. Natural variation in photosynthetic capacity, growth, and yield in 64 field-grown wheat genotypes. *Journal of Experimental Botany*, 65(17), 4959–4973.

Dubcovsky, J. & Dvorak, J., 2007. Genome Plasticity a Key Factor. *Science*, 316(5833), 1862–1866.

Ducat, D.C. & Silver, P.A., 2012. Improving carbon fixation pathways. *Current Opinion in Chemical Biology*, 16(3–4), 337–344.

Dunn, J., Hunt, L., Afsharinafar, M., Al Meselmani, M., Mitchell, A., Howells, R., Wallington, E., Fleming, A.J. & Gray, J.E., 2019. Reduced stomatal density in bread wheat leads to increased water-use efficiency. *Journal of Experimental Botany*, erz248

Dunstone, R. & Evans, L., 1974. Role of Changes in Cell Size in the Evolution of Wheat. *Australian Journal of Plant Physiology*, 1(1), 157.

Earles, J.M., Theroux-Rancourt, G., Roddy, A.B., Gilbert, M.E., McElrone, A.J. & Brodersen, C.R., 2018. Beyond Porosity: 3D Leaf Intercellular Airspace Traits That Impact Mesophyll Conductance. *Plant Physiology*, 178(1), 148–162.

Earles, J.M., Buckley, T.N., Brodersen, C.R., Busch, F.A., Cano, F.J., Choat, B., Evans, J.R., Farquhar, G.D., Harwood, R., Huynh, M., John, G.P., Miller, M.L., Rockwell, F.E., Sack, L., Scoffoni, C., Struik, P.C., Wu, A. Yin, X. & Barbour, M.M., 2019. Embracing 3D Complexity in Leaf Carbon–Water Exchange. *Trends in Plant Science*, 24(1), 15–24.

Endo, H. & Torii, K.U., 2019. Stomatal Development and Perspectives toward Agricultural Improvement. Cold Spring Harbor perspectives in biology, 11(5), a034660.

Evans, J.R., 2013. Improving Photosynthesis. *Plant Physiology*, 162(4), 1780–1793.

Evans, J.R., 1983. Nitrogen and Photosynthesis in the Flag Leaf of Wheat (*Triticum aestivum* L.). *Plant physiology*, 72(2), 297–302.

Evans, J.R., 1989. Photosynthesis and nitrogen relationships in leaves of C3 plants, *Oecologica,* 78, 9–19.

Evans, J.R., Kaldenhoff, R., Genty, B. & Terashima, I., 2009. Resistances along the CO_2diffusion pathway inside leaves. *Journal of Experimental Botany*, 60(8), 2235–2248.

Evans, J.R. & Santiago, L.S., 2014. Prometheus wiki gold leaf protocol: Gas exchange using LI-COR 6400. *Functional Plant Biology*, 41(3), 223–226.

Evans, J.R. & Seemann, J.R., 1984. Differences between Wheat Genotypes in Specific Activity of Ribulose-1,5-bisphosphate Carboxylase and the Relationship to Photosynthesis. *Plant physiology*, 74(4), 759–65.

Facette, M.R. & Smith, L.G., 2012. Division polarity in developing stomata. *Current Opinion in Plant Biology*, 15(6), 585–592.

Faralli, M., Cockram, J., Ober, E., Wall, S., Galle, A., Van Rie, J., Raines, C.A. & Lawson, T., 2019. Genotypic, Developmental and Environmental Effects on the Rapidity of gs in Wheat: Impacts on Carbon Gain and Water-Use Efficiency. *Frontiers in Plant Science*, 10, 492.

Faralli, M., Matthews, J. & Lawson, T., 2019. Exploiting natural variation and genetic manipulation of stomatal conductance for crop improvement. *Current Opinion in Plant Biology*, 49, 1–7.

Farquhar, G. & Richards, R., 1984. Isotopic Composition of Plant Carbon Correlates With Water-Use Efficiency of Wheat Genotypes. *Australian Journal of Plant Physiology*, 11(6), 539.

Farquhar, G.D., Caemmerer, S. & Berry, J.A., 1980. A biochemical model of photosynthetic CO_2 assimilation in leaves of C3 species. *Planta*, 149(1), 78–90.

Farquhar, G.D. & Sharkey, T.D., 1982. Stomatal Conductance and Photosynthesis. *Annual Review of Plant Physiology*, 33(1), 317–345.

Feild, T.S. & Brodribb, T.J., 2013. Hydraulic tuning of vein cell microstructure in the evolution of angiosperm venation networks. *New Phytologist*, 199(3), 720–726.

Feldman, A.B., Leung, H., Baraoidan, M., Elmido-Mabilangan, A., Canicosa, I., Quick, W.P., Sheehy, J. & Murchie, E.H., 2017. Increasing Leaf Vein Density via Mutagenesis in Rice Results in an Enhanced Rate of Photosynthesis, Smaller Cell Sizes and Can Reduce Interveinal Mesophyll Cell Number. *Frontiers in Plant Science*, 8, 1883.

Fischer, R.A., Rees, D., Sayre, K.D., Lu, Z.M., Condon, A.G. & Saavedra, A.L., 1998. Wheat yield progress associated with higher stomatal conductance and photosynthetic rate, and cooler canopies. *Crop Science*, 38(6), 1467–1475.

Flannery, B.P., Deckman, H.W., Roberge, W.G. & D'Amico, K.L. 1987. Three-dimensional x-ray microtomography. *Science*, 237(4821), 1439–1444.

Flavel, R.J., Guppy, C.N., Tighe, M., Watt, M., McNeill, A. & Young, I.M., 2012. Non-destructive quantification of cereal roots in soil using high-resolution X-ray tomography. *Journal of Experimental Botany*, 63(7), 2503–2511.

Fleming, A.J., 2006. The integration of cell proliferation and growth in leaf morphogenesis. *Journal of Plant Research*, 119, 31–36.

Flexas, J., Niinemets, Ü., Gallé, A., Barbour, M.M., Centritto, M., Diaz-Espejo, A., Douthe, C., Galmés, J., Ribas-Carbo, M., Rodriguez, P.L., Rosselló, F., Soolanayakanahally, R., Tomas, M., Wright, I.J., Farquhar, G.D. & Medrano, H., 2013. Diffusional conductances to CO2 as a target for increasing photosynthesis and photosynthetic water-use efficiency. *Photosynthesis Research*, 117(1–3), 45–59.

Flexas, J., 2016. Genetic improvement of leaf photosynthesis and intrinsic water use efficiency in C3 plants: why so much little success? *Plant Science*. 251, 155–161.

Flexas, J., Ribas-Carbó, M., Diaz-Espejo, A., Galmés, J. & Medrano, H., 2008. Mesophyll conductance to CO_2: current knowledge and future prospects. *Plant, Cell & Environment*, 31(5), 602–621.

Flexas, J., Díaz-Espejo, A., Conesa, M.A., Coopman, R.E., Douthe, C., Gago, J., Gallé, A., Galmés, J., Medrano, H., Ribas-Carbo, M., Tomàs, M. & Niinemets, U., 2016. Mesophyll conductance to CO_2 and Rubisco as targets for improving intrinsic water use efficiency in C_3 plants. *Plant, Cell & Environment*, 39(5), 965–982.

Flexas, J., Barbour, M.M., Brendel, O., Cabrera, H.M., Carriquí, M., Diaz-Espejo, A., Douthe, C., Dreyer, E., Ferrio, J.P., Gago, J., Gallé, A., Galmes, J., Kodama, N., Medrano, H., Niinemets, U., Peguero-Pina, J.J., Pou, P., Ribas-Carbo, M., Tomas, M., Tosens, T. & Warren, C.R., 2012. Mesophyll diffusion conductance to CO_2: an unappreciated central player in photosynthesis. *Plant Science*, 193–194, 70–84.

Franks, P.J., W. Doheny-Adams, T., Britton-Harper, Z.J. & Gray, J.E., 2015. Increasing water-use efficiency directly through genetic manipulation of stomatal density. *New Phytologist*, 207(1), 188–195.

Franks, P.J. & Beerling, D.J., 2009. Maximum leaf conductance driven by CO2 effects on stomatal size and density over geologic time. *Proceedings of the National Academy of Sciences of the United States of America*, 106(25), 10343–10347.

Franks, P.J., Drake, P.L. & Beerling, D.J., 2009. Plasticity in maximum stomatal conductance constrained by negative correlation between stomatal size and density: An analysis using Eucalyptus globulus. *Plant, Cell and Environment*, 32(12), 1737–1748.

Franks, P.J. & Farquhar, G.D., 2006. The Mechanical Diversity of Stomata and Its Significance in Gas-Exchange Control. *Plant Physiology*, 143(1), 78–87.

Gaju, O., DeSilva, J., Carvalho, P., Hawkesford, M.J., Griffiths, S., Greenland, A. & Foulkes, M.J., 2016. Leaf photosynthesis and associations with grain yield, biomass and nitrogen-use efficiency in landraces, synthetic-derived lines and cultivars in wheat. *Field Crops Research*, 193, 1–15.

Gaju, O., Reynolds, M.P., Sparkes, D.L., Mayes, S., Ribas-Vargas, G., Crossa, J. & Foulkes, M.J., 2014. Relationships between physiological traits, grain number and yield potential in a wheat DH population of large spike phenotype. *Field Crops Research*, 164(1), 126–135.

Gegas, V.C., Nazari, A., Griffiths, S., Simmonds, J., Fish, L., Orford, S., Sayers, L., Doonan, J.H. & Snape, J.W., 2010. A genetic framework for grain size and shape variation in wheat. *The Plant Cell*, 22(4), 1046–56.

Giannoutsou, E., Sotiriou, P., Apostolakos, P. & Galatis, B., 2013. Early local differentiation of the cell wall matrix defines the contact sites in lobed mesophyll cells of *Zea mays*. *Annals of Botany*, 112(6), 1067–81.

Gilbert, M.E., Zwieniecki, M.A. & Holbrook, N.M., 2011. Independent variation in photosynthetic capacity and stomatal conductance leads to differences in intrinsic water use efficiency in 11 soybean genotypes before and during mild drought. *Journal of Experimental Botany*, 62(8), 2875–2887.

Giuliani, R., Koteyeva, N., Voznesenskaya, E., Evans, M.A., Cousins, A.B. & Edwards, G.E., 2013. Coordination of Leaf Photosynthesis, Transpiration, and Structural Traits in Rice and Wild Relatives (Genus Oryza). *Plant Physiology*, 162(3), 1632–1651.

Godfray, H.C.J., Beddington, J.R., Crute, I.R., Haddad, L., Lawrence, D., Muir, J.F., Pretty, J., Robinson, S., Thomas, S.M. & Toulmin, C., 2010. Food Security: The Challenge of Feeding 9 Billion People. *Science,* 327(5967), 812–818.

Grewal, S., Edwards, S.H., Yang, C.Y., Scholefield, D., Ashling, S., Burridge, A., Wilkinson, P.A., King, I.P. & King, J.,2018. Detection of *T. urartu* Introgressions in Wheat and Development of a Panel of Interspecific Introgression Lines. *Frontiers in Plant Science*, 9, 1565.

Griffiths, H. & Helliker, B.R., 2013. Mesophyll conductance: Internal insights of leaf carbon exchange. *Plant, Cell and Environment*, 36(4), 733–735.

Haas, M., Schreiber, M. & Mascher, M., 2019. Domestication and crop evolution of wheat and barley: Genes, genomics, and future directions. *Journal of Integrative Plant Biology*, 61(3), 204–225.

Hamblin, J., Stefanova, K. & Angessa, T.T., 2014. Variation in Chlorophyll Content per Unit Leaf Area in Spring Wheat and Implications for Selection in Segregating Material. *PLoS ONE*, 9(3), 92529.

Hawkesford, M.J., Araus, J.L., Park, R., Calderini, D., Miralles, D., Shen, T., Zhang, J. & Parry, M.A., 2013. Prospects of Doubling Global Wheat Yields. *Food and Energy Security*, 2(1), 34–48.

Hepler, P.K. & Gunning, B.E.S., 1998. Confocal fluorescence microscopy of plant cells. *Protoplasma,* 201(3), 121–157.

Hepworth, C., Doheny-Adams, T., Hunt, L., Cameron, D.D. & Gray, J.E., 2015. Manipulating stomatal density enhances drought tolerance without deleterious effect on nutrient uptake. *New Phytologist*, 208(2), 336–341.

Hepworth, C., Caine, R.S., Harrison, E.L., Sloan, J. & Gray, J.E.,2018. Stomatal development: focusing on the grasses. *Current Opinion in Plant Biology*, 41, 1–7.

Herremans, E., Verboven, P., Verlinden, B.E., Cantre, D., Abera, M., Wevers, M. & Nicolaï, B.M., 2015. Automatic analysis of the 3-D microstructure of fruit parenchyma tissue using X-ray micro-CT explains differences in aeration. *BMC Plant Biology*, 15(1), 264.

Ho, Q.T., Verboven, P., Yin, X., Struik, P.C. & Nicolaï, B.M., 2012. A microscale model for combined CO_2 diffusion and photosynthesis in leaves. *PloS one*, 7(11), p.e48376.

Ho, Q.T., Berghuijs, H.N., Watté, R., Verboven, P., Herremans, E., Yin, X., Retta, M.A., Aernouts, B., Saeys, W., Helfen, L. & Farquhar, G.D., 2016. 3-D microscale modeling of CO2 transport and light propagation in tomato leaves enlightens photosynthesis. *Plant, Cell & Environment*, 39(1), 50-61.

Holbrook, G.P., Keys, A.J. & Leech, R.M., 1984. Biochemistry of photosynthesis in species of triticum of differing ploidy. *Plant physiology*, 74(1), 12–5.

Hubbart, S., Peng, S., Horton, P., Chen, Y. & Murchie, E.H., 2007. Trends in leaf photosynthesis in historical rice varieties developed in the Philippines since 1966. *Journal of Experimental Botany*, 58(12), 3429–3438.

Hubick, K. & Farquhar, G., 1989. Carbon isotope discrimination and the ratio of carbon gained to water lost in barley cultivars. *Plant, Cell & Environment*, 12(8), 795–804.

Hughes, J., Hepworth, C., Dutton, C., Dunn, J.A., Hunt, L., Stephens, J., Waugh, R., Cameron, D.D. & Gray, J.E., 2017. Reducing Stomatal Density in Barley Improves Drought Tolerance without Impacting on Yield. *Plant Physiology*, 174(2), 776-787.

Hughes, N., Oliveira, H.R., Fradgley, N., Corke, F.M., Cockram, J., Doonan, J.H. & Nibau, C., 2019. μCT trait analysis reveals morphometric differences between domesticated temperate small grain cereals and their wild relatives. *The Plant Journal,* 99(1), 98-111.

Hutzler, P., 1998. Tissue localization of phenolic compounds in plants by confocal laser scanning microscopy. *Journal of Experimental Botany*, 49(323), 953–965.

Ichiro, T., Hiroki, O., Takashi, F. & Riichi, O., 2016. Light environment within a leaf. II. Progress in the past one-third century. *Journal of Plant Research*, 129(3),1–11.

Ishizaki, K., 2015. Development of schizogenous intercellular spaces in plants. *Frontiers in Plant Science,* 6, 497.

Jahan, E., Amthor, J.S., Farquhar, G.D., Trethowan, R. & Barbour, M.M., 2014. Variation in mesophyll conductance among Australian wheat genotypes. *Functional Plant Biology*, 41(6), 568–580.

Jarvis, M.C., Briggs, S.P.H. & Knox, J.P., 2003. Intercellular adhesion and cell separation in plants. *Plant, Cell and Environment*, 26(7), 977–989.

Jeffree, C.E., Dale, J.E. & Fry, S.C., 1986. The genesis of intercellular spaces in developing leaves of Phaseolus vulgaris L. *Protoplasma*, 132(1–2), 90–98.

Jellings, A.J. & Leech, R., 1984. Anatomical Variation in First Leaves of Nine Tritucum Genotypes, and Its Relationship To Photosynthetic Capacity. *New Phytologist*, 96(3), 371–382.

Jhala, V.M. & Thaker, V.S., 2015. X-ray computed tomography to study rice (*Oryza sativa* L.) panicle development. *Journal of Experimental Botany*, 66(21), 6819–6825.

John, G.P., Scoffoni, C. & Sack, L., 2013. Allometry of cells and tissues within leaves. *American Journal of Botany*, 100(10), 1936–1948.

Johnson, G. & Murchie, E., 2011. Gas exchange measurements for the determination of photosynthetic efficiency in Arabidopsis leaves. *Methods in molecular biology (Clifton, N.J.)*, 775, 311–26.

Jung, G. & Wernicke, W., 1990. Cell shaping and mierotubules in developing mesophyll of wheat (*Triticum aestivum* L.). *Protoplasma,* 153(3), 141–148.

Jung, G., Hellmann, A. & Wernike, W., 1993. Changes in the density of microtubular networks in mesophyll cells and mesophyll derived protoplasts of Nicotiana and Triticum during leaf development. *Planta*, 190, 10–16.

Kaldenhoff, R., 2012. Mechanisms underlying CO2 diffusion in leaves. *Current Opinion in Plant Biology*, 15(3), 276–281.

Kalve, S., Saini, K., Vissenberg, K., Beeckman, T. & Beemster, G., 2015. Transverse Sectioning of Arabidopsis thaliana Leaves Using Resin Embedding. *Bio-protocol,* 5(18), e1592.

Kaminski, A., Austin, R.B., Ford, M.A. & Morgan, C.L., 1990. Flag Leaf Anatomy of Triticum and Aegilops Species in Relation to Photosynthetic Rate. *Annals of Botany*, 66(3), 359–365.

Kaplan, D.R., 2001. Fundamental Concepts of Leaf Morphology and Morphogenesis: A Contribution to the Interpretation of Molecular Genetic Mutants. *International Journal of Plant Sciences,* 162(3), 465–474.

Kaplan, D.R., 1973. The Problem of Leaf Morphology and Evolution in the Monocotyledons. *The Quarterly Review of Biology*, 48(3), 437–457.

Katagiri, Y., Hasegawa, J., Fujikura, U., Hoshino, R., Matsunaga, S. & Tsukaya, H., 2016. The coordination of ploidy and cell size differs between cell layers in leaves. *Development* , 143(7), 1120–5.

Kessler, S. & Sinha, N., 2004. Shaping up: the genetic control of leaf shape. *Current Opinion in Plant Biology*, 7(1),.65–72.

Khazaei, H., Mohammady, S.D., Zaharieva, M. & Monneveux, P., 2009. Carbon isotope discrimination and water use efficiency in Iranian diploid, tetraploid and hexaploid wheats grown under well-watered conditions. *Genetic Resources and Crop Evolution*, 56(1), 105–114.

Khazaei, H., Monneveux, P., Hongbo, S. & Mohammady, S., 2010.Variation for stomatal characteristics and water use efficiency among diploid, tetraploid and hexaploid Iranian wheat landraces. *Genetic Resources and Crop Evolution*, 57(2), 307–314.

Kierzkowski, D., Nakayama, N., Routier-Kierzkowska, A.L., Weber, A., Bayer, E., Schorderet, M., Reinhardt, D., Kuhlemeier, C. & Smith, R.S., 2012. Elastic Domains Regulate Growth and Organogenesis in the Plant Shoot Apical Meristem. *Science*, 335(6072), 1096–1099.

Kirchhoff, H., 2013. Architectural switches in plant thylakoid membranes. *Photosynthesis Research*, 116,481–487.

Knox, J.P., 1992. Cell adhesion, cell separation and plant morphogenesis. *The Plant Journal*, 2(2), 137–141.

Kondorosi, E., Roudier, F. & Gendreau, E., 2000. Plant cell-size control: Growing by ploidy? *Current Opinion in Plant Biology*, 3(6), 488–492.

Kurihara, D., Mizuta, Y., Sato, Y. & Higashiyama, T., 2015. ClearSee: a rapid optical clearing reagent for whole-plant fluorescence imaging. *Development*, 4168–4179.

Landis, E.N. & Keane, D.T., 2010. X-ray microtomography. *Materials Characterization*, 61(12), 1305–1316.

Lawson, T. & Blatt, M.R., 2014. Stomatal Size, Speed, and Responsiveness Impact on Photosynthesis and Water Use Efficiency. *Plant Physiology*, 164(4), 1556–1570.

Lawson, T. & Vialet-Chabrand, S., 2019. Speedy stomata, photosynthesis and plant water use efficiency. *New Phytologist*, 221(1), 93–98.

Leakey, A.D., Ferguson, J.N., Pignon, C.P., Wu, A., Jin, Z., Hammer, G.L. & Lobell, D.B., Water Use Efficiency as a Constraint and Target for Improving the Resilience and Productivity of C_3 and C_4 Crops. *Annual Review of Plant Biology*, 70(1), 781–808.

Lehmeier, C., Pajor, R., Lundgren, M.R., Mathers, A., Sloan, J., Bauch, M., Mitchell, A., Bellasio, C., Green, A., Bouyer, D., Schnittger, A., Osborne, C.P., Rolfe, S., Mooney, S. & Fleming A.J., 2017. Cell density and airspace patterning in the leaf can be manipulated to increase leaf photosynthetic capacity. *The Plant Journal*, 92(6), 981–994.

Leinonen, I., Grant, O.M., Tagliavia, C.P.P., Chaves, M.M. & Jones, H.G., 2006. Estimating stomatal conductance with thermal imagery. *Plant, Cell and Environment*, 29(8), 1508–1518.

Lewis, M.W. & Hake, S., 2016. Keep on growing: building and patterning leaves in the grasses. *Current Opinion in Plant Biology*, 29, 80–86.

Lightner, J., James Jr, D.W., Dooner, H.K. & Browse, J., 1994. Altered body morphology is caused by increased stearate levels in a mutant of Arabidopsis. *The Plant Journal*, 6(3), 401–412.

Linkert, M., Rueden, C.T., Allan, C., Burel, J.M., Moore, W., Patterson, A., Loranger, B., Moore, J., Neves, C., MacDonald, D. & Tarkowska, A., 2010. Metadata matters: access to image data in the real world. *The Journal of Cell Biology*, 189(5), 777–782.

Littlejohn, G.R., Mansfield, J.C., Christmas, J.T., Witterick, E., Fricker, M.D., Grant, M.R., Smirnoff, N., Everson, R.M., Moger, J. & Love, J., 2014. An update: improvements in imaging perfluorocarbon-mounted plant leaves with implications for studies of plant pathology, physiology, development and cell biology. *Frontiers in Plant Science*, 5, 140.

Littlejohn, G.R., Gouveia, J.D., Edner, C., Smirnoff, N. & Love, J., 2010. Perfluorodecalin enhances in vivo confocal microscopy resolution of *Arabidopsis thaliana* mesophyll. *New Phytologist*, 186(4), 1018–1025.

Liu, T., Ohashi-Ito, K. & Bergmann, D.C., 2009. Orthologs of *Arabidopsis thaliana* stomatal bHLH genes and regulation of stomatal development in grasses. *Development*, 136(13), 2265–2276.

Lobell, D.B., Schlenker, W. & Costa-Roberts, J., 2011. Climate Trends and Global Crop Production Since 1980. *Science*, 333(6042), 616–620.

Long, S.P., Farage, P.K., Bolhár-Nordenkampf, H.R. & Rohrhofer, U., 1989. Separating the contribution of the upper and lower mesophyll to photosynthesis in Zea mays L. leaves. *Planta*, 177(2), 207–216.

Long, S.P. & Bernacchi, C.J., 2003. Gas exchange measurements, what can they tell us about the underlying limitations to photosynthesis? Procedures and sources of error. *Journal of Experimental Botany*, 54(392), 2393–2401.

Long, S.P., Marshall-Colon, A. & Zhu, X.-G., 2015. Meeting the Global Food Demand of the Future by Engineering Crop Photosynthesis and Yield Potential. *Cell*, 161(1), 56–66.

Loreto, F., Harley, P. C., Di Marco, G., & Sharkey, T. D. 1992. Estimation of Mesophyll Conductance to CO2 Flux by Three Different Methods. *Plant Physiology*, 98(4), 1437–1443.

Loreto, F., Di Marco, G., Tricoli, D., & Sharkey, T. D. 1994. Measurements of mesophyll conductance, photosynthetic electron transport and alternative electron sinks of field grown wheat leaves. *Photosynthesis research*, 41(3), 397–403.

Lundgren, M.R., Mathers, A., Baillie, A.L., Dunn, J., Wilson, M.J., Hunt, L., Pajor, R., Fradera-Soler, M., Rolfe, S., Osborne, C.P., Sturrock, C.J., Gray, J.E., Mooney, S.J, & Fleming A.J., 2019. Mesophyll porosity is modulated by the presence of functional stomata. *Nature Communications*, 10(1), 2825.

Maccaferri, M., Harris, N.S., Twardziok, S.O., Pasam, R.K., Gundlach, H., Spannagl, M., Ormanbekova, D., Lux, T., Prade, V.M., Milner, S.G., Himmelbach, A., Mascher, M., Bagnaresi, P., Faccioli, P., Cozzi, P., Lauria, M., Lazzari, B., Stella, A., Manocni, A., Gnocchi, M., Moscatelli, M., Avni, R., Deek, J., Biyiklioglu, S., Frascaroli, E., Corneti, S., Salvi, S., Sonnante, G., Desiderio, F., Marè, C., Crosatti, C., Mica, E., Özkan, H., Kilian, B., De Vita, P., Marone, D., Joukhadar, R., Mazzucotelli, E., Nigro, D., Gadaleta, A., Chao, S., Faris, J.D., Melo, A.T.O., Pumphrey, M., Pecchioni, N., Milanesi, L., Wiebe, K., Ens, J., MacLachlan, R.P., Clarke, J.M., Sharpe, A.G., Koh, C.S., Liang, K.Y.H., Taylor, G.J., Knox, R., Budak, H., Mastrangelo, A.M., Xu, S.S., Stein, N., Hale, I., Distelfeld, A., Hayden, M.J., Tuberosa, R., Walkowiak, S., Mayer, K.F.X., Ceriotti, A., Pozniak, C.J. & Cattivelli, L., 2019. Durum wheat genome highlights past domestication signatures and future improvement targets. *Nature Genetics*, 51(5), 885–895.

Maosong, L., Chunyan, W., Jiqing, S., Yonggang, C., Xiufen, W. & Yongfeng, W., 2008. Evolutional trends of leaf stomatal and photosynthetic characteristics in wheat evolutions. *Acta Ecologica Sinica*, 28(11), 5385–5391.

Marcussen, T., Sandve, S.R., Heier, L., Spannagl, M., Pfeifer, M., Jakobsen, K.S., Wulff, B.B., Steuernagel, B., Mayer, K.F., Olsen, O.A., International Wheat Genome Sequencing Consortium, Jakobsen, K.S., Wulff, B.B.H., Steuernagel, B., Mayer, K.F.X. Olsen, O.A., 2014. Ancient hybridizations among the ancestral genomes of bread wheat. *Science (New York, N.Y.)*, 345(6194), 1250092.

Martin, C. & Glover, B., 2007. Functional aspects of cell patterning in aerial epidermis. *Current Opinion in Plant Biology*, 10(1), 70–82.

Masterson, J., 1994. Stomatal Size in Fossil Plants: Evidence for Polyploidy in Majority of Angiosperms. *Science*, 264, 421–424.

Mathers, A.W., Hepworth, C., Baillie, A.L., Sloan, J., Jones, H., Lundgren, M., Fleming, A.J., Mooney, S.J. and Sturrock, C.J., 2018. Investigating the microstructure of plant leaves in 3D with lab-based X-ray computed tomography. *Plant Methods*, 14(1), 99.

Matthews, J.S.A., Vialet-Chabrand, S.R.M. & Lawson, T., 2017. Diurnal Variation in Gas Exchange: The Balance between Carbon Fixation and Water Loss. *Plant Physiology*, 174(2), 614–623.

Mayo, S.C., Chen, F. & Evans, R., 2010. Micron-scale 3D imaging of wood and plant microstructure using high-resolution X-ray phase-contrast microtomography. *Journal of Structural Biology*, 171(2), 182–188.

McAusland, L., Davey, P.A., Kanwal, N., Baker, N.R. and Lawson, T., 2013. A novel system for spatial and temporal imaging of intrinsic plant water use efficiency. *Journal of Experimental Botany*, 64(16), 4993–5007.

McElwain, J.C., Yiotis, C. & Lawson, T., 2015. Using modern plant trait relationships between observed and theoretical maximum stomatal conductance and vein density to examine patterns of plant macroevolution. *New Phytologist*, 209(1), 94–103.

Merah, O., Monneveux, P. & Deléens, E., 2001. Relationships between flag leaf carbon isotope discrimination and several morpho-physiological traits in durum wheat genotypes under Mediterranean conditions. *Environmental and Experimental Botany*, 45(1), 63–71.

Meyer, R.S., DuVal, A.E. & Jensen, H.R., 2012. Patterns and processes in crop domestication: an historical review and quantitative analysis of 203 global food crops. *New Phytologist*, 196(1), 29–48.

Milla, R., Osborne, C. P., Turcotte, M. M., & Violle, C., 2015. Plant domestication through an ecological lens. *Trends in Ecology & Evolution*, 30(8), 463–469.

Milla, R. & Matesanz, S., 2017. Growing larger with domestication: a matter of physiology, morphology or allocation? *Plant Biology*, 19(3), 475–483.

Miner, G.L., Bauerle, W.L. & Baldocchi, D.D., 2017. Estimating the sensitivity of stomatal conductance to photosynthesis: a review. *Plant, Cell & Environment*, 40(7), 1214–1238.

Mishra, M.K., 1997. Stomatal Characteristics at Different Ploidy Levels in Coffea. *Annals of Botany*, 80(5),.689–692.

Mizukami, Y., 2001. A matter of size: Developmental control of organ size in plants. *Current Opinion in Plant Biology*, 4(6), 533–539.

Mohammed, U., Caine, R.S., Atkinson, J.A., Harrison, E.L., Wells, D., Chater, C.C., Gray, J.E., Swarup, R. & Murchie, E.H., 2019. Rice plants overexpressing OsEPF1 show reduced stomatal density and increased root cortical aerenchyma formation. *Scientific Reports*, 9(1), 5584.

Montenegro-Johnson, T., Strauss, S., Jackson, M.D., Walker, L., Smith, R.S. & Bassel, G.W., 2019. 3DCellAtlas Meristem: a tool for the global cellular annotation of shoot apical meristems. *Plant Methods*, 15(1), 33.

Montenegro-Johnson, T.D., Stamm, P., Strauss, S., Topham, A.T., Tsagris, M., Wood, A.T., Smith, R.S. & Bassel, G.W., *et al.*, 2015. Digital Single-Cell Analysis of Plant Organ Development Using 3DCellAtlas. *The Plant Cell*, 27(4), 1018–1033.

Mooney, S. J., Pridmore, T. P., Helliwell, J., & Bennett, M. J., 2012. Developing X-ray Computed Tomography to non-invasively image 3-D root systems architecture in soil. *Plant and Soil*, 352(1-2), 1–22.

Mott, K.A., Berg, D.G., Hunt, S.M. & Peak, D., 2014. Is the signal from the mesophyll to the guard cells a vapour-phase ion? *Plant, Cell & Environment*, 37(5), 1184–1191.

Mott, K.A., Sibbernsen, E.D. & Shope, J.C., 2008. The role of the mesophyll in stomatal responses to light and CO_2. *Plant, Cell & Environment*, 31(9), 1299–1306.

Navea, C., Terrazas, T., Delgado-Salinas, A. & Ramírez-Vallejo, P., 2002. Foliar response of wild and domesticated *Phaseolus vulgaris L.* to water stress. *Genetic Resources and Crop Evolution*, 49(2), 125–132.

Nelissen, H., Gonzalez, N. & Inzé, D., 2016. Leaf growth in dicots and monocots: so different yet so alike. *Current Opinion in Plant Biology*, 33, 72–76.

Nevo, E., Carver, B.F. & Beiles, A., 1991. Photosynthetic performance in wild emmer wheat, *Triticum dicoccoides*: ecological and genetic predictability. *Theoretical and Applied Genetics*, 81(4), 445–460.

Niinemets, Ü., Díaz-Espejo, A., Flexas, J., Galmés, J. & Warren, C.R., 2009. Role of mesophyll diffusion conductance in constraining potential photosynthetic productivity in the field. *Journal of Experimental Botany*, 60(8), 2249–2270.

Ocheltree, T.W., Nippert, J.B. & Prasad, P.V.V, 2012. Changes in stomatal conductance along grass blades reflect changes in leaf structure. *Plant, Eell & Environment*, 35(6), 1040–9.

Oguchi, R., Hikosaka, K. & Hirose, T., 2005. Leaf anatomy as a constraint for photosynthetic acclimation: Differential responses in leaf anatomy to increasing growth irradiance among three deciduous trees. *Plant, Cell and Environment*, 28(7), 916–927.

Oi, T., Enomoto, S., Nakao, T., Arai, S., Yamane, K. & Taniguchi, M., 2017. Three-dimensional intracellular structure of a whole rice mesophyll cell observed with FIB-SEM. *Annals of Botany*, 120(1), 21–28.

Olsovska, K., Kovar, M., Brestic, M., Zivcak, M., Slamka, P. & Shao, H.B., 2016. Genotypically Identifying Wheat Mesophyll Conductance Regulation under Progressive Drought Stress. *Frontiers in Plant Science*, 7, 1111.

Omasa, K., Konishi, A., Tamura, H. & Hosoi, F., 2008. 3D confocal laser scanning microscopy for the analysis of chlorophyll fluorescence parameters of chloroplasts in intact leaf tissues. *Plant and Cell Physiology*, 50(1), 90–105.

Ouyang, W., Struik, P.C., Yin, X. & Yang, J., 2017. Stomatal conductance, mesophyll conductance, and transpiration efficiency in relation to leaf anatomy in rice and wheat genotypes under drought. *Journal of Experimental Botany*, 68(18), 5191–5205.

Ovečka, M., von Wangenheim, D., Tomančák, P., Šamajová, O., Komis, G. & Šamaj, J., 2018. Multiscale imaging of plant development by light-sheet fluorescence microscopy. *Nature Plants*, 4(9), 639–650.

Paddock, S.W., 2000. Principles and practices of laser scanning confocal microscopy. *Molecular Biotechnology*, 16(2), 127–149.

Pajor, R., Fleming, A., Osborne, C.P., Rolfe, S.A., Sturrock, C.J. & Mooney, S.J., 2013. Seeing space: visualization and quantification of plant leaf structure using X-ray micro-computed tomography. *Journal of experimental botany*, 64(2), 385–90.

Palmer, W.M., Martin, A.P., Flynn, J.R., Reed, S.L., White, R.G., Furbank, R.T. & Grof, C.P., 2015. PEA-CLARITY: 3D molecular imaging of whole plant organs. *Scientific Reports*, 5(1), 13492.

Panteris, E. & Galatis, B., 2005. The morphogenesis of lobed plant cells in the mesophyll and epidermis: Organization and distinct roles of cortical microtubules and actin filaments. *New Phytologist*, 167(3), 721–732.

Parker, M.L. & Ford, M. A., 1982. The structure of the mesophyll of flag leaves in three Triticum species. *Annals of Botany*, 49, 65–176.

Parry, M.A., Reynolds, M., Salvucci, M.E., Raines, C., Andralojc, P.J., Zhu, X.G., Price, G.D., Condon, A.G. & Furbank, R.T., 2010. Raising yield potential of wheat. II. Increasing photosynthetic capacity and efficiency. *Journal of Experimental Botany*, 62(2), 453–467.

Parsons, J.L., Martin, S.L., James, T., Golenia, G., Boudko, E.A. & Hepworth, S.R., 2019. Polyploidization for the Genetic Improvement of *Cannabis sativa*. *Frontiers in Plant Science*, 10.

Pautler, M., Tanaka, W., Hirano, H.Y. & Jackson, D., 2013. Grass Meristems I: Shoot Apical Meristem Maintenance, Axillary Meristem Determinacy and the Floral Transition. *Plant and Cell Physiology*, 54(3), 302–312.

Peng, J.H., Sun, D. & Nevo, E., 2011. Domestication evolution, genetics and genomics in wheat. *Molecular Breeding*, 28(3), 281–301.

Pillitteri, L.J. & Torii, K.U., 2012. Mechanisms of Stomatal Development. *Annual Review of Plant Biology*, 63(1), 591–614.

Pons, T.L., Flexas, J., Von Caemmerer, S., Evans, J.R., Genty, B., Ribas-Carbo, M. & Brugnoli, E., 2009. Estimating mesophyll conductance to CO2: methodology, potential errors, and recommendations. *Journal of Experimental Botany*, 60(8), 2217–2234.

Porra, R.J., Thompson, W.A. & Kriedemann, P.E., 1989. Determination of accurate extinction coefficients and simultaneous equations for assaying chlorophylls a and b extracted with four different solvents: verification of the concentration of chlorophyll standards by atomic absorption spectroscopy. *Biochimica et Biophysica Acta (BBA) - Bioenergetics*, 975(3), 384–394.

Preece, C., Livarda, A., Christin, P.A., Wallace, M., Martin, G., Charles, M., Jones, G., Rees, M. & Osborne, C.P., 2017. How did the domestication of Fertile Crescent grain crops increase their yields? *Functional Ecology*, 31(2), 387–397.

Preece, C., Livarda, A., Wallace, M., Martin, G., Charles, M., Christin, P.A., Jones, G., Rees, M. &Osborne, C.P., 2015. Were Fertile Crescent crop progenitors higher yielding than other wild species that were never domesticated? *New Phytologist*, 207(3), 905-913.

Preibisch, S., Saalfeld, S. & Tomancak, P., 2009. Globally optimal stitching of tiled 3D microscopic image acquisitions. *Bioinformatics*, 25(11), 1463–1465.

Prins, A., Orr, D.J., Andralojc, P.J., Reynolds, M.P., Carmo-Silva, E. & Parry, M.A., 2016. Rubisco catalytic properties of wild and domesticated relatives provide scope for improving wheat photosynthesis. *Journal of Experimental Botany*, 67(6), 1827–38.

Purugganan, M.D. & Fuller, D.Q., 2009. The nature of selecion during plant domestication. *Nature*, 457, 843–848.

Pyke, K. A, Jellings, A J. & Leech, R.M., 1990. Variation in mesophyll cell number and size in wheat leaves. *Annals of Botany*, 65(6), 679.

Raines, C. A, 2003. The Calvin cycle revisited. *Photosynthesis research*, 75(1), 1–10.

Raissig, M.T., Abrash, E., Bettadapur, A., Vogel, J.P. & Bergmann, D.C., 2016. Grasses use an alternatively wired bHLH transcription factor network to establish stomatal identity. *Proceedings of the National Academy of Sciences of the United States of America*, 113(29), 8326–31.

Rajabi, A., Griffiths, H., Ober, E.S., Kromdijk, W. & Pidgeon, J.D., 2008. Genetic characteristics of water-use related traits in sugar beet. *Euphytica*, 160(2), 175–187.

Ramírez-González, R.H., Borrill, P., Lang, D., Harrington, S.A., Brinton, J., Venturini, L., Davey, M., Jacobs, J., Van Ex, F., Pasha, A., Khedikar, Y., Robinson, S.J., Cory, A.T., Florio, T., Concia, L., Juery, C., Schoonbeek, H., Steuernagel, B., Xiang, D., Ridout, C.J., Chalhoub, B., Mayer, K.F.X., Benhamed, M., Latrasse, D., Bendahmane, A., International Wheat Genome Sequencing Consortium, Wulff B.B.H., Appels, A., Tiwari, V., Datla, R., Choulet, F., Pozniak, C.J., Provart., N.J., Sharpe, A.G., Paux, E., Spannagl, M., Brautigam, A. & Uauy C., 2018. The transcriptional landscape of polyploid wheat. *Science*, 361(6403), eaar6089.

Ray, D.K., Ramankutty, N., Mueller, N.D., West, P.C. & Foley, J.A., 2012. Recent patterns of crop yield growth and stagnation. *Nature Communications*, 3, 1293.

Ray, D.K., Mueller, N.D., West, P.C. & Foley, J.A.,2013. Yield Trends Are Insufficient to Double Global Crop Production by 2050. *PloS one*, 8(6), e66428.

Rebetzke, G.J., Botwright, T.L., Moore, C.S., Richards, R.A. & Condon, A.G., 2004. Genotypic variation in specific leaf area for genetic improvement of early vigour in wheat. *Field Crops Research*, 88(2–3), 179–189.

Rebetzke, G.J., Condon, A.G., Richards, R.A. and Read, J.J., 2001. Phenotypic variation and sampling for leaf conductance in wheat (*Triticum aestivum* L.) breeding populations. *Euphytica,* 121(3), 335–341.

Rebetzke, G.J., Condon, A.G., Richards, R.A. & Farquhar, G.D., 2002. Selection for reduced carbon isotope discrimination increases aerial biomass and grain yield of rainfed bread wheat. *Crop Science*, 42(3), 739–745.

Ren, T., Weraduwage, S.M. & Sharkey, T.D., 2019. Prospects for enhancing leaf photosynthetic capacity by manipulating mesophyll cell morphology. *Journal of Experimental Botany*, 70(4), 1153–1165.

Renny-Byfield, S. & Wendel, J.F., 2014. Doubling down on genomes: Polyploidy and crop plants. *American Journal of Botany*, 101(10), 1711–1725.

Reynolds, M., Foulkes, J., Furbank, R., Griffiths, S., King, J., Murchie, E., Parry, M. & Slafer, G., 2012. Achieving yield gains in wheat. *Plant, Cell & Environment*, 35(10), 1799–1823.

Richards, R. A, 2000. Selectable traits to increase crop photosynthesis and yield of grain crops. *Journal of Experimental Botany*, 51, 447–458.

Ritman, E.L., 2011. Current Status of Developments and Applications of Micro-CT. *Annual Review of Biomedical Engineering*, 13(1), 531–552.

Rizza, F., Ghashghaie, J., Meyer, S., Matteu, L., Mastrangelo, A.M. & Badeck, F.W., 2012. Constitutive differences in water use efficiency between two durum wheat cultivars. *Field Crops Research*, 125, 49–60.

Rockwell, F.E. & Holbrook, N.M., 2017. Leaf Hydraulic Architecture and Stomatal Conductance: A Functional Perspective. *Plant Physiology*, 174(4), 1996–2007.

Sachs, T., 1979. Cellular Interactions in the Development of Stomatal Patterns in *Vinca major L. Annals of Botany*, 43(6), 693–700.

Sack, L. & Holbrook, N.M., 2006. Leaf Hydraulics. *Annual Review of Plant Biology*, 57(1), 361–381.

Sack, L. & Scoffoni, C., 2013. T Leaf venation: structure, function, development, evolution, ecology and applications in the past, present and future. *New Phytologist,* 198(4), 983–1000.

Sadras, V.O., Lawson, C. & Montoro, A., 2012. Photosynthetic traits in Australian wheat varieties released between 1958 and 2007. *Field Crops Research*, 134, 19–29.

Sage, T.L. & Sage, R.F., 2009. The functional anatomy of rice leaves: Implications for refixation of photorespiratory CO2 and efforts to engineer C4 photosynthesis into rice. *Plant and Cell Physiology*, 50(4), 756–772.

Salman-Minkov, A., Sabath, N. & Mayrose, I., 2016. Whole-genome duplication as a key factor in crop domestication. *Nature Plants*, 2(8), 16115.

Salvo, L., Suéry, M., Marmottant, A., Limodin, N. and Bernard, D., *et al.*, 2010. 3D imaging in material science: Application of X-ray tomography. *Comptes Rendus Physique*, 11(9–10), 641–649.

Sattler, M.C., Carvalho, C.R. & Clarindo, W.R., 2016. The polyploidy and its key role in plant breeding. *Planta*, 243(2), 281–296.

Schindelin, J., Rueden, C.T., Hiner, M.C. & Eliceiri, K.W., 2015. The ImageJ ecosystem: An open platform for biomedical image analysis. *Molecular Reproduction and Development*, 82(7–8), 518–529.

Schneider, J.V., Rabenstein, R., Wesenberg, J., Wesche, K., Zizka, G. & Habersetzer, J., 2018. Improved non-destructive 2D and 3D X-ray imaging of leaf venation. *Plant Methods*, 14, 7.

Seibt, U., Rajabi, A., Griffiths, H. and Berry, J.A., 2008. Carbon isotopes and water use efficiency: Sense and sensitivity. *Oecologia*, 155(3), 441–454.

Serna, L., 2015. Development: Early events in asymmetric division. *Nature Plants*, 1(2), 15008.

Sezgin, M. & Sankur, B., 2004. Survey over image thresholding techniques and quantitative performance evaluation. *Journal of Electronic Imaging*, 13(1), 146–166.

Sharkey, T.D., Bernacchi, C.J., Farquhar, G.D. & Singsaas, E.L., 2007. Fitting photosynthetic carbon dioxide response curves for C_3 leaves. *Plant, Cell & Environment*, 30(9), 1035–1040.

Sharkey, T.D., 2016. What gas exchange data can tell us about photosynthesis. *Plant, Cell & Environment*, 39(6), 1161–1163.

Shewry, P.R., 2009. Wheat. *Journal of Experimental Botany*, 60(6), 1537–1553.

Shiferaw, B., Smale, M., Braun, H.J., Duveiller, E., Reynolds, M. & Muricho, G., 2013. Crops that feed the world 10. Past successes and future challenges to the role played by wheat in global food security. *Food Security*, 5(3), 291–317.

Sid'ko, A.F., Botvich, I.Y., Pisman, T.I. and Shevyrnogov, A.P., 2017. Estimation of chlorophyll content and yield of wheat crops from reflectance spectra obtained by ground-based remote measurements. *Field Crops Research*, 207, 24–29.

Sluis, A. & Hake, S., 2015. Organogenesis in plants: initiation and elaboration of leaves. *Trends in Genetics*, 31(6), 300–306.

Smillie, I.R.., Pyke, K.A. & Murchie, E.H., 2012. Variation in vein density and mesophyll cell architecture in a methylation and chromatin patterning. *Journal of Experimental Botany*, 63(2), 695–709.

Smith, L.G., 2001. Plant cell division: building walls in the right places. *Nature Reviews – Molecular Cell Biology*, 2, 3–9.

Souza, N.M., Topham, A.T. & Bassel, G.W., 2017. Quantitative analysis of the 3D cell shape changes driving soybean germination. *Journal of Experimental Botany*, 68(7), 1531–1537.

Staedler, Y.M., Masson, D. & Schönenberger, J., 2013. Plant Tissues in 3D via X-Ray Tomography: Simple Contrasting Methods Allow High Resolution Imaging. *PLoS ONE*, 8(9), 75295.

Steppe, K., Cnudde, V., Girard, C., Lemeur, R., Cnudde, J.P. & Jacobs, P.,2004. Use of X-ray computed microtomography for non-invasive determination of wood anatomical characteristics. *Journal of Structural Biology*, 148(1), 11–21.

Strock, C.F., Schneider, H.M., Galindo-Castañeda, T., Hall, B.T., Van Gansbeke, B., Mather, D.E., Roth, M.G., Chilvers, M.I., Guo, X., Brown, K. & Lynch, J.P., 2019. Laser ablation tomography for visualization of root colonization by edaphic organisms. *Journal of Experimental Botany*, erz271.

Stuppy, W.H., Maisano, J.A., Colbert, M.W., Rudall, P.J. & Rowe, T.B., 2003. Three-dimensional analysis of plant structure using high-resolution X-ray computed tomography. *Trends in Plant Science*, 8(1), 2–6.

Sugiyama, S.I., 2005. Polyploidy and cellular mechanisms changing leaf size: Comparison of diploid and autotetraploid populations in two species of Lolium. *Annals of Botany*, 96(5), 931–938.

Sun, J., Sun, J. & Feng, Z., 2015. Modelling photosynthesis in flag leaves of winter wheat (*Triticum aestivum*) considering the variation in photosynthesis parameters during development. *Functional Plant Biology*, 42(11), 1036–1044.

Takahashi, K., Mineuchi, K., Nakamura, T., Koizumi, M. & Kano, H., 1994. A system for imaging transverse distribution of scattered light and chlorophyll fluorescence in intact rice leaves. *Plant, Cell & Environment*, 17(1), 105–110.

Tanaka, Y., Sugano, S.S., Shimada, T. & Hara-Nishimura, I., 2013. 2013. Enhancement of leaf photosynthetic capacity through increased stomatal density in Arabidopsis. *New Phytologist*, 198(3), 757–764.

Tazoe, Y., Von Caemmerer, S., Badger, M.R. and Evans, J.R., 2009.2009. Light and CO2 do not affect the mesophyll conductance to CO_2 diffusion in wheat leaves. *Journal of Experimental Botany*, 60(8), 2291–2301.

Terashima, I., Hanba, Y.T., Tholen, D. & Niinemets, Ü., 2011. 2011. Leaf Functional Anatomy in Relation to Photosynthesis. *Plant Physiology*, 155(1), 108–116.

Théroux-Rancourt, G., Earles, J.M., Gilbert, M.E., Zwieniecki, M.A., Boyce, C.K., McElrone, A.J. & Brodersen, C.R., 2017. The bias of a two-dimensional view: comparing two-dimensional and three-dimensional mesophyll surface area estimates using noninvasive imaging. *New Phytologist*, 215(4), 1609–1622.

Tholen, D., Boom, C. & Zhu, X.G., 2012. 2012. Variable mesophyll conductance revisited: theoretical background and experimental implications. *Plant, Cell & Environment*, 35(12), 2087–2103.

Tholen, D., Boom, C. & Zhu, X.-G., 2012. Opinion: Prospects for improving photosynthesis by altering leaf anatomy. *Plant Science*, 197, 92–101.

Tholen, D., Ethier, G. & Genty, B., 2014. Mesophyll conductance with a twist. *Plant, Cell & Environment*, 2456–2458.

Tomás, M., Flexas, J., Copolovici, L., Galmés, J., Hallik, L., Medrano, H., Ribas-Carbó, M., Tosens, T., Vislap, V. & Niinemets, Ü., 2013. Importance of leaf anatomy in determining mesophyll diffusion conductance to CO2 across species: quantitative limitations and scaling up by models. *Journal of Experimental Botany*, 64(8), 2269–2281.

Tosens, T., Niinemets, U., Vislap, V., Eichelmann, H. & Castro Diez, P., 2012. Developmental changes in mesophyll diffusion conductance and photosynthetic capacity under different light and water availabilities in Populus tremula: how structure constrains function. *Plant, Cell & Environment*, 35(5), 839–856.

Tracy, S.R., Gómez, J.F., Sturrock, C.J., Wilson, Z.A. & Ferguson, A.C., 2017. Non-destructive determination of floral staging in cereals using X-ray micro computed tomography (μCT). *Plant Methods*, 13(1), 9.

Tracy, S.R., Black, C.R., Roberts, J.A., McNeill, A., Davidson, R., Tester, M., Samec, M., Korošak, D., Sturrock, C. & Mooney, S.J. 2012. Quantifying the effect of soil compaction on three varieties of wheat (*Triticum aestivum* L.) using X-ray Micro Computed Tomography (CT). *Plant and Soil*, 353(1–2), 195–208.

Truernit, E., Bauby, H., Dubreucq, B., Grandjean, O., Runions, J., Barthélémy, J. & Palauqui, J.C., 2008. High-Resolution Whole-Mount Imaging of Three-Dimensional Tissue Organization and Gene Expression Enables the Study of Phloem Development and Structure in Arabidopsis. *the Plant Cell Online*, 20(6), 1494–1503.

Tsukaya, H., 2013. Does ploidy level directly control cell size? Counterevidence from Arabidopsis genetics. *PLoS ONE*, 8(12), 1–7.

Tsukaya, H., 2019. Has the impact of endoreduplication on cell size been overestimated? *New Phytologist*, 223(1), 11–15.

Vandenhout, H., Ortiz, R., Vuylsteke, D., Swennen, R., & Bai, K. V., 1995. Effect of ploidy on stomatal and other quantitative traits in plantain and banana hybrids. *Euphytica*, 83(2), 117–122.

Vatén, A. & Bergmann, D.C., 2012. Mechanisms of stomatal development: an evolutionary view. *EvoDevo*, 3, 11.

Verboven, P., Herremans, E., Helfen, L., Ho, Q.T., Abera, M., Baumbach, T., Wevers, M. & Nicolaï, B.M., 2014. Synchrotron X-ray computed laminography of the three-dimensional anatomy of tomato leaves. *The Plant Journal,* 81(1) 169–182.

Vergauwen, D. & De Smet, I., 2017. From early farmers to Norman Borlaug — the making of modern wheat. *Current Biology*, 27(17), 858–862.

Vialet-Chabrand, S.R.M., Matthews, J.S., McAusland, L., Blatt, M.R., Griffiths, H. & Lawson, T., 2017. Temporal Dynamics of Stomatal Behavior: Modeling and Implications for Photosynthesis and Water Use. *Plant Physiology*, 174(2), 603–613.

Vlad, D., Kierzkowski, D., Rast, M.I., Vuolo, F., Ioio, R.D., Galinha, C., Gan, X., Hajheidari, M., Hay, A., Smith, R.S., Huijser, P., Bailey, C.D. & Tsiantis, M., 2014. Leaf shape evolution through duplication, regulatory diversification and loss of a homeobox gene. *Science*, 343(6172), 780–783.

Vogelmann, T.C. & Evans, J.R., 2002. Profiles of light absorption and chlorophyll within spinach leaves from chlorophyll fluorescence. *Plant, Cell and Environment*, 25(10), 1313–1323.

Walker, B.J., Orr, D.J., Carmo-Silva, E., Parry, M.A., Bernacchi, C.J. & Ort, D.R.,2017. Uncertainty in measurements of the photorespiratory CO2 compensation point and its impact on models of leaf photosynthesis. *Photosynthesis Research*, 132(3), 245–255.

Wang, H. & Clarke, J.M., 1993. Genotypic, intraplant, and environmental variation in stomatal frequency and size in wheat. *Canadian Journal of Plant Science*, 73(3), 671–678.

Wang, P., Karki, S., Biswal, A.K., Lin, H.C., Dionora, M.J., Rizal, G., Yin, X., Schuler, M.L., Hughes, T., Fouracre, J.P., Jamous, B.A., Sedelnikova, O., Lo, S.F., Bandyopadhyay, A., Yu, S.M., Kelly,. S., Quick, W.P. & Langdale, J., 2017. Candidate regulators of Early Leaf Development in Maize Perturb Hormone Signalling and Secondary Cell Wall Formation When Constitutively Expressed in Rice. *Scientific Reports*, 7(1), 4535.

Wang, S.G., Jia, S.S., Sun, D.Z., Wang, H.Y., Dong, F.F., Ma, H.X., Jing, R.L. & Ma, G., 2015. Genetic basis of traits related to stomatal conductance in wheat cultivars in response to drought stress. *Photosynthetica*, 53(2), 299–305.

Warner, D.A. & Edwards, G.E., 1993. Effects of polyploidy on photosynthesis. *Photosynthesis Research*, 35(2), 135–147.

Watanabe, N., Evans, J.R. & Chow, W.S., 1994. Changes in the photosynthetic properties of Australian wheat cultivars over the last century. *Australian Journal of Plant Physiology*, 21(2), 169–183.

Wheeler, T., & Von Braun, J., 2013. Climate change impacts on global food security. *Science*, 341(6145), 508–513.

Willats, W.G., Orfila, C., Limberg, G., Buchholt, H.C., van Alebeek, G.J.W., Voragen, A.G., Marcus, S.E., Christensen, T.M., Mikkelsen, J.D., Murray, B.S. & Knox, J.P., 2001. Modulation of the Degree and Pattern of Methyl-esterification of Pectic Homogalacturonan in Plant Cell Walls. Implications for pectin methyl esterase action, matrix properties, and cell adhesion. *Journal of Biological Chemistry*, 276(22), 19404–19413.

Wilson, D. & Cooper, J.P., 1970. Effect of selection for mesophyll cell size on growth and assimilation in *Lolium perenne* L. *New Phytologist*, 69(2), 233–245.

Wu, A., Hammer, G.L., Doherty, A., von Caemmerer, S. & Farquhar, G.D.,2019. Quantifying impacts of enhancing photosynthesis on crop yield. *Nature Plants*, 5(4), 380–388.

Wuyts, N., Palauqui, J.C., Conejero, G., Verdeil, J.L., Granier, C. & Massonnet, C., 2010. High-contrast three-dimensional imaging of the Arabidopsis leaf enables the analysis of cell dimensions in the epidermis and mesophyll. *Plant methods*, 6(11), 17.

Xiao, Y., Tholen, D. & Zhu, X.G., 2016. The influence of leaf anatomy on the internal light environment and photosynthetic electron transport rate: Exploration with a new leaf ray tracing model. *Journal of Experimental Botany*, 67(21), 6021–6035.

Xiong, D., Flexas, J., Yu, T., Peng, S. & Huang, J., 2016. Leaf anatomy mediates coordination of leaf hydraulic conductance and mesophyll conductance to CO_2 in Oryza. *New Phytologist*, 213(2), 572–583.

Xiong, Y.C., Li, F.M. & Zhang, T., 2006. Performance of wheat crops with different chromosome ploidy: Root-sourced signals, drought tolerance, and yield performance. *Planta*, 224(3), 710–718.

Yin, X., Struik, P.C., Romero, P., Harbinson, J., Evers, J.B., Van Der Putten, P.E. & Vos, J.A.N., 2009. Using combined measurements of gas exchange and chlorophyll fluorescence to estimate parameters of a biochemical C_3 photosynthesis model: a critical appraisal and a new integrated approach applied to leaves in a wheat (*Triticum aestivum*) canopy. *Plant, Cell & Environment*, 32(5), 448–464.

Yoshida, S., de Reuille, P.B., Lane, B., Bassel, G.W., Prusinkiewicz, P., Smith, R.S. & Weijers, D., 2014. Genetic Control of Plant Development by Overriding a Geometric Division Rule. *Developmental Cell*, 29(1), 75–87.

Zhang, Y., Wang, B., Qi, S., Dong, M., Wang, Z., Li, Y., Chen, S., Li, B. & Zhang, J., 2019. Ploidy and hybridity effects on leaf size, cell size and related genes expression in triploids, diploids and their parents in Populus. *Planta*, 249, 635–646.

Zhu, X.-G., Long, S.P. & Ort, D.R., 2010. Improving Photosynthetic Efficiency for Greater Yield. *Annual Review of Plant Biology*, 61(1), 235–261.

Zhu, X.-G., Long, S.P. & Ort, D.R., 2008. What is the maximum efficiency with which photosynthesis can convert solar energy into biomass? *Current opinion in biotechnology*, 19(2), 153–9.

Appendices

Appendix 1. Significance tables for Chapter 2

A summary of the lines used in this thesis (including ploidy number, species name and domestication status) is available in Table 2.1.

Lines which could be significantly distinguished from one another (at $P = <0.01$) following a post-hoc test are shown by an asterisk (*). Ploidy level is indicated by colour. Lines coded white are diploid, orange are tetraploid and blue are hexaploid.

Appendix 1.1. Significance table for Figure 2.3A

	TRI 18344	TRI 19028	TRI 6735	TRI 17128	TRI 28870	TRI 18513	TRI 16599	TRI 18505	TRI 18530	TRI 16877	Anvergur	Aventadur	Surmesur	Voilur	Cashel	Conqueror	Conversion	Cougar	Crusoe	Gallant	Sacramento	Scout	Shamrock	Shango	Skyfall	Stigg
TRI 18344		*	ns	*	*	*	*	*	*	*	*	*	*	*	*	*	*	*	*	*	*	*	*	*	*	*
TRI 19028	*		ns	ns	ns	*	*	*	*	*	*	*	*	*	*	*	*	*	*	*	*	*	*	*	*	*
TRI 6735	ns	ns		ns	ns	*	*	*	*	*	*	*	*	*	*	*	*	*	*	*	*	*	*	*	*	*
TRI 17128	*	ns	ns		ns	*	*	*	*	*	*	*	*	*	*	*	*	*	*	*	*	*	*	*	*	*
TRI 28870	*	ns	ns	ns		*	*	*	ns	*	*	*	*	*	*	*	*	*	*	*	*	*	*	*	*	*
TRI 18513	*	*	*	*	*		ns	ns	ns	ns	ns	ns	ns	ns	ns	ns	ns	ns	ns	ns	*	ns	ns	ns	ns	ns
TRI 16599	*	*	*	*	*	ns		ns	ns	ns	ns	ns	ns	ns	ns	ns	ns	ns	ns	ns	*	ns	ns	ns	ns	ns
TRI 18505	*	*	*	*	*	ns	ns		ns	ns	ns	ns	ns	ns	ns	ns	ns	ns	*	*	ns	ns	ns	ns	ns	ns
TRI 18530	*	*	*	*	ns	ns	ns	ns		ns	ns	*	ns	ns	*	*	ns	*	*	*	*	*	ns	*	*	ns
TRI 16877	*	*	*	*	*	ns	ns	ns	ns		ns	ns	ns	ns	ns	ns	ns	ns	ns	ns	*	ns	ns	ns	ns	ns
Anvergur	*	*	*	*	*	ns	ns	ns	ns	ns		ns	ns	ns	ns	ns	ns	ns	ns	ns	*	ns	ns	ns	ns	ns
Aventadur	*	*	*	*	*	ns	ns	ns	*	ns	ns		ns	*	ns	ns	ns	ns	ns	ns	ns	ns	ns	ns	ns	ns
Surmesur	*	*	*	*	*	ns	ns	ns	ns	ns	ns	ns		ns	ns	ns	ns	ns	ns	ns	ns	ns	ns	ns	ns	ns
Voilur	*	*	*	*	*	ns	ns	ns	ns	ns	ns	*	ns		ns	ns	ns	*	ns	*	*	ns	ns	ns	ns	ns
Cashel	*	*	*	*	*	ns	ns	ns	*	ns	ns	ns	ns	ns		ns	ns	ns	ns	ns	ns	ns	ns	ns	ns	ns
Conqueror	*	*	*	*	*	ns	ns	ns	*	ns	ns	ns	ns	ns	ns		ns	ns	ns	ns	ns	ns	ns	ns	ns	ns
Conversion	*	*	*	*	*	ns	ns	ns	ns	ns	ns	ns	ns	ns	ns	ns		ns	ns	ns	ns	ns	ns	ns	ns	ns
Cougar	*	*	*	*	*	ns	ns	ns	*	ns	ns	ns	ns	*	ns	ns	ns		ns	ns	ns	ns	ns	ns	ns	ns
Crusoe	*	*	*	*	*	ns	ns	ns	*	ns	ns	ns	ns	ns	ns	ns	ns	ns		ns	ns	ns	ns	ns	ns	ns
Gallant	*	*	*	*	*	ns	ns	*	*	ns	ns	ns	ns	*	ns	ns	ns	ns	ns		ns	ns	ns	ns	ns	ns
Sacramento	*	*	*	*	*	*	*	*	*	*	*	ns	ns	*	ns	ns	ns	ns	ns	ns		ns	ns	ns	ns	*
Scout	*	*	*	*	*	ns	ns	ns	*	ns	ns	ns	ns	ns	ns	ns	ns	ns	ns	ns	ns		ns	ns	ns	ns
Shamrock	*	*	*	*	*	ns	ns	ns	ns	ns	ns	ns	ns	ns	ns	ns	ns	ns	ns	ns	ns	ns		ns	ns	ns
Shango	*	*	*	*	*	ns	ns	ns	*	ns	ns	ns	ns	ns	ns	ns	ns	ns	ns	ns	ns	ns	ns		ns	ns
Skyfall	*	*	*	*	*	ns	ns	ns	*	ns	ns	ns	ns	ns	ns	ns	ns	ns	ns	ns	ns	ns	ns	ns		ns
Stigg	*	*	*	*	*	ns	ns	ns	ns	ns	ns	ns	ns	ns	ns	ns	ns	ns	ns	ns	*	ns	ns	ns	ns	

Appendix 1.2. Significance table for Figure 2.5A

	TRI 18344	TRI 6735	TRI 28870	TRI 18513	TRI 18505	TRI 16877	Anvergur	Voilur	Cougar	Crusoe	Shango
TRI 18344		ns	ns	*	*	*	*	*	*	*	*
TRI 6735	ns		ns	*	*	*	*	*	*	*	*
TRI 28870	ns	ns		*	*	*	*	*	*	*	*
TRI 18513	*	*	*		*	*	ns	ns	*	*	*
TRI 18505	*	*	*	*		ns	ns	ns	*	ns	ns
TRI 16877	*	*	*	*	ns		ns	*	*	ns	ns
Anvergur	*	*	*	ns	ns	ns		ns	*	*	ns
Voilur	*	*	*	ns	ns	*	ns		*	*	*
Cougar	*	*	*	*	*	*	*	*		ns	ns
Crusoe	*	*	*	*	ns	ns	*	*	ns		ns
Shango	*	*	*	*	ns	ns	ns	*	ns	ns	

Appendix 1.3. Significance table for Figure 2.5C

	TRI 18344	TRI 6735	TRI 28870	TRI 18513	TRI 18505	TRI 16877	Anvergur	Voilur	Cougar	Crusoe	Shango
TRI 18344		ns	ns	*	*	ns	*	ns	*	*	*
TRI 6735	ns		ns	*	*	*	*	ns	*	*	*
TRI 28870	ns	ns		*	*	*	*	*	*	*	*
TRI 18513	*	*	*		ns	ns	ns	ns	*	*	*
TRI 18505	*	*	*	ns		ns	ns	ns	*	*	*
TRI 16877	ns	*	*	ns	ns		ns	ns	*	*	*
Anvergur	*	*	*	ns	ns	ns		ns	*	*	*
Voilur	ns	ns	*	ns	ns	ns	ns		*	*	*
Cougar	*	*	*	*	*	*	*	*		ns	ns
Crusoe	*	*	*	*	*	*	*	*	ns		ns
Shango	*	*	*	*	*	*	*	*	ns	ns	

Appendix 1.4. Significance table for Figure 2.5E

	TRI 18344	TRI 6735	TRI 28870	TRI 18513	TRI 18505	TRI 16877	Anvergur	Voilur	Cougar	Crusoe	Shango
TRI 18344		ns	ns	*	*	*	*	*	*	*	*
TRI 6735	ns		ns	*	*	*	*	*	*	*	*
TRI 28870	ns	ns		*	*	*	*	*	*	*	*
TRI 18513	*	*	*		ns	ns	ns	ns	*	*	*
TRI 18505	*	*	*	ns		ns	ns	ns	*	*	*
TRI 16877	*	*	*	ns	ns		ns	ns	*	*	*
Anvergur	*	*	*	ns	ns	ns		*	*	*	*
Voilur	*	*	*	ns	ns	ns	*		*	*	*
Cougar	*	*	*	*	*	*	*	*		ns	ns
Crusoe	*	*	*	*	*	*	*	*	ns		ns
Shango	*	*	*	*	*	*	*	*	ns	ns	

Appendix 1.5. Significance table for Figure 2.6

	TRI 18344	TRI 6735	TRI 28870	TRI 18513	TRI 18505	TRI 16877	Anvergur	Voilur	Cougar	Crusoe	Shango
TRI 18344		ns	ns	ns	ns	ns	ns	ns	*	*	*
TRI 6735	ns		ns	ns	ns	ns	ns	ns	ns	ns	ns
TRI 28870	ns	ns		ns	ns	ns	ns	ns	*	*	*
TRI 18513	ns	ns	ns		ns	ns	ns	ns	*	*	*
TRI 18505	ns	ns	ns	ns		ns	ns	ns	ns	ns	ns
TRI 16877	ns	ns	ns	ns	ns		ns	ns	ns	ns	ns
Anvergur	ns	ns	ns	ns	ns	ns		ns	ns	ns	ns
Voilur	ns	ns	ns	ns	ns	ns	ns		ns	ns	ns
Cougar	*	ns	*	*	ns	ns	ns	ns		ns	ns
Crusoe	*	ns	*	*	ns	ns	ns	ns	ns		ns
Shango	*	ns	*	*	ns	ns	ns	ns	ns	ns	

Appendix 1.6. Significance table for Figure 2.7A

	TRI 18344	TRI 6735	TRI 28870	TRI 18513	TRI 18505	TRI 16877	Anvergur	Voilur	Cougar	Crusoe	Shango
TRI 18344		ns	ns	*	ns	ns	*	*	*	*	*
TRI 6735	ns		ns	ns	ns	ns	*	*	*	*	*
TRI 28870	ns	ns		*	*	ns	*	*	*	*	*
TRI 18513	*	ns	*		ns	ns	ns	ns	ns	ns	ns
TRI 18505	ns	ns	*	ns		ns	ns	ns	ns	ns	ns
TRI 16877	ns	ns	ns	ns	ns		ns	ns	ns	ns	ns
Anvergur	*	*	*	ns	ns	ns		ns	ns	ns	ns
Voilur	*	*	*	ns	ns	ns	ns		ns	ns	ns
Cougar	*	*	*	ns	ns	ns	ns	ns		ns	ns
Crusoe	*	*	*	ns	ns	ns	ns	ns	ns		ns
Shango	*	*	*	ns	ns	ns	ns	ns	ns	ns	

Appendix 1.7. Significance table for Figure 2.7C

	TRI 18344	TRI 6735	TRI 28870	TRI 18513	TRI 18505	TRI 16877	Anvergur	Voilur	Cougar	Crusoe	Shango
TRI 18344		ns	ns	*	*	*	*	*	*	*	*
TRI 6735	ns		ns	ns	*	ns	*	ns	*	*	*
TRI 28870	ns	ns		*	*	ns	*	*	*	*	*
TRI 18513	*	ns	*		ns	ns	ns	ns	ns	ns	ns
TRI 18505	*	*	*	ns		ns	ns	ns	ns	ns	ns
TRI 16877	*	ns	ns	ns	ns		ns	ns	ns	ns	ns
Anvergur	*	*	*	ns	ns	ns		ns	ns	ns	ns
Voilur	*	Ns	*	ns	ns	ns	ns		ns	ns	ns
Cougar	*	*	*	ns	ns	ns	ns	ns		ns	ns
Crusoe	*	*	*	ns	ns	ns	ns	ns	ns		ns
Shango	*	*	*	ns	ns	ns	ns	ns	ns	ns	

Appendix 1.8. Significance table for Figure 2.7E

	TRI 18344	TRI 6735	TRI 28870	TRI 18513	TRI 18505	TRI 16877	Anvergur	Voilur	Cougar	Crusoe	Shango
TRI 18344		ns	ns	*	*	ns	*	*	*	*	*
TRI 6735	ns		ns	*	*	ns	*	*	*	*	*
TRI 28870	ns	ns		*	*	ns	*	*	*	*	*
TRI 18513	*	*	*		ns	ns	ns	ns	*	*	*
TRI 18505	*	*	*	ns		ns	ns	ns	*	ns	*
TRI 16877	ns	ns	ns	ns	ns		ns	ns	*	*	*
Anvergur	*	*	*	ns	ns	ns		ns	ns	ns	ns
Voilur	*	*	*	ns	ns	ns	ns		ns	ns	ns
Cougar	*	*	*	*	*	*	ns	ns		ns	ns
Crusoe	*	*	*	*	ns	*	ns	ns	ns		ns
Shango	*	*	*	*	*	*	ns	ns	ns	ns	

Appendix 1.9. Significance table for Figure 2.8A

	TRI 18344	TRI 6735	TRI 28870	TRI 18513	TRI 18505	TRI 16877	Anvergur	Voilur	Cougar	Crusoe	Shango
TRI 18344		ns	ns	ns	ns	*	*	*	*	*	*
TRI 6735	ns		ns	ns	ns	*	*	*	*	*	*
TRI 28870	ns	ns		ns	ns	*	*	*	*	*	*
TRI 18513	ns	ns	ns		ns	*	*	*	ns	*	*
TRI 18505	ns	ns	ns	ns		*	*	*	ns	*	*
TRI 16877	*	*	*	*	*		ns	ns	*	ns	ns
Anvergur	*	*	*	*	*	ns		ns	*	*	ns
Voilur	*	*	*	*	*	ns	ns		*	*	ns
Cougar	*	*	*	ns	ns	*	*	*		ns	*
Crusoe	*	*	*	*	*	ns	*	*	ns		*
Shango	*	*	*	*	*	ns	ns	ns	*	*	

Appendix 1.10. Significance table for Figure 2.8C

	TRI 18344	TRI 6735	TRI 28870	TRI 18513	TRI 18505	TRI 16877	Anvergur	Voilur	Cougar	Crusoe	Shango
TRI 18344		ns	ns	ns	*	*	*	ns	ns	*	*
TRI 6735	ns		ns	ns	*	*	ns	ns	ns	*	*
TRI 28870	ns	ns		ns	*	*	ns	ns	ns	*	*
TRI 18513	ns	ns	ns		*	*	*	ns	ns	*	*
TRI 18505	*	*	*	*		ns	*	*	*	ns	*
TRI 16877	*	*	*	*	ns		*	*	*	ns	ns
Anvergur	*	ns	ns	*	*	*		ns	ns	ns	ns
Voilur	ns	ns	ns	ns	*	*	ns		ns	ns	ns
Cougar	ns	ns	ns	ns	*	*	ns	ns		ns	ns
Crusoe	*	*	*	*	ns	ns	ns	ns	ns		ns
Shango	*	*	*	*	*	ns	ns	ns	ns	ns	

Appendix 1.11. Significance table for Figure 2.8E

	TRI 18344	TRI 6735	TRI 28870	TRI 18513	TRI 18505	TRI 16877	Anvergur	Voilur	Cougar	Crusoe	Shango
TRI 18344		ns	ns	ns	*	*	*	*	*	*	*
TRI 6735	ns		ns	ns	*	*	*	*	*	*	*
TRI 28870	ns	ns		ns	*	*	*	*	*	*	*
TRI 18513	ns	ns	ns		*	*	*	*	*	*	*
TRI 18505	*	*	*	*		*	ns	ns	ns	ns	*
TRI 16877	*	*	*	*	*		ns	ns	*	ns	ns
Anvergur	*	*	*	*	ns	ns		ns	*	ns	ns
Voilur	*	*	*	*	ns	ns	ns		*	ns	ns
Cougar	*	*	*	*	ns	*	*	*		ns	*
Crusoe	*	*	*	*	ns	ns	ns	ns	ns		ns
Shango	*	*	*	*	*	ns	ns	ns	*	ns	

Appendix 1.12. Significance table for Figure 2.9A

	TRI 18344	TRI 6735	TRI 28870	TRI 18513	TRI 18505	TRI 16877	Anvergur	Voilur	Cougar	Crusoe	Shango
TRI 18344		ns	ns	*	*	ns	*	*	*	*	*
TRI 6735	ns		ns	*	*	ns	*	*	*	*	*
TRI 28870	ns	ns		*	*	*	*	*	*	*	*
TRI 18513	*	*	*		ns	ns	*	ns	*	ns	ns
TRI 18505	*	*	*	ns		*	ns	ns	ns	ns	ns
TRI 16877	ns	ns	*	ns	*		*	*	*	*	ns
Anvergur	*	*	*	*	ns	*		ns	ns	ns	ns
Voilur	*	*	*	ns	ns	*	ns		ns	ns	ns
Cougar	*	*	*	*	ns	*	ns	ns		ns	*
Crusoe	*	*	*	ns	ns	*	ns	ns	ns		ns
Shango	*	*	*	ns	ns	ns	ns	ns	*	ns	

Appendix 1.13. Significance table for Figure 2.9C

	TRI 18344	TRI 6735	TRI 28870	TRI 18513	TRI 18505	TRI 16877	Anvergur	Voilur	Cougar	Crusoe	Shango
TRI 18344		ns	ns	ns	*	ns	*	*	*	*	*
TRI 6735	ns		ns	*	*	ns	*	*	*	*	*
TRI 28870	ns	ns		*	*	ns	*	*	*	*	*
TRI 18513	ns	*	*		ns	ns	*	ns	*	*	ns
TRI 18505	*	*	*	ns		*	*	ns	*	ns	ns
TRI 16877	ns	ns	ns	ns	*		*	*	*	*	*
Anvergur	*	*	*	*	*	*		ns	ns	ns	ns
Voilur	*	*	*	ns	ns	*	ns		ns	ns	ns
Cougar	*	*	*	*	*	*	ns	ns		ns	ns
Crusoe	*	*	*	*	ns	*	ns	ns	ns		ns
Shango	*	*	*	ns	ns	*	ns	ns	ns	ns	

Appendix 1.14. Significance table for Figure 2.10A

	TRI 18344	TRI 6735	TRI 28870	TRI 18513	TRI 18505	TRI 16877	Anvergur	Voilur	Cougar	Crusoe	Shango
TRI 18344		ns	*	ns	ns	ns	ns	ns	ns	ns	ns
TRI 6735	ns		ns	ns	*	ns	ns	ns	ns	ns	ns
TRI 28870	*	ns		*	*	*	*	ns	*	ns	ns
TRI 18513	ns	ns	*		ns	ns	ns	ns	ns	ns	ns
TRI 18505	ns	*	*	ns		ns	ns	*	ns	*	ns
TRI 16877	ns	ns	*	ns	ns		ns	ns	ns	ns	ns
Anvergur	ns	ns	*	ns	ns	ns		ns	ns	ns	ns
Voilur	ns	ns	ns	ns	*	ns	ns		ns	ns	ns
Cougar	ns	ns	*	ns	ns	ns	ns	ns		ns	ns
Crusoe	ns	ns	ns	ns	*	ns	ns	ns	ns		ns
Shango	ns	ns	ns	ns	ns	ns	ns	ns	ns	ns	

Appendix 1.15. Significance table for Figure 2.11A

	TRI 18344	TRI 19028	TRI 6735	TRI 17128	TRI 28870	TRI 18513	TRI 16599	TRI 18505	TRI 18530	TRI 16877	Anvergur	Aventadur	Surmesur	Voilur	Cashel	Conqueror	Conversion	Cougar	Crusoe	Gallant	Sacramento	Scout	Shamrock	Shango	Skyfall	Stigg
TRI 18344		ns	ns	ns	*	ns	ns	ns	ns	ns	ns	ns	ns	ns	ns	ns	ns	ns	ns	ns	ns	ns	ns	ns	ns	ns
TRI 19028	ns		ns	ns	*	ns	ns	ns	ns	ns	ns	ns	ns	ns	ns	ns	ns	ns	ns	ns	ns	ns	ns	ns	ns	ns
TRI 6735	ns	ns		ns	*	ns	ns	ns	ns	ns	ns	ns	ns	ns	ns	ns	ns	ns	ns	ns	ns	ns	ns	ns	ns	ns
TRI 17128	ns	ns			ns	ns	ns	ns	ns	ns	ns	ns	ns	ns	ns	ns	ns	ns	ns	ns	ns	ns	ns	ns	ns	ns
TRI 28870	*	*	*	ns		ns	*	*	*	ns	ns	ns	ns	ns	ns	ns	*	ns	ns	ns	ns	ns	ns	*	ns	*
TRI 18513	ns	ns	ns	ns	ns		ns	ns	ns	ns	ns	ns	ns	ns	ns	ns	ns	ns	ns	ns	ns	ns	ns	ns	ns	ns
TRI 16599	ns	ns	ns	ns	*	ns		ns	ns	ns	ns	ns	ns	ns	ns	ns	ns	ns	ns	ns	ns	ns	ns	ns	ns	ns
TRI 18505	ns	ns	ns	ns	*	ns	ns		ns	ns	ns	ns	ns	ns	ns	ns	ns	ns	ns	ns	ns	ns	ns	ns	ns	ns
TRI 18530	ns	ns	ns	ns	*	ns	ns	ns		ns	ns	ns	ns	ns	ns	ns	ns	ns	ns	ns	ns	ns	ns	ns	ns	ns
TRI 16877	ns	ns	ns	ns	ns	ns	ns	ns	ns		ns	ns	ns	ns	ns	ns	ns	ns	ns	ns	ns	ns	ns	ns	ns	ns
Anvergur	ns	ns	ns	ns	ns	ns	ns	ns	ns	ns		ns	ns	ns	ns	ns	ns	ns	ns	ns	ns	ns	ns	ns	ns	ns
Aventadur	ns	ns	ns	ns	ns	ns	ns	ns	ns	ns	ns		ns	ns	ns	ns	ns	ns	ns	ns	ns	ns	ns	ns	ns	ns
Surmesur	ns	ns	ns	ns	ns	ns	ns	ns	ns	ns	ns	ns		ns	ns	ns	ns	ns	ns	ns	ns	ns	ns	ns	ns	ns
Voilur	ns	ns	ns	ns	ns	ns	ns	ns	ns	ns	ns	ns	ns		ns	ns	ns	ns	ns	ns	ns	ns	ns	ns	ns	ns
Cashel	ns	ns	ns	ns	ns	ns	ns	ns	ns	ns	ns	ns	ns	ns		ns	ns	ns	ns	ns	ns	ns	ns	ns	ns	ns
Conqueror	ns	ns	ns	ns	ns	ns	ns	ns	ns	ns	ns	ns	ns	ns	ns		ns	ns	ns	ns	ns	ns	ns	ns	ns	ns
Conversion	ns	ns	ns	ns	*	ns	ns	ns	ns	ns	ns	ns	ns	ns	ns	ns		ns	ns	ns	ns	ns	ns	ns	ns	ns
Cougar	ns	ns	ns	ns	ns	ns	ns	ns	ns	ns	ns	ns	ns	ns	ns	ns	ns		ns	ns	ns	ns	ns	ns	ns	ns
Crusoe	ns	ns	ns	ns	ns	ns	ns	ns	ns	ns	ns	ns	ns	ns	ns	ns	ns	ns		ns	ns	ns	ns	ns	ns	ns
Gallant	ns	ns	ns	ns	ns	ns	ns	ns	ns	ns	ns	ns	ns	ns	ns	ns	ns	ns	ns		ns	ns	ns	ns	ns	ns
Sacramento	ns	ns	ns	ns	ns	ns	ns	ns	ns	ns	ns	ns	ns	ns	ns	ns	ns	ns	ns	ns		ns	ns	ns	ns	ns
Scout	ns	ns	ns	ns	ns	ns	ns	ns	ns	ns	ns	ns	ns	ns	ns	ns	ns	ns	ns	ns	ns		ns	ns	ns	ns
Shamrock	ns	ns	ns	ns	ns	ns	ns	ns	ns	ns	ns	ns	ns	ns	ns	ns	ns	ns	ns	ns	ns	ns		ns	ns	ns
Shango	ns	ns	ns	ns	*	ns	ns	ns	ns	ns	ns	ns	ns	ns	ns	ns	ns	ns	ns	ns	ns	ns	ns		ns	ns
Skyfall	ns	ns	ns	ns	ns	ns	ns	ns	ns	ns	ns	ns	ns	ns	ns	ns	ns	ns	ns	ns	ns	ns	ns	ns		ns
Stigg	ns	ns	ns	ns	*	ns	ns	ns	ns	ns	ns	ns	ns	ns	ns	ns	ns	ns	ns	ns	ns	ns	ns	ns	ns	

Appendix 1.16. Significance table for Figure 2.11C

	TRI 18344	TRI 19028	TRI 6735	TRI 17128	TRI 28870	TRI 18513	TRI 16599	TRI 18505	TRI 18530	TRI 16877	Anvergur	Aventadur	Surmesur	Voilur	Cashel	Conqueror	Conversion	Cougar	Crusoe	Gallant	Sacramento	Scout	Shamrock	Shango	Skyfall	Stigg
TRI 18344		ns	ns	ns	ns	ns	ns	ns	ns	*	ns	*	*	*	*	*	*	*	*	*	*	*	*	*	*	*
TRI 19028	ns		ns	ns	ns	ns	ns	ns	ns	*	ns	*	*	*	*	*	*	*	*	*	*	*	*	*	*	*
TRI 6735	ns	ns		ns	ns	ns	ns	ns	ns	ns	ns	ns	ns	ns	ns	ns	ns	ns	*	*	ns	*	*	ns	ns	ns
TRI 17128	ns	ns	ns		ns	ns	ns	ns	ns	ns	ns	ns	ns	ns	ns	ns	ns	ns	ns	ns	ns	ns	ns	ns	ns	ns
TRI 28870	ns	ns	ns	ns		ns	ns	ns	ns	ns	ns	ns	ns	ns	ns	ns	ns	ns	ns	ns	ns	ns	ns	ns	ns	ns
TRI 18513	ns	ns	ns	ns	ns		ns	ns	ns	ns	ns	ns	ns	ns	ns	ns	ns	ns	ns	ns	ns	ns	ns	ns	ns	ns
TRI 16599	ns	ns	ns	ns	ns	ns		ns	ns	ns	ns	ns	ns	ns	ns	ns	ns	ns	ns	ns	ns	ns	ns	ns	ns	ns
TRI 18505	ns	ns	ns	ns	ns	ns	ns		ns	*	ns	*	*	*	*	*	*	*	*	*	*	*	*	*	*	*
TRI 18530	ns	ns	ns	ns	ns	ns	ns	ns		ns	ns	ns	ns	ns	ns	ns	ns	ns	ns	ns	ns	ns	ns	ns	ns	ns
TRI 16877	*	*	ns	ns	ns	ns	ns	*	ns		ns	ns	ns	ns	ns	ns	ns	ns	ns	ns	ns	ns	ns	ns	ns	ns
Anvergur	ns	ns	ns	ns	ns	ns	ns	ns	ns	ns		ns	ns	ns	ns	ns	ns	ns	ns	ns	ns	ns	ns	ns	ns	ns
Aventadur	*	*	ns	ns	ns	ns	ns	*	ns	ns	ns		ns	ns	ns	ns	ns	ns	ns	ns	ns	ns	ns	ns	ns	ns
Surmesur	*	*	ns	ns	ns	ns	ns	*	ns	ns	ns	ns		ns	ns	ns	ns	ns	ns	ns	ns	ns	ns	ns	ns	ns
Voilur	*	*	ns	ns	ns	ns	ns	*	ns	ns	ns	ns	ns		ns	ns	ns	ns	ns	ns	ns	ns	ns	ns	ns	ns
Cashel	*	*	ns	ns	ns	ns	ns	*	ns	ns	ns	ns	ns	ns		ns	ns	ns	ns	ns	ns	ns	ns	ns	ns	ns
Conqueror	*	*	ns	ns	ns	ns	ns	*	ns	ns	ns	ns	ns	ns	ns		ns	ns	ns	ns	ns	ns	ns	ns	ns	ns
Conversion	*	*	ns	ns	ns	ns	ns	*	ns	ns	ns	ns	ns	ns	ns	ns		ns	ns	ns	ns	ns	ns	ns	ns	ns
Cougar	*	*	ns	ns	ns	ns	ns	*	ns	ns	ns	ns	ns	ns	ns	ns	ns		ns	ns	ns	ns	ns	ns	ns	ns
Crusoe	*	*	*	ns	ns	ns	ns	*	ns	ns	ns	ns	ns	ns	ns	ns	ns	ns		ns	ns	ns	ns	ns	ns	ns
Gallant	*	*	*	ns	ns	ns	ns	*	ns	ns	ns	ns	ns	ns	ns	ns	ns	ns	ns		ns	ns	ns	ns	ns	ns
Sacramento	*	*	ns	ns	ns	ns	ns	*	ns	ns	ns	ns	ns	ns	ns	ns	ns	ns	ns	ns		ns	ns	ns	ns	ns
Scout	*	*	*	ns	ns	ns	ns	*	ns	ns	ns	ns	ns	ns	ns	ns	ns	ns	ns	ns	ns		ns	ns	ns	ns
Shamrock	*	*	*	ns	ns	ns	ns	*	ns	ns	ns	ns	ns	ns	ns	ns	ns	ns	ns	ns	ns	ns		ns	ns	ns
Shango	*	*	ns	ns	ns	ns	ns	*	ns	ns	ns	ns	ns	ns	ns	ns	ns	ns	ns	ns	ns	ns	ns		ns	ns
Skyfall	*	*	ns	ns	ns	ns	ns	*	ns	ns	ns	ns	ns	ns	ns	ns	ns	ns	ns	ns	ns	ns	ns	ns		ns
Stigg	*	*	ns	ns	ns	ns	ns	*	ns	ns	ns	ns	ns	ns	ns	ns	ns	ns	ns	ns	ns	ns	ns	ns	ns	

Appendix 1.17. Significance table for Figure 2.11E

	TRI 18344	TRI 19028	TRI 6735	TRI 17128	TRI 28870	TRI 18513	TRI 16599	TRI 18505	TRI 18530	TRI 16877	Anvergur	Aventadur	Surmesur	Voilur	Cashel	Conqueror	Conversion	Cougar	Crusoe	Gallant	Sacramento	Scout	Shamrock	Shango	Skyfall	Stigg
TRI 18344		ns	ns	ns	ns	ns	ns	ns	ns	ns	ns	ns	*	ns	ns	*	*	*	*	*	ns	*	*	*	ns	ns
TRI 19028	ns		ns	ns	ns	ns	ns	ns	ns	ns	ns	ns	*	ns	ns	*	*	*	*	*	ns	*	*	*	ns	ns
TRI 6735	ns	ns		ns	ns	ns	ns	ns	ns	ns	ns	ns	ns	ns	ns	*	*	ns	*	*	ns	*	ns	ns	ns	ns
TRI 17128	ns	ns	ns		ns	ns	ns	ns	ns	ns	ns	ns	ns	ns	ns	*	*	ns	*	*	ns	*	ns	ns	ns	ns
TRI 28870	ns	ns	ns	ns		ns	ns	ns	ns	ns	ns	ns	ns	ns	ns	ns	ns	ns	ns	ns	ns	ns	ns	ns	ns	ns
TRI 18513	ns	ns	ns	ns	ns		ns	ns	ns	ns	ns	ns	ns	ns	ns	ns	ns	ns	ns	ns	ns	ns	ns	ns	ns	ns
TRI 16599	ns	ns	ns	ns	ns	ns		ns	ns	ns	ns	ns	ns	ns	ns	ns	ns	ns	ns	ns	ns	ns	ns	ns	ns	ns
TRI 18505	ns	ns	ns	ns	ns	ns	ns		ns	ns	ns	ns	*	ns	ns	*	*	*	*	*	ns	*	*	*	ns	ns
TRI 18530	ns	ns	ns	ns	ns	ns	ns	ns		ns	ns	ns	ns	ns	ns	*	*	ns	*	*	ns	*	ns	ns	ns	ns
TRI 16877	ns	ns	ns	ns	ns	ns	ns	ns	ns		ns	ns	ns	ns	ns	ns	ns	ns	ns	ns	ns	ns	ns	ns	ns	ns
Anvergur	ns	ns	ns	ns	ns	ns	ns	ns	ns	ns		ns	ns	ns	ns	ns	ns	ns	ns	ns	ns	ns	ns	ns	ns	ns
Aventadur	ns	ns	ns	ns	ns	ns	ns	ns	ns	ns	ns		ns	ns	ns	ns	ns	ns	ns	ns	ns	ns	ns	ns	ns	ns
Surmesur	*	*	ns	ns	ns	ns	ns	*	ns	ns	ns	ns		ns	ns	ns	ns	ns	ns	ns	ns	ns	ns	ns	ns	ns
Voilur	ns	ns	ns	ns	ns	ns	ns	ns	ns	ns	ns	ns	ns		ns	ns	ns	ns	ns	ns	ns	ns	ns	ns	ns	ns
Cashel	ns	ns	ns	ns	ns	ns	ns	ns	ns	ns	ns	ns	ns	ns		ns	ns	ns	ns	ns	ns	ns	ns	ns	ns	ns
Conqueror	*	*	*	*	ns	ns	ns	*	*	ns	ns	ns	ns	ns	ns		ns	ns	ns	ns	ns	ns	ns	ns	ns	ns
Conversion	*	*	*	*	ns	ns	ns	*	*	ns	ns	ns	ns	ns	ns	ns		ns	ns	ns	ns	ns	ns	ns	ns	ns
Cougar	*	*	ns	ns	ns	ns	ns	*	ns	ns	ns	ns	ns	ns	ns	ns	ns		ns	ns	ns	ns	ns	ns	ns	ns
Crusoe	*	*	*	*	ns	ns	ns	*	*	ns	ns	ns	ns	ns	ns	ns	ns	ns		ns	ns	ns	ns	ns	ns	ns
Gallant	*	*	*	*	ns	ns	ns	*	*	ns	ns	ns	ns	ns	ns	ns	ns	ns	ns		ns	ns	ns	ns	ns	ns
Sacramento	ns	ns	ns	ns	ns	ns	ns	ns	ns	ns	ns	ns	ns	ns	ns	ns	ns	ns	ns	ns		ns	ns	ns	ns	ns
Scout	*	*	*	*	ns	ns	ns	*	*	ns	ns	ns	ns	ns	ns	ns	ns	ns	ns	ns	ns		ns	ns	ns	ns
Shamrock	*	*	ns	ns	ns	ns	ns	*	ns	ns	ns	ns	ns	ns	ns	ns	ns	ns	ns	ns	ns	ns		ns	ns	ns
Shango	*	*	ns	ns	ns	ns	ns	*	ns	ns	ns	ns	ns	ns	ns	ns	ns	ns	ns	ns	ns	ns	ns		ns	ns
Skyfall	ns	ns	ns	ns	ns	ns	ns	ns	ns	ns	ns	ns	ns	ns	ns	ns	ns	ns	ns	ns	ns	ns	ns	ns		ns
Stigg	ns	ns	ns	ns	ns	ns	ns	ns	ns	ns	ns	ns	ns	ns	ns	ns	ns	ns	ns	ns	ns	ns	ns	ns	ns	

Appendix 2. Significance tables for Chapter 3

A summary of the lines used in this thesis (including ploidy number, species name and domestication status) is available in Table 2.1.

Lines which could be significantly distinguished from one another (at P= <0.01) following a post-hoc test are shown by an asterisk (*). Ploidy level is indicated by colour. Lines coded white are diploid, orange are tetraploid and blue are hexaploid.

Appendix 2.1. Significance table for Figure 3.3A

	TRI 18344	TRI 6735	TRI 28870	TRI 18513	TRI 18505	TRI 16877	Anvergur	Voilur	Cougar	Crusoe	Shango
TRI 18344		ns	ns	ns	ns	ns	ns	ns	*	*	ns
TRI 6735	ns		ns	ns	ns	ns	ns	ns	*	*	ns
TRI 28870	ns	ns		ns	ns	ns	ns	ns	ns	ns	ns
TRI 18513	ns	ns	ns		ns	ns	ns	ns	ns	ns	ns
TRI 18505	ns	ns	ns	ns		ns	ns	ns	*	*	ns
TRI 16877	ns	ns	ns	ns	ns		ns	ns	*	*	ns
Anvergur	ns	ns	ns	ns	ns	ns		ns	ns	ns	ns
Voilur	ns	ns	ns	ns	ns	ns	ns		ns	ns	ns
Cougar	*	*	ns	ns	*	*	ns	ns		ns	ns
Crusoe	*	*	ns	ns	*	*	ns	ns	ns		ns
Shango	ns	ns	ns	ns	ns	ns	ns	ns	ns	ns	

Appendix 2.2. Significance table for Figure 3.5A

	TRI 18344	TRI 6735	TRI 28870	TRI 18513	TRI 18505	TRI 16877	Anvergur	Voilur	Cougar	Crusoe	Shango
TRI 18344		ns	ns	ns	ns	ns	ns	ns	ns	ns	ns
TRI 6735	ns		ns	ns	ns	ns	ns	ns	ns	ns	ns
TRI 28870	ns	ns		ns	ns	ns	ns	ns	ns	ns	ns
TRI 18513	ns	ns	ns		ns	ns	ns	ns	ns	ns	ns
TRI 18505	ns	ns	ns	ns		ns	ns	ns	ns	ns	ns
TRI 16877	ns	ns	ns	ns	ns		ns	ns	ns	ns	ns
Anvergur	ns	ns	ns	ns	ns	ns		ns	ns	ns	ns
Voilur	ns	ns	ns	ns	ns	ns	ns		ns	ns	ns
Cougar	ns	ns	ns	ns	ns	ns	ns	ns		ns	ns
Crusoe	ns	ns	ns	ns	ns	ns	ns	ns	ns		ns
Shango	ns	ns	ns	ns	ns	ns	ns	ns	ns	ns	

Appendix 2.3. Significance table for Figure 3.7A

	TRI 18344	TRI 6735	TRI 28870	TRI 18513	TRI 18505	TRI 16877	Anvergur	Voilur	Cougar	Crusoe	Shango
TRI 18344		ns	ns	ns	ns	ns	ns	ns	ns	ns	ns
TRI 6735	ns		ns	ns	ns	ns	ns	ns	ns	ns	ns
TRI 28870	ns	ns		ns	ns	ns	ns	ns	ns	ns	ns
TRI 18513	ns	ns	ns		ns	ns	ns	ns	ns	ns	ns
TRI 18505	ns	ns	ns	ns		ns	ns	ns	ns	ns	ns
TRI 16877	ns	ns	ns	ns	ns		ns	ns	ns	ns	ns
Anvergur	ns	ns	ns	ns	ns	ns		ns	ns	ns	ns
Voilur	ns	ns	ns	ns	ns	ns	ns		ns	ns	ns
Cougar	ns	ns	ns	ns	ns	ns	ns	ns		ns	ns
Crusoe	ns	ns	ns	ns	ns	ns	ns	ns	ns		ns
Shango	ns	ns	ns	ns	ns	ns	ns	ns	ns	ns	

Appendix 2.4. Significance table for Figure 3.7C

	TRI 18344	TRI 6735	TRI 28870	TRI 18513	TRI 18505	TRI 16877	Anvergur	Voilur	Cougar	Crusoe	Shango
TRI 18344		ns	ns	ns	ns	ns	ns	ns	ns	ns	ns
TRI 6735	ns		ns	ns	ns	ns	ns	ns	ns	ns	ns
TRI 28870	ns	ns		ns	ns	ns	ns	ns	ns	ns	ns
TRI 18513	ns	ns	ns		ns	ns	ns	ns	ns	*	ns
TRI 18505	ns	ns	ns	ns		ns	ns	ns	ns	*	ns
TRI 16877	ns	ns	ns	ns	ns		ns	ns	*	*	ns
Anvergur	ns	ns	ns	ns	ns	ns		ns	ns	*	ns
Voilur	ns	ns	ns	ns	ns	ns	ns		ns	ns	ns
Cougar	ns	ns	ns	ns	ns	*	ns	ns		ns	ns
Crusoe	ns	ns	ns	*	*	*	*	ns	ns		ns
Shango	ns	ns	ns	ns	ns	ns	ns	ns	ns	ns	

Appendix 2.5. Significance table for Figure 3.9A

	TRI 18344	TRI 6735	TRI 28870	TRI 18513	TRI 18505	TRI 16877	Anvergur	Voilur	Cougar	Crusoe	Shango
TRI 18344		ns	ns	ns	ns	ns	ns	ns	*	ns	ns
TRI 6735	ns		ns	ns	ns	ns	ns	ns	*	ns	ns
TRI 28870	ns	ns		ns	ns	ns	ns	ns	*	ns	ns
TRI 18513	ns	ns	ns		ns	ns	ns	ns	ns	ns	ns
TRI 18505	ns	ns	ns	ns		ns	ns	ns	ns	ns	ns
TRI 16877	ns	ns	ns	ns	ns		ns	ns	ns	ns	ns
Anvergur	ns	ns	ns	ns	ns	ns		ns	ns	ns	ns
Voilur	ns	ns	ns	ns	ns	ns	ns		ns	ns	ns
Cougar	*	*	*	ns	*	ns	ns	ns		ns	ns
Crusoe	ns	ns	ns	ns	ns	ns	ns	ns	ns		ns
Shango	ns	ns	ns	ns	ns	ns	ns	ns	ns	ns	

Appendix 2.6. Significance table for Figure 3.9C

	TRI 18344	TRI 6735	TRI 28870	TRI 18513	TRI 18505	TRI 16877	Anvergur	Voilur	Cougar	Crusoe	Shango
TRI 18344		ns	ns	ns	*	*	ns	ns	*	*	*
TRI 6735	ns		ns	ns	*	ns	ns	ns	ns	ns	ns
TRI 28870	ns	ns		ns	*	ns	ns	ns	ns	ns	ns
TRI 18513	ns	ns	ns		*	ns	ns	ns	ns	ns	ns
TRI 18505	*	*	*	*		ns	*	*	ns	ns	ns
TRI 16877	*	ns	ns	ns	ns		ns	ns	ns	ns	ns
Anvergur	ns	ns	ns	ns	*	ns		ns	ns	ns	ns
Voilur	ns	ns	ns	ns	*	ns	ns		ns	*	ns
Cougar	*	ns	ns	ns	ns	ns	ns	ns		ns	ns
Crusoe	*	ns	ns	ns	ns	ns	ns	*	ns		ns
Shango	*	ns	ns	ns	ns	ns	ns	ns	ns	ns	

Appendix 2.7. Significance table for Figure 3.10A

	TRI 18344	TRI 6735	TRI 28870	TRI 18513	TRI 18505	TRI 16877	Anvergur	Voilur	Cougar	Crusoe	Shango
TRI 18344		ns	ns	ns	*	ns	ns	ns	*	*	*
TRI 6735	ns		ns	ns	*	ns	ns	ns	*	*	*
TRI 28870	ns	ns		ns	*	ns	ns	ns	*	*	*
TRI 18513	ns	ns	ns		ns	ns	ns	ns	*	*	ns
TRI 18505	*	*	*	ns		ns	ns	ns	ns	ns	ns
TRI 16877	ns	ns	ns	ns	ns		ns	ns	ns	ns	ns
Anvergur	ns	ns	ns	ns	ns	ns		ns	ns	ns	ns
Voilur	ns	ns	ns	ns	ns	ns	ns		*	*	ns
Cougar	*	*	*	*	ns	ns	ns	*		ns	ns
Crusoe	*	*	*	*	ns	ns	ns	*	ns		ns
Shango	*	*	*	ns	ns	ns	ns	ns	ns	ns	

Appendix 2.8. Significance table for Figure 3.10C

	TRI 18344	TRI 6735	TRI 28870	TRI 18513	TRI 18505	TRI 16877	Anvergur	Voilur	Cougar	Crusoe	Shango
TRI 18344		ns	ns	ns	*	ns	ns	ns	*	*	ns
TRI 6735	ns		ns	ns	*	ns	ns	ns	ns	*	ns
TRI 28870	ns	ns		ns	*	ns	ns	ns	*	*	ns
TRI 18513	ns	ns	ns		*	ns	ns	ns	ns	*	ns
TRI 18505	*	*	*	*		ns	ns	*	ns	ns	ns
TRI 16877	ns	ns	ns	ns	ns		ns	ns	ns	ns	ns
Anvergur	ns	ns	ns	ns	ns	ns		ns	ns	ns	ns
Voilur	ns	ns	ns	ns	*	ns	ns		ns	ns	ns
Cougar	*	ns	*	ns	ns	ns	ns	ns		ns	ns
Crusoe	*	*	*	*	ns	ns	ns	ns	ns		ns
Shango	ns	ns	ns	ns	ns	ns	ns	ns	ns	ns	

Appendix 2.9. Significance table for Figure 3.11A

	TRI 18344	TRI 6735	TRI 28870	TRI 18513	TRI 18505	TRI 16877	Anvergur	Voilur	Cougar	Crusoe	Shango
TRI 18344		ns	ns	ns	ns	ns	ns	ns	ns	ns	ns
TRI 6735	ns		ns	ns	ns	ns	ns	ns	ns	ns	ns
TRI 28870	ns	ns		ns	ns	ns	ns	ns	ns	ns	ns
TRI 18513	ns	ns	ns		ns	ns	ns	ns	ns	ns	ns
TRI 18505	ns	ns	ns	ns		ns	ns	ns	ns	ns	ns
TRI 16877	ns	ns	ns	ns	ns		ns	ns	ns	ns	ns
Anvergur	ns	ns	ns	ns	ns	ns		ns	*	ns	ns
Voilur	ns	ns	ns	ns	ns	ns	ns		ns	ns	ns
Cougar	ns	ns	ns	ns	ns	ns	*	ns		ns	ns
Crusoe	ns	ns	ns	ns	ns	ns	ns	ns	ns		ns
Shango	ns	ns	ns	ns	ns	ns	ns	ns	ns	ns	

Appendix 2.10. Significance table for Figure 3.12A

	TRI 18344	TRI 6735	TRI 28870	TRI 18513	TRI 18505	TRI 16877	Anvergur	Voilur	Cougar	Crusoe	Shango
TRI 18344		ns	ns	ns	ns	ns	ns	ns	ns	ns	ns
TRI 6735	ns		ns	ns	ns	ns	ns	ns	ns	ns	ns
TRI 28870	ns	ns		ns	ns	ns	ns	ns	ns	ns	ns
TRI 18513	ns	ns	ns		ns	ns	ns	ns	ns	ns	ns
TRI 18505	ns	ns	ns	ns		ns	ns	ns	ns	ns	ns
TRI 16877	ns	ns	ns	ns	ns		ns	ns	*	ns	ns
Anvergur	ns	ns	ns	ns	ns	ns		ns	ns	ns	ns
Voilur	ns	ns	ns	ns	ns	ns	ns		ns	ns	ns
Cougar	ns	ns	ns	ns	ns	*	ns	ns		ns	ns
Crusoe	ns	ns	ns	ns	ns	ns	ns	ns	ns		ns
Shango	ns	ns	ns	ns	ns	ns	ns	ns	ns	ns	

Appendix 2.11. Significance table for Figure 3.12C

	TRI 18344	TRI 6735	TRI 28870	TRI 18513	TRI 18505	TRI 16877	Anvergur	Voilur	Cougar	Crusoe	Shango
TRI 18344		ns	ns	ns	ns	ns	ns	ns	ns	ns	ns
TRI 6735	ns		ns	ns	ns	ns	ns	ns	ns	ns	ns
TRI 28870	ns	ns		ns	ns	ns	ns	ns	ns	ns	ns
TRI 18513	ns	ns	ns		ns	ns	ns	ns	ns	ns	ns
TRI 18505	ns	ns	ns	ns		ns	ns	ns	ns	ns	ns
TRI 16877	ns	ns	ns	ns	ns		ns	ns	ns	ns	ns
Anvergur	ns	ns	ns	ns	ns	ns		ns	ns	ns	ns
Voilur	ns	ns	ns	ns	ns	ns	ns		ns	ns	ns
Cougar	ns	ns	ns	ns	ns	ns	ns	ns		ns	ns
Crusoe	ns	ns	ns	ns	ns	ns	ns	ns	ns		ns
Shango	ns	ns	ns	ns	ns	ns	ns	ns	ns	ns	

Appendix 2.12. Significance table for Figure 3.13A

	TRI 18344	TRI 6735	TRI 28870	TRI 18513	TRI 18505	TRI 16877	Anvergur	Voilur	Cougar	Crusoe	Shango
TRI 18344		ns	ns	ns	ns	ns	ns	ns	ns	ns	ns
TRI 6735	ns		ns	ns	ns	ns	ns	ns	ns	ns	ns
TRI 28870	ns	ns		ns	ns	ns	ns	ns	ns	ns	ns
TRI 18513	ns	ns	ns		ns	ns	ns	ns	ns	ns	ns
TRI 18505	ns	ns	ns	ns		ns	ns	ns	ns	ns	ns
TRI 16877	ns	ns	ns	ns	ns		ns	ns	ns	ns	ns
Anvergur	ns	ns	ns	ns	ns	ns		ns	ns	ns	ns
Voilur	ns	ns	ns	ns	ns	ns	ns		ns	ns	ns
Cougar	ns	ns	ns	ns	ns	ns	ns	ns		ns	ns
Crusoe	ns	ns	ns	ns	ns	ns	ns	ns	ns		ns
Shango	ns	ns	ns	ns	ns	ns	ns	ns	ns	ns	

Appendix 3. Significance tables for Chapter 4

A summary of the lines used in this thesis (including ploidy number, species name and domestication status) is available in Table 2.1.

Lines which could be significantly distinguished from one another (at P= <0.01) following a post-hoc test are shown by an asterisk (*). Ploidy level is indicated by colour. Lines coded white are diploid, orange are tetraploid and blue are hexaploid.

Appendix 3.1. Significance table for Figure 4.5A

	TRI 18344	TRI 6735	TRI 28870	TRI 18513	TRI 18505	TRI 16877	Anvergur	Voilur	Cougar	Crusoe	Shango
TRI 18344		ns	ns	ns	ns	ns	ns	*	*	*	*
TRI 6735	ns		ns	ns	ns	ns	ns	ns	ns	*	ns
TRI 28870	ns	ns		ns	ns	ns	ns	ns	*	*	*
TRI 18513	ns	ns	ns		ns	ns	ns	ns	ns	*	ns
TRI 18505	ns	ns	ns	ns		ns	ns	ns	ns	ns	ns
TRI 16877	ns	ns	ns	ns	ns		ns	ns	ns	ns	ns
Anvergur	ns	ns	ns	ns	ns	ns		ns	ns	ns	ns
Voilur	*	ns	ns	ns	ns	ns	ns		ns	ns	ns
Cougar	*	ns	*	ns	ns	ns	ns	ns		ns	ns
Crusoe	*	*	*	*	ns	ns	ns	ns	ns		ns
Shango	*	ns	*	ns	ns	ns	ns	ns	ns	ns	

Appendix 3.2. Significance table for Figure 4.6A

	TRI 18344	TRI 6735	TRI 28870	TRI 18513	TRI 18505	TRI 16877	Anvergur	Voilur	Cougar	Crusoe	Shango
TRI 18344		ns	ns	ns	ns	ns	ns	ns	*	*	ns
TRI 6735	ns		ns	ns	ns	ns	ns	ns	ns	*	ns
TRI 28870	ns	ns		ns	ns	ns	ns	ns	*	*	ns
TRI 18513	ns	ns	ns		ns	ns	ns	ns	ns	ns	ns
TRI 18505	ns	ns	ns	ns		ns	ns	ns	ns	ns	ns
TRI 16877	ns	ns	ns	ns	ns		ns	ns	ns	ns	ns
Anvergur	ns	ns	ns	ns	ns	ns		ns	ns	ns	ns
Voilur	ns	ns	ns	ns	ns	ns	ns		ns	ns	ns
Cougar	*	ns	*	ns	ns	ns	ns	ns		ns	ns
Crusoe	*	*	*	ns	ns	ns	ns	ns	ns		ns
Shango	ns	ns	ns	ns	ns	ns	ns	ns	ns	ns	

Appendix 3.3. Significance table for Figure 4.8A

	TRI 18344	TRI 6735	TRI 28870	TRI 18513	TRI 18505	TRI 16877	Anvergur	Voilur	Cougar	Crusoe	Shango
TRI 18344		ns	ns	ns	ns	ns	ns	ns	ns	ns	ns
TRI 6735	ns		ns	ns	ns	ns	ns	ns	ns	ns	ns
TRI 28870	ns	ns		ns	ns	ns	ns	ns	ns	ns	ns
TRI 18513	ns	ns	ns		ns	ns	ns	ns	ns	ns	ns
TRI 18505	ns	ns	ns	ns		ns	ns	ns	ns	ns	ns
TRI 16877	ns	ns	ns	ns	ns		ns	ns	ns	ns	ns
Anvergur	ns	ns	ns	ns	ns	ns		ns	ns	ns	ns
Voilur	ns	ns	ns	ns	ns	ns	ns		ns	ns	ns
Cougar	ns	ns	ns	ns	ns	ns	ns	ns		ns	ns
Crusoe	ns	ns	ns	ns	ns	ns	ns	ns	ns		ns
Shango	ns	ns	ns	ns	ns	ns	ns	ns	ns	ns	

Appendix 3.4. Significance table for Figure 4.9A

	TRI 18344	TRI 6735	TRI 28870	TRI 18513	TRI 18505	TRI 16877	Anvergur	Voilur	Cougar	Crusoe	Shango
TRI 18344		ns	ns	ns	ns	ns	ns	ns	*	*	ns
TRI 6735	ns		ns	ns	ns	ns	ns	ns	*	ns	ns
TRI 28870	ns	ns		ns	ns	ns	ns	ns	*	ns	ns
TRI 18513	ns	ns	ns		ns	ns	ns	ns	ns	ns	ns
TRI 18505	ns	ns	ns	ns		ns	ns	ns	ns	ns	ns
TRI 16877	ns	ns	ns	ns	ns		ns	ns	ns	ns	ns
Anvergur	ns	ns	ns	ns	ns	ns		ns	ns	ns	ns
Voilur	ns	ns	ns	ns	ns	ns	ns		ns	ns	ns
Cougar	*	*	*	ns	ns	ns	ns	ns		ns	ns
Crusoe	*	ns	ns	ns	ns	ns	ns	ns	ns		ns
Shango	ns	ns	ns	ns	ns	ns	ns	ns	ns	ns	